Investigating the Potential Role of the M1 Muscarinic Acetylcholine Receptor in Misfolded Protein Propagation

Jose Andres Alepuz Guillen

BSc, MSc

Submitted in fulfilment of the requirements of the Degree of

Doctor of Philosophy

Institute of Molecular Biosciences

College of Medical, Veterinary & Life Sciences

University of Glasgow

May 2024

Abstract

Prion diseases are a variety of fatal neurodegenerative diseases characterised by the misfolding, aggregation and propagation of the prion protein. There are currently no disease modifying treatments available that can slow the progression of the disease (Scarpa et al., 2020). However, previous data from our group suggests that the activation of the M1 muscarinic acetylcholine receptor (mAChR) can both restore memory deficits as well as slow the accumulation of misfolded scrapie prion protein (PrP^{Sc}) in a *in vivo* murine prion disease model (Bradley et al., 2017; Dwomoh, Rossi, et al., 2022). These findings pose a question around the mechanism via which the M1 mAChR signalling acts in a neuroprotective mode against neurodegeneration by slowing down the propagation of misfolded prion.

In this study, PrP^{Sc} from diseased animals was purified and administered to primary neuronal cultures to evaluate prion infection and propagation. In prion protein overexpressing neurons, infection with PrP^{Sc} resulted in the progressive accumulation and propagation of PrP^{Sc} over time. In contrast, prion protein knockout cultures showed a gradual degradation of PrP^{Sc} after infection due to the lack of endogenous cellular prion (PrP^{C}) to act as a substrate for propagation. In this study, results confirmed the successful infection and propagation of PrP^{Sc} *in vitro* suggesting that PrP^{C} is required for PrP^{Sc} propagation but not for infection.

To understand the role of the M1 mAChR in prion infection and propagation, neurons from M1 wildtype, M1 knockout, M1-DREADD (designer receptor exclusively activated by designer drugs) and M1-PD (phosphorylation deficient) mice were used. These primary neuronal cultures were also chronically treated for 7 days, after infection, with several muscarinic ligands with different potencies, efficacies and affinities to test the impact of muscarinic downstream signalling on prion infection and misfolding. No significant differences in PrP^{Sc} accumulation were observed in all strains, with or without ligand treatment. This data suggests that the action of the receptor could be more important in the presence of glia, requiring the expression of these cell types for a reduction in PrP^{Sc} to be observed.

A proteomic study of this novel prion model in primary neuronal cultures showed several dysregulations in mitochondrial, ribosomal and neuronal-associated proteins as a consequence of PrP^{Sc} infection. Results revealed dysregulation of neuronal proteins which had not been previously observed *in vivo* prion disease mouse models, possibly hindered by the high upregulation of neuroinflammatory-associated proteins. It also highlighted several cytoskeletal-associated proteins that could potentially be involved in the mechanisms of PrP^{Sc} infection and propagation.

These findings validate this model to specifically study infection and propagation of PrP^{Sc} in neurons, with the advantage of no neuronal degeneration and disease. Further research into the role of muscarinics and other proteins in prion infection and propagation utilising this *in vitro* primary neuronal cell model may allow to develop novel drug candidates with disease modifying effects.

Table of Contents

Abstract i

Table of Contents iii

List of Tables viii

List of Figures x

Acknowledgement xiii

Author's Declaration xiv

Definitions/Abbreviations xv

Chapter 1 Introduction 1

1.1 PRIONS AND PROTEIN MISFOLDING DISEASES 2

1.1.1 Prion diseases 2

1.1.2 The prion protein 5

1.1.3 Mechanisms of protein misfolding, aggregation and propagation 8

1.1.4 Prion strains 10

1.1.5 Therapeutic targets for prion diseases 13

1.1.6 Protein misfolding Diseases 15

1.1.6.1 Parkinson's disease 15

1.1.6.2 Amyotrophic lateral sclerosis 17

1.1.6.3 Frontotemporal lobar degeneration 17

1.1.6.4 Alzheimer's disease 18

1.2 PRION-LIKE PROTEINS 21

1.2.1 α-synuclein 21

1.2.2 TDP-43 22

1.2.3 Amyloid-β and tau 23

1.3 MUSCARINIC ACETYLCHOLINE RECEPTORS 26

1.3.1 Overview of muscarinic acetylcholine receptors 26

1.3.2 Muscarinic receptor signalling 28

1.3.3 M1 muscarinic acetylcholine receptor 29

1.3.4 M1 mAChR in neurodegenerative diseases 30

1.3.5 Engineered M1 mAChR versions 31

1.3.6 mAChR ligands 34

1.3.7 M1 mAChR ligands in neurodegenerative diseases 36

1.4 M1 MACHR AS A POTENTIAL TARGET FOR PRION DISEASE 37

1.5 GENERAL AIMS OF THE THESIS 38
Chapter 2 Materials and Methods 40
2.1 MATERIALS 41
2.1.1 General materials and reagents 41
2.1.2 Materials and reagents used in cell and tissue culture 42
2.1.3 Muscarinic pharmacological ligands 43
2.1.4 Primary antibodies (Western blotting and immunocytochemistry) ... 43
2.1.5 Secondary antibodies (Western blotting and immunocytochemistry) 44
2.1.6 Materials and reagents used for Mass Spectrometry sample preparation 45
2.1.7 Mass Spectrometry Buffer recipes 46
2.1.8 Recipes for Buffers and Solutions 46
2.2 EXPERIMENTAL ANIMALS 47
2.2.1 Ethics statement 48
2.2.2 Mouse prion Infection 48
2.2.3 Tissue Harvest 49
2.3 CHO CELL CULTURE 49
2.3.1 Production of CHO Flp-In™ cell lines 49
2.3.2 Maintenance of CHO Flp-In cell lines 49
2.3.3 Determination of cell viability 49
2.3.4 Cryopreservation of CHO Flp-In cell lines 50
2.4 PRIMARY NEURONAL CELL CULTURE 50
2.5 PHARMACOLOGICAL ASSAYS 51
2.5.1 IP1 Accumulation Assay 51
2.5.2 Radioligand Binding Assay 51
2.6 PRION ENRICHMENT AND NEURONAL INFECTION 52
2.7 IMMUNOBLOTTING 53
2.7.1 Lysate preparation from cultured CHO cells 53
2.7.2 Immunoprecipitation of HA-tagged proteins 53
2.7.3 Lysate preparation of neuronal cultures 53
2.7.4 Protein Quantification BCA Assay 54
2.7.5 SDS-PAGE 54
2.7.6 Probing and detection 54
2.7.7 Sample proteinase K digestion 55
2.8 IMMUNOCYTOCHEMISTRY 55

2.8.1 Cell fixation 55
2.8.2 Immunostaining 55
2.9 PROTEOMICS 56
2.9.1 Lysate preparation 56
2.9.2 Sample reduction, alkylation and digestion 56
2.9.3 Peptide labelling 57
2.9.4 Sample fractionation 58
2.9.5 Mass spectrometry analysis 58
2.9.6 Protein identification 58
2.10 DATA ANALYSIS 59
2.10.1 Neuronal Sample Size 59
2.10.2 General statistical analysis 59
2.10.3 Analysis of Binding Saturation Assays 60
2.10.4 Analysis of Proteomic data 60
Chapter 3 *In vitro* characterisation of the prion protein and the M1 muscarinic acetylcholine receptor 61
3.1 INTRODUCTION 62
3.1.1 Prion Protein and M1 mAChR 62
3.1.2 Aims 63
3.2 RESULTS 63
3.2.1 M1 mAChR expression in non-transfected, wild-type and DREADD mutant M1 mAChR CHO Flp-In cells 63
3.2.2 M1 mAChR pharmacological evaluation in non-transfected, wild-type and DREADD mutant M1 mAChR on CHO Flp-In cells 66
3.2.3 M1 mAChR and prion characterisation of *in vitro* primary neuronal cultures from different GEMMs 69
3.2.4 M1 mAChR pharmacological evaluation of primary neuronal cultures from several GEMMs 77
3.3 DISCUSSION 80
Chapter 4 Role of the M1 mAChR in a new prion infection model of *in vitro* primary neuronal cultures 86
4.1 INTRODUCTION 87
4.1.1 Prion disease mouse model 87
4.1.2 Cellular models of prion 88
4.1.3 Muscarinic receptors and prion 90

4.1.4 Aims 91
4.2 SPECIFIC METHODOLOGY 92
4.2.1 Novel protocol of prion purification from prion diseased mice 92
4.3 RESULTS 94
4.3.1 Characterisation of the novel prion purification protocol 94
4.3.2 Optimisation of novel *in vitro* model of PrP^{Sc} infection and propagation in primary neuronal cultures 95
4.3.3 Characterisation of the novel prion infection and propagation model 99
4.3.4 Effect of M1 mAChR expression in PrP^{Sc} infection and propagation .103
4.3.5 Muscarinic receptor activation effect on prion infection and propagation.....105
4.3.6 M1 mAChR expression and signalling after chronic receptor activation 107
4.3.7 Muscarinic receptor activation effect on prion infection and propagation in a M1 mAChR phosphorylation-deficient mutant primary neuronal culture 111
4.3.8 M1 mAChR expression and signalling after chronic receptor activation in a M1 mAChR phosphorylation-deficient mutant primary neuronal culture 112
4.4 DISCUSSION 114
Chapter 5 Proteomic study of the new prion infection model of *in vitro* primary neuronal cultures 121
5.1 INTRODUCTION 122
5.1.1 Proteomic Studies of Protein Misfolding Diseases 122
5.1.2 Proteomic Studies in Prion Disease Models 123
5.1.3 Aims 124
5.2 SPECIFIC METHODOLOGY 126
5.2.1 Proteomic sample experimental outline 126
5.3 RESULTS 127
5.3.1 Initial analysis of uninfected, NBH control-treated and RML prion-infected neuronal cultures' samples 127
5.3.2 General comparison between all 3 group samples 129
5.3.3 Impact of NBH control-treatment in primary neuronal cultures 130
5.3.4 Impact of RML prion-infection in primary neuronal cultures 131

5.3.5 RML prion-infection vs NBH control-treated primary neuronal cultures 134
5.4 DISCUSSION 139
Chapter 6 Final Discussion 147
Appendices 154
List of References 159

List of Tables

Table 1-1 Summary of the distinct PrP^{Sc} strains found in same and different animal species. 11
Table 2-1 List of general materials and reagents used..... 41
Table 2-2 List of Chinese Hamster Ovary (CHO) cells lines used 42
Table 2-3 List of materials and reagents used in cell and tissue culture..... 43
Table 2-4 List of muscarinic pharmacological ligands used 43
Table 2-5 List of primary antibodies used in Western blotting (WB) and immunocytochemistry (ICC) experiments 44
Table 2-6 List of secondary antibodies used in Western blotting and immunocytochemistry experiments 44
Table 2-7 List of materials and reagents used in for mass spectrometry sample preparation 45
Table 2-8 List of different GEMMs used..... 48
Table 3-1 Potency and efficacy values of muscarinic receptor ligands in Gq signalling. 67
Table 3-2 Maximum specific binding and affinity values of muscarinic receptor ligands in Gq signalling of primary neuronal cultures. 77
Table 3-3 Potency and efficacy values of muscarinic receptor ligands in Gq signalling of primary neuronal cultures..... 79
Table 4-1 Muscarinic expression and efficacy on the outer membrane of 6x Prion neuronal cultures after daily treatment of Oxotremorine-M for 7 days..... 109
Table 4-2 Muscarinic expression and efficacy on the plasma membrane and inside the cytoplasm of 6x Prion neuronal cultures after daily treatment of Oxotremorine-M for 7 days. 110
Table 4-3 Muscarinic expression and efficacy of M1-PD neuronal cultures after daily treatment of Oxotremorine-M for 7 days. 114

Table S-1 Protein names of the significantly different proteins in NBH control-treated neurons compared to uninfected neurons..... 154
Table S-2 Protein names of the significantly different proteins in RML prion-infected neurons compared to uninfected neurons..... 155
Table S-3 Protein names and functions of the 28 significantly upregulated proteins. 156

Table S-4 Protein names and functions of the 44 significantly downregulated proteins. 157

List of Figures

Figure 1-1 Diagrammatic representation of the mechanism in which prions and prionoids misfold, nucleate and fragmentate. 3
Figure 1-2 Sequence alignment of Bovine, Human and Mouse Prion protein. 6
Figure 1-3 Structure of the human PrP^C. 7
Figure 1-4 Diagrammatic representation of the different mechanisms involved in the release and uptake of prions and prionoids by cells..... 9
Figure 1-5 Diagram of the several strategies utilised to slow down and stop prion misfolding, propagation and diseased. 14
Figure 1-6 Diagram illustrating the major hallmarks of Alzheimer's Disease..... 20
Figure 1-7 Misfolded protein aggregate deposition and their respective CNS disorders..... 21
Figure 1-8 Diagrammatic representation of the human APP proteolytic pathways. 24
Figure 1-9 The six human tau isoforms found in the brain. 26
Figure 1-10 Downstream signalling pathways within the sub-family of muscarinic acetylcholine receptors. 27
Figure 1-11 Snake plots of the humanised and moused M1-HA mAChR. 32
Figure 1-12 Snake plots of the humanised and moused M1-DREADD mAChR..... 33
Figure 1-13 Snake plots of the moused M1-PD mAChR. 34
Figure 1-14 Chemical structures of different mAChR ligands. 35
Figure 3-1 Expression of the M1 mAChR in CHO cells..... 63
Figure 3-2 M1 mAChR expression in CHO cells..... 64
Figure 3-3 Inositol phosphate (IP1) accumulation concentration-response curves in CHO cells via Gq coupled pathways..... 66
Figure 3-4 Neuron development at DIV7 and DIV14..... 68
Figure 3-5 Expression of the M1 mAChR and total prion in Prion-KO and 6x prion protein primary neuronal cultures from GEMM..... 70
Figure 3-6 Expression of the M1 mAChR and total prion in M1-HA Wt, M1-KO and M1-DREADD-HA primary neuronal cultures from genetically engineered embryonic mice. 72
Figure 3-7 M1 mAChR and total prion expression in primary neuronal cultures.. 74
Figure 3-8 Muscarinic receptor expression levels across different primary neuronal cultures from different GEMMs. 76

Figure 3-9 Inositol phosphate (IP1) accumulation concentration-response curves in primary neuronal cultures via Gq coupled pathways. 78
Figure 4-1 Novel protocol for prion protein enrichment from mouse brains. 93
Figure 4-2 Prion protein enrichment from control and prion mouse brains..... 94
Figure 4-3 PrPSc deposition increases with higher concentrations of enriched substrate infections..... 96
Figure 4-4 Enriched PrP^{Sc} can infect both in Prion-KO and 6x Prion neuronal cultures, however, propagation can only be observed in 6x Prion cultures. 98
Figure 4-5 Infection with enriched prion from control mouse brains does not have any visible effect on 6x Prion neuronal cultures over a period of 7 days. 100
Figure 4-6 Infection with enriched prion from prion mouse brains does not have any visible effect on 6x Prion neuronal cultures over a period of 7 days. 101
Figure 4-7 Neuron PrP^{Sc} infection does not have an adverse impact on neuronal health. 102
Figure 4-8 Equal levels of PrPSc deposition were observed across M1-WT, M1-DREADD and M1-KO neuronal cultures. 104
Figure 4-9 Activation of muscarinic receptors does not change the course of infection and propagation across different muscarinic GEMM neuronal culture strains. 106
Figure 4-10 Expression and activation levels of muscarinic receptors on the plasma membrane of neuronal cultures decrease after daily treatment of Oxotremorine-M for 7 days. 108
Figure 4-11 Daily treatment of Oxotremorine-M for 7 days leads to the reduced expression of muscarinic receptors both in the outer membrane and cytoplasm of 6x Prion neurons. 110
Figure 4-12 Activation of the phospho-deficient M1 muscarinic receptor does not change the course of infection and propagation neuronal cultures..... 111
Figure 4-13 Expression and activation levels of muscarinic receptors on the plasma membrane and in the cytoplasm decrease in M1-PD neuronal cultures after daily treatment of Oxotremorine-M for 7 days. 113
Figure 5-1 Flow diagram outlining the procedure carried out for the proteomic study between uninfected (blue), NBH control-treated (yellow) and RML prion-infected (red) 6x Prion primary neuronal cultures. 126
Figure 5-2 Density plots and PCA of all samples from the three groups. 128

Figure 5-3 Heatmaps and significant protein changes between all three groups. 129
Figure 5-4 Upregulated and downregulated proteins by p-value in NBH control-treated vs uninfected neurons. 131
Figure 5-5 Upregulated and downregulated proteins by p-value in RML prion-infected vs uninfected neurons. 132
Figure 5-6 Upregulated and downregulated proteins by p-value in RML prion-infected vs NBH control-treated neurons. 133
Figure 5-7 Top 10 upregulated proteins. 135
Figure 5-8 Top 10 downregulated proteins..... 137
Figure 5-9 Upregulated proteins by p-value and log2fold. 138
Figure 5-10 STRING map of all differentially expressed proteins between RML prion-infected and NBH control-treated neurons. 146

Acknowledgement

I would like to start thanking my two supervisors, Professors Andrew Tobin and Graeme Milligan. I would like to thank you for the opportunity you gave me to perform my PhD in your labs, for all the mentoring and advice, as well as help and support throughout this whole process. Your help has been essential to guide me through this project and to obtain my PhD. I would also like to thank the postdocs in the lab, Gonzalo, Louis, Aisling, Natasja, Sara and Mario, who provided me with all their help and time, teaching me new techniques and troubleshooting all the problems encountered, as well as dealing with my loudness. I would also like to thank Colin for all the animal help, and for all the great conversations and laughs we had.

I want to thank everyone I met throughout my PhD, colleagues that became friends, that helped in the low moments and that celebrated the highs. I want to specially thank Niniola, Miriam and Eloise. The three of you have gotten me through this PhD, I could not have asked for three better people to go through this process with. You were always there in the lab to help with anything, put smiles in my face and joke around, and I hope this does not stop. Wandia and Yazzed, thanks for the great time we had together at the Davidson, it was a big shame not having you guys at the ARC. I would also like to thank the other PhD students and technicians in the lab, Kat, Abdul, Zhaoyang, Becca, Sarah, Jessica, Beth S., Luca, Elaine, Pietro, Laura, Mags and Beth D. for all the help and support.

I could not have done this without the help and support of my whole family, my mum, my dad, my grandma, uncle, aunt and cousins. You have always had my back and have always supported me to better myself. Mama, papa, moltes gracies als dos, aso no haguera segut posible sense vosatros.

Finally, I would like to give my biggest thanks to Emily and Innes. The two of you have made my PhD, cannot imagine this journey without the two of you. Em, you have always encouraged me, believed in me when I did not, helped me with everything and even proofreading this thesis. I will always be grateful to you for being there during this time and I cannot wait for our new adventure in Boston with our wee man.

Author’s Declaration

May 2024

“I declare that, except where explicit reference is made to the contribution of others, this thesis is the result of my own work and has not been submitted for any other degree at the University of Glasgow or any other institution.”

Jose Andres Alepuz Guillen

Definitions/Abbreviations

ABCA1	ATP binding cassette subfamily A member 1
ACh	Acetylcholine
ACTBL2	Actin-beta like 2 protein
ACTN4	Actinin alpha 4
AD	Alzheimer's Disease
AFAP1	Actin-associated filament protein 1
AGC	Automatic gain control
AICD	APP intracellular domain
ALS	Amyotrophic Lateral Sclerosis
ANOVA	Analysis of variance
AP2	Adaptor protein 2
ApoE	Apolipoprotein E
APP	Amyloid precursor protein
ASOs	Antisense oligonucleotides
BOLA1	BolA family member 1
BQCA	Benzyl quinolone carboxylic acid
BSA	Bovine serum albumin
BSE	Bovine Spongiform Encephalitis
cAMP	Cyclic adenosine monophosphate
CAV1	Caveolin 1
CC	Charged clusters
CCM2	CCM2 scaffold protein
ChAT	Choline acetyltransferase
CHO	Chinese hamster ovary
CJD	Creutzfeldt Jakob Disease
CNO	Clozapine-N-oxide
CNS	Central nervous system
COQ6	Coenzyme Q6, monooxygenase
CTF	C-terminal fragment
CWD	Chronic Wasting Disease
d.p.i.	days post infection
DAPI	4′,6-diamidino-2-phenylindole
DCTN3	Dynactin subunit 3

DIV	Days *in vitro*
DMSO	Dimethyl sulfoxide
DPBS	Dulbecco phosphate-buffered saline
DREADD	Designer receptor exclusively activated by designer drug
DYNLT3	Dynein light chain Tctex-type 3
ECL	Extracellular loop
ECM	Extracellular matrix
EDTA	Ethylenediaminetetraacetic acid
EEG	Electroencephalogram
ER	Endoplasmatic reticulum
ERG28	Ergosterol biosynthesis 28 homolog
ERK	Extracellular signal-regulated kinase
FAM169A	Family with sequence similarity 169 member A
FBS	Foetal bovine serum
FFI	Fatal familial insomnia
FMNL1	Formin like 1
FRET	Fluorescence resonance energy transfer
FTLD	Frontotemporal Lobe Dementia
FTMS	Fourier transform mass spectrometer
GDP	Guanosine diphosphate
GEMMs	Genetically engineered mouse models
GFAP	Glial fibrillary acidic protein
GNA11	Gα protein subunit 11
GPCRs	G protein-coupled receptors
GRKs	G protein-coupled receptor kinases
GSN	Gelsolin
GTP	Guanosine triphosphate
HA	Hemagglutinin
HAPLN1	Hyaluronan and proteoglycan link protein 1
HAPLN2	Hyaluronan and proteoglycan link protein 2
HBSS	Hank's Balanced Salt Solution
HEPES	4-(2-hydroxyethyl)-1-piperazineethanesulfonic acid
HPLC	High-performance liquid chromatography
HSPGs	Heparan sulphate proteoglycans
IAA	Iodoacetamide

ICC	Immunocytochemistry
ICL	Intracellular loop
IP1	Inositol-1-phosphate
IP3	Inositol triphosphate
ITGB6	Integrin subunit beta 6
KCTN2	Potassium sodium-associated channel subfamily T member 2
KIAA0319L	KIAA0319-like protein
LBs	Lewy bodies
LC-MS/MS	Liquid chromatography–tandem mass spectrometry
Limma	Linear Models for Microarray Data
LIMS1	LIM zinc finger containing domain 1
LSM2	LSM2 homolog, U6 small nuclear RNA and mRNA degradation associated
M1-PD	Phosphorylation-deficient M1 mAChR
mAChR	Muscarinic acetylcholine receptor
MAPK	Mitogen-activated protein kinases
MAPT	Microtubule-associated protein tau
MBP	Myelin basic protein
MCEE	Methylmalonyl-CoA epimerase
mEGFP	Monomeric enhanced green fluorescent protein
mGuR1	Metabotropic glutamate receptor 1
MPTP	1-methyl-4-phenyl-1,2,3,6-tetrahydropyridine
MRPS22	Mitochondrial ribosomal protein S22
MTs	Microtubules
NAA38	N-alpha-acetyltransferase 38
NAMs	Negative allosteric modulators
NBH	Normal brain homogenate
NDs	Neurodegenerative diseases
NDUFA10	NADH:ubiquinone oxidoreductase subunit A10
NDUFA5	NADH:ubiquinone oxidoreductase subunit A5
NFIA	Nuclear factor I A
NHLRC3	NHL repeat containing 3
NMR	Nuclear magnetic resonance
NMS	N-methyl scopolamine
NO	Nitric oxide

NSB	Non-specific binding
ORPI	Octapeptide repeat insertions
OTUD7A	OTU deubiquitinase 7A
Oxo	Oxotremorine M
PAMs	Positive allosteric modulators
PD	Parkinson's Disease
PDZRN3	PDZ domain containing ring finger 3
PFA	Paraformaldehyde
PHACTR1	Phosphatase and actin regulator 1
pK	Proteinase K
PMSF	Phenylmethylsulfonyl fluoride
PrP^{C}	Cellular prion
PrP^{Sc}	Scrapie prion
PrP^{Tot}	Total prion
QNB	3-quinuclidinyl benzilate
RGS13	Regulator of G protein 13
RHOG	Ras homolog family member G
RIPA	Radioimmunoprecipitation assay
RML	Rocky Mountain Laboratories
RND2	RHO family GTPase 2
RNF2	Ring finger protein 2
ROS	Reactive oxygen species
RT-QuIC	Real-time quake-inducing conversion
SDS	Sodium dodecyl sulphate
TBS	Tris buffered saline
TCAF1	TRPM8 channel associated factor 1
TCEP	Tris(2-carboxyethyl)phosphine
TEAB	Triethylammonium Bicarbonate
TFA	Trifluoracetic acid
TIAM2	TIAM Rac1 associated GEF 2
TM	Transmembrane
TNF	Tumour necrosis factor
TPT1	Translational controlled tumour protein 1
TTC1	Tetratricopeptide repeat domain 1
VMA21	Vacuolar ATPase assembly factor 21

VU846	VU0486846
w.p.i.	weeks post inoculation
WB	Western blot
Wt	Wild-type

Chapter 1 Introduction

1.1 Prions and protein misfolding diseases

1.1.1 Prion diseases

Prion diseases (or Transmissible Spongiform Encephalopathies) are a variety of fatal multifaceted neurodegenerative diseases (NDs), either genetic, acquired or spontaneous, caused by unique infectious pathogens called prions (Prusiner, 1998). These infectious agents arise from the conformational misfolding of the endogenous cellular prion protein (PrP^{C}), into the pathological, disease-causing scrapie prion protein (PrP^{Sc}) (Kovacs & Budka, 2008). The first human prion cases were described between 1921 and 1923 by Alfons Jakob, which he thought were similar to other cases reported by Hans Creutzfeldt in 1920 (Creutzfeldt, 1989; Jakob, 1989). Prion diseases were originally thought to be caused by "slow viruses", due to their transmissibility and prolonged incubation periods (Prusiner, 1998). It was Stanley Prusiner, who was able to isolate the scrapie agent, confirming the "slow virus" to be a misfolded protein, which he referred to as a "proteinaceous infectious particle", or a prion (Prusiner, 1998). Prion disease occurs when the pathological disease-causing PrP^{Sc} acts as a template for PrP^{C}, changing its conformation and structure from PrP^{C} into PrP^{Sc}. Misfolding is followed by the aggregation of the insoluble PrP^{Sc} molecules, forming oligomers, protofibrils and fibrils (Fig. 1-1). It is the propagation of these misfolded prion aggregates across the distinct regions of the brain which results in different prion diseases. Human prion diseases are characterised by their three distinct mechanisms for the disease to originate: genetic (familial), spontaneous (sporadic), and acquired (infectious or transmitted). Genetic occurring prion diseases include familial Creutzfeldt-Jakob Disease (CJD) and Fatal Familial Insomnia (FFI), as well as other *PRNP* gene (encoding prion protein) mutation related diseases. Sporadic CJD is an example of spontaneous prion disease, whilst variant CJD, iatrogenic CJD and Kuru are all acquired prion diseases. Prion diseases also occur in different animal species, including Bovine Spongiform Encephalopathy (BSE) in cattle, Scrapie in sheep and goat, and Chronic Wasting Disease (CWD) in deer and elk. Murine prion models also exist; however, these are not naturally occurring, and were created after the inoculation of brain homogenates from scrapie-diseased goats into the brain of a mouse (Chandler,

1961), which are currently used as terminal neurodegenerative disease mouse models.

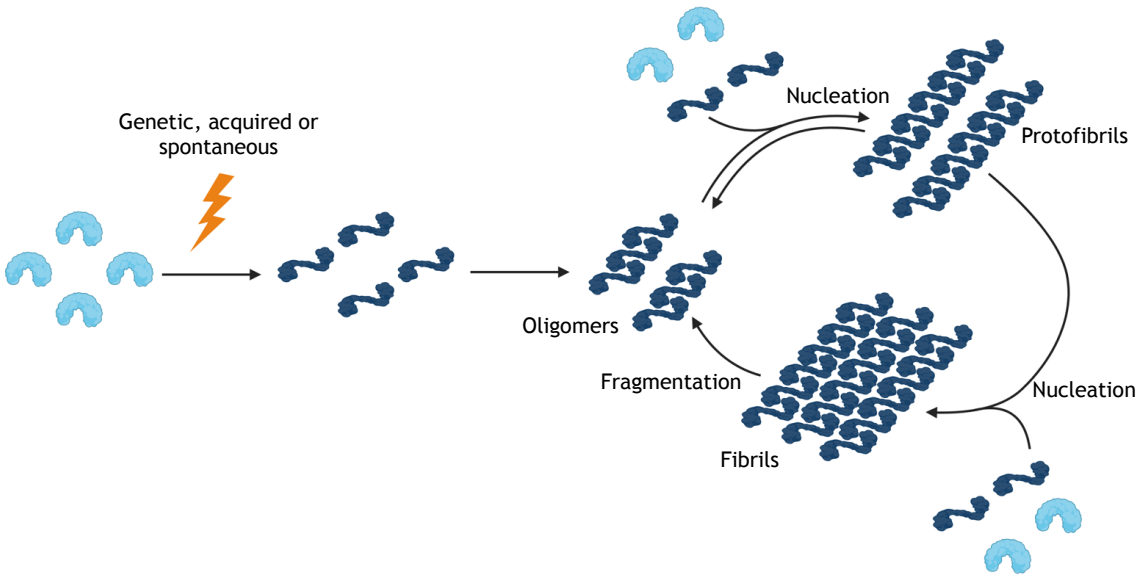

Figure 1-1 Diagrammatic representation of the mechanism in which prions and prionoids misfold, nucleate and fragmentate. (Adapted from Scheckel and Aguzzi, 2018).

Genetic prion diseases include familial CJD and FFI. Prion disease originating from *PRNP* mutations are mainly from missense mutations, however, stop codon mutations and octapeptide repeat insertion (OPRI) mutations can also occur (Lloyd et al., 2013). Familial CJD is the most common genetic prion disease, with more than 20 *PRNP* mutations behind the disease. Rapid progressive dementia with ataxia and other motor problems is the typical symptomology of familial CJD, with onsets occurring between the ages of 30 and 55 years (Geschwind, 2015). The E200K mutation is most common *PRNP* mutation resulting in familial CJD (Brown & Mastrianni, 2010), with it being the most common in European countries and the third most common amongst Chinese patients (Gambetti et al., 2003). In contrast, FFI is a very rare genetic disease, with a single point *PRNP* mutation (D178N with the cis codon 129M) (Geschwind, 2015). Within this mutation, distinctive pathological outcomes depending on the codon 129 polymorphism are observed, as patients with a cis methionine at codon 129 develop FFI whilst those with a cis valine present as familial CJD (McLean et al., 1997). Severe progressive insomnia is the main symptom in patients, with the development of dysautonomia (hyperpyrexia, tachycardia and hyperhidrosis) occurring in the late stage of

disease. FFI onset is typically between the ages of 45 and 50 years, with a life expectancy of about 18 months (Brown & Mastrianni, 2010).

The most common sporadic prion disease is sporadic CJD, with onset occurring between the ages of 55 and 75 years, and an average survival of 6 months since onset. The typical symptomology of sporadic CJD is a rapid progressive dementia, similar to familial CJD, as well as behaviour changes, ataxia, and at later stages, myoclonus (Puoti et al., 2012; Rabinovici et al., 2006). Recently, a novel form of sporadic CJD has been reported, referred to as variably protease-sensitive prionopathy, due to the rare protease-resistant PrP^{Sc} observed when samples are analysed on Western blot (Geschwind, 2015). Variably protease-sensitive prionopathy is similar to the original sporadic CJD in the symptomology presented by patients, however, onset occurs between the ages of 65 and 75 years, with life expectancy lasting from 18 to 40 months, rather than 6 months (Puoti et al., 2012).

Acquired forms of prion disease in humans are very rare and naturally declining. There are several forms of acquired prion disease that are either infected or transmitted. Variant CJD is the only form of human prion disease, to date, known to have been directly transmitted from animals to humans. It was first identified in the mid 1990s in the United Kingdom, where the consumption of cow meat exposed humans to BSE, which made a portion of these humans develop variant CJD (Brown & Mastrianni, 2010). The origin of BSE was pin-pointed to the consumption of scrapie contaminated sheep product by cattle, therefore resulting in the development of BSE. Very few cases of variant CJD have been reported since 2015, all being located in western European countries, the USA, Saudi Arabia, Japan and Taiwan. Symptoms present after onset in variant CJD patients include cognitive dysfunction, cerebellar dysfunction, dysesthesia and a range of involuntary movements, with an average life expectancy of around 15 months after onset. Another form of acquired prion disease is iatrogenic CJD, which consists of the iatrogenic human-to-human transmission of prion disease, including transmission through infected blood transfusions, electroencephalogram (EEG) depth electrodes, corneal transplants, and most commonly, transplants of human pituitary hormone and dura mater from diseases humans (Brown et al., 2006; Will, 2003). Human growth hormone injections have been the result of 226 cases of

iatrogenic CJD worldwide, with patients presenting with brainstem and cerebellar signs followed by cognitive dysfunction, with incubation periods ranging from 5 to 42 years (Abrams et al., 2011). Another 228 reported cases of iatrogenic CJD have been linked to dura mater transplants, showing very similar pathology to that of sporadic CJD, and an average survival of 12 years (Hamaguchi et al., 2013). Since the discovery of the origin of both human growth hormone and dura mater-related iatrogenic CJD cases in the 1990s, cases of this form of prion disease have drastically decreased (Brown & Mastrianni, 2010). However, due to the very long incubation periods, cases are still expected to rise from transplants which occurred during and before the 1990s. Finally, the last of the acquired prion disease forms is Kuru disease. This disease primarily impacts the Fore linguistic group of the Eastern Highlands in Papua New Guinea (Wadsworth, Joiner, Linehan, Asante, et al., 2008). Its transmission is very different to that of iatrogenic CJD. Instead of transplants, transfusions and injections as a cause of the disease, Kuru is characterised by transmission through the consumption of an individual with sporadic CJD (Alpers & Rail, 1971). This original transmission is responsible for the development of Kuru disease, and the propagation of the disease within the rest of the Fore linguistic group is due to the continued consumption of individuals which developed Kuru. The disease is divided into three reported stages, starting with ambulatory, then sedentary and the final tertiary stage, with progressive cerebellar ataxia being the most dominant clinical symptom (Collinge, 2005; Collinge et al., 2006). Studies have shown similarities within the molecular characteristics and transmission properties of variant CJD and Kuru disease (Wadsworth, Joiner, Linehan, Desbruslais, et al., 2008), linking the origin of Kuru to the consumption of an individual suffering from sporadic CJD.

1.1.2 The prion protein

The endogenous PrP^{C} is expressed in many tissues and is most abundantly expressed in the central nervous system (Koyama et al., 2022). This protein is highly conserved across mammals, including mouse and bovine, as well as with other vertebrates such as frogs and fish (Rivera-Milla et al., 2003; Strumbo et al., 2001). The sequence of the single copy gene is also highly conserved between mammalian species (Lysek et al., 2005), with the human sequence sharing 88.5% and 89% of its sequence with the bovine and murine prion proteins (Figure 1-2).

However, the chromosome location varies between species, with it being located in chromosome 20 in humans and in a homologous position in chromosome 2 for mice (Sparkes et al., 1986). Whilst the function of the protein has not yet been determined, its glycosylphosphatidylinositol (GPI)-anchor feature (Prusiner, 1998) has led to speculation of its potential role in signalling processes or cell adhesion. Studies with genetically engineered mouse models (GEMMs) lacking PrP^C after knocking out the *PRNP* gene have shown no phenotype changes compared to wild-type mice (Büeler et al., 1992; Manson et al., 1994), with the exception to being fully resistant to prion diseases (Büeler et al., 1993; Matamoros-Angles et al., 2022; Sailer et al., 1994).

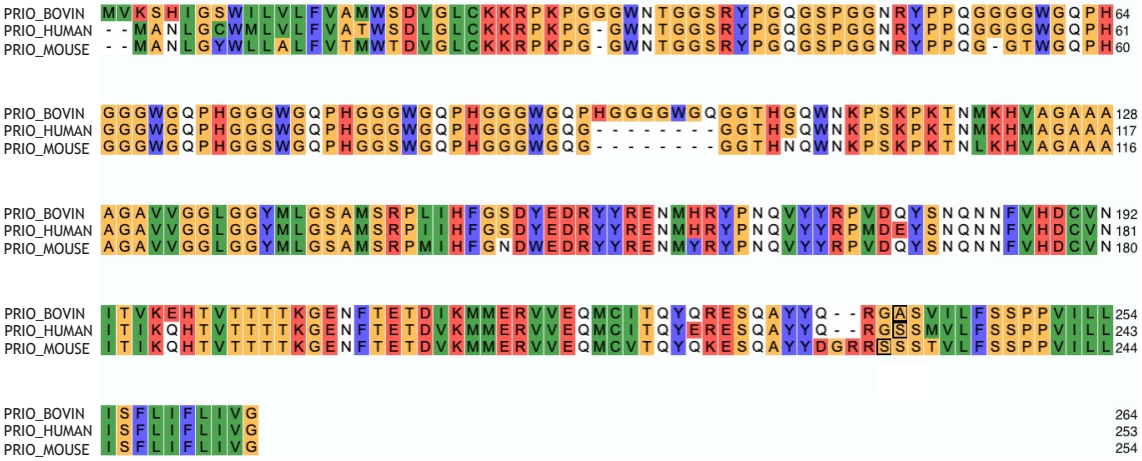

Figure 1-2 Sequence alignment of Bovine, Human and Mouse Prion protein. Amino acid sequences were obtained using UniProtKB and Clustal Omega was used for multiple sequence alignment.

The structure of the natively folded PrP^C was first observed in 1996 using nuclear magnetic resonance (NMR) spectroscopy, followed by a high-resolution three-dimensional crystal structure in 2001 (Knaus et al., 2001; Riek et al., 1996). The N-terminal half of the protein is composed of a flexible tail with a random-coil sequence (Shmerling et al., 1998), containing two positively charged clusters (CC) flanking an octapeptide repeat region (Figure 1-3A). Within the C-terminal domain of the protein, secondary structures can be observed (Figure 1-3B), including an antiparallel β-pleated sheet and three α-helices (3% and 45% of the protein content, respectively) (Riek et al., 1996). A disulphide bond can also be observed between C179 and C214 (Riek et al., 1996).

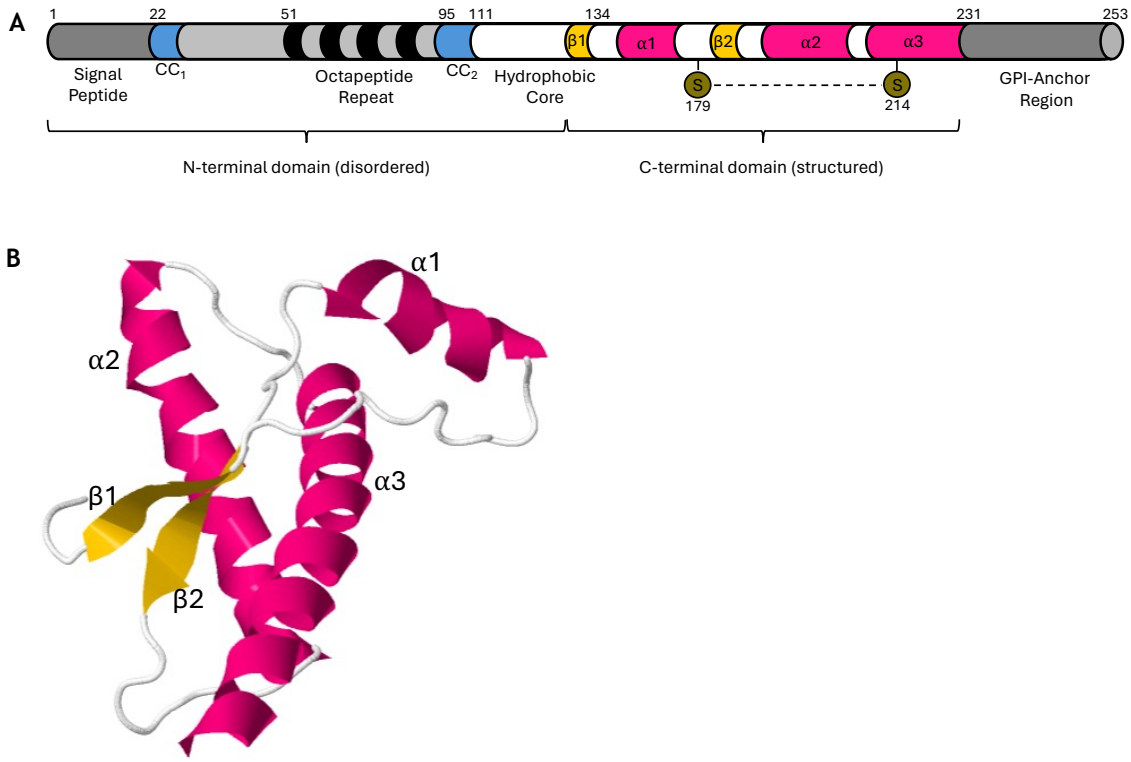

Figure 1-3 Structure of the human PrP^C. (A) Primary structure of PrP^C, including a secretory signal peptide residue at the N-terminus, charged clusters (CC), an octapeptide repeat, a hydrophobic core, a disulphide bridge between S179-S214 and a GPI-anchor region. The secondary structures are represented as β1/β2 (gold) for β-sheets and α1/α2/α3 (pink) for α-helices, respectively, within the structured C-terminal domain. The numbers represent the position of the respective amino acids. **(B)** Ribbon diagram of the human PrP^C (121-230), representing the structured C-terminal domain (PDB core 1QLZ). Antiparallel two-stranded β-sheets are shown in gold, α-helices are shown in pink and the connecting loops are displayed in white. Image was obtained from the RCSB Protein Data Bank.

Until recently, the structure of the misfolded disease-causing PrP^{Sc} had been poorly understood due to obstacles for X-ray crystallisation and NMR spectroscopy caused by misfolded prion aggregates. Some challenges included the different sized aggregates, glycosylation forms within the aggregates as well as their high molecular weights (Diaz-Espinoza & Soto, 2012). However, using Fourier-transform infrared (Pan et al., 1993) and circular dichroism spectroscopy (Safar et al., 1994), it was reported that PrP^{Sc} has a major shift in its secondary structures, with a β-sheet content of around 40% and 30% for α-helices, demonstrating a conformational change between PrP^C and PrP^{Sc}. Most recently, the use of cryo-EM has revealed the near-atomic resolution structures of several prion strains, demonstrating differences between the infectious forms and their synthetic fibrils, including larger ordered cores in the infectious strains (Artikis et al., 2022; Kraus et al., 2021).

1.1.3 Mechanisms of protein misfolding, aggregation and propagation

Under physiological conditions, the folding of the polypeptide chain leads to the formation of the stable and native state of the protein (Depta et al., 2022). However, problems encountered during this folding process result in misfolded proteins, leading to diseases known as proteinopathies or protein misfolding diseases. Protein misfolding occurs when polypeptides deviate from their precise folding mechanism (Hebert & Molinari, 2007). This can occur due to mistakes in post-translational modifications, protein environment alterations, oxidative stress and increased accumulation of degradation products (Pagel et al., 2015). Once misfolding occurs, the next step is protein aggregation, a very common pathophysiology seen in protein misfolding disease. The misfolded prions and prionoids (disease-causing proteins) accumulate throughout the brain causing disease.

The concept of protein aggregation was developed following the theory that prions and prionoids multiply in a nucleation and fragmentation manner. This means that misfolded protein oligomers incorporate endogenous correctly folded proteins, inducing their conformational change, becoming misfolded and growing in size (Scheckel & Aguzzi, 2018). *In vitro* studies have demonstrated that these oligomers would then aggregate, forming protofibrils and fibrils (Saborio et al., 2001), which through fragmentation would come back to their previous oligomeric form and continue with the misfolding of more endogenous protein (Fig. 1-1). Other studies have shown that partially folded or misfolded intermediates make assembly and aggregation between them easier as a result of their patches of surface hydrophobicity (Stefani, 2010), growing into oligomers, protofibrils and aggregated protein fibrils. *In vivo* studies with prion knock-out mice showed that the lack of PrP^{C} stopped PrP^{Sc} from propagating, as it did not have any endogenous PrP^{C} around to trigger its misfolding.

Misfolding and aggregation of prions and prionoids throughout the brain requires the propagation of these disease-causing misfolded proteins from one neuron to another, where the misfolded aggregates escape one neuron and are taken up by another (Figure 1-4). Several mechanisms of protein uptake have been discovered,

such as macropinocytosis, a mechanism followed by misfolded α-synuclein and tau (Frost et al., 2009; Holmes et al., 2013). Macropinocytosis is a type of fluid-phase uptake which produces vesicles ranging in size, with the ability to internalise large protein aggregates. For this process to occur, prions and prionoids first bind to heparan sulphate proteoglycans (HSPGs), glycolipid-anchored core proteins (Holmes et al., 2013). HSPGs have been shown to be required by misfolded prions (Horonchik et al., 2005) and Aβ (Kanekiyo et al., 2011) for infection of cultured cells, and by tau and α-synuclein (Holmes et al., 2013) for infection, seeding and propagation in both immortalised cells and primary neurons. These proteins are able to then escape these endocytosed vesicles after rupturing their membrane, allowing them to carry on with their propagation. Another uptake mechanism of prion and prionoids is the direct transfer of misfolded aggregates from one neuron to another through tunnelling nanotubules (Costanzo et al., 2013; Gousset et al., 2009). It has also been hypothesised that prions and prionoids could possibly enter neurons by receptor-mediated endocytosis, however, no conclusive evidence has been reported.

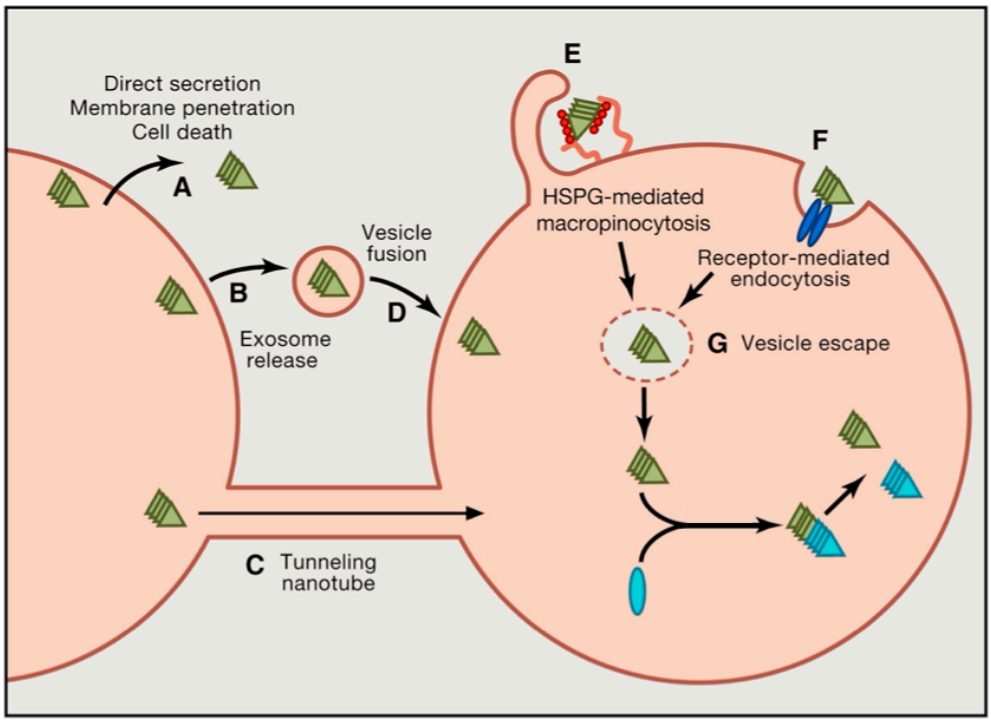

Figure 1-4 Diagrammatic representation of the different mechanisms involved in the release and uptake of prions and prionoids by cells. (A) Direct release into the extracellular space and **(B)** exosome release are two options through which prions can be released out of neurons. Prion scan be trafficked directly into neighbouring neurons via **(C)** tunnelling nanotubules, avoiding the extracellular space and an uptake mechanism. Prions released into the extracellular space undergo one of the several uptake process ranging from **(D)** vesicle fusion, **(E)** HSPGs-mediated macropinocytosis and **(F)** receptor-mediated endocytosis. Once internalised, prions undergo **(G)** vesicle escape, before acting as seeds for PrP^C monomers to undergo misfolding and aggregation. (Taken from Sanders et al. 2016).

Whilst mechanisms for protein uptake have been discovered and characterised, the mechanisms by which neurons release prions into the extracellular space are still undergoing investigation. Several mechanisms involving exosomes (Saman et al., 2012) and ectosomes (Dujardin et al., 2014) have been suggested as well as the secretion of soluble protein (Chai et al., 2012; Karch et al., 2012; Santa-Maria et al., 2012) and the escape into the extracellular space after membrane rupture due to cell death (Palmio et al., 2009).

1.1.4 Prion strains

Prion strains are described as infectious isolates that exhibit different disease phenotypes after transmission to identical hosts (Aguzzi et al., 2007). Distinct strains were first discovered in 1961 after different clinical phenotypes were observed in goats when infected with the same PrP^{Sc} agents (Pattison & Millson, 1961). At this time, the phenotypic outcome was thought to be species-specific (Chesebro, 1998). However, further studies showed that differences in PrP^{Sc} molecule conformation, with distinct biochemical properties, were behind the distinctive clinical phenotypes within the same and different animal species (Bessen et al., 1995; Morales et al., 2007; Tanaka et al., 2004). Over time, many PrP^{Sc} species from the same and different animal species have been reported, some of which are listed in Table 1-1. The main reason behind such a variety of strains within the same and different animal species is due to “strain mutation” occurring within an infected host (Bruce & Dickinson, 1987). The propagated strain’s biochemical and pathogenetic characteristics are altered, and no longer correspond to that of the inoculum, resulting in new strains being formed (Solforosi et al., 2013). Infection can occur within the same animal species or a different one, such as C-BSE, which originated from scrapie contamination of cattle feed, therefore crossing from sheep to bovine. In addition, bovine prion can cross-species to humans, as seen by the Mad Cow outbreak which occurred in the United Kingdom in the 1980s and 1990s. Although some prion strains have been reported and shown to cross the species barrier (Kurt & Sigurdson, 2016), there have been no reports of mouse prion transmission to humans. The lack of cross-species infection from mouse to human allows for the safe investigation into prion disease using mouse models.

STRAIN	SPECIES	ORIGIN	LOCALISATION
RML	Mouse	Derived from the Moredun Institute's sheep scrapie brain pool (Carroll et al., 2015)	Localised in neurons, astrocytes and microglia (Carroll et al., 2015)
22L	Mouse	Anchorless prions derived from Tg44 mice (Brandner & Jaunmuktane, 2017)	Localised in neurons, astrocytes and microglia (Carroll et al., 2015)
ME7	Mouse	Transmission of natural scrapie of Suffolk sheep directly into mice (Dickinson et al., 1968)	Always localised in neurons and neuropil (van Keulen et al., 2015)
263K	Hamster	Drowsy goat-derived PrP^{Sc}-infected in mice, followed by infection in rats, and finally into golden hamsters (Kimberlin & Walker, 1978)	Higher levels of PrP^{Sc} found in the thalamus, cortex and hippocampus of different hamster species (Meade-White et al., 2009)
21K slow	Sheep	Natural sheep scrapie isolated prions (Le Dur et al., 2017)	Habenula, thalamus and hypothalamus (Nakić et al., 2021)
CH1641	Sheep	Natural case of scrapie from Cheviot sheep (Foster & Dickinson, 1988)	Thalamus, cerebral cortex and hippocampus (Nakić et al., 2021)
C-BSE	Cattle	Scrapie contamination of cattle feed (Will, 2008)	Higher levels of PrP^{Sc} found in the cerebellum, midbrain, cranial and caudal medulla oblongata (Priemer et al., 2013)

Table 1-1 Summary of the distinct PrP^{Sc} strains found in same and different animal species. Table including a summary of the origin of each strain as well as the localisation of the misfolded prions in the brain of their respective species after infection.

Rocky Mountain Laboratory (RML), 22L and ME7 are the three strains most commonly used in mouse prion research. Structurally, RML and ME7 fibril morphology resemble each other, however they are distinguished by their helical

assemblies with different orientations of the N- and C-terminal lobes (Manka et al., 2023). The 22L strain shows an overall flatter monomer shape in comparison to RML, as well as having its characteristic anchorless conformational feature compared to the anchored RML and ME7 (Hoyt et al., 2022). It is these conformational differences between the different prion strains that leads to the different biochemical and phenotypic properties when infected into mice, some of which are listed in Table 1-1.

Studies have shown that these strongly neuroinvasive prions are able to diffuse through the whole brain and rapidly progress to terminal disease stage after intracerebral inoculation (Bett et al., 2012). Biochemical analysis of different brain regions has shown differences in PrP^{Sc} deposition across several brain regions. The thalamus is one of the first regions where scrapie deposition can be observed, with 22L showing higher levels of deposition compared to RML and ME7 at earlier stages (Carroll et al., 2016). Other studies have shown similar time-course propagation of RML in different brain regions during disease, with similar PrP^{Sc} deposition across cortex, hippocampus and striatum (Scarpa, 2022). Immunohistochemical images have shown the prion strains to have surprising host cell tropism, with different patterns of PrP^{Sc} localization in different brain cells across different brain regions. Within the thalamus, PrP^{Sc} localises in glial cells in RML and 22L infected mice, however, in the ME7 brains, PrP^{Sc} is only localised in neurons and neuropil (Carroll et al., 2015, 2016; van Keulen et al., 2015). In the hippocampus and cortex, 22L and ME7 prion infected brains showed the same cell distribution, while RML is found in neurons and neuropil (Bett et al., 2012). The different strains can also lead to different levels of astrocytic and microglia activation in different regions of the brain, showing different phenotypic outcomes. In previous studies (Makarava et al., 2021), 22L prion-infected mice have been shown to have high levels of astrocyte activation in the thalamus, cortex and hippocampus, in comparison to ME7, whilst RML showed distinct gliosis depending on the brain region being studied. Although it has been reported that the different strains lead to different biochemical and phenotypic properties, survival studies have shown a similar disease time-course across all three strains, reaching terminal stage at similar time-points (Bett et al., 2012).

1.1.5 Therapeutic targets for prion diseases

Over the years, different strategies have been adopted in the design and development of anti-prion drugs (Figure 1-5). Inhibiting the conversion of PrP^{C} to PrP^{Sc} and clearing the levels of PrP^{Sc} have been the main research focus behind the therapeutics for prion disease, including the use of polyanions and small-molecules (Giles et al., 2017). Some examples of anti-prion compounds are Congo red, quinacrine and LD7. Congo red was one of the first compounds used as an anti-prion drug, with the ability to bind to purified prions, to inhibit the replication of prions in cell cultures and to increase survival of prion diseased hamsters when inoculated peripherally (Caughey & Race, 1992; Levey et al., 1995; Prusiner et al., 1983). Quinacrine, a widely used antimalarial drug, was identified as a potential anti-prion compound, with the ability to cross the blood brain barrier (BBB) and exhibit a high potency for the inhibition of prion conversion in neuroblastoma cell lines (Doh-ura et al., 2000). In contrast to *in vitro* data, when quinacrine was examined in several *in vivo* studies (Barret et al., 2003; Doh-ura et al., 2000) and clinical trials (Geschwind et al., 2013; Haïk et al., 2004), no significant difference in survival extension was observed due to the restricted inflow of quinacrine through the BBB (Ahn et al., 2012). LD7 is one of the latest compounds showing great potential to reduce levels of proteinase K resistant PrP^{Sc} in *in vitro* studies using ScN2a cells, PrP^{Sc} infected N2a cells (Imberdis et al., 2016). However, in contrast to Congo red, surface plasmon resonance has shown that PrP^{C} is not the molecular target of LD7, demonstrating that the indirect targeting of LD7 leads to the reduction of PrP^{Sc} accumulation in prion infected neuroblastoma cells (Mercer & Harris, 2019). Although this strategy targets the conversion and clearance of PrP^{Sc}, some disadvantages have risen from the design of drugs following this approach, the most important one being strain specificity. Various anti-prion drugs have been shown to be strain-specific, inhibiting the conversion of certain prion strains and not others, therefore limiting their potential for the overall spectrum of prion diseases (Giles et al., 2015; L. Sim, 2012).

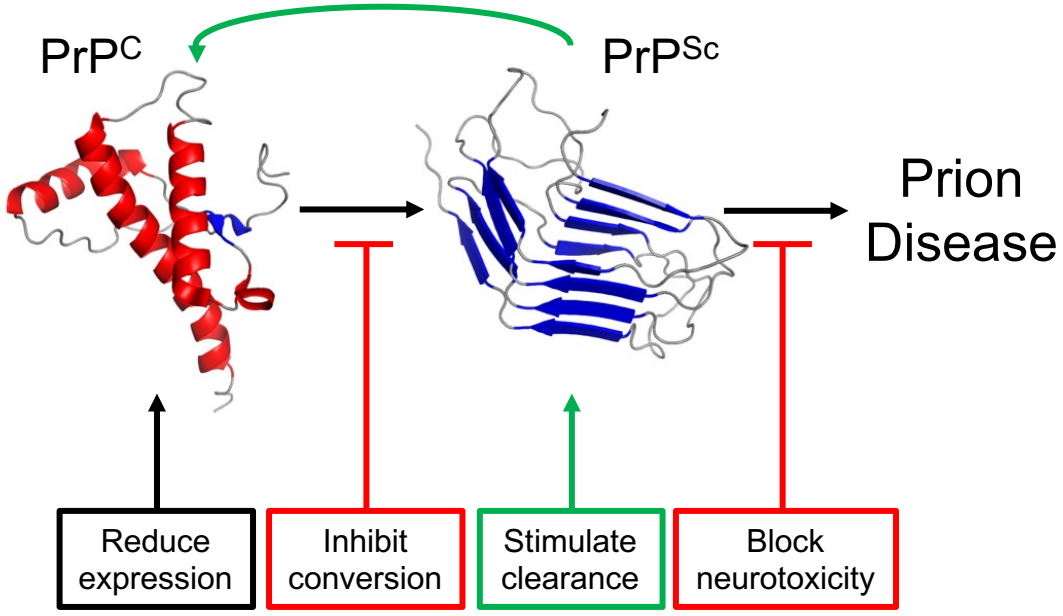

Figure 1-5 Diagram of the several strategies utilised to slow down and stop prion misfolding, propagation and diseased. (Adapted from Krance et al. (2020).

Another therapeutic strategy has focused on decreasing the levels of *PRNP* gene expression and therefore reducing the expression of PrP^{C}. Antisense oligonucleotides (ASOs) are the latest advancement in the prion disease field and are small sequences of single-stranded DNA-like molecules which lower the levels of specific target proteins (Dhuri et al., 2020). These molecules are already in ongoing clinical trials for other NDs such as Alzheimer's Disease (AD), Parkinson's Disease (PD) and Amyotrophic Lateral Sclerosis (ALS), and have shown great potential in *in vivo* studies to degrade prion mRNA and extend survival in prion diseased mice (Mothe & Brander, 2020; Raymond et al., 2019; Vallabh et al., 2020).

A different therapeutic approach for prion disease is the design of compounds to block the neurotoxicity caused by the PrP^{Sc} accumulation in the brain. High levels of PrP^{Sc} in the brain lead to neurotoxic outcomes, including synaptic and dendritic dysfunction and loss, astrogliosis, and neuronal death (Soto & Satani, 2011). Targeting the symptomatic stages has led to the discovery of key proteins involved in the neurotoxic pathways of prion diseases. One of these key players is p38 mitogen-activated protein kinases (MAPK), which is involved in the response to all cell stress stimuli (Han et al., 2020). *In vitro* studies of p38 MAPK inhibition and genetic suppression have shown to prevent PrP^{Sc} induced neurotoxic consequences, therefore making MAPKs potential targets for blocking the

neurotoxicity consequences of prion disease (Astolfi et al., 2020). With such a wide range of strategies to tackle prion disease at different points in its disease course, further research is needed in the development of drugs that can directly and/or indirectly target the prion protein or other proteins to slow the progression of this neurodegenerative disease.

1.1.6 Protein misfolding Diseases

The majority of NDs are characterised by the same mechanism of misfolding, aggregation and oligomerisation of different neuronal proteins such as prion diseases, making these proteins prime therapeutic targets. Examples of these NDs characterised by this pathology are AD, PD, Frontotemporal lobar degeneration (FTLD) and ALS (Chaudhuri & Paul, 2006; Halliday & Mallucci, 2015; Zhang et al., 2018). These protein misfolding diseases are the result of genetic, acquired or spontaneous gain of toxic activity or loss of normal function after the misfolding and aggregation of insoluble proteins (Bayer, 2015; Marsh, 2019). AD's two main neuropathological hallmarks are the cerebral aggregation and spread of amyloid-beta (Aβ) and hyperphosphorylated tau (Nelson et al., 2012). Tau aggregates can also be found in different NDs such as Pick's disease, corticobasal degeneration and progressive supranuclear palsy (Ballatore et al., 2007; Kertesz & Munoz, 2004). PD neurodegeneration comprises of the accumulation of α-synuclein, whilst ALS shows the deposition and inclusion of TAR DNA-binding protein 43 (TDP-43) in motor neurons and glia (McAlary et al., 2020). In FTLD patients, the majority of cases show accumulation of either misfolded tau or TDP-43. Not only does protein misfolding characterise NDs, but it is also responsible for many p53-mediated cancers. In both NDs and cancers, the conformational and structural changes suffered by misfolded proteins leads to aggregated masses, resulting in cellular toxicity and death.

1.1.6.1 Parkinson's disease

PD is the second most common neurodegenerative disease after AD (Rizek et al., 2016). It is characterised by the accumulation and aggregation of the pathological form of the α-synuclein protein leading to the formation of Lewy bodies (LBs), as well as the progressive loss of dopaminergic neurons in the substantia nigra

projecting to the striatum (Xu & Pu, 2016). This dopamine deficiency in the striatum is responsible for the classic motor symptoms that PD patients exhibit, including postural instability, muscular rigidity, resting tremor and bradykinesia (Politis et al., 2010). These motor symptoms tend to manifest after a decrease of 60-80% of dopamine within the striatum region of the brain (Dauer & Przedborski, 2003; Lee et al., 1996). Before these symptoms are present, Parkinson's patients experience non-motor symptoms including cognitive deficits, sleep disturbances and mood disorders such as anxiety and depression (Kalia & Lang, 2015; Schapira et al., 2017). Post-mortem studies of Parkinson's patients' brains show the presence of LBs within the substantia nigra, directly correlating the presence of α-synuclein with the main affected brain regions in PD (Beach et al., 2009). Neuroinflammation also plays a key role in PD, with the accumulation and aggregation of α-synuclein triggering the activation of glia, enhancing neuroinflammation followed by the degeneration of striatal neurons (Orr et al., 2005). The progression of neuronal cell death in PD has been shown to be modulated by several inflammatory mediators derived from glial cells such as reactive oxygen species (ROS), nitric oxide (NO) and tumour necrosis factor α (TNF)-α (Glass et al., 2010; Hirsch & Hunot, 2009). These data suggest a synergistic role played by α-synuclein pathology and inflammation in PD.

To date, several medications have been developed for PD to target the dopaminergic system, including levodopa, an immediate precursor to dopamine (Hauser, 2009), dopamine agonists to activate dopaminergic receptors (Brooks, 2000), as well as catechol-O-methyl transferase inhibitors and monoamine oxidase aldehyde dehydrogenase B inhibitors to inhibit the breakdown of levodopa and dopamine (Kaakkola, 2000; Riederer & Laux, 2011). These drugs increase the levels of dopamine within the brain, attempting to counteract the reduced levels of dopamine endogenously present due to the reduction of neurons within the substantia nigra and striatum. Alternative drugs are also used to alleviate other symptoms of Parkinson's such as hallucinations and depression (Powell et al., 2022; Veazey et al., 2005). However, none of these treatments impact the progression of disease. Instead, they target symptoms and improve the patient´s quality of life, highlighting the requirement for treatments that can impact disease progression.

1.1.6.2 Amyotrophic lateral sclerosis

ALS is the most prevalent motor neuron degenerative disease, characterised by the progressive degeneration and loss of lower and upper motor neurons (Wijesekera & Leigh, 2009). ALS symptoms vary between patients, as well as the location of the initial symptoms suffered by each individual (Morris, 2015; Swinnen & Robberecht, 2014). Disease site onset is key in the severity and progression of motor neuron loss, with individual patients experiencing different symptoms and progression times, however, progressive muscle weakness and paralysis are experienced by all ALS patients (Ravits et al., 2007; Ravits & La Spada, 2009). Braak et al. (2013) have shown that ALS pathology can be divided into four progressive stages depending on where TDP-43 inclusions are observed in the brain. Initial stages of disease show the presence of phosphorylated TDP-43 aggregates in projection neurons of the agranular motor cortex and somatosensory neurons of the brain stem and spinal cord, followed by inclusions found in the prefrontal cortex, striatum and basal ganglia and finally progressing to the temporal lobe, entorhinal cortex and hippocampus (Braak et al., 2013). The same studies have shown that progression of TDP-43 inclusions in the brain correlates with motor neuron degeneration and loss.

1.1.6.3 Frontotemporal lobar degeneration

Another neurodegenerative disease caused by TDP-43 is FTLD. This progressive fatal neurodegenerative disease is characterised by a decline in behaviour and language skills linked to frontal and anterior temporal lobe degeneration in the brain (Rabinovici & Miller, 2010). TDP-43 inclusions, as well as tau aggregates, are clear histopathological hallmarks of FTLD (Mackenzie et al., 2011; Shi et al., 2005) and are mainly localised in neurons and glia of the affected regions. Whilst TDP-43 mutations are rarely associated with FTLD cases, around 50% of all FTLD cases show TDP-43 inclusions within neurons and glia in the frontal and anterior temporal lobes (Cairns et al., 2007; Weihl et al., 2008). The accumulation and propagation pattern of phosphorylated TDP-43 aggregates is similar to the observed with ALS, as well as being divided into four stages. In FTLD, initial inclusions are located in the basal and neocortex regions of the prefrontal neocortex and in the amygdala, followed by propagation to the striatum and

regions of the thalamus, motor cortex and spinal cord, and finally spreading to the visual centre of the brain, the occipital neocortex (Geser et al., 2009; Mackenzie et al., 2011). Again, propagation of these aggregates is linked to the behaviour and language deficits seen in patients, as inclusions affect the prefrontal cortex, hippocampus and amygdala from early stages of the disease (McKhann et al., 2001; Mioshi et al., 2010)

1.1.6.4 Alzheimer's disease

AD is the most common type of neurodegenerative disease, with a non-stop increase in cases due to the growing elderly population worldwide (Qiu et al., 2009). This fatal form of dementia is characterised by changes in behaviour, progressive cognitive impairment and memory loss (Halliday & Mallucci, 2015). AD's two main neuropathological hallmarks are the cerebral aggregation and spreading of Aβ and hyperphosphorylated tau (Nelson et al., 2012), making AD a protein misfolding disease. These two pathological features are linked by a cascade of events. The aggregation of Aβ peptides lead to the formation of senile plaques, whose accumulation is thought to induce the formation of neurofibrillary tangles (NFTs) composed of the hyperphosphorylated tau (Iqbal et al., 2016; Kametani & Hasegawa, 2018; Mandelkow et al., 1995). The misfolding and aggregation of tau, leading to the formation of NFTs, is likely to be associated with both loss-of-function and gain of neurotoxic properties (Winklhofer et al., 2008). The aggregation and spreading of NFTs, characterised by the 'Braak Stages', has been linked to the progression of AD and its symptoms, starting with memory deficits, followed by progressive cognitive decline and neuropsychiatric symptoms (Nelson et al., 2012; Okamura & Yanai, 2017). Post mortem studies have revealed that in individuals with AD, pathological tau will first appear in the locus coeruleus and transentorhinal cortex, further spreading to the entorhinal and hippocampal regions and reaching the basal temporal cortex and the insular cortex (Braak & Braak, 1991). However, the spreading of Aβ pathology in AD patients follows a distinct pattern to that of tau pathology. Aβ plaques start emerging at the orbitofrontal neocortex and basal temporal cortex, spreading towards the neocortex and finally reaching the midbrain, hippocampus, cerebellum and brainstem (Hampel et al., 2021). The spreading patterns of these two proteins have been further confirmed from post mortem studies with PET imaging,

visualising the propagation of both Aβ and tau pathology in the same patients (Insel et al., 2020).

In addition to the misfolding, aggregation and propagation of Aβ and tau, AD is also characterised by other neuropathological hallmarks. These include neuroinflammation, oxidative stress, mitochondrial and autophagy dysfunction (Figure 1-6), as well as cholinergic hypofunction which will be discussed later. Neuroinflammation is a key hallmark in AD and the majority of NDs, with increased reactive astrocytes and astrogliosis occurring in the brain (Wang et al., 2015). Several studies have identified inflammatory cytokines, such as interleukin-6 and TNF-α (Lourenco et al., 2013; Wang et al., 2015), and toxic mediators being released by glia as the cause of synaptic dysfunction (Ferreira et al., 2014), tau phosphorylation (Quintanilla et al., 2004) and learning deficits (Burton & Johnson, 2012; Heyser et al., 1997).

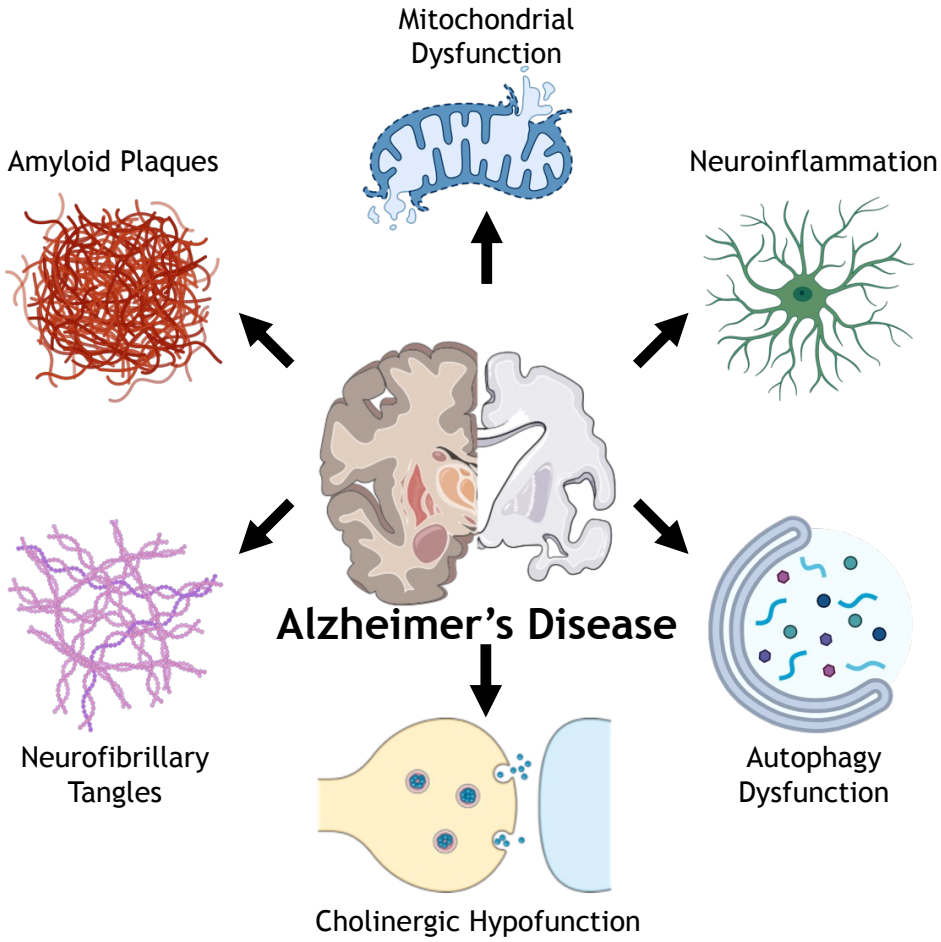

Figure 1-6 Diagram illustrating the major hallmarks of Alzheimer's Disease. Accumulation of Aβ plaques and hyperphosphorylated tau neurofibrillary tangles, neuroinflammation, cholinergic hypofunction, and both mitochondrial and autophagy dysfunction are identified hallmarks in AD patients' brains (Adapted from Dhapola et al. 2021).

Current AD treatments consist of drugs such as donepezil and rivastigmine, acetylcholinesterase inhibitors with the aim to reduce the amounts of ACh being broken down to compensate for the lower quantities released into the synaptic cleft. Although not having a disease modifying effect, these drugs help patients with counteracting early symptoms of AD. Lately, new drugs are being researched in order to reduce both Aβ and tau aggregation, with some showing great promise in animal models (Iqbal et al., 2018). However, to date, none of these drugs have been shown to be effective in human patients with AD (Selkoe & Hardy, 2016).

1.2 Prion-like proteins

As mentioned before, many NDs, such prion disease, are characterised by loss of function or toxicity gain due to protein misfolding and aggregation. As a consequence of the similarities in the misfolding mechanism between the prion protein and the other neurodegenerative disease-causing proteins, these are referred to as prion-like proteins. Some examples of prion-like proteins include α-synuclein, TDP43, Aβ and tau (Figure 1-7).

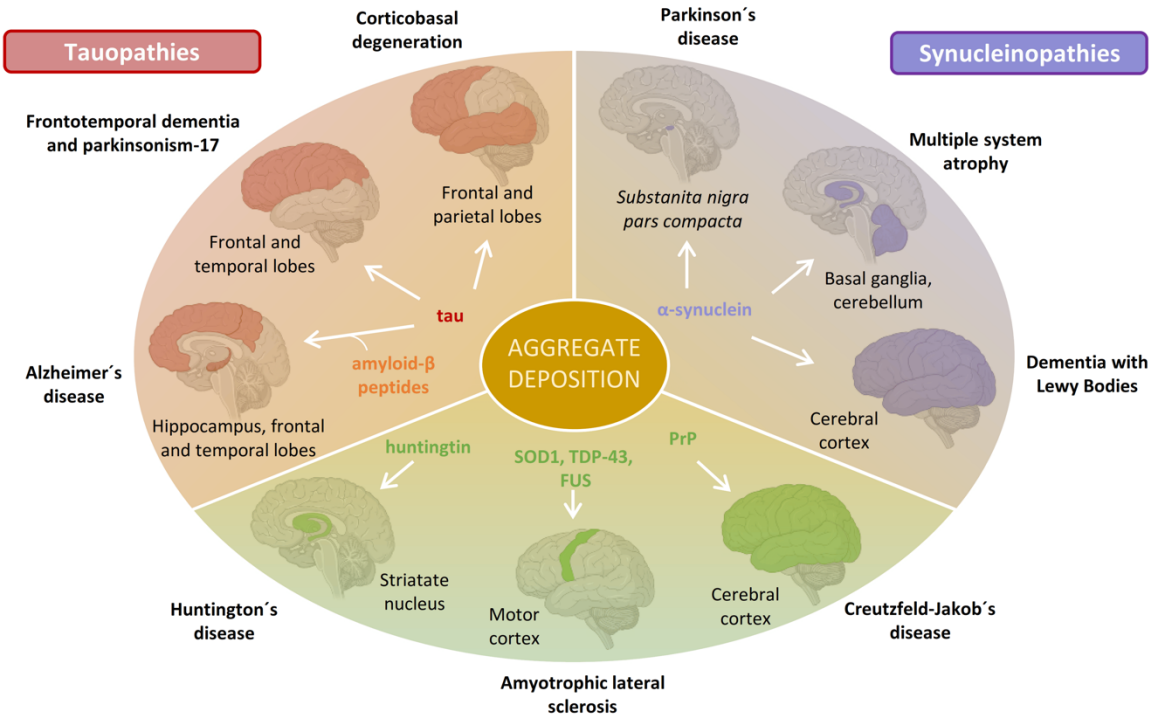

Figure 1-7 Misfolded protein aggregate deposition and their respective CNS disorders. Diagram showing the different prion-like proteins and their respective NDs depending on their solo or group aggregation as well as localisation within the brain regions. (Taken from Franco et al. 2021).

1.2.1 α-synuclein

α-synuclein is a presynaptic neuronal protein directly responsible for PD through a toxic gain-of-function (Oikawa et al., 2016). Studies investigating genetic mutations in the α-synuclein protein have revealed a direct link between α-synuclein and PD (Polymeropoulos et al., 1997). Multiple system atrophy and Dementia with Lewy Bodies are two other disorders cause by α-synuclein with different characteristics to PD. α-synuclein is a member of the synuclein protein

family, comprised of two more proteins called β- and γ-synuclein (George, 2002). All proteins within this family are neuronal proteins which localise in presynaptic terminals under physiological conditions. α-synuclein is abundantly expressed within the CNS, consisting of around 1% of the total cytosolic proteins expressed in the brain (Stefanis, 2012). Whilst immunohistochemical analysis has demonstrated its high expression in presynaptic terminals of neurons, α-synuclein is expressed at a much lower level in glial cells (Xilouri et al., 2022). The function of α-synuclein is unknown, however, it has been proposed that this protein may play a role in membrane-associated functions at presynaptic terminals, for example, as a negative regulator of dopamine neurotransmission (Abeliovich et al., 2000). α-synuclein has the ability to produce β-sheet structures under certain circumstances, leading to the aggregation of α-synuclein molecules, forming amyloid-like fibrils (Conway et al., 2000). These fibrils end up forming large abnormal clumps of β-sheeted α-synuclein molecules called LBs (Butler et al., 2022). LBs are considered a histological hallmark for PD, with neuronal loss occurring in the same sites as where LBs are found in diseased patients with PD (Wakabayashi et al., 2007). Post-mortem studies have validated that the prion-like pathogenic form of α-synuclein, structured with β-sheets, is the pathogenesis driver of PD (Butler et al., 2022).

1.2.2 TDP-43

TDP-43 is a highly conserved nuclear RNA/DNA-binding protein involved in RNA processing regulation, including mRNA stabilization, transcriptional regulation and alternative splicing (Nakielny & Dreyfuss, 1997; Scotter et al., 2015). In physiological conditions, TDP-43 is expressed within the nucleus of cells, playing an essential role in mRNA stabilization (Geuens et al., 2016; Neumann et al., 2006). However, under pathological conditions, TDP-43 experiences post-translational modifications such as hyperphosphorylation, ubiquitination and cleavage, resulting in pathological inclusions (Hasegawa et al., 2008; Neumann et al., 2006; Zhang et al., 2009). It is the accumulation of these TDP-43 aggregates in the CNS that are commonly observed in several NDs, such as ALS, FTLD and AD (Huang et al., 2020; Jo et al., 2020; Scotter et al., 2015). TDP-43 follows the same mechanism of seed-dependant propagation by cell-to-cell protein transfer as other prion-like proteins (McAlary et al., 2019). Mutations within the protein and

aberrant post-translational modifications are responsible for the irreverseble aggregation of TDP inclusions. Many mutations in the TDP-43 protein have been directly linked to both ALS and FTLD, the majority found within the C-terminal domain (Johnson et al., 2009). Examples of these mutations include A315T, which increases protein aggregation and leads to neurotoxicity (Guo et al., 2011), as well as G294V, G294A, and G295S, which have been shown to form twisted amyloid-like fibres (Sun et al., 2014). Out of all ALS cases, only 10% are genetic, with around 4% of the familial ALS cases originating from mutations within the gene encoding for the TDP-43 protein, *TARDBP* (Jo et al., 2020). In addition, more than 90% of all ALS patients show TDP-43 pathology, demonstrating the role of TDP-43 mutations and post-translational modifications in this motor neuron disease.

1.2.3 Amyloid-β and tau

Aβ and tau are the two proteins responsible for AD, the most prevalent dementia disease worldwide. Whilst they are both present in AD patients' brains, their role and time-frame of aggregation and propagation throughout the disease differs between them.

Aβ is a product derived from the normal cellular metabolism of the amyloid precursor protein (APP) (O'Brien & Wong, 2011), a 695-770 amino acid protein involved in the regulation of synaptic formation and repair, iron export and anterograde neuronal transport (Duce et al., 2010; Priller et al., 2006; Turner et al., 2003). APP is comprised of a long extracellular glycosylated N-terminus, a single membrane-spanning domain and a short cytoplasmic C-terminal domain (O'Brien & Wong, 2011). It is synthesised in the endoplasmatic reticulum (ER), and the Golgi apparatus is responsible for its maturation and transport to the plasma membrane. APP proteolysis can result in a disease-associated amyloidogenic product, Aβ, or in a normal non-amyloidogenic product, P3. The products formed depend on the secretases involved in the cleavage process of APP (Figure 1-8). Aβ is generated by the successive cleavage of APP by β- and γ-secretase (Haass et al., 1992), making a 37 to 49 amino acid residue peptide, after which it remains associated to the plasma membrane, or it's released into the extracellular space. Depending on the site of cleavage of γ-secretase, distinct sized Aβ monomers are formed, with the 40-amino acid (Aβ20) and 42-amino acid (Aβ42) fragments being

the final forms (Olsson et al., 2014; Takami et al., 2009). Amyloidogenic Aβ tends to aggregate in the extracellular matrix, forming fibrils and growing into different sized oligomers (Jin et al., 2016). These aggregates are formed in different sizes, including oligomers, protofibrils and amyloid fibrils. Oligomers are known to be soluble and capable of spreading throughout the brain, whilst the larger amyloid fibrils end up forming the plaques seen in post-mortem examinations of AD patients (Mondal et al., 2023). These larger amyloid plaques are formed by the aggregation of Aβ fragments, which according to the "amyloid cascade hypothesis" (Karran et al., 2011), are responsible for the neurotoxic and dementia pathologies observed in AD patients (Hensley et al., 1994).

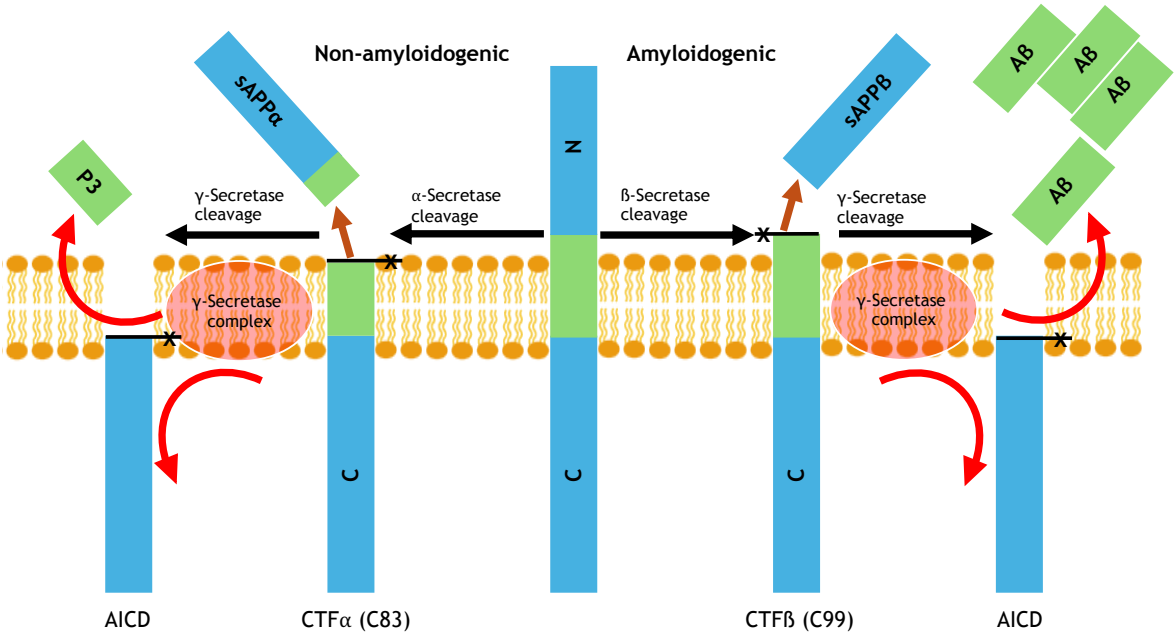

Figure 1-8 Diagrammatic representation of the human APP proteolytic pathways. The non-amyloidogenic pathway consists of APP being firstly processed by α-secretase, cleaving APP within the Aβ domain, generating the N-terminal fragment sAPPα and the membrane-tethered C-terminal fragment (CTF) α. CTFα is finally cleaved by γ-secretase, forming the APP intracellular domain (AICD) and the extracellular P3 fragment. The amyloidogenic pathways consists of the sequential cleavage of APP by β-secretase and γ-secretase. The first cleavage by β-secretase cleaves APP into the N-terminal sAPPß and the membrane-tethered CTFβ. CTFβ is subsequently cleaved by γ-secretases into the APP intracellular domain (AICD) and the extracellular Aβ. (Adapted from Chen et al., 2017).

As for tau, its main function is to stabilise microtubules (MTs) in neurons. Under physiological conditions, tau is in a regulated dynamic equilibrium both on and off the MTs, having a central role in maintaining effective axonal transport (Ballatore et al., 2007). Additionally, other functions linked to tau involve tau phosphorylation, which allow neurons to escape from acute apoptotic death by

stabilising β-catenin (H. L. Li et al., 2007). In humans, a total of six isoforms of the tau protein are expressed, after the alternative splicing of the microtubule-associated protein tau (*MAPT*) gene located on chromosome 17q21 (Goedert et al., 1989). The alternative splicing of exons 2 and 3 results in variants containing either zero (0), one (1N) or two (2N) inserts at the N-terminal domain (Figure 1-9). On top of the alternative splicing, the presence or absence of exon 10 results in tau proteins with either three (3R) or four (4R) C-terminus microtubule-binding domains (Panda et al., 2003). The combination of all leads to six different isoforms, which include 3R0N, 3R1N, 3R2N, 4R0N, 4R1N, and 4R2N. The variation from an equal ratio of tau protein expression between 3R and 4R tau in humans, has been linked with several genetic diseases (Poorkaj et al., 1998; Spillantini et al., 1998). Phosphorylation is a key post-translational modification of the tau protein with around 2 to 3 residues on tau proteins in the brain being phosphorylated. In contrast, this is significantly increased to around 9 or 10 phosphate molecules in AD (Iqbal et al., 1986). This hyperphosphorylation of tau is linked to a disruption in the equilibrium of tau phosphates and tau kinases. Tau hyperphosphorylation lowers the affinity of tau for microtubules and increases its resistance to ubiquitin-proteosome degradation (Iqbal et al., 2009). In the long run, tau hyperphosphorylation results in the generation and aggregation of NFTs (Alonso et al., 2001, 2004). The accumulation of hyperphosphorylated NFTs propagating through the brain following the 'Braak Stages' (Braak & Braak, 1991), dictates the progressive symptoms suffered by AD patients.

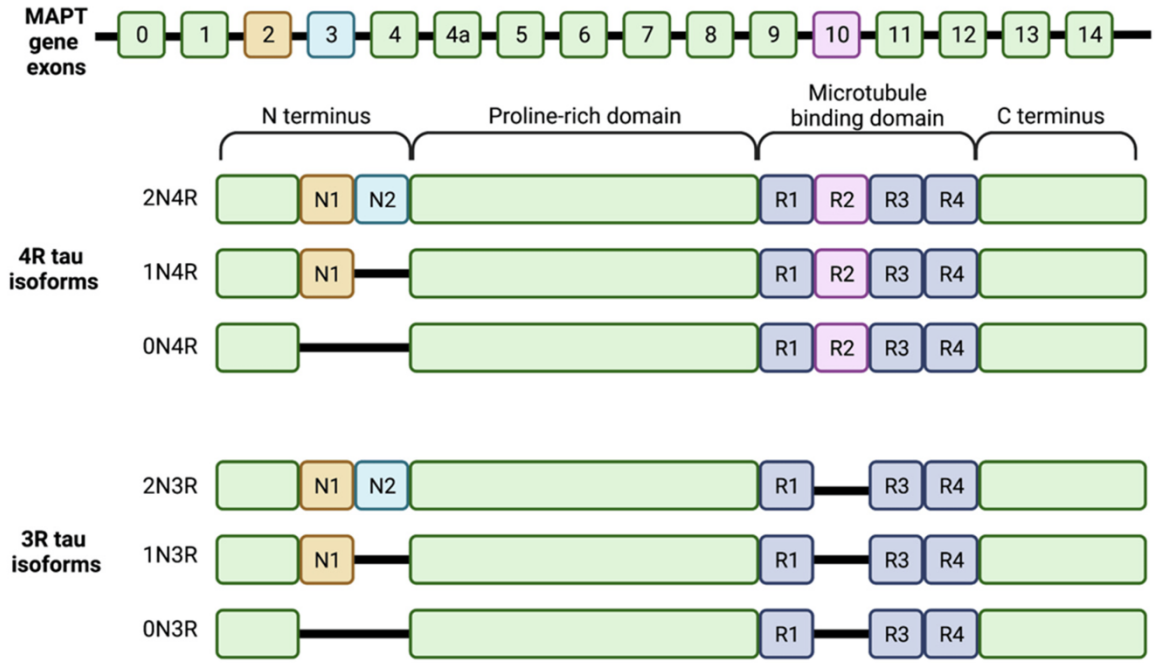

Figure 1-9 The six human tau isoforms found in the brain. (Taken from Holper et al. 2022).

1.3 Muscarinic acetylcholine receptors

1.3.1 Overview of muscarinic acetylcholine receptors

G Protein-Coupled Receptors (GPCRs) are the largest superfamily of human membrane-bound receptors, including five different classes and over 800 different members (Hauser et al., 2017). They are formed of 7 membrane-spanning α-helical domains, separated by alternating extracellular and intracellular loops (Rosenbaum et al., 2009). These receptors are expressed everywhere in the human body, including all vital organs, in which they signal a vast range of responses to different stimuli. One of these families is the muscarinic acetylcholine receptor (mAChR) family and it is a member of the cholinergic system. This family comprises of 5 different receptors (M1 to M5) and are all activated by the endogenous orthosteric neurotransmitter acetylcholine (ACh) (Fig. 1-10) The five subtypes are highly conserved, sharing between 64 and 82% sequence identity, mainly due to the high degree of similarity in their transmembrane regions (Maeda et al., 2019). They can be divided by coupling specificity and their signalling pathways, with the M1, M3 and M5 mAChRs coupling to $G\alpha_{q/11}$-proteins, and the M2 and M4 coupling to $G\alpha_{i/o}$-proteins. After activation by ACh occurs, protein

kinases negatively regulate the receptors by serine-threonine phosphorylation of the receptor's C-terminus and the binding of arrestin. The binding of arrestin to the receptor triggers the desensitisation and internalisation of muscarinic receptors, inhibiting the G-proteins from binding to the receptors and therefore stopping the G-protein signalling cascade. Arrestin binding also leads to the recruitment and regulation of the activation of an extracellular signal-regulated kinase (ERK) cascade (Jung et al., 2017).

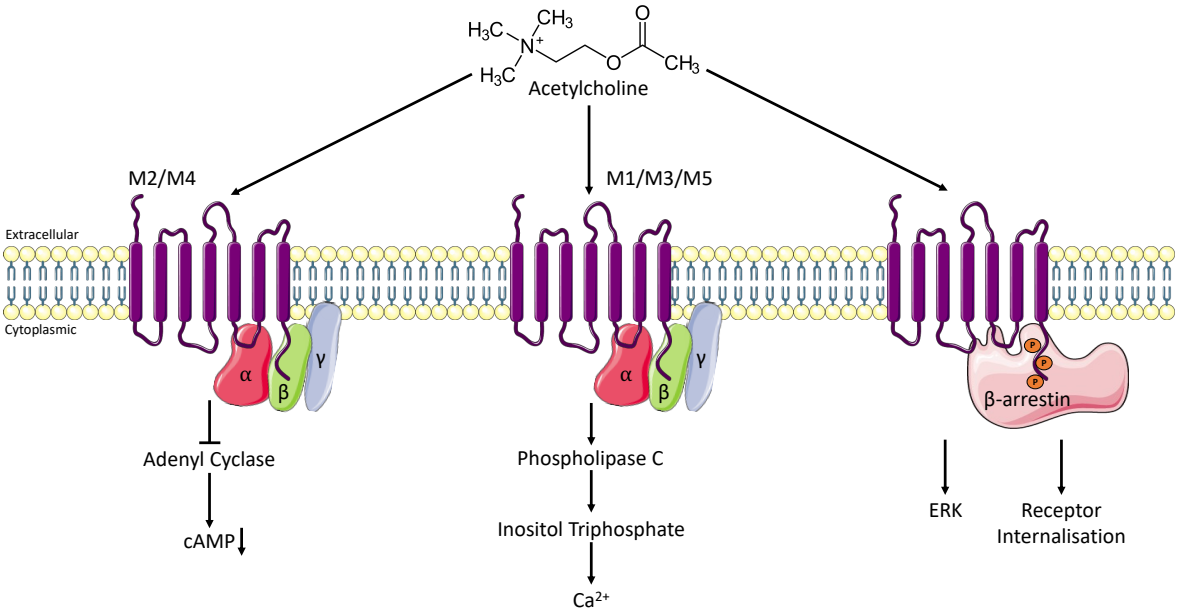

Figure 1-10 Downstream signalling pathways within the sub-family of muscarinic acetylcholine receptors. (Adapted from Dwomoh, Tejeda, et al. (2022).

These receptors can also be categorised by tissue distribution, playing essential roles in many physiological systems such as the central nervous system (CNS), gastrointestinal tract and lungs (Lebois et al., 2018). The M2 mAChR is predominantly expressed in the cardiovascular system and is involved in the control of the heart rate (Krejčí & Tuček, 2002; Nenasheva et al., 2013), whilst the M1, M3 and M5 mAChRs are expressed in the vasculature, suggesting roles in blood pressure regulation (Gericke et al., 2011; Krejčí & Tuček, 2002). The M4 mAChR has been shown to regulate potassium currents in atrial cardiomyocytes, as well as being widely expressed in the brain, specifically in the corpus striatum, putamen and co-expressed with dopamine receptors in striatal projection neurons (Klawonn et al., 2018). However, out of all 5 receptors, the M1 mAChR is the most abundantly expressed in the CNS, especially in the hippocampus and cerebral cortex (Bradley et al., 2017). This receptor is located postsynaptically in neuronal

cells, in both excitatory glutamatergic neurons (Levey, 1996), as well as in inhibitory GABAergic synapses within cholinergic terminals (Takács et al., 2018). The M1 mAChRs expressed within cholinergic synapses (Scarr, 2012), which form part of the muscarinic cholinergic system, have a primary role in learning and memory processes (Hasselmo & Sarter, 2011). The M1 mAChR has been shown to regulate particular memory processes such as episodic memory, spatial working memory and acquisition, retention and consolidation (Nathan et al., 2013). Extensive research into this system has suggested that AD and schizophrenia patients have an impaired cholinergic system through muscarinic receptors (Scarpa et al., 2020). Therefore, as the M1 mAChR is the most abundant in the brain, it makes it a clear target for NDs such as AD and prion disease.

1.3.2 Muscarinic receptor signalling

The downstream signalling of a muscarinic receptor is dependent on the receptor itself. GPCR signalling consists of both G-protein dependent and G-protein independent signalling pathways. Not only do the same receptors signal through several pathways, but activation of the receptor with different ligands can lead to bias signalling with preference to one or more pathways.

Receptor activation by stimulus or ligand binding results in conformational changes, leading to the exchange of guanosine diphosphate (GDP) for guanosine triphosphate (GTP) induced by guanine nucleotide-exchange factors (GEFs) (Neves et al., 2002). This conformational change results in the uncoupling of the GTP-bound $G\alpha$ and $G\beta\gamma$ subunits (Janetopoulos et al., 2001; Oldham & Hamm, 2008). For muscarinic receptors, this triggers the disassociated G protein subunits to transduce the signal to produce intracellular second messengers. M1, M3 and M5 $G\alpha_{q/11}$-signalling mAChRs lead to the production of inositol triphosphate (IP3) and increases the levels of Ca^{2+} (Hulme et al., 1990; Ilyaskina et al., 2018), whilst M2 and M4 $G\alpha_{i/o}$-signalling mAChRs result in decreased concentrations of intracellular cyclic adenosine monophosphate (cAMP) (Hulme et al., 2003). Signalling is then terminated by the Ras-like GTPases domain of the $G\alpha$ subunit, hydrolysing GTP to GDP, and triggering the recoupling of the $G\alpha$ and $G\beta\gamma$ subunits back to the receptor (Mann et al., 2016).

Receptor phosphorylation also terminates GPCR signalling after ligand activation. Multiple serine and threonine residues within intracellular loop (ICL) 3 and the C-terminal tail are phosphorylated by GPCR kinases (GRKs) (Tobin, 2008). Phosphorylation of these intracellular domains increases the affinity for arrestins to bind to the receptors (Carman & Benovic, 1998). Arrestin coupling to the receptor is the end of G protein-dependent signalling (signalling desensitisation), as it induces the steric hindrance displacement of G proteins (Shukla et al., 2013; Staus et al., 2020). Through the interaction with clathrin and adaptor protein 2 (AP2), arrestins act as scaffolds leading to receptor endocytosis/internalisation (Goodman et al., 1996). Arrestins can also result in G protein-independent signalling by activating signalling partners such as MAPK (Jiménez & Montiel, 2005). Recently, phosphorylation-deficient cell lines and GEMMs have been designed to further investigate the importance of phosphorylation in muscarinic signalling and disease (Bradley et al., 2020; Scarpa et al., 2021).

1.3.3 M1 muscarinic acetylcholine receptor

Muscarinic receptor expression in humans is mainly comprised of the M1 mAChR receptor, constituting around 50% of total muscarinic expression (Levey, 1993). It is significantly expressed within the CNS, salivary glands and sympathetic ganglia (Levey, 1993). Within the brain, the hippocampus and cortex represent the two main regions with the majority of M1 mAChR expression, having a key role in cognition, specifically learning and memory (Hasselmo & Sarter, 2011; Volpicelli & Levey, 2004). The M1 mAChR accounts for 60% of all muscarinic receptors expressed in the brain, demonstrating its higher levels of expression in comparison to other muscarinics. As mentioned before, the M1 mAChR belongs to a very conserved family of GPCRs, with very similar orthosteric pockets, lying within the 3-, 5- and 7-transmembrane (TM) domains (Hulme et al., 2003; Lebon et al., 2009; Wess, 1993). This high conserved orthosteric pocket has been thoroughly characterised with high-resolution X-ray crystallography (Thal et al., 2016). It is in the intracellular and extracellular domains where differences can be observed between the different muscarinic receptors. These differences include a large extracellular vestibule, a dynamic structure found in muscarinic receptors, containing M1 specific residues which contributes to the allosteric binding pocket and its higher specificity (Hollingsworth et al., 2019).

Single-particle cryo-EM has recently allowed to obtain the structure of the M1 mAChR bound to iperoxo, a potent muscarinic agonist, forming a complex with the heterotrimeric $G\alpha_{11}$ protein (Maeda et al., 2019). By obtaining this structure complex and comparing it to the inactive receptor bound to tiotropium, an inverse agonist, it has allowed the activation mechanism of the M1 mAChR to be determined (Thal et al., 2016). Activation of the M1 mAChR results in the outer displacement of the TM6, moving closer to the extracellular loop (ECL) 2 and contracting the extracellular vestibule, a movement of the TM5 towards the TM6 and a small rotation of the helix. The conformational changes observed in the active structure compared to the inactive, allows the C-terminal helix of the $G\alpha$ subunit to engage with the TM5 in core of the M1 mAChR (Maeda et al., 2019), initiating G-protein dependent downstream signalling.

1.3.4 M1 mAChR in neurodegenerative diseases

The cholinergic system has a major role in cognitive function and cortical plasticity, with ACh as its main neurotransmitter activating mAChRs and nicotinic receptors. Disruption of this system has been linked with memory deficits and cognitive disturbances, symptoms observed in many NDs such as AD (Schliebs & Arendt, 2006). Specifically, presynaptic cholinergic hypofunction has been identified as another neuropathological hallmark of AD, with loss of cortex and hippocampal cholinergic innervation (Giacobini & Becker, 2007). Further research led to the 'cholinergic hypothesis', postulating that the activation and maintenance of the cholinergic system can reverse the effects of cholinergic hypofunction and restore cognitive impairment (Fisher, 2012). Acetylcholinesterase inhibitors are still currently being used for AD patients, providing important treatment and ameliorating symptoms during early stages of disease. However, these specific drugs are not disease modifying and do not stop disease progression, requiring further investigation of the cholinergic system and different targets. As mentioned above, mAChRs are involved in different signalling pathways including the modulation of neuronal excitability, synaptic plasticity, cognitive function and feedback regulation of ACh release. Recently, some studies have shown that in both prion diseased mouse brains and human AD brains, the expression of M1 mAChRs was unchanged (Bradley et al., 2017). Not only does the disease not change the expression of M1 mAChRs, but its activation has shown the

potential to alter AD hallmarks, reducing both the levels of plaques (Fisher et al., 2003) and NFTs (Forlenza et al., 2000). These studies identify the M1 mAChR as a major potential target in reversing both the effects of AD and the disease itself.

More selective approaches are now being proposed to reverse symptoms of AD, particularly cholinergic hypofunction, using selective M1 mAChR ligands which can act to increase receptor activation and reduce precognitive effects (Wess et al., 2007). The use of M1 positive allosteric modulators (PAMs) in prion animal models has also shown an attenuation of memory deficits, a slowing down of neurodegeneration, and with this, a disease-modifying effect (Bradley et al., 2017). This data highlights the muscarinic receptors as a possible target due to their potential involvement in the mechanism of misfolded protein infectivity and propagation.

1.3.5 Engineered M1 mAChR versions

In the pharmacology field, tags and mutations have been introduced within GPCR sequences to facilitate their study, both *in vitro* and *in vivo*. These tools have already been generated and used for the M1 mAChR, to easily track the receptor and improve our understanding of its physiological function. They also allow to investigate selective activation of the receptors and to understand the bias signalling of the receptor and its ligands.

Tags such as hemagglutinin (HA) tags are commonly used to track the receptor, with the HA-epitope sequence (YPYDVPDYA) added at the end of the C-terminal of the receptor (Bradley et al., 2020). These tags have been incorporated to both the human and mouse M1 mAChR sequences and are used in both *in vitro* and *in vivo* (Figure 1-11). The use of these tags has allowed for a more detailed characterisation and localisation of the M1 mAChR receptor in the brain.

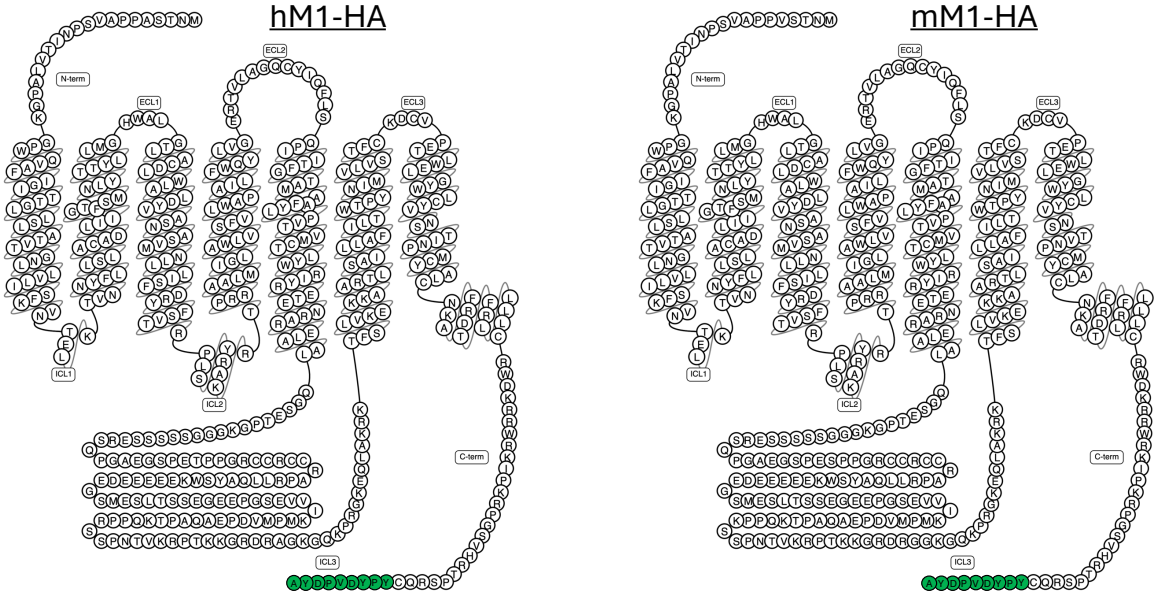

Figure 1-11 Snake plots of the humanised and moused M1-HA mAChR. Sequence diagrams of the human and mouse M1 mAChR combined with the sequence of an HA-tag at the end of the C-terminus tail. Original M1 mAChR sequences were obtained from the GPCR database (GPCRdb.org).

Another pharmacological tool is the use of the Designer Receptor Exclusively Activated by Designer Drug (DREADD) technology (Armbruster et al., 2007). This tool introduces a two-point mutation within the orthosteric pocket of the M1 mAChR (Y106C, A196C), preventing the binding of its natural ligand acetylcholine (Figure 1-12). Instead, synthetic designer drug, clozapine-N-oxide (CNO), is used to activate the M1-DREADD receptor, leading to its downstream signalling. This tool allows the study of receptor families with the same natural ligand and very conserved orthosteric pockets, allowing the selective deactivation of the receptor in the presence of the endogenous ligand and therefore acting as a knock-out. However, when treating this same receptor with the synthetic ligand, specific activation of this receptor is achieved (Armbruster et al., 2007). In the case of the M1-DREADD receptor, this permits the further investigation of its specific role and 'druggability' of the receptor (Bradley et al., 2020). Studies using the M1-DREADD receptor identified phenotypes in the M1-KO mice, such as anxiety and hyperactivity. However, the treatment with CNO corrects these phenotypes, indicating the role and regulation of the M1 mAChR in anxiety and locomotion (Bradley et al., 2020).

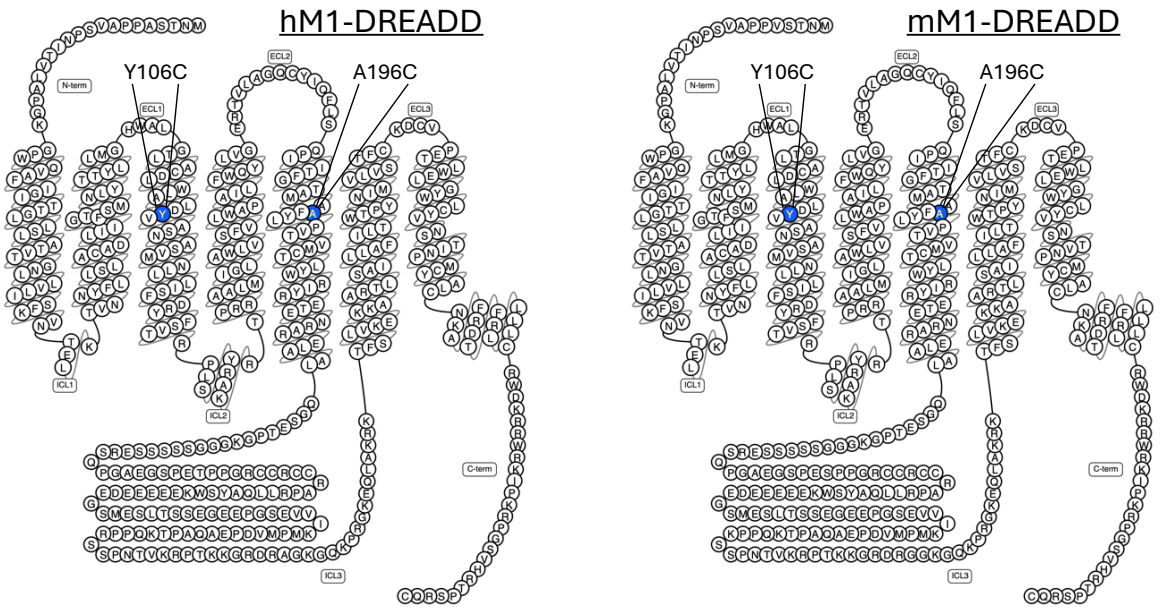

Figure 1-12 Snake plots of the humanised and moused M1-DREADD mAChR. Sequence diagrams of the human and mouse M1 mAChR with a two-point mutation withing the 3rd and 5th intracellular domains, making them DREADD receptors. Original M1 mAChR sequences were obtained from the GPCR database (GPCRdb.org).

In addition, investigation of signalling bias in GPCRs can be performed by mutating the serine phosphorylation sites within the intracellular domain regions of the receptor sequence. When these mutations are introduced within the 3rd intracellular loop and the C-terminal tail of the M1 mAChR, it permits the normal coupling of $G_{q/11}$ and their downstream signalling pathways. However, this significantly reduces the ability of the receptor to recruit arrestins after agonist treatment, leading to a deficit in internalisation of the receptor (Bradley et al., 2020) and creating a phosphorylation-deficient M1 mAChR (M1-PD) (Figure 1-13). *In vivo* studies using mice expressing the M1-PD receptor demonstrated higher anxiolytic responses of M1-PD mice compared to wild-type, which highlights the role of M1 mAChR phosphorylation in positive anxiety regulation. Locomotion tests revealed that M1-PD mice have similar locomotor behaviour to wild-type mice, suggesting that this behaviour is not dependent on receptor phosphorylation. These studies (Bradley et al., 2020), reveal that different behaviours and phenotypes are regulated by different signalling pathways of the same receptor, demonstrating 'bias signalling' within the M1 mAChR.

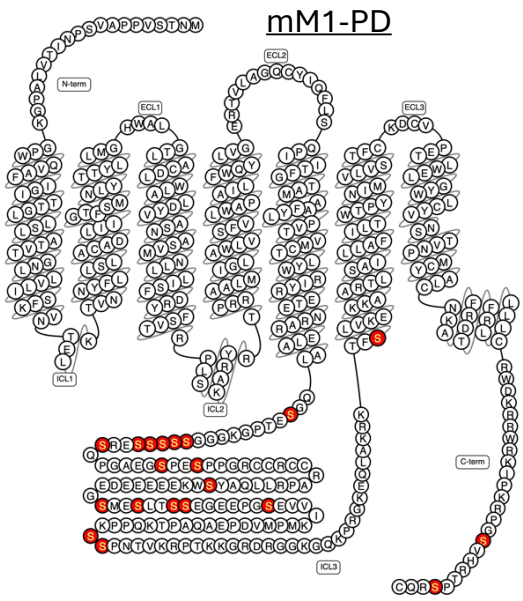

Figure 1-13 Snake plots of the moused M1-PD mAChR. Sequence diagram of the mouse M1 mAChR in which all identified phosphorylation sites and potential phosphorylation serine residues have been identified and mutated. Original M1 mAChR sequence were obtained from the GPCR database (GPCRdb.org).

As described above, these pharmacological tools have previously been used to characterise the M1 mAChR both *in vivo* and *in vitro* to understand the function of the receptor. In this study, they will be employed to further understand the role of the M1 mAChR in misfolded protein infection and propagation in primary neuronal cultures.

1.3.6 mAChR ligands

Affinity and efficacy define the pharmacological parameters of ligands. Affinity describes the strength of the interaction between individual ligands and their binding site. The efficacy of a ligand represents its ability to trigger receptor response, such as activating downstream signalling pathways. A key component to the pharmacology of a ligand is its interaction with the receptor, and therefore, ligands can be divided into different types depending on their binding site, referred to as orthosteric, allosteric or bitopic ligands. Orthosteric ligands bind to the site of the natural endogenous ligand, and in the case of muscarinics, the binding site of ACh. Allosteric ligands bind to a topologically distinct site from the orthosteric pocket. Finally, bitopic ligands have the ability to bind to both the orthosteric and allosteric sites of the same receptor (Valant et al., 2012).

Within the orthosteric ligands, affinity, efficacy and potency parameters dictate the subtypes of the receptor (Nussinov & Tsai, 2012). They are divided into full, partial or inverse agonists and neutral antagonists orthosteric ligands (Berg & Clarke, 2018). Full agonists display full activation of the downstream signalling pathway they activate, whilst partial agonists produce partial stimulation, therefore inducing partial response of the signal. Neutral antagonists compete with other agonists; however, they do not affect the basal signal induced. Finally, inverse agonists inhibit basal and constitutive activity of the receptor, resulting in receptor inactivity and no downstream signalling. Examples of these ligands include: ACh, the natural endogenous orthosteric ligand for muscarinic receptors, which activates all sub-types; Oxotremorine-M (Oxo), a full muscarinic agonist, with the ability to bind to all 5 muscarinic receptor sub-types; CNO (Armbruster et al., 2007), a synthetic ligand designed to bind to the orthosteric pockets of DREADD mutated receptors and HTL9936 (Brown et al., 2021), a partial agonist selective for the M1 and M4 mAChR (Figure 1-14).

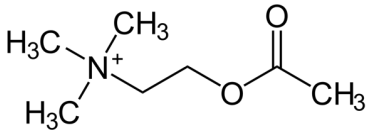

Acetylcholine
(endogenous muscarinic neurotransmitter)

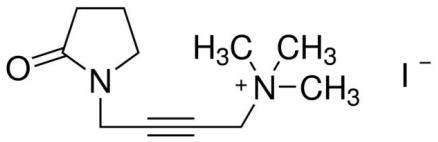

Oxotremorine-M
(muscarinic receptor agonist)

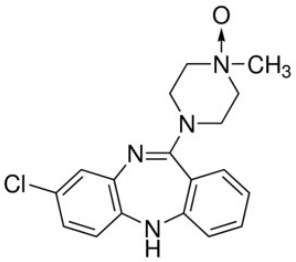

Clozapine-N-Oxide
(synthetic agonist to DREADD receptors)

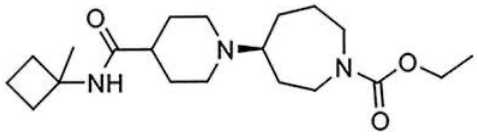

HTL9936
(M1 & M4 muscarinic partial agonist)

Figure 1-14 Chemical structures of different mAChR ligands. Structures of several muscarinic receptor agonists, including the endogenous neurotransmitter, acetylcholine, a full agonist, oxotremorine-M, a synthetic ligand designed to activate DREADD receptors, clozapine-N-oxide, and a partial M1 and M4-selective ligand, HTL9936.

On the contrary, allosteric ligands are more complicated to fully define due to the variations in the active state adopted by the receptor when interacting with ligand(s) and G proteins (Stallaert et al., 2011). These ligands can be divided into allosteric agonists, neutral allosteric antagonists, PAMs and negative allosteric modulators (NAMs). Allosteric agonists display full downstream signalling whilst allosteric antagonists inhibit all signalling. PAMS enhance the signal induced by orthosteric ligands, whilst NAMs reduce the signal generated by the orthosteric ligand (Christopoulos, 2014). Each subgroup of allosteric ligands displays distinct 'signalling bias', preferentially activating one downstream pathway over another (Luttrell & Kenakin, 2011). As allosteric ligands target a different site to the orthosteric site, more selective ligands can be developed to target specific subclasses of the muscarinic receptors (Bradley et al., 2017). An example of such allosteric ligands is VU0486846 (VU846), a next-generation M1 mAChR-selective PAM (Dwomoh, Rossi, et al., 2022).

1.3.7 M1 mAChR ligands in neurodegenerative diseases

Lately, the pharmacological manipulation of the M1 muscarinic receptor has been thought to be the key to positive therapeutic effects in different NDs (Thomas et al., 2008). Studies investigating M1 mAChR orthosteric agonists and antagonists have reported few selective receptor molecules. Orthosteric agonists such as Xanomeline, a M1/M4 selective partial agonist, have shown positive antipsychotic results in Alzheimer's and schizophrenia trials. However, this results in several side effects such as salivation, nausea, vomiting and diarrhea, which are all linked to the peripheral expression of the receptor (Bodick et al., 1997). More recently, PAMs, ligands which bind to topographically distinct sites to the orthosteric site, have been investigated to potentiate the activation of the M1 mAChR with the same levels of endogenous acetylcholine present (Christopoulos et al., 2014). Different PAMs such as PF-06764427 and MK-7622, have demonstrated the potential to potentiate the M1 mAChR activity both alone and when used alongside an orthosteric agonist, whilst other PAMS such as VU0550164 and VU0453595 have only shown receptor overactivation when an orthosteric ligand is present (Moran et al., 2018). Whilst many orthosteric ligands have gone through complete clinical stages, PAMs are still being developed as well as being tested in early clinical

stages, which could expand the therapeutic treatment window of dementia patients through combined drug treatments.

All the ligands mentioned above have different functional selectivity on its receptor target and do not all produce the same downstream signalling. This receptor characteristic has led to another approach to study M1 mAChR ligands, focussing on 'biased agonism'. This is the ligand's ability to differentially activate specific downstream signalling pathways within the same receptor (Michel & Charlton, 2018). The ligand, in this case, will only activate one specific downstream signalling pathway instead of having a balanced effect on the whole set of downstream signalling pathways induced by one receptor (Jarpe et al., 1998; Patel et al., 2010; Wootten et al., 2018). This has become crucial in drug discovery, as it will allow receptor signalling pathways to be specifically targeted, which could positively impact disease symptoms and the disease itself.

1.4 M1 mAChR as a potential target for prion disease

As shown by data previously published by the Tobin group (Bradley et al., 2017; Scarpa et al., 2021; Dwomoh et al., 2022), studies into both the disruption of part of the M1 mAChR receptor signalling and activation of the M1 mAChR with both orthosteric and allosteric ligands has highlighted the potential for the M1 mAChR as a target for prion disease. Bradley et al. (2017) demonstrated that treatment of prion-diseased mice with Xanomeline can restore learning and memory deficits. The same study revealed that treatment of prion-diseased mice with benzyl quinolone carboxylic acid (BQCA), an M1 PAM, could restore fear-conditioning learning and memory deficits as well as significantly increase survival of the mice. Scarpa et al. (2021) showed that the genetically modified inhibition of part of the M1 mAChR signalling pathway, in this case the phosphorylation of the receptor by mutating all serine phosphorylation sites in the intracellular domain of the receptor, making the M1-PD. This mutation on the M1 mAChR leads to an acceleration in PrP^{Sc} accumulation, prion disease progression and shorter survival compared to Wt mice. The study also revealed higher levels of neuroinflammatory markers in the M1-PD at the same time-point as in the Wt mice. Lastly, Dwomoh, Rossi, et al. (2022) corroborated that M1 mAChR activation with M1 PAMs slows down prion propagation and prion disease. The study showed that treatment of

prion-infected mice with VU846, a next-generation M1 selective PAM, could again reduce learning and memory deficits like BQCA. The same study performed a global proteomic analysis of isolated hippocampi from control-infected and prion-infected mice, as well as prion-infected mice treated with vehicle and VU846, revealing that VU846 down-regulated the up-regulated neuroinflammatory and neurodegenerative markers seen in prion-infected mice compared to control-infected mice. Neuroinflammatory markers such as glial fibrillary acid protein (GFAP), Vimentin and Galectin-1 were all shown to be down-regulated as a consequence of VU846 treatment, as well as AD-associated markers of neurodegeneration like apolipoprotein E (ApoE), ApoD and ApoC. VU846 was also able to increase expression of synaptic protein like SNAp-25 and syntaxin1A/1B, which had previously been shown to be down regulated in prion disease.

This data generated by our group directly points at the M1 mAChR as a major potential target in the slowing down of prion disease. Further research to understand the direct mechanism by which the M1 mAChR influences prion disease is required for the development of therapeutics which can be taken to clinical studies for human prion disease.

1.5 General aims of the thesis

Given that the literature highlights the M1 mAChR as a major potential target for prion disease, further investigation into the mechanism by which this receptor impacts PrP^{Sc} infection and propagation is required. M1-PD studies by Scarpa et al. (2021) demonstrate the importance of the receptor phosphorylation in disease progression, accelerating the propagation and accumulation of PrP^{Sc} in the brain. In addition, Dwomoh, Rossi, et al. (2022) demonstrated that exogenous activation of the M1 mAChR can slow down propagation of PrP^{Sc}. Therefore, we hypothesise that the activation of the M1 mAChR has a protective effect in prion disease and plays a role in the infection and propagation mechanism of PrP^{Sc} in neurons. Improving our understanding of these mechanisms may permit to development of specific ligands which can modify misfolded prion propagation and disease progression. This study therefore aimed to

1. Biochemically and pharmacologically characterise the prion protein and M1 mAChR in immortalised cell lines and primary neuronal cell cultures (Chapter 3).

2. Create a novel model of PrP^{Sc} infection and propagation in primary neuronal cultures and to use this model to investigate the role of M1 mAChR expression and activation in PrP^{Sc} infection and propagation (Chapter 4).

3. Conduct a proteomic analysis to thoroughly evaluate the impact of PrP^{Sc} infection in primary neuronal cultures in comparison to control treated neurons (Chapter 5).

Chapter 2 Materials and Methods

2.1 Materials

2.1.1 General materials and reagents

Supplier	Description	Cat. No.
Beckman Coulter	26.3mL Polycarbonate Bottle with Cap Assembly, 25 x 89mm	355618
	Type 70 Ti Fixed-Angle Titanium Rotor	337922
Bio-Rad Laboratories Ltd	Precision Plus Protein™ All Blue Prestained Protein Standards	#1610373
	Resolving Gel Buffer for PAGE	#1610798
	Stacking Gel Buffer for PAGE	#1610799
Fisher Chemicals	Ammonium Persulphate	A/6160/60
	Dimethyl Sulfoxide (DMSO)	D/4120/PB08
	Ethylenediaminetetraacetic acid (EDTA) disodium salt dihydrate	D/0700/60
Merck Life Sciences	Proteinase k	P2308
Perkin-Elmer – Cisbio	IP-One – Gq KIT	62IPAPEC
Sigma-Aldrich	Anti-HA Affinity Matrix	11815016001
	β-glycerol phosphate	G5422
	cOmplete™ Mini, EDTA-free Protease Inhibitor Cocktail	11836170001
	EDTA	27285
	Glycerol	G6279
	Glycine	G7126
	Goat Serum	G9023
	IGEPAL® CA-630	I3021
	Lithium Chloride	L4408
	N-Lauroylsarcosine sodium salt (Sarcosyl)	61747
	PhosSTOP™	04906837001
	phenylmethylsulfonyl fluoride (PMSF)	P7626
	Sodium chloride	S7653
	Sodium deoxycholate	D6750
	Sodium dodecyl sulphate (SDS)	L6026
	N,N,N',N'-Tetramethylethylenediamine (TEMED)	T9281

	Trizma® base	T1503
	Trizma® hydrochloride	T3253
	TWEEN® 20	P1379
Severn Biotech Ltd	Acrylamide Bis-Acrylamide Stock Solution, 30% Acrylamide (w/v) Ratio 37.5:1	20-2100-10
ThermoFisher Scientific	Dulbecco's Phosphate-Buffered Salines (DPBS)	14190094
	HBSS (10X) [+] $CaCl_2$, [+] $MgCl_2$ – Hank's Balanced Salt Solution	14065-049
	Pierce™ BCA Protein Assay Kit	23227
	Pierce™ Silver Stain Kit	24612
	Restore™ PLUS Western Blot Stripping Buffer	46430
	Sodium Bicarbonate (7.5%)	25080-094
VWR Chemicals	Ammonium Sulphate	21333.296
VWR Chemicals	Calcium Chloride Dihydrate	22322.295
	4-(2-hydroxyethyl)-1-piperazineethanesulfonic acid (HEPES)	441485H
	Potassium Chloride	26764.260

Table 2-1 List of general materials and reagents used

2.1.2 Materials and reagents used in cell and tissue culture

Cell Lines
Wild-type Chinese Hamster Ovary (CHO)
Wild-type human M1 mAChR HA-tagged transfected CHO
Wild-type human M1 mAChR DREADD HA-tagged transfected CHO

Table 2-2 List of Chinese Hamster Ovary (CHO) cells lines used

Supplier	Description	Cat. No.
Invitrogen	Ethylenediaminetetraacetic acid (EDTA) 0.5M, pH 8.0	15575-038
ThermoFisher Scientific	B-27™ Plus Neuronal Culture System	A3653401
	DMEM, high glucose	41965
	Foetal Bovine Serum (FBS)	10500064
	GlutaMAX™ Supplement	35050038

	Laminin Mouse Protein, Natural	23017015
	Penicillin/Streptomycin	15140122
Santa Cruz Biotechnologies	Hygromycin B solution	sc-29067
Sigma-Aldrich	Nutrient Mixture F-12 Ham with L-glutamine and Sodium Bicarbonate	N6658
	Poly-D-Lysine Hydrobromide	P6407
	Trypan Blue Solution	T8154

Table 2-3 List of materials and reagents used in cell and tissue culture

2.1.3 Muscarinic pharmacological ligands

Supplier	Description	Cat. No.
Sigma-Aldrich	Acetylcholine Chloride	A6625
	Atropine Sulphate Salt	A-0257
	Oxotremorine M	O100
Tocris	Clozapine-N-Oxide	4636/50
Sosei Heptares	HTL9936	N/A
PerkinElmer	[^{3}H]-NMS Scopolamine methyl chloride	NET636001MC
	Quinuclidinyl benzilate L-[benzilic-4,4`-3H(N)]-(QNB)	NET656001MC

Table 2-4 List of muscarinic pharmacological ligands used

2.1.4 Primary antibodies (Western blotting and immunocytochemistry)

Supplier	Antigen	Species	Working Dilution	Cat. No.	RRID
Abcam	Anti-alpha actinin 4	Rabbit	1:1,000 (WB)	ab108198	AB_10858236
	Anti-alpha-tubulin [DM1A]	Mouse	1:5,000 (WB)	ab7291	AB_2241126
	Anti-NeuN [1B7]	Mouse	1:1,000 (WB)	ab104224	AB_10711040
	Anti-myelin basic protein	Rabbit	1:1,000 (WB)	ab218011	AB_2895537

	Anti-p62 antibody [2c11]	Mouse	1:1,000 (WB)	ab56416	AB_945626
	Anti-prion protein PrP antibody [8H4]	Mouse	1:1,000 (WB/ ICC)	ab61409	AB_944979
Cell Signalling Technology	c-Fos antibody	Rabbit	1:1,000 (WB)	4384	AB_2106617
	Caspase-3 antibody	Rabbit	1:1,000 (WB)	9662	AB_331439
Novus Biotech	LC3B antibody	Rabbit	1:1,000 (WB)	NB100-2220	AB_10003146
Santa Cruz Biotech.	mAChR M1 antibody (G-9)	Mouse	1:1,000 (WB)	sc-365966	AB_10847359
Sigma-Aldrich	Anti-HA-Peroxidase	Rat	1:1,000 (WB), 1:500 (ICC)	12013819001	AB_390917

Table 2-5 List of primary antibodies used in Western blotting (WB) and immunocytochemistry (ICC) experiments

2.1.5 Secondary antibodies (Western blotting and immunocytochemistry)

Supplier	Antibody	Working Dilution	Cat. No	RRID
Invitrogen	Fluoromount™, with 4′,6-diamidino-2-phenylindole (DAPI)	-	00-4959-52	-
	Goat anti-Mouse IgG (H+L) Alexa Fluor™ 594	1:500 (ICC)	A11005	AB_2534073
	Goat anti-Rat IgG (H+L) Alexa Fluor™ 488	1:500 (ICC)	A11006	AB_141373
LI-COR biotechnology	IRDye 800CW Donkey anti-Mouse IgG (H + L)	1:10,000 (WB)	926-32212	AB_621847
	IRDye 800CW Donkey anti-Rabbit IgG (H+L)	1:10,000 (WB)	926-32213	AB_621848
	IRDye 800CW Goat anti-Rat IgG (H + L)	1:10,000 (WB)	926-32219	AB_1850025
	Revert™ 700 Total Protein Stain	-	926-11021	-

Table 2-6 List of secondary antibodies used in WB and ICC experiments

2.1.6 Materials and reagents used for Mass Spectrometry sample preparation

Supplier	Description	Cat. No.
Eppendorf	Eppendorf SmartBlock 15ml	5366000021
	ThermoMixer C	5382000031
Fisher Chemicals	Trifluoroacetic Acid (TFA), 0.1%	LS119-1
Profiti	S-Trap Midi Columns	N/A
Promega	Trypsin-LysC	V5073
Qiagen	Qiagen Stainless Steel Bead, 5mm	69989
	Qiagen TissueLyser LT	85600
Sigma-Aldrich	Hydroxylamine	467804
	Iodoacetamide (IAA)	I6125
	Methanol for HPLC	34860-1L-R
	Triethylammonium Bicarbonate (TEAB)	18597
	Tris(2-carboxyethyl)phosphine (TCEP)	75259
	Trypsin from Bovine Pancreas	T1426
ThermoFisher Scientific	Acetonitrile, LC-MS Grade	51101
	Acetonitrile, Anhydrous	043166.AK
	Formic acid	85178
	Formic Acid, 0.1%	85170
	Low Binding tubes 1.5ml	90410
	Low Binding tubes 2.0ml	88379
	Oil Free Vacuum Pump	OFP400-230
	Pierce High-pH Reversed-phase Peptide Fractionation Kit	84868
	pH Test Strips	P-4661
	Savant Refrigerated Vapor Trap	RVT5105
	Savant SpeedVac Vacuum Concentrator	SPD140DDA
	Sodium dodecyl sulphate (SDS), 10%	71736
	TMT 10plex	90110
	TMT 11	A37724
	Trifluoroacetic Acid (TFA) , LC-MS Grade	85183
VWR Chemicals	Water for high-performance liquid chromatography (HPLC)	23595.328
WATERS	WATERS Sep-Pak C18 columns	WAT054960

Table 2-7 List of materials and reagents used in for mass spectrometry sample preparation.

2.1.7 Mass Spectrometry Buffer recipes

Lysis Buffer – 2% SDS, 10mM TEAB, pH 8.
S-Trap Buffer – 90% methanol for HPLC, 100mM TEAB.
Digestion Buffer – 50mM TEAB in water for HPLC.
Elution Buffer 1 – 0.2% Formic Acid in water for HPLC.
Elution Buffer 2 – 80% Acetonitrile, 0.2% Formic Acid
Elution Buffer 3 – 50% Acetonitrile, 0.15% Formic Acid

2.1.8 Recipes for Buffers and Solutions

CHO Cell Medium – Sigma's Nutrient Mixture F12 Ham containing 10% FBS, and penicillin/streptomycin (100 U/mL)
Neurobasal Complete Medium + - B-27™ Plus Neuronal Culture System containing 1% GlutaMAX™ Supplement (100X) and penicillin/streptomycin (100 U/mL)
T/E Buffer – 10mM Tris-HCl pH 8.0, 1mM EDTA.
T/E+ Purification Buffer – 10mM Tris-HCl pH 8.0, 1mM EDTA, 1mM PMSF, 10mM β-glycerol phosphate.
Radioimmunoprecipitation Assay (RIPA) Buffer – 50 mM Tris-HCl pH 8, 150 mM NaCl, 0.5% (w/v) Na-deoxycholate, 1% (v/v) IGEPAL CA-630, 0.1% (v/v) SDS.
Laemmli Sample Buffer (4x) – 250 mM Tris-base, pH 6.8, 4% (w/v) SDS, 40% (v/v) glycerol, 10% Β-mercaptoethanol and 0.04% (w/v) bromophenol blue.
Tris-Glycine SDS Running Buffer – 25 mM Tris-base, 192 mM glycine, 0.1% SDS.
Transfer Buffer – 25 mM Tris-base, 192 mM glycine, and 20% ethanol.
Tris Buffered Saline (TBS) - 20 mM Tris-HCl, pH 7.6, 137 mM NaCl.
TBS-T – TBS and 0.1% (v/v) Tween-20.
Fixing Solution – 4% (w/v) Paraformaldehyde (PFA) in DPBS.
Blocking Buffer for ICC – 0.1% Triton-X100, 1% BSA, and 3% goat serum in DPBS.
IP1 Stimulation Buffer – HBSS (1X) [+] $CaCl_2$, [+] $MgCl_2$, 10mM HEPES, 0.035% $NaHCO_3$, pH 7.4.
IP1 Treatment Buffer – HBSS (1X) [+] $CaCl_2$, [+] $MgCl_2$, 10mM HEPES, 0.035% $NaHCO_3$, 50mM $LiCl_2$, pH 7.4.
Binding Assay Buffer – 110 mM NaCl, 5.4 mM KCl, 1.8 mM $CaCl_2$, 1 mM $MgSO_4$, 25 mM glucose, 20 mM HEPES, 58 mM sucrose.

2.2 Experimental animals

The following animals were all used throughout the project:

Animal Strain	Background	Genotype	Genetic Mutations	Obtained from/by
Prion-KO	FVB/N	Homozygous	Knock-out of the *PRNP* gene	(Mallucci et al., 2002)
Tg37 hemizygous (3x Prion)	FVB/N	Hemizygous	Expresses 3 copies of the *PRNP* gene	Mating of Prion-KO with 6x Prion mice
Tg37 homozygous (6x Prion)	FVB/N	Homozygous	Expresses 6 copies of the *PRNP* gene	(Mallucci et al., 2003)
M1-HA Wt	C57BL/6	Homozygous	Knock-in of an HA-tagged M1 mAChR on the C-terminus	GenOway
M1-KO	C57BL/6	Homozygous	Knock-in of an inducible HA-tagged M1 mAChR on the C-terminus with mutations in the third intracellular loop and C-terminus tail replacing 20 threonine/serine residues with alanine making the receptor phosphorylation deficient	GenOway
M1-DREADD	C57BL/6	Homozygous	Knock-in of a constitutive HA-tagged M1 mAChR on the C-terminus with two-point mutations Y106A and A196C which render the receptor insensitive to Acetylcholine and promotes Clozapine-N-Oxide sensitivity	GenOway

M1-PD	C57BL/6	Homozygous	Knock-in of a constitutive HA-tagged M1 mAChR on the C-terminus with mutations in the third intracellular loop and C-terminus tail replacing 20 threonine/serine residues with alanine making the receptor phosphorylation deficient	GenOway

Table 2-8 List of different GEMMs used

The first litter of every mating was always genotyped by Transnetyx. All animals were housed in a regulatory unit at room temperature under 12-hour light/dark cycles, and were fed normal chow. Both female and male adult mice were used for purification experimental procedures, and only female pregnant mice were used to obtain the 16/17-day old embryos for primary neuronal cultures.

2.2.1 Ethics statement

All procedures were conducted in accordance with the Animals (Scientific Procedures) Act 1986 under personal licence I96136800, held by me, and project licences PP0894775 or PP7704105, held by Prof Andrew B. Tobin (University of Glasgow).

2.2.2 Mouse prion Infection

Mice aged 3 to 4 weeks from the 3x Prion strain were inoculated by intracerebral injection with 1% brain homogenate infected with RML prion into the left parietal lobe as previously described (Mallucci et al., 2003). All inoculations were performed using a free-hand injection method, to maximise consistency, by the same animal technician. RML prion-infected brain homogenate inoculum was obtained from RML mouse-passaged PrP^{Sc} originally derived from the "drowsy goat" line (Chandler, 1961; Kimberlin & Walker, 1978). Injections of 1% normal brain homogenate (NBH) (20 µl) were used as the control.

2.2.3 Tissue Harvest

Cerebral tissue was harvested at sacrifice by cervical dislocation. Harvested tissue was snap frozen in dry ice and stored at − 80°C until required.

2.3 CHO cell culture

2.3.1 Production of CHO Flp-In™ cell lines

The Flp-In™ system was used on CHO cells to stably and constitutively express two different versions of the M1 mAChR with a HA epitope tag fused to the receptor's C-terminus to facilitate detection.
The two versions generated were the:

- hM1-HA (human wild type M1 mAChR with an HA-tag on the C-terminus)
- hM1-DREADD-HA (human DREADD of the M1 mAChR with an HA tag on the C-terminus)

2.3.2 Maintenance of CHO Flp-In cell lines

CHO cells were cultured in a humidified atmosphere at 37°C and 5% CO_2 levels. Once cells reach 80-90% confluency, cell medium was aspirated followed by a quick DPBS wash. Cells were then detached from cell flask surface using PBS-EDTA at 37°C for 4 min, proceeded by resuspension in cell medium. Stably transfected CHO cells (hM1-HA and hM1-DREADD-HA) medium was supplemented with 0.4µg/mL Hygromycin. Once cells were resuspended, a 5 min 1000 x g centrifugation was used to pellet all cells and discard the medium containing PBS-EDTA. After the medium was aspirated, cells were resuspended with 10X the desired dilution of their respective medium. Finally, the cell suspension was transferred into new cell flasks and an appropriate volume of medium was added in order for the cells to grow.

2.3.3 Determination of cell viability

Trypan blue staining and an automated cell counter (Countess™ 3, Invitrogen) were used in order to calculate cell viability. A 1-in-1 0.4% trypan blue and cell

suspension mix was prepared, gently mixing to avoid cell damage. 10µL of the suspension mix was added onto a Countess™ cell counting chamber slide and inserted into the automated cell counter (Countess™ 3, Invitrogen), obtaining an accurate number of viable cells per mL of the suspension.

2.3.4 Cryopreservation of CHO Flp-In cell lines

Cells were grown to 80-90% confluency to be for cryopreserved. Medium was aspirated from the cell flask, followed by a quick DPBS wash and a 4 min incubation in PBS-EDTA for allow cells to detach from the flask surface. CHO medium was added to neutralise PBS-EDTA and followed by a 5 min 100 x g centrifugation to aspirate the PBS-EDTA containing medium from the cell pellet. Cells were resuspended in a 10% DMSO-PBS solution, then transferred into a cryotube and frozen at -80 ˚C, before storing in liquid nitrogen for long term.

2.4 Primary neuronal cell culture

Hippocampal and cortical regions of 16/17 day old embryos were dissected in order to prepare primary neuronal cultures from the different strain mice mentioned before. Brain regions were incubated in TrypLE™ Express Enzyme at 37˚C for 10 minutes to dissociate all adherent cells in the dissected brain regions. Neurobasal Complete Medium+ was then added to neutralise the TrypLE™ Express Enzyme and cells were then centrifuged in order to aspirate the TrypLE™ Express Enzyme containing medium from the pellet. The neuronal pellet was again resuspended with Neurobasal Complete Medium+ and cell viability was determined in the same manner as described before. Once number of viable cells had been calculated, the neuronal suspension was further diluted in order to plate the desired concentration of cells in 6, 24 and 96-well plates previously coated with 6µg of laminin and 4µg of poly-D-lysine. Every 7 days, 50% of the medium was replaced with new fresh medium.

2.5 Pharmacological Assays

2.5.1 IP1 Accumulation Assay

Inositol-1-phosphate (IP1) accumulation assays were performed, to measure Gαq protein downstream signalling, with the IP-One – Gq KIT (CisBio). Assay was performed according to manufacturers' instructions. CHO cells were plated at 25,000 cells/well in 96-well plates and grown overnight before assay was performed. Neurons were plated at 25,000 cells/well in 96-well plates and left to grow for 7 or 14 days before performing the assay, depending on the experiment. Cells were washed with Stimulation Buffer 3 times and then incubated in the same buffer for 1 hr at 37°C. Cells were then incubated with 90µl of Treatment Buffer (same as Stimulation with the addition of $LiCl_2$) and 10µl of 10X concentrated muscarinic ligands (Table 2-4) for 1 hr at 37°C. Treatment buffer with ligands was then removed and cells were lysed with IP1 assay kit lysis buffer. 96-well plates were then shaken for 15 min and cell suspension was pipetted into a 384-well white proxiplates (PerkinElmer). IP1 standards and antibody conjugates were prepared according to manufacturers' instructions. Same volume of IP1 standards as of cell suspension was added to the proxiplates wells and 3 µL of each antibody was added to each well containing cell suspension or IP1 kit standards. Plate was then incubated for 1-24 hrs at room temperature and time resolved fluorescence (wavelengths 665 nm and 620 nm) was measured using a PHERAstar plate reader (BMG Labtech). Absorbance ratio at 665/620 nm was calculated and IP1 concentrations were extrapolated from the standards provided by the kit. Results were normalised to maximal stimulation response of acetylcholine for all CHO cell line and neuronal cultures, except for the DREADD lines/cultures which were normalised to CNO. Concentration–response curves obtained were fitted according to a four-parameter logistic equation in GraphPad Prism 10. The potency (EC_{50}) and efficacy (E_{max}) of the tested ligands were determined with a stimulation non-linear regression curve model.

2.5.2 Radioligand Binding Assay

Neurons were plated at 50,000 cells/well on clear poly-D-lysine and laminin coated 24-well plates and left to grow and spread their processes for 7 days, or

14 days with daily 10μM dosing of Oxotremorine M from day 7 to day 13. At DIV7 or DIV14, neurons were washed twice with warm Binding Assay Buffer, followed by a two-hour incubation at 37°C containing increasing concentrations of the tritiated radioligands [3H]-NMS and [3H]-QNB in Binding Assay Buffer. 10 μM atropine was added to one of each radioligand concentration triplicates to determine the Non-Specific Binding (NSB). After the two-hour incubation, two washes with 0.9% NaCl were performed to remove unbound radioligand, followed by solubilisation of the neurons with 0.1 M NaOH for 30 min before being transferred to scintillation vials. Bound radioactivity was determined with a liquid scintillation counter (Liquid Scintillation Analyzer Tri-Carb® 2910 TR; PerkinElmer). Data was analysed using GraphPad Prism 7 to obtain non-linear regression curves, and Bmax and Kd values.

2.6 Prion enrichment and neuronal infection

NBH (control) and RML (prion) infected 3x Prion mouse brains were homogenated in TE + Purification Buffer. Homogenates were firstly centrifuged for 10 min, at 4°C and 500xg. Supernatant was discarded and the pellet was resuspended in 10mL TE+ buffer. This step was repeated twice. The supernatant was again discarded, and the pellet was resuspended in DPBS, followed by an ultracentrifugation for 20 minutes, at 4°C and 20,000xg. The supernatant was discarded, and the pellet was resuspended with 10mL of 1% Sarcosyl-DPBS to solubilise the insoluble protein left. The resuspended pellet spun on a rotation wheel for 1 hour at 4°C. The sample was further ultracentrifuged for 20 minutes, at 4°C and 100,000xg. The newly formed pellet was collected for analysis, and the supernatant was again ultracentrifuged for 20 minutes, at 4°C and 100,000xg. The new pellet was again resuspended in PBS, and one last time ultracentrifuged for 40 minutes, at 4°C and 100,000xg. This final pellet was resuspended in DPBS to be used for neuronal culture infections. The purified brain sample was then stored at -80°C. This process was repeated with the brains of a large number of animals, to create a homogenous large batch of control and prion purified brain sample.

2.7 Immunoblotting

2.7.1 Lysate preparation from cultured CHO cells

CHO cells were cultured from 150cm^2 tissue culture flasks once cells reached confluency after 1-2 days of splitting. Cells were washed twice with ice-cold PBS and lysed with RIPA buffer with both proteinase and phosphatase inhibitor tablets. Lysed cells were scraped of the tissue flask surface and collected in microcentrifuge tubes. Samples were centrifuged for 15min, 21,000xg at 4°C and supernatants were then collected in new tubes. Protein quantification using a Pierce™ BCA Protein Assay Kit was performed, and samples were all adjusted to the sample concentration.

2.7.2 Immunoprecipitation of HA-tagged proteins

After centrifugation and supernatant collection step mentioned above, 50µl of Anti-HA Affinity Matrix beads were added and incubated at 4°C overnight. Samples were centrifuged the following day for 1min, 1,000xg at 4°C, supernatants were discarded, and beads were washed in ice-cold DPBS. This step was repeated twice before resuspending the beads in Laemmli Buffer. Beads were heated to 60°C for 5min, before centrifuging again for 2min, 1,000xg at 4°C. Finally, supernatant was collected in new tubes ready for Western blot.

2.7.3 Lysate preparation of neuronal cultures

Neuronal cultures were allowed to grow until desired day (7, 14, 21 days *in vitro*). Once reached the end of the experiments, cells were washed twice with ice-cold PBS and lysed with RIPA buffer with both proteinase and phosphatase inhibitor tablets. Lysed cells were scraped of the 6-well plates' surface and collected in microcentrifuge tubes. Samples were centrifuged for 15min, 21,000xg at 4°C to separate pellet (insoluble protein) from supernatant (soluble protein). Pellet was then resuspended with 1% SDS RIPA Buffer and sonicated to solubilise all proteins in the pellet. Protein quantification of both pellet and supernatant was performed using a Pierce™ BCA Protein Assay Kit and samples were all adjusted to the sample

concentration. Pellet resuspensions were used to detect PrP^{Sc} whilst supernatants were used to detect all other proteins.

2.7.4 Protein Quantification BCA Assay

BCA protein quantification assay was performed according to manufacturers' protocol to measure to the total protein of each individual sample. A volume of 5µl of each sample was pipetted into a 96-well plate in duplicate alongside known BSA protein standards (0-20mg/ml in duplicates too. 200µl of BCA assay mix was added to all sample wells and incubated for 30min at 37°C. Absorbance at 562nm was recorded using a PHERAstar microplate reader (BMG Labtech). All sample were then adjusted to have equal protein concentrations followed by the addition of 4X Laemmli sample buffer to achieve a 1X final concentration. Samples were then heated at 95°C for 5 min before being loaded onto a gel.

2.7.5 SDS-PAGE

Bio-Rad mini-Protean III equipment was used to cast sodium dodecyl sulphate polyacrylamide resolving gels. 1.5 mm thick 15 % acrylamide gels were made to observe proteins under 50kDa. For any other proteins sized between 50-200kDa, a 10% acrylamide resolving gel was made. The stacking gel above the resolving contained 5% acrylamide. Laemmli-containing samples were then loaded into casted gels and electrophoresed in TrysGlycine SDS running buffer at 90 V for 2 hrs.

2.7.6 Probing and detection

After gel electrophoresis is finished, a nitrocellulose membrane was placed in direct contact with the gel and placed within two 1mm Whatman chromatography paper sandwich. This sandwich was then placed within two transfer sponges in a transfer cassette, which was placed inside a transfer tank full of transfer buffer. The wet-transfer was allowed to run for 2 hrs at a constant voltage of 25 V. Once transfer was complete, a brief incubation in ponceau red was performed in order to visualise if transfer onto the nitrocellulose membrane had been successful. Once all ponceau red had been washed off with TBS-T, membranes were blocked

with 5% (w/v) non-fat milk powder in TBS-T for 1 hr at room temperature. Primary antibody (Table 2-5) in TBS-T was added to the membranes and incubated with at 4°C overnight. Membranes were then washed several times with TBS-T before incubating with corresponding secondary antibodies (Table 2-6) for 1 hr at room temperature. For total protein stain, membranes were incubated with Revert™ 700 Total Protein Stain for 15 min. Finally, blots were washed again with TBS-T before visualising them using the Odyssey M Imager scanner and analysing them with the Empiria Studio software.

2.7.7 Sample proteinase K digestion

In order to determine PrP^{Sc} levels, lysates from brain tissue and neuronal cultures were digested with proteinase K (pK) before running on a Western blot. Lysed samples were incubated with proteinase K for 30 min at 37°C. The pK-to-protein concentration ratio was 1:1. 4X Laemmli Buffer to achieve a final concentration of 1X was added to stop pK digestion activity. Samples were then incubated for 5 min at 95°C before being loaded onto a 15% acrylamide gel.

2.8 Immunocytochemistry

2.8.1 Cell fixation

CHO cells were grown to 70-80% confluency and neuronal cultures were allowed to grow for 7 and 14 days *in vitro* on 30 mm round coverslips in 6-well plates. Cells were washed 3 times for 5 min with DPBS and then fixed for 30min with 4% paraformaldehyde (PFA) (v/v) at 4°C. Coverslips were washed again with DPBD 3 times for 5 min before either being stored at 4°C or carrying on with the immunostaining.

2.8.2 Immunostaining

Coverslips were once again washed 3 times for 5 min in DPBS followed by a 30 min incubation with Blocking Buffer at room temperature. Buffer was then removed and Primary antibody (Table 2-5) in Blocking Buffer at room temperature overnight. Samples were then washed again 3 times for 5 min in DPS followed by

incubation with Secondary antibody (Table 2-6) in Blocking Buffer at room temperature for 1 hr. Coverslips were washed 3 times for 5 min in DPBS and finally mounted using Vectashield mounting media containing DAPI on glass slides. Cells were imaged with an LSM 880 confocal laser scanning microscope (Zeiss) using the x20, x40 and x63 objectives.

2.9 Proteomics

2.9.1 Lysate preparation

Neuronal lysates were prepared by scraping neuronal cells from 6-well plates with a total of 400µL Lysis Buffer per sample condition into low binding microcentrifuge tubes. Lysates were topped up to 600µl volume with Lysis Buffer and 1 Qiagen Stainless Steel Bead (5mm) was added to each tube before homogenising the samples with 3x30 sec high-speed pulses on a Qiagen TissueLyser LT at 4°C. Samples were rested for 5 min in ice, before transferring the sample solutions into new low binding microcentrifuge tubes. Samples were then sonicated 3x10 sec, followed by a 10 min, 10,000xg centrifugation at 4°C. Supernatant was collected, and protein concentration was measured using the Pierce™ BCA Protein Assay Kit following manufacturer's instructions. Sample concentrations were adjusted to equal concentrations before continuing.

2.9.2 Sample reduction, alkylation and digestion

Sample reduction was performed by adding 10mM TCEP final concentration in each sample, followed by 30min, 60°C, 1100 RPM incubation on a Eppendorf ThermoMixer® C with lid on. Samples were rested at 24°C for 5 min. A final concentration of 40mM IAA was added to each sample, followed by 30min, 60°C, 1100 RPM incubation on a Eppendorf ThermoMixer® C with lid on for the alkylation step. Alkylation was quenched with a 5mM final concentration of TCEP and Eppendorf ThermoMixer® C incubation for 10 min, 1100 RPM at room temperature. Sample digestion continued with the addition at a final concentration of 5% SDS, 1% TFA and S-Trap buffer before transferring the solutions into the S-Trap columns in 15mL falcon tubes. Tubes were then centrifuged for 5 min, 2600 RPM at room

temperature on a Eppendorf Centrifuge 5418 R to trap protein in the column. Column was further washed with S-Trap Buffer and centrifuged under the same conditions 4 times. Buffer collected in the falcons was discarded, and both Trypsin-LysC and Bovine Pancreas Trypsin were added to each column. S-Trap columns inside falcons were incubated at 47°C for 1h 20min with no shaking on a Thermomixer followed by an overnight room temperature incubation. Digested peptides were eluted by a 2 min, 2,000 RPM at room temperature centrifugation on a Eppendorf Centrifuge 5418 R using 50mM TEAB, Elution Buffer 1 and Elution Buffer 2 in this order. After Elution Buffer 2 was collected, samples were transferred into low binding microcentrifuge to snap-freeze in liquid nitrogen and then dried in a SpeedVac. Dried peptides were resuspended in 1% TFA and incubated on a Eppendorf ThermoMixer® C for 30 min, 1,850 RPM at room temperature. Resuspended peptides were then transferred into pre-equilibrated WATERS columns, according to manufacturer's instructions, and eluted by gravity twice. Columns were transferred into 15mL falcon tubes followed by 4 washes and centrifugations with 0.15% formic acid at 200RPM, RT for 2 min on a Eppendorf Centrifuge 5418 R. Columns were then eluted 3 times using Elution Buffer 3, followed by another snap-freeze in liquid nitrogen and drying in a SpeedVac.

2.9.3 Peptide labelling

Dried samples were resuspended with 50mM TEAB and centrifuged for 30 min, 1,800 RPM at room temperature on a Eppendorf Centrifuge 5418 R. Supernatants were transferred into new low binding microcentrifuge tubes. Pre-resuspended TMT reagents in 100% anhydrous ACN was added to each individual sample and incubated on a Eppendorf ThermoMixer® C for 2 hrs, 1,200 RPM at room temperature. The TMT-to-peptide ratio was 2.5:1. Quality control of the TMT labelling was performed at this stage, 1 solution containing 2µL of each individual sample was sent for liquid chromatography–tandem MS (LC-MS/MS) analysis at the University of Warwick, Research Technology Platforms Centre. Once quality control abundances were received, samples were normalised per the abundances, followed by the final concentration addition of 0.17% hydroxylamine. All samples were then pooled together, followed by being snap-frozen and dried.

2.9.4 Sample fractionation

Pooled dried sample was resuspended with 0.1% formic acid followed by fractionation using the Pierce High-pH Reversed-phase Peptide Fractionation Kit according to manufacturer's instructions, into 12 fractions. Fractions were snap-frozen in liquid nitrogen and dried in a SpeedVac. All 12 dried fractions were sent for LC-MS/MS analysis at the University of Warwick.

2.9.5 Mass spectrometry analysis

Mass spectrometry analysis was outsourced to Andrew Bottrill from the Proteomics Facility at the University of Warwick and performed as previously described by Dwomoh et al. (2022). A LTQ Orbitrap Velos mass spectrometer (Thermo Fisher Scientific) was used to analyse the samples. The samples were then loaded at a high flow rate onto a reversed-phase trap column containing 5-mm C18 300-Å Acclaim PepMap medium. Peptides were eluted passed through a reversed-phase PicoFrit capillary column. Peptides were eluted again, being sprayed directly into the nanospray ion source of the LTQ Orbitrap Velos mass spectrometer. The LTQ Orbitrap Velos mass spectrometer was set to acquire a one-microscan Fourier transform mass spectrometer (FTMS) scan event at 60,000 resolutions over the mass/charge ratio range of 300 to 2000 Da in positive ion mode. Maximum injection time for MS was 500 ms, and the automatic gain control (AGC) target setting was 1 × 106. Up to 10 data-dependent higher-energy collision dissociation MS/MS were triggered from the FTMS scan. Isolation width was 2.0 Da, with a normalized collision energy of 42.5. Maximum injection time was 250 ms for MS/MS, and the AGC target was set to 5 × 104.

2.9.6 Protein identification

Proteome Discoverer (version 2.5.0.400, Thermo Fisher Scientific) was used to process the raw data obtained from the individual LC-MS/MS acquisitions. Mascot (version 2.7.07, Matrix Science Ltd.) was used to search each file against the UniProtKB-SwissProt database. The tolerances for peptide and MS/MS were set to 10 parts per million and 0.02 Da, respectively. A decoy database search was performed. Scaffold Q + S (version 4.11.0, Proteome Software) was utilised to

further process the Proteome Discoverer processed raw data. X!Tandem (Global Proteome Machine Organization) was used to search the data after import. PeptideProphet and ProteinProphet (Institute for Systems Biology) probability thresholds of 95% were determined from the decoy searches, and an improved 95% peptide and protein probability threshold based on the data from the two different search algorithms was calculated using Scaffold.

2.10 Data Analysis

2.10.1 Neuronal Sample Size

The sample size (number of biological replicates) used for primary neuronal experiments was equivalent (n=3) to the sample size used in previous studies by our group (Marsango et al., 2022; Scarpa et al., 2021).

2.10.2 General statistical analysis

GraphPad Prism 10 software was utilised for statistical analysis. Parametric tests were used to statistically analyse the differences between, normally distributed, groups of measures. Two-tailed unpaired student's t test was used for the analysis of 2 or less groups of measure, and one- or two-way Analysis Of Variance (ANOVA) were used for 3 or more groups, depending on the number of independent variables. If the number of independent variables is one (EC_{50}, E_{max}, Bmax and K_D between different CHO and neuronal cells), one-way ANOVA is used, whilst if it is two independent variables (PrP^{Sc} levels after control and prion-infection across different neuronal cultures), a two-way ANOVA is performed. Several types of multiple-comparisons post hoc corrections were used after performing ANOVAs, including Tukey, Dunnett and Šídák. Tukey's multiple comparisons post hoc corrections were used when comparing the means of every group to each other. Dunnett's multiple comparisons post hoc corrections were used when comparing all groups mean to one reference group. And Šídák's multiple comparisons post hoc corrections were used to compare only selected sets of means.

2.10.3 Analysis of Binding Saturation Assays

Two different radiolabelled muscarinic antagonists were used to assess ligand affinity. [^{3}H]-NMS, a non-permeable radioligand, and [^{3}H]-QNB, a permeable radioligand, were utilised in saturation binding assays to determine muscarinic receptor affinity and expression at the plasma membrane and cytosol of neurons.

This saturation binding assay permits to calculate the maximum specific binding, in terms of Bmax, corresponding to muscarinic receptor expression. The assay also allows the calculation of the equilibrium binding constant (KD), corresponding to the ligand concentration required to occupy half of all receptors bound, allowing to calculate ligand affinity. The parameters used to calculate the Bmax and K_D were established by GraphPad Prism using the following model of for one-site specific binding , where X is the radioligand concentration:

$$Specific\ binding\ (Y) = \frac{Bmax \times X}{Kd + X}$$

2.10.4 Analysis of Proteomic data

Microsoft Excel (version 2016), Perseus (version 1.6.12.0), and Scaffold (version 4.11.0) analytical suites were used to upload and analyse raw count data. In order to include a specific protein in the analysis, its corresponding peptides are required to be present in at least three of the four independent datasets. Proteins “only identified by site”, reverse hits and contaminants were excluded from the analysis. Statistical analysis was performed using the Linear Models for Microarray Data (Limma) Package from the R Studio package. Significance was defined as $p < 0.01$. Graphs and plots were made using the R Studio software. Spearman’s correlation was used to create the sample correlation heatmap between all samples from all three groups.

Chapter 3 *In vitro* characterisation of the prion protein and the M1 muscarinic acetylcholine receptor

3.1 Introduction

3.1.1 Prion Protein and M1 mAChR

PrP^C and muscarinic receptors, especially the M1 mAChR, are abundantly expressed in the CNS, specifically in neurons and are mainly localised at the plasma membrane (Levey et al., 1995; Wulf et al., 2017). The prion protein can be seen expressed across all regions of the brain, as well as in the rest of the body, however, no definitive function has been pin-pointed to it. GEMMs knocking out the prion protein have been designed to understand the function behind this highly expressed protein, with mice suffering no detrimental impact from no prion expression, only becoming protected from misfolded prion infection, propagation and disease. Similarly to the prion protein, the M1 mAChR is also abundantly expressed in the brain, especially in neurons in the cerebral cortex and hippocampus (Bradley et al., 2017). The M1 mAChR is the most expressed muscarinic receptor in the brain, having major roles in synaptic plasticity, and in learning and memory mechanisms (Scarr, 2012). GEMMs with the ablation of the *CHRM1* gene (encoding the M1 mAChR) or mutations in the orthosteric pocket or phosphorylation sites have shown a range of phenotypical changes on important functions of the central nervous system including mouse behaviour, and learning and memory (Bradley et al., 2017; Hamilton et al., 1997), pointing out the importance of the M1 mAChR. These same studies have revealed that ablation or mutation of the M1 mAChR has no direct impact on the expression of PrP^C (Scarpa et al., 2021), however, there have been no studies on the impact of PRNP modifications on the expression the M1 mAChR. Connections previously established by our lab (Bradley et al., 2017, 2020; Dwomoh, Rossi, et al., 2022; Scarpa et al., 2021), as mentioned in Chapter 1.4, have demonstrated that the activation of the M1 mAChR has a positive impact on prion diseased mice, making muscarinic receptors a major target for this protein misfolding diseases. Whilst *in vivo* studies have already been performed demonstrating the positive impact of M1 mAChR activation, further assessment of the receptor's pharmacology in primary neuronal cultures utilising a wider range of muscarinic ligands would provide further information in the planification and development of a strategy to treat misfolding prion disease in *in vivo* studies.

3.1.2 Aims

The aims of this chapter are to understand the expression of PrP^C and the M1 mAChR through Western blotting, immunocytochemistry and radioligand binding assays, and to pharmacologically assess the $G\alpha_q$ downstream signalling pathway of the M1 mAChR upon stimulation with muscarinic receptor agonists using a FRET-based IP1 accumulation assay. Distinct immortalised CHO cell lines and primary neuronal culture from several GEMMs will be utilised to assess these aims. The data obtained will be required to later create an *in vitro* model of misfolded prion propagation in primary neuronal cultures, to assess the impact of muscarinic activation on prion propagation.

3.2 Results

3.2.1 M1 mAChR expression in non-transfected, wild-type and DREADD mutant M1 mAChR CHO Flp-In cells

In order to characterise the muscarinic ligands which would be later tested in a model of misfolded prion propagation in neuronal cultures, several initial studies with CHO cell lines were performed to gain a better understanding of the pharmacological properties of these compounds.

Lysates, with the same protein concentration, from CHO cells stably expressing human M1 mAChR or M1-DREADD, both tagged with haemagglutinin (HA) in the C-terminal region, were immunoprecipitated using HA-beads, followed by Western blotting to confirm receptor expression. Immunoblots confirmed the expression of the M1 mAChR and M1-DREADD mAChR receptors in their corresponding cell lines, as seen in Figure 3-1. Expression of the two versions of the hM1 mAChR was validated by the bands present at 45, 55 and 75kDa, representing the different glycosylated forms of the M1 mAChR. As expected, no bands were observed from the non-transfected CHO cell lysates, indicating the lack of M1 mAChR receptor in this cell line.

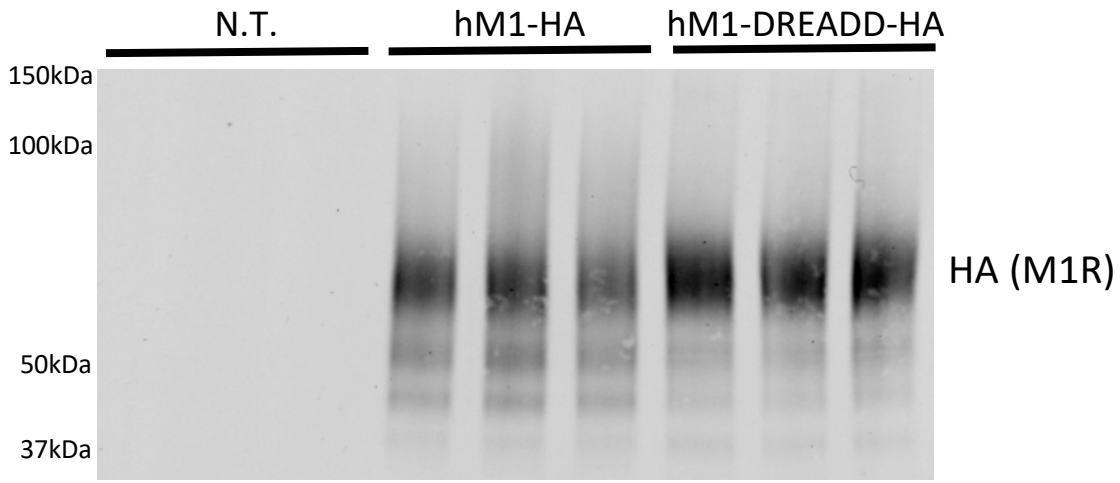

Figure 3-1 Expression of the M1 mAChR in CHO cells. Western blot analysis using anti-HA antibody to confirm M1 mAChR receptor expression in non-transfected CHO cells, hM1-HA wild-type stably transfected CHO cells and hM1-DREADD stably transfected CHO cell lysates after overnight HA pull-down (15µg). Bands come from three independent experiments. (n=3).

To further investigate the receptor expression and localisation, immunocytochemical staining of the three CHO cell lines was performed, probing against the receptor HA-tag. Cells were also stained with DAPI to visualise the cells' nuclei, and therefore understand the localisation of the receptor in respect of the cell's nucleus. Both hM1-HA and hM1-DREADD-HA cells lines showed similar levels of hM1 mAChR expression with the fused HA-tag, mainly distributed at the plasma membrane surface, with smaller levels of expression at cytosolic region of the cell (Figure 3-2). As expected, and already seen with the Western blots, non-transfected wild-type CHO cells showed no staining with the anti-HA antibody, demonstrating that the M1 mAChR is not endogenously expressed by this cell line.

Western blots and immunocytochemical staining allowed to validate the expression of these two versions of the M1 mAChR in their corresponding cell lines, before attempting pharmacological assays to assess the specificity, efficacy and potency of different muscarinic ligands.

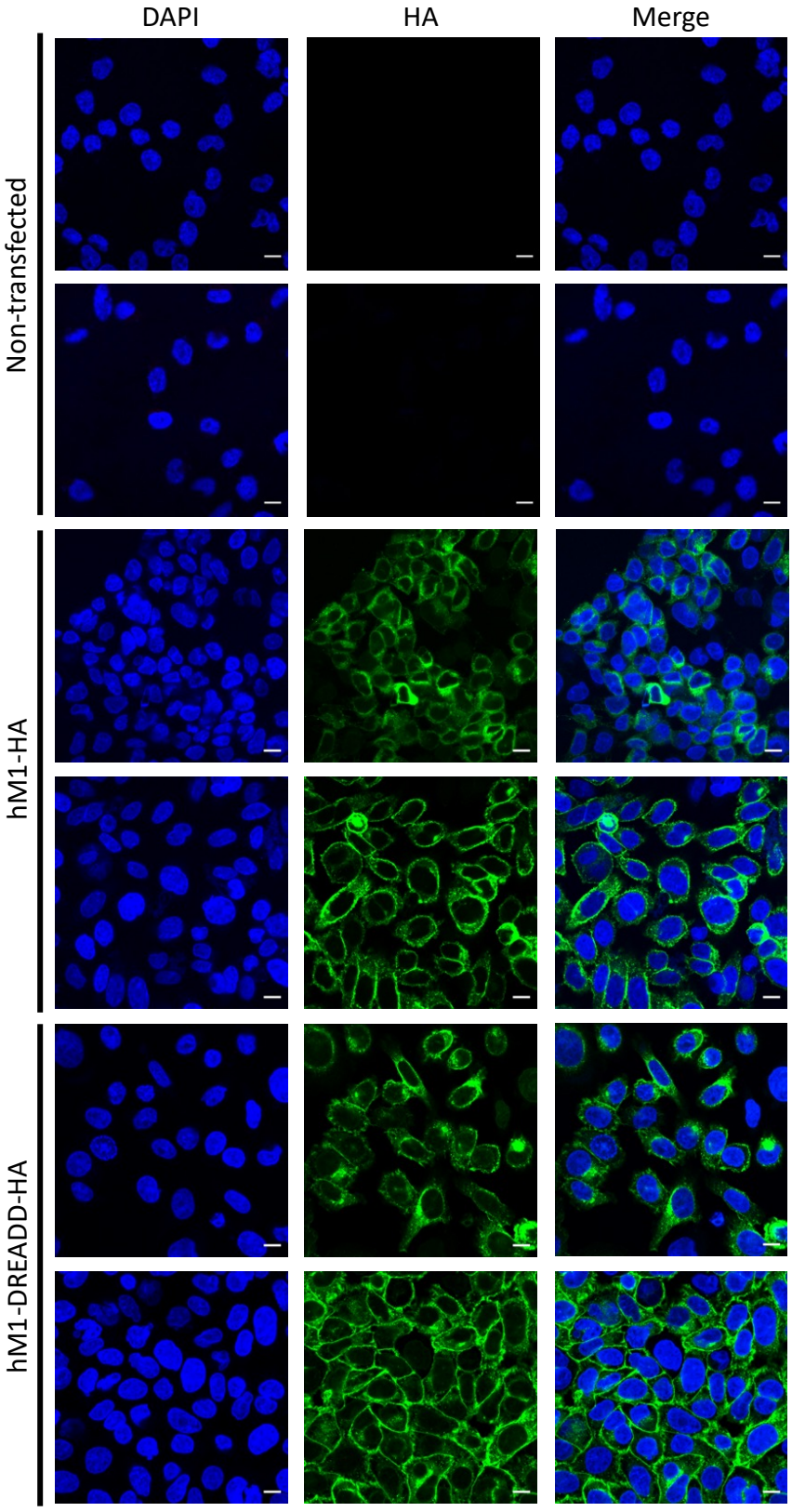

Figure 3-2 M1 mAChR expression in CHO cells. Immunocytochemical staining of non-transfected CHO cells, hM1-HA wild-type stably transfected CHO cells and hM1-DREADD-HA stably transfected CHO cells, using anti-HA antibodies to observe the expression of hM1-HA wild-type and hM1-DREADD-HA receptors. DAPI stained nuclei (blue) and Ha-tagged receptor (green). Scale bar = 10μM.

3.2.2 M1 mAChR pharmacological evaluation in non-transfected, wild-type and DREADD mutant M1 mAChR on CHO Flp-In cells

The M1 mAChR couples to $G\alpha_{q/11}$ proteins, which triggers a canonical downstream signalling pathway leading to calcium release and the activation of the inositide signalling pathway (Dwomoh et al., 2022). A reliable method to measure $G\alpha_{q/11}$ signalling is by testing the accumulation of inositol phosphate (IP1), a substrate of IP3 and by-product of the inositide signalling pathway, with a fluorescence resonance energy transfer (FRET)-based assay. Several muscarinic ligands were used to obtain concentration-response curves for IP1 accumulation enabling us to assess the specificity, potency ($logEC_{50}$) and efficacy (E_{max}) of each compound for the two versions of the hM1 mAChR (Figure 3-3). Acetylcholine, as the natural neurotransmitter of muscarinic receptors, was used as a control to compare against the other ligands being investigated. The other three compounds were: Oxotremorine-M, a full agonist for muscarinic receptors, clozapine-N-oxide, a synthetic ligand which only activates DREADD receptors, and HTL9936, a partial M1 and M4-selective orthosteric ligand (Brown et al., 2021).

Treatment of non-transfected CHO cells (Figure 3-3A) with all four ligands showed no increase in IP1 accumulation due to the lack of expression of $G\alpha_{q/11}$ signalling mAChRs. The same low concentration of IP1 could be detected across all four ligands at all their concentrations, showing a basal constitutive IP1 production by CHO cells. This basal IP1 concentration could also be observed at the lowest ligand concentrations in the other two cell lines, showing the same constitutive production of IP1 by CHO cells. In the stably transfected hM1-HA CHO cells (Figure 3-3B), ACh and Oxo showed identical potency and efficacy, followed by HTL9936 with a significantly reduced potency compared to ACh ($p=0.007$, one-way ANOVA) but high efficacy at the highest concentration (Table 3-1). CNO showed no IP1 accumulation and therefore, no activation of the hM1 mAChR. In contrast and as expected, CNO showed robust potency and efficacy in the hM1-DREADD-HA CHO cells (Figure 3-3C), with Oxo showing high efficacy at 1mM drug treatment concentrations, but potency was reduced by around 2.5-fold, with their $logEC_{50}$ values being -8.15± 0.10 and -4.79± 0.05 ($p=0.004$, one-way ANOVA), respectively (Table 3-1). Acetylcholine and HTL9936 showed no IP1 accumulation when added

to the hM1-DREADD-HA CHO cells, demonstrating that DREADD receptor mutation fully inhibits the receptor activation with the endogenous orthosteric ligand.

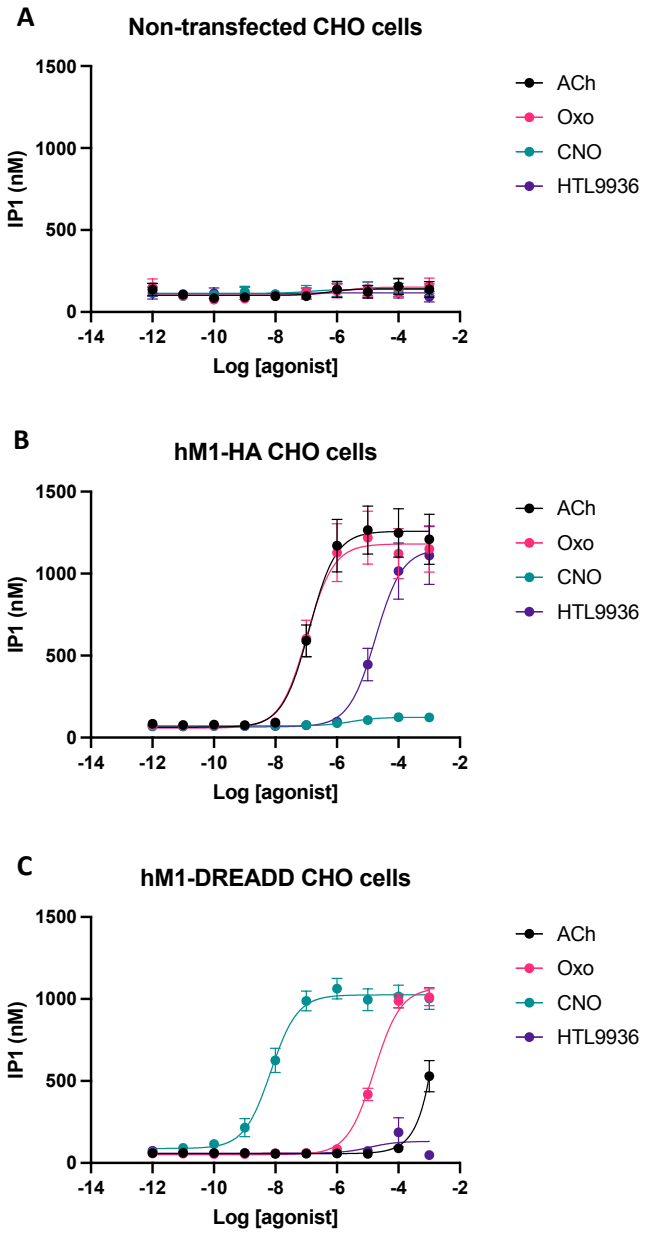

Figure 3-3 Inositol phosphate (IP1) accumulation concentration-response curves in CHO cells via Gq coupled pathways. Agonist-induced IP1 accumulation was measured in **(A)** non-transfected CHO cells, in (**B**) hM1-HA wild-type stably transfected CHO cells and in **(C)** hM1-DREADD-HA stably transfected CHO cells, following treatment with muscarinic receptor ligands. Cells were stimulated with muscarinic receptor agonists for 1 hour ranging from 1mM down to 1pM to allow for an IP1 accumulation concentration-response curve. Results are mean ± SEM of three independent experiments (n=3).

A	IP1 Accumulation LogEC50 (Mean ± SEM) / p-value				N
Ligand	hM1-HA CHO		hM1-DREADD-HA CHO		
	Log EC50	P	Log EC50	P	
Acetylcholine	-6.90 ± 0.15		N.R.	-	3
Oxotremorine M	-6.98 ± 0.16	0.99	-4.79 ± 0.05	0.0004 ***	3
Clozapine-N-Oxide	N.R.	-	-8.15 ± 0.10		3
HTL9936	-4.75 ± 0.14	0.0007 ***	N.R.	-	3

B	IP1 Accumulation Emax (Mean ± SEM) / p-value				N
Ligand	hM1-HA CHO		hM1-DREADD-HA CHO		
	Emax	P	Emax	P	
Acetylcholine	1263 ± 303		N.R.	-	3
Oxotremorine M	1167 ± 310	0.99	1073 ± 80.7	>0.99	3
Clozapine-N-Oxide	N.R.	-	1030 ± 115		3
HTL9936	1066 ± 357	0.93	N.R.	-	3

Table 3-1 Potency and efficacy values of muscarinic receptor ligands in Gq signalling. **(A)** Potency (LogEC50) and **(B)** efficacy (Emax) values were derived from (Figure 3-2). Statistical analysis conducted was ordinary one-way ANOVA (Dunnett's multiple comparisons). Results are mean ± SEM of three independent experiments. (n=3). N.R. = no response. ***=P<0.001.

3.2.3 M1 mAChR and prion characterisation of *in vitro* primary neuronal cultures from different GEMMs

In order to facilitate the use of a more physiologically relevant cell models, M1 mAChR and prion protein expression were characterised in neuronal cultures from several GEMMs (Table 2-8). Time-points of DIV7 and DIV14 were chosen as neuronal cultures display maturity after 7 days of culture (Biffi et al., 2013)and these are the time-points at which other biochemical and pharmacological assays would be later performed. An increased number of processes was observed in neuronal cultures from DIV7 to DIV14 (Figure 3-4), indicating continued neuronal growth as cells attempts to connect with further cells beyond DIV7.

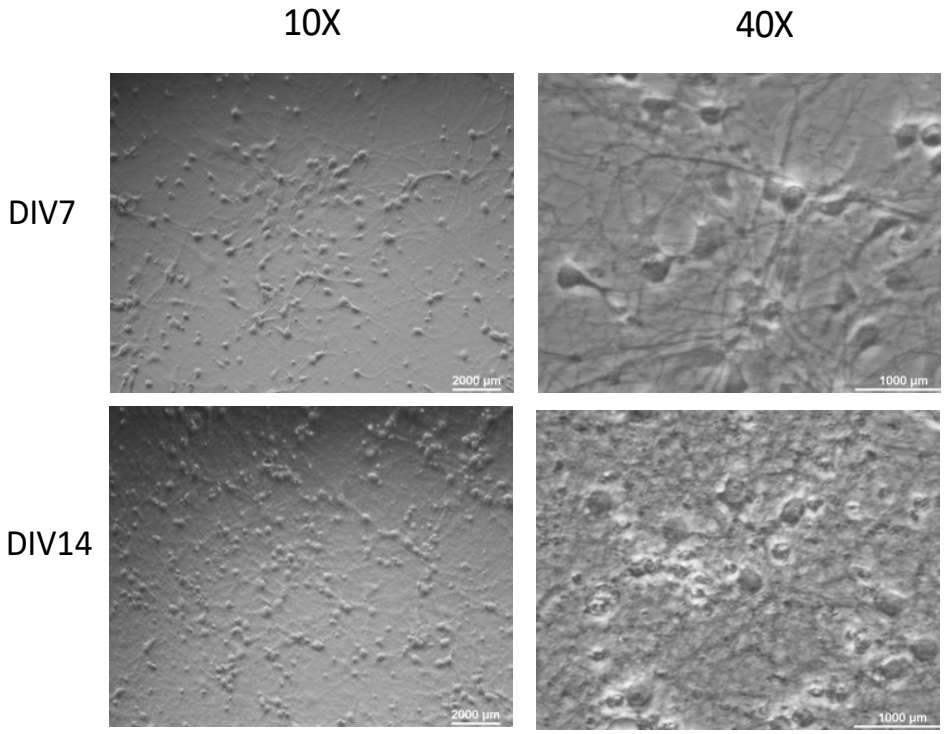

Figure 3-4 Neuron development at DIV7 and DIV14. Light microscope images (10x and 40x magnification) of embryonic mouse primary neuronal cells. Images show neuronal differentiation and growth from at DIV7 and DIV14 since dissection and plating. 10x scale bar = 2000µM, 40x scale bar = 1000µM.

When probing with anti-prion antibody, Prion-KO blots revealed no bands at either time-point as expected, due to the PRNP gene being knocked out from this mouse model (Figure 3-5A). In contrast, Tg37 homozygous (6x Prion) neuronal culture immunoblots showed the typical three band pattern of endogenous prion protein between 30 and 25 kDa as expected; these three bands are likely the unglycosylated, monoglycosylated and diglycosylated forms of the protein (Riesner, 2003). Significantly increased expression levels of endogenous PrP^C over-time were observed, from DIV7 to DIV14 ($p<0.0001$, two-way ANOVA) (Figure 3-5B). When comparing the same time-point, Prion-KO neurons showed a significant reduction in prion expression compared to 6x Prion neurons at both time-points (DIV7 $p=0.016$, DIV14 $p<0.0001$, two-way ANOVA), due to the ablation of the PRNP in the Prion-KO neurons.

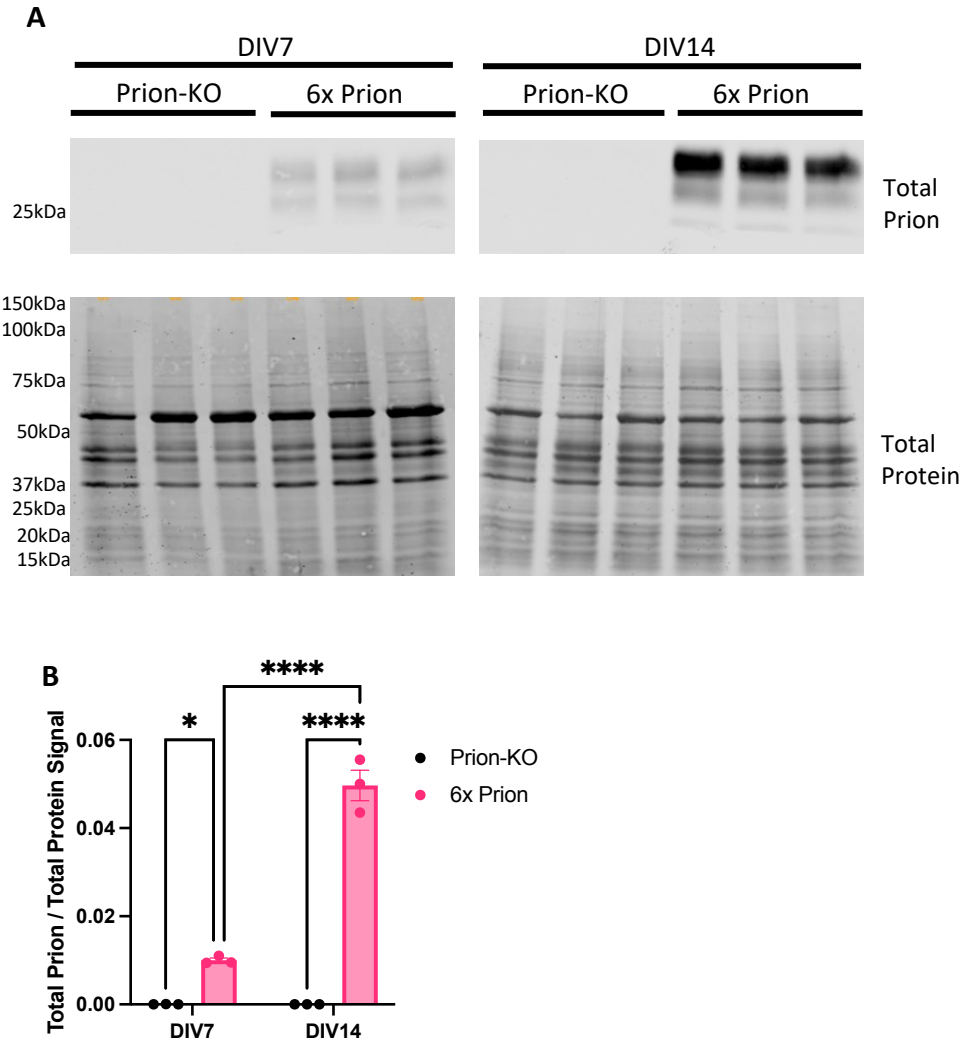

Figure 3-5 Expression of total prion in Prion-KO and 6x prion protein primary neuronal cultures from genetically engineered embryonic mice. (A) Western blot analysis using anti-prion antibodies to confirm and observe changes in protein expression between DIV7 and DIV14 Prion-KO and 6x Prion neuronal culture lysates (10µg). Band pixel intensity signal analysis (EmpiriaStudio) between DIV7 and DIV14 **(B)** prion protein expression normalised to total protein. Statistical analysis conducted was two-way ANOVA (Šídák's multiple comparisons). Data is expressed as mean ± SEM of three independent experiments. (n=3). *=P<0.05, **=P<0.01, ***=P<0.001, ****=P<0.0001.

Analysis of the endogenous levels of PrP^C demonstrated an increasing trend was observed from DIV7 to DIV14 in all 3 strains (Figure 3-6A,B), with only M1-HA Wt demonstrating a significant increase in prion expression (p=0.014, two-way ANOVA). More interestingly, M1-HA Wt neurons showed significantly higher levels of PrP^C compared to the M1-DREADD (p=0.026, two-way ANOVA) strains at DIV14 but not at DIV7.

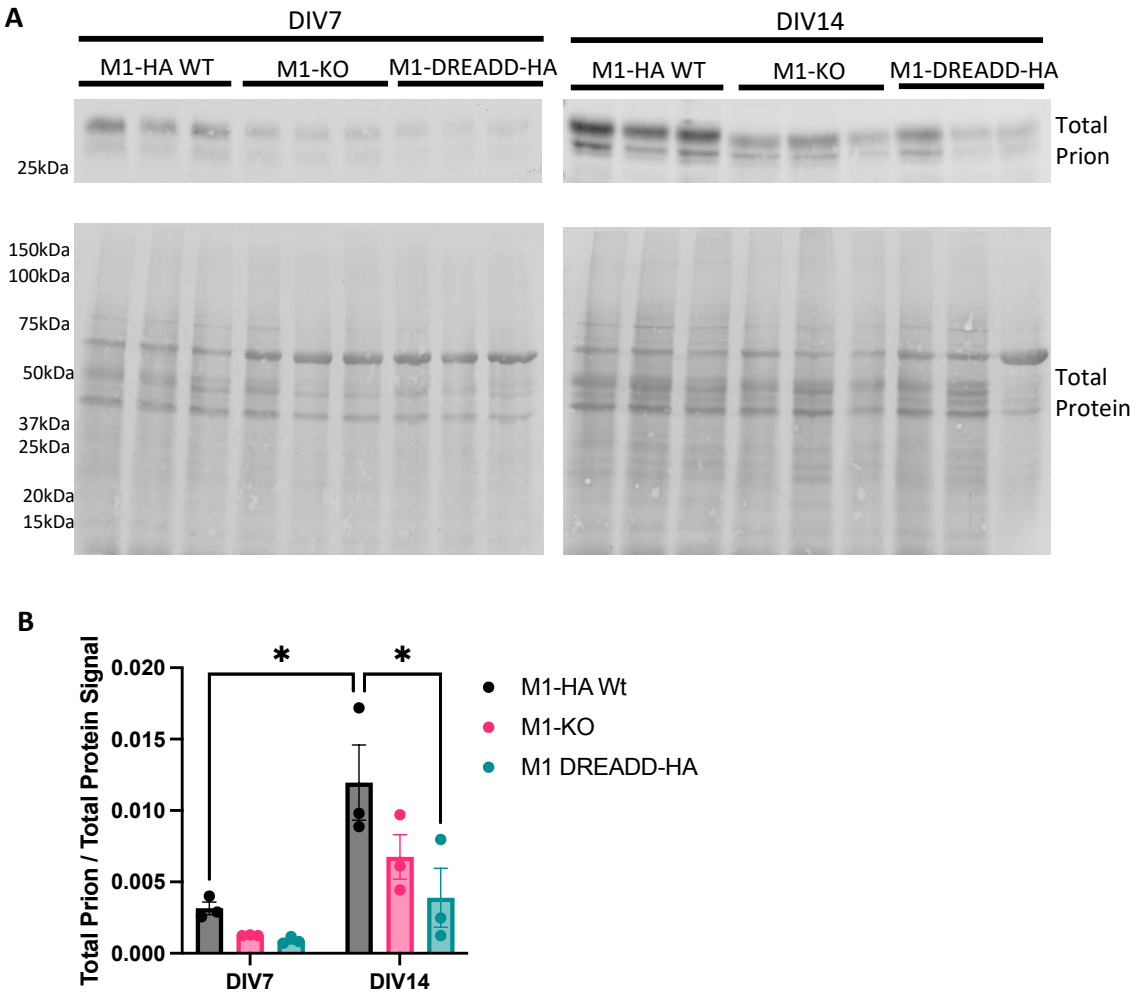

Figure 3-6 Expression of total prion in M1-HA Wt, M1-KO and M1-DREADD-HA primary neuronal cultures from genetically engineered embryonic mice. (A) Western blot analysis using anti-prion antibodies to confirm and observe changes in protein expression between DIV7 and DIV14 M1-HA Wt, M1.KO and M1-DREADD-HA neuronal culture lysates (10µg). Band pixel intensity signal analysis (EmpiriaStudio) between DIV7 and DIV14 **(B)** prion protein expression normalised to total protein. Statistical analysis conducted was two-way ANOVA (Šídák's multiple comparisons). Data is expressed as mean ± SEM of three independent experiments. (n=3). *=P<0.05, **=P<0.01.

Immunocytochemistry of DIV14 neuronal allowed for observation of the location of receptor or prion protein within the neurons. As expected, Prion-KO cultures showed no expression of the endogenous PrP^C (Figure 3-7A, validating the results obtain from the Western blots (Figure 1-5). In contrast, 6x Prion showed very high levels of endogenous prion expression in the cultures, with the majority expressed in the outer membrane of processes and cell bodies of all neurons (Figure 3-7B).

Staining with anti-HA antibody for the HA tagged M1 mAChR demonstrated expression in both the M1-HA Wt and M1-DREADD-HA neurons, with high levels of expression being located in the plasma membrane of both processes and cell

bodies of the neurons (Figure 3-7D,E). Meanwhile M1-KO neurons were negative for HA staining (Figure 3-7C). Interestingly, M1 mAChR expression was also observed in the soma in the M1-DREADD-HA strain, suggesting potential constitutive internalisation of the receptor (Figure 3-7E). M1-HA, M1-KO and M1-DREADD-HA neurons all showed PrP^C expression in a consistent manner, being expressed across the outer membrane of all neurons and showing the same distribution as the 6x Prion strain.

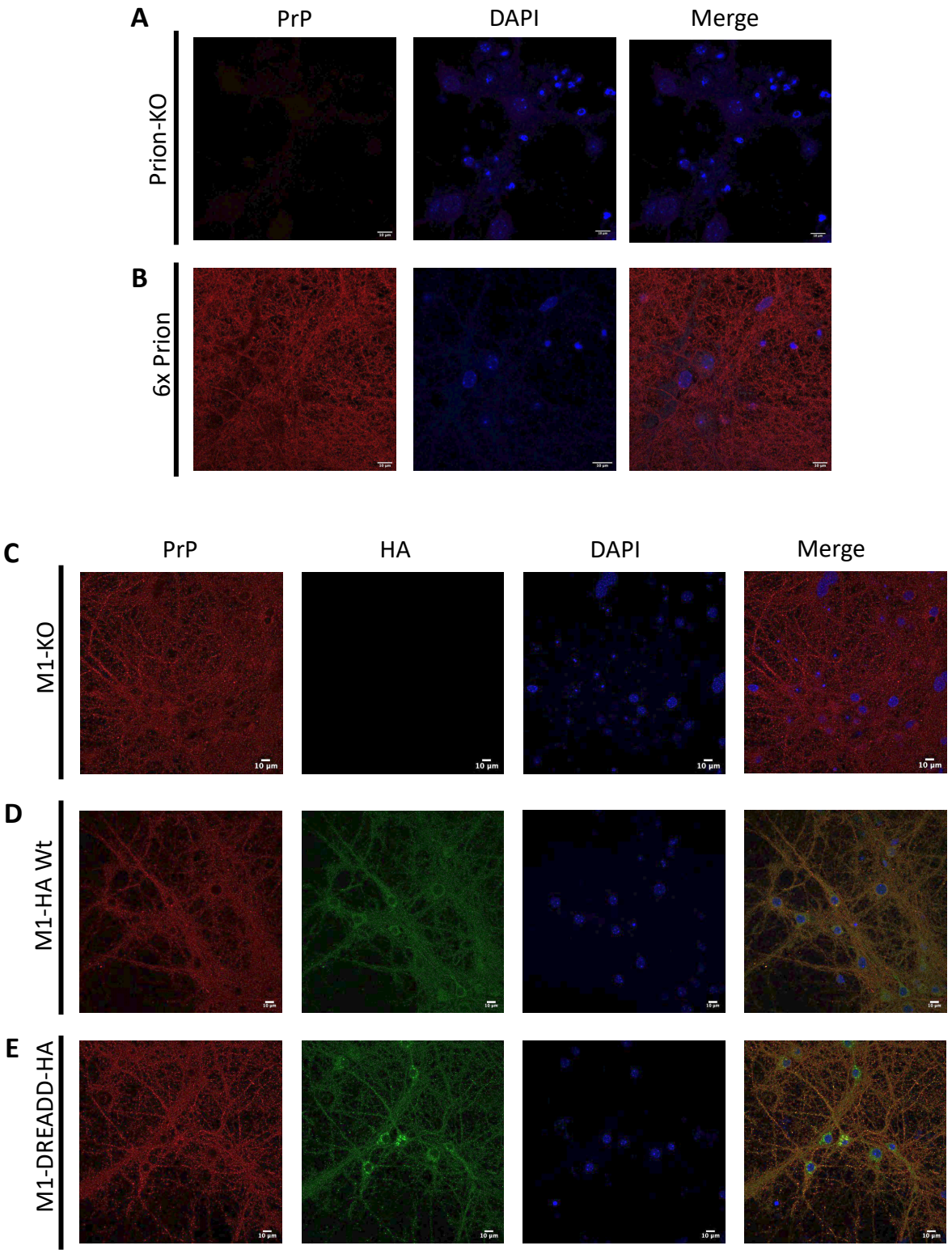

Figure 3-7 M1 mAChR and total prion expression in primary neuronal cultures. Immunocytochemical staining at DIV14 of **(A)** Prion-KO, **(B)** 6x Prion, **(C)** M1-KO, **(D)** M1-HA Wt and **(E)** M1-DREADD-HA. Scale bar = 10µm. PrP stained prion (red), HA stained HA-tagged receptor (green) and DAPI stained the nuclei (blue). Scale bar = 10µM.

Radioligand saturation binding assays, using tritiated N-methyl-scopolamine ([3H]-NMS), were performed to further quantify the expression levels of muscarinic receptors at the neuron cell surface. NMS is an antagonist for all five muscarinic receptors, binding to their orthosteric site. The assays were carried out on all prion-expressing neuronal cultures: 6x Prion, M1-HA, M1-KO and M1-DREADD-HA neurons.

M1-HA Wt neuronal cultures expressed comparable levels of all muscarinic acetylcholine receptors compared to 6x Prion (Figure 3-8A,B), with similar K_D (equilibrium disassociation constant) and Bmax (total concentration of receptors) values (M1-HA Wt K_D = 0.40 and Bmax = 630.2 fmol/mg; 6x Prion K_D = 0.27 and Bmax = 686.4 fmol/mg) (Table 3-2). M1-KO neurons showed a significant reduction in the Bmax (223.1 fmol/mg) compared to the 6x Prion ($p=0.0002$, one-way ANOVA) (Figure 3-8C). Finally, the M1-DREADD-HA neurons (Figure 3-8D) showed similar levels of muscarinic expression as the M1-KO (Bmax = 269 223.1 fmol/mg) and significantly lower than 6x Prion ($p=0.0004$, one-way ANOVA). Muscarinic receptor affinity for ([3H]-NMS) showed no significant difference when comparing M1-KO and M1-DREADD-HA neurons to M1-HA Wt (M1-KO $p=0.93$; M1 DREADD $p=0.4$, one-way ANOVA) (Table 3-2).

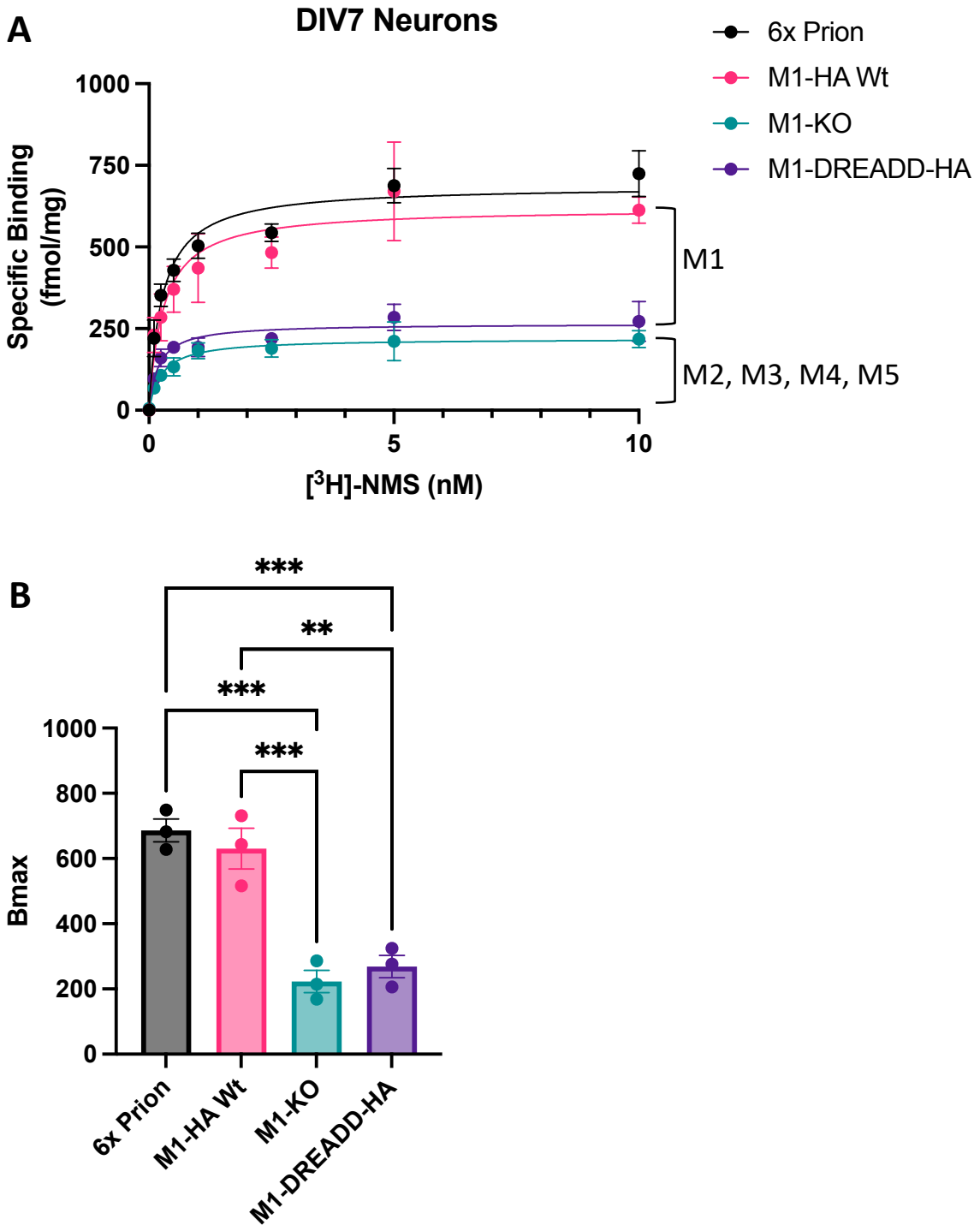

Figure 3-8 Muscarinic receptor expression levels across different primary neuronal cultures from different GEMMs. (A) Radioligand saturation concentration-response curve and **(B)** maximum specific binding (Bmax) values comparing of DIV7 6x Prion, M1-HA, M1-KO and M1-DREADD-HA primary neuronal cultures, following treatment with muscarinic receptor specific radioligand [^{3}H]-NMS. Neurons were stimulated for 2 hours with [^{3}H]-NMS concentrations ranging from 10nM to 0.1nM for a radioligand saturation concentration-response curve. Statistical analysis conducted was ordinary one-way ANOVA (Sidaks multiple comparisons). Results are mean ± SEM of three independent experiments (n=3). Specific binding results were normalised to the protein concentration of three independent wells with the same number of plated neurons. **=P<0.01, ***=P<0.001.

Strains	[^{3}H]-NMS Saturation Binding				*N*
	Bmax ± SEM	***P***	**Kd ± SEM**	***P***	
6x Prion	686.4 ± 35.0		0.27 ± 0.03		3
M1-Wt	630.2 ± 62.5	0.77	0.40 ± 0.18	0.75	3
M1-KO	223.1 ± 34.4	0.0002 ***	0.31 ± 0.12	0.99	3
M1-DREADD-HA	269.0 ± 34.1	0.0004 **	0.21 ± 0.05	0.96	3

Table 3-2 Maximum specific binding and affinity values of muscarinic receptor ligands in Gq signalling of primary neuronal cultures. Maximum specific binding (Bmax) and affinity (Kd) values were derived from (Figure 3-8). Statistical analysis conducted was ordinary one-way ANOVA (Dunnett's multiple comparisons) comparing each individual strain to 6x Prion. Results are mean ± SEM of three independent experiments. (n=3). **=P<0.01, ***=P<0.001.

3.2.4 M1 mAChR pharmacological evaluation of primary neuronal cultures from several GEMMs

IP1 accumulation assays were used again to characterise the same orthosteric ligands discussed before (Chapter 1.2.2) in several strains of primary neuronal cultures to understand $G\alpha_{q/11}$ protein-dependent signalling. In the 6x Prion and M1-HA Wt neuronal cultures, Oxo-M induced IP1 accumulation with similar potency ($logEC_{50}$) and efficacy (E_{max}) compared to the endogenous neurotransmitter ACh (Figure 3-9A,B and Table 3-3A,B). HTL9936, the partial M1 and M4 selective agonist, showed a nearly significant reduction in potency and significantly reduced efficacy ($logEC_{50}$ p=0.05, E_{max} p=0.0007, one-way ANOVA) compared to ACh in 6x Prion neurons, and significantly reduced efficacy (E_{max} p=0.0001, one-way ANOVA) compared to ACh in M1-HA Wt neurons. In both neuronal strains, CNO induced no IP1 accumulation, as expected. In contrast, the M1-KO neurons showed no IP1 accumulation from either CNO or HTL9936 treatment, but very low levels of IP1 accumulation were observed with both ACh and Oxo-M (Figure 3-9C). When assessing the M1-DREADD-HA neurons, treatment with ACh and Oxo-M induced

similar IP1 accumulation compared to M1-HA Wt cultures (Figure 3-9D). CNO, the synthetic ligand designed for the M1-DREADD-HA receptor, did activate the modified receptor with a similar potency to ACh and Oxo, however efficacy was reduced by 50% in comparison (Figure 3-9D and Table 3-3A,B). HTL9936 showed no response in M1-DREADD-HA neurons.

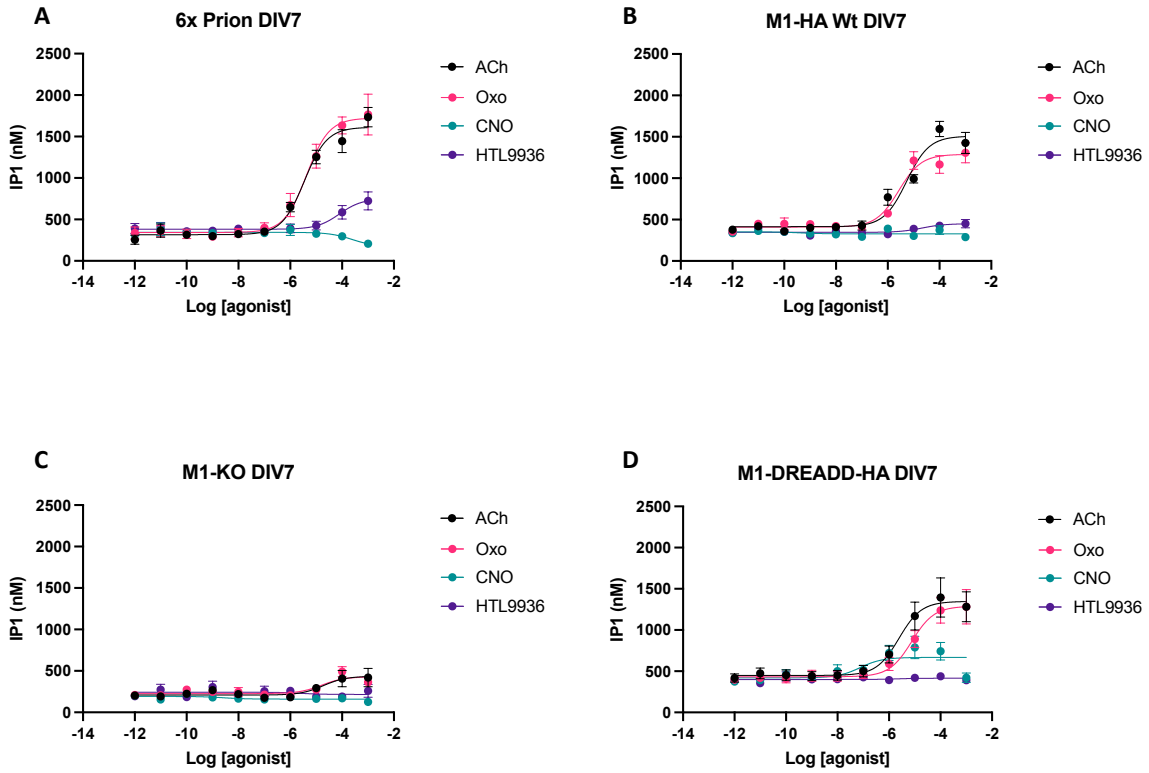

Figure 3-9 Inositol phosphate (IP1) accumulation concentration-response curves in primary neuronal cultures via Gq coupled pathways. Agonist-induced IP1 accumulation was measured in DIV7 **(A)** 6x Prion, **(B)** M1-HA, **(C)** M1-KO and **(D)** M1-DREADD-HA primary neuronal cultures, following treatment with muscarinic receptor ligands. Cells were stimulated with muscarinic receptor agonists for 1 hour ranging from 1mM down to 1pM to allow for an IP1 accumulation concentration-response curve. Results are mean ± SEM of three independent experiments and six for the M1-DREADD-HA neurons (n=3/6).

A	IP1 Accumulation LogEC50 (Mean ± SEM) / p-value								N
Ligand	6x Prion		M1-HA Wt		M1-KO		M1-DREADD-HA		
	Log EC50	P	Log EC50	P	Log EC50	P	Log EC50	P	
Acetylcholine	-5.47 ± 0.07		-5.27 ± 0.13		-4.73 ± 0.42		-5.69 ± 0.26	0.84	3
Oxotremorine M	-5.37 ± 0.09	0.99	-5.58 ± 0.16	0.97	-4.78 ± 0.44	0.99	-5.06 ± 0.22	0.67	3
Clozapine-N-Oxide	N.R.	-	N.R.	-	N.R.	-	-6.91 ± 0.55		3
HTL9936	-4.11 ± 0.16	0.007 **	-4.68 ± 0.67	0.58	N.R.	-	N.R.	-	3

B	IP1 Accumulation Emax (Mean ± SEM) / p-value								N
Ligand	6x Prion		M1-HA Wt		M1-KO		M1-DREADD-HA		
	Emax	P	Emax	P	Emax	P	Emax	P	
Acetylcholine	1619 ± 234		1526 ± 109		569 ± 202		1874 ± 406	0.14	3
Oxotremorine M	1698 ± 282	0.99	1294 ± 44.5	0.24	417 ± 16.7	0.67	1760 ± 388	0.20	3
Clozapine-N-Oxide	N.R.	-	N.R.	-	N.R.	-	911 ± 52.1		3
HTL9936	751 ± 218	0.05	541 ± 133	0.0001 ***	N.R.	-	N.R.	-	3

Table 3-3 Potency and efficacy values of muscarinic receptor ligands in Gq signalling of primary neuronal cultures. (A) Potency ($LogEC_{50}$) and **(B)** efficacy (Emax) values were derived from (Figure 3-9). Statistical analysis conducted was ordinary one-way ANOVA (Dunnett's multiple comparisons). Results are mean ± SEM of three independent experiments and six for the M1-DREADD-HA neurons (n=3/6). Normalised response graphs used acetylcholine (ACh) as the reference agonist for both 6x Prion and M1-HA neuronal cultures, and ACh from M1-HA neurons was used as reference for M1-KO neuronal cultures. Clozapine-N-Oxide (CNO) was used as reference for the M1-DREADD-HA neuronal culture experiments. N.R. = no response. **=P<0.01, ***=P<0.001.

3.3 Discussion

In this chapter, the aim was to characterise the expression of both PrP^C and M1 mAChR across several immortalised and primary cellular models. In addition, canonical signalling properties of muscarinic receptors were tested, specifically the M1 mAChR, with both natural and synthetic muscarinic receptor ligands. CHO cell lines showed high expression of the different human M1 mAChR variants expressed, and the FRET-based IP1 accumulation assay demonstrated the potency, efficacy and affinity of all the ligands to the different M1 mutants. Several primary neuronal culture strains were used as a more translational approach, in which differences in prion and M1 mAChR expression across the neuronal cultures tested were observed. Expression of prion was shown through Western blotting, whilst radioligand binding assays demonstrated higher quality in determining the expression of the muscarinic receptors, specifically the M1. Immunocytochemical images revealed the localisation of PrP^C and M1 mAChR in the different neuronal strains. IP1 accumulation assays provided further insight of the specificity of each ligand for the M1 mAChR, the $G\alpha_q$ signalling attributed to the M3 and M5 mAChRs, and an unexpected activation of the M1-DREADD-HA mAChR with ACh.

Robust expression of the hM1 mAChR variants was first demonstrated in the distinct CHO cell lines, before performing $G\alpha_{q/11}$ signalling assays to test several muscarinic compounds. An interesting observation from the immunoblots showing M1 mAChR expression in both the HA and DREADD cell lines was the different bands seen for the hM1 mAChR, at 45, 55 and 75kDa. This suggests the presence of post-translationally modified forms of the M1 mAChR (Liang et al., 1987), with the most intense band at 75kDa reflecting the mature form of the receptor. As muscarinic receptors are glycoproteins, with the M1 mAChR having two potential N-glycosylation sites (Haga, 2013), difference in carbohydrate moiety between receptor forms could explain the presence several bands. In addition, Ohara et al. (1990) have previously shown a decrease in the M1 mAChR size by 20kDa after treatment with endoglycosidase-F, catalysing the deglycosylation of the receptor, corroborating the distinct size bands observed for M1 mAChR.

FRET-based IP1 accumulation assays reiterated data previously published on the distinct ligands' pharmacological properties when activating variants of the hM1

mAChR. ACh and Oxo demonstrated efficacious and potent hM1 mAChR activation of the hM1-HA, previously reported by Khajehali et al., (2020). In contrast, CNO showed no response in this cell line (Thompson et al., 2018; Bradley et al., 2020), due to the absence of any DREADD receptor. HTL9936 managed to reach a similar efficacy as both ACh and Oxo, however, a much reduced potency due to its partial agonist properties (Brown et al., 2021). Assessment of the hM1-DREADD-HA cells showed no response by ACh up to the highest concentration, 1μM, resulting in a peak accumulation of IP1. Whilst the receptor mutation is designed to be unresponsive to the endogenous neurotransmitter, the IP1 accumulation response could potentially be a result of the capability of the hM1-DREADD-HA receptor to bind ACh at very high concentrations. This has previously been reported using the same hM1-DREADD-HA receptor (Khajehali et al., 2020; Thompson et al., 2018), using the hM3-DREADD receptor and ACh (Armbruster et al., 2007) and also in different DREADD-mutated GPCRs, such as FFA2-DREADD (Bolognini et al., 2019), where the endogenous ligand propionate, is able to activate the mutated receptor at similar high concentrations. A binding affinity assay could be performed at this stage to test this hypothesis, however, due to the high concentration of ACh required to activate the hM1-DREADD-HA receptor, this result is acknowledged as a non-physiological concentration which could impact further studies. CNO provided the highest potency and efficacy of all four ligands in the M1-DREADD-HA cell line, as this ligand was specifically synthesised to activate DREADD mutated receptors (Armbruster et al., 2007). In addition, Oxo showed good efficacy, however a much lower potency than CNO, suggesting a lower affinity of Oxo for the M1-DREADD modified orthosteric pocket compared to the wild-type orthosteric pocket. Finally, HTL9936 showed no response due to the receptor's mutation (Khajehali et al., 2020). These pharmacological experiments corroborated data previously published on ligand specificity, potency and efficacy in the different CHO cell lines, but also allowed us to first-hand test this assay and compounds before moving into primary cultures, where data with several of these ligands and neuronal strains planned to be used, had never been published before.

As the main aim of this project was to create an *in vitro* model of prion infection and propagation in primary neuronal cultures in which to test the impact of different muscarinic ligands in PrP^{Sc} deposition, understanding if expression or mutations of PrP^{C} and the M1 mAChR have a direct impact on one another was the

initial characterisation required. Investigation of the muscarinic neuronal strains revealed PrP^C to have a decreasing trend in expression in M1-KO and a significant reduction in M1-DREADD-HA neurons compared to the M1-HA Wt neurons at DIV14. This could potentially suggest that the ablation of M1 mAChR, or lack of endogenous activation, has an detrimental impact on PrP^C expression. However, immuno-stained images of M1-HA Wt, M1-KO and M1-DREADD-HA neurons at the same time-point showed similar levels and pattern of PrP^C expression across all three neuronal strains. These images correlate with transcript data showing no difference in PrP^C transcript levels between M1-HA Wt and M1-KO mice (Scarpa et al., 2021), and although no transcript data for the M1-DREADD-HA mice is available, it was expected to have similar levels to the M1-HA Wt and M1-KO mice. In addition, PrP^C was shown to increase from DIV7 to DIV14 in the majority of neuronal strains. Primary neurons, in contrast to immortalised CHO cells, are non-proliferating primary cells which differentiate, expanding their axons and dendrites, making connections between them (Gordon et al., 2013). This continuous growth of neuron size over time is directly responsible for the increase in protein expression from DIV7 to DIV14, with the maturation process continuing, changing the biochemistry and physiology of the neurons (Dawson & Dawson, 1996).

Immuno-stained images of the neuronal strains revealed PrP^C expression throughout all cultures, except in Prion-KO neurons. This data agrees with previous studies which show that the endogenous prion protein is expressed abundantly in the outer membrane of neuronal cells (Mironov et al., 2003; Wulf et al., 2017). M1 mAChR showed similar localisation to PrP^C, with its expression covering the plasma membrane of all neurons, as previously observed in other studies (Levey et al., 1995). In addition, both M1-HA Wt and M1-DREADD-HA neurons showed some receptor expression within the cytoplasm. Intracellular expression of the M1 mAChR has previously been reported in rat hippocampal neurons in components corresponding to the Endoplasmatic Reticulum and Golgi apparatus (Anisuzzaman et al., 2013), were the M1 mAChR is synthesised, modified and trafficked.

M1 mAChR expression in neuronal cultures was further investigated with radioligand binding assay, to validate expression at a higher quality than

performed with immunoblots. Similar Bmax and K_D levels between 6x Prion and M1-HA Wt neurons demonstrated that the addition of an HA-tag to the endogenous M1 mAChR does not affect receptor expression or the affinity of ligands at the orthosteric pocket. This is also observed in neuronal cultures and animal tissue from mice with a mEGFP tag on the M1 mAChR (Marsango et al., 2022), demonstrating that the addition of a tag to the C-terminal of the receptor does not alter expression or orthosteric pocket binding. The significant Bmax reduction observed in the M1-KO neurons corresponds to the ablation of the CHRM1 gene from this strain, revealing that two thirds of muscarinic expression in 6x Prion and M1-HA Wt neurons is M1 mAChR, whilst the other third of muscarinic receptor expression is divided between the other four receptors. This has previously been reported by Marsango et al. (2022), where they have shown around 50% reduction in muscarinic receptor expression in cortical and hippocampal tissue of M1-KO mice compared to M1-WT mice. Several other studies have also shown that the M1 mAChR accounts for around 60% of all muscarinic receptors expressed within the brain (Buckley et al., 1988; Levey, 1993; Volpicelli & Levey, 2004). All this data also reveals the ablation of the CHRM1 gene does not lead to increased expression of any other muscarinic receptor in order to compensate the lack of M1 mAChR expression and subsequent downstream signalling. M1-DREADD-HA neurons showed a similar Bmax to M1-KO neurons, consistent with previous results from our lab (Brooke, 2018), due to the orthosteric radioligand used in this assay being unable to bind to the mutated M1 DREADD mAChR. However, immuno-stained images clearly demonstrate that the M1-DREADD-HA neurons do express a mutated version of the M1 mAChR.

$G\alpha_{q/11}$ downstream signalling was tested to understand the specificity, efficacy and potency of the distinct ligands across the different M1 mAChR variant neuronal strains, to later test the same compounds in the neuronal *in vitro* model of prion infection and propagation. Similar potency and efficacy levels of ACh and Oxo in both 6x Prion and M1-HA Wt neuronal cultures demonstrated again that the HA-tag in the C-terminus of the receptor does not alter the orthosteric binding pocket or the $G\alpha_{q/11}$ downstream signalling. Marsango et al. (2022) also showed no changes in $G\alpha_{q/11}$ downstream signalling when investigating M1 mAChR tagged with mEGFP compared to M1-WT, corroborating the IP1 data obtained with 6x Prion and M1-HA Wt neuronal cultures. Treatment of the same two strains with

CNO resulted in no IP1 accumulation, as previously seen in the hM1-HA CHO cell lines, whilst HTL9936 revealed reduced levels of IP1 accumulation in comparison to ACh and Oxo, with both reduced efficacy and potency due to only activating the M1 mAChR and its partial agonistic properties (Brown et al., 2021). M1-KO neurons showed no IP1 accumulation by CNO, as no DREADD receptor was expressed, and by HTL9936, due to the lack of M1 mAChR expression in these cultures. The highest concentrations of ACh and Oxo showed limited IP1 accumulation in comparison to levels seen in 6x Prion and M1-HA Wt neurons due to the absence of M1 expression. The observed IP1 accumulation is a result of M3 and M5 mAChR activation (Dwomoh et al., 2022), the other two muscarinic receptors which signal through $G\alpha_{q/11}$ proteins, which are still expressed in these M1-KO cells as seen from the radioligand binding assays. Treatment of M1-DREADD-HA neurons resulted in very unexpected IP1 accumulation from ACh and Oxo treatments, at similar concentrations as seen with CNO activation. Whilst the EC_{50} for all three ligands was very similar, the efficacy, although not significantly different, was doubled by both ACh and Oxo compared to CNO. This was unforeseen, as the levels of IP1 accumulation expected from ACh and Oxo in M1-DREADD-HA neurons were to be similar to the levels observed in the M1-KO strain. These results were contrary to the data observed with the hM1-DREADD CHO cells, as the wild-type M1 mAChR is ablated from the M1-DREADD-HA animals before knocking in the mutated M1 DREADD mAChR, inhibiting the binding and activation of ACh to the receptor, therefore expecting a lower level of accumulation from only M3 and M5 mAChR activation. Results were also contrary to *in vivo* and *ex vivo* experiments with M1-DREADD-HA mice and tissue performed by our lab (Bradley et al., 2020). IP1 accumulation data from the M1-KO neurons demonstrates however, that the IP1 accumulation observed from these treatments is not an off target effect. This suggests the possibility of $G\alpha_q$ downstream signalling from a heterodimer complex formation by M1-DREADD and the other muscarinic receptors. This can occur through two ways; the formation of the heterodimer changes the predominant second messenger through which a protomer signals, or the ligand for one of the heterodimer's receptors is able to transactivate both receptors through the hetoromer (Dale et al., 2022). To begin, Goin & Nathanson (2006) have previously reported through BRET studies the ability of the M1 mAChR to form stable heterodimers with the M2 and M3 mAChR, proving the possibility of muscarinic heterodimers occurring in the M1-DREADD-HA

neurons. In addition, heterodimer studies have demonstrated the change from $G\alpha_s$ to $G\alpha_l$ coupling of the D1 dopamine receptor when forming a heteromer with the H3 histamice receptor (Jarrahian et al., 2004), as well as the change from $G\alpha_i$ to $G\alpha_s$ coupling of the CB1 cannabinoid receptor when forming a heteromer with the D2 dopamine receptor (Ferrada et al., 2009), suggesting the possibility of a predominant second messenger change after the muscarinic heteromer formation. Another possibility, as previously reported for the heterodimer formed of the MT2 melatonin receptor and 5-HT_{2C} serotonin receptor, is that melatonin is able to transactivate the 5-HT_{2C} receptor within the MT2-5-HT_{2C} receptor heteromer (Kamal et al., 2015). These GPCR heteromer result support the possibility of $G\alpha_q$ downstream signalling after ACh and Oxo activation of any M1-DREADD heterodimers formed in the M1-DREADD-HA neuronal cultures, providing a possible explanation for the high concentration of IP1 accumulation observed in this data.

The biochemical and pharmacological characterisation of both proteins of interest in this chapter will allow us to design and carry out the next stage of this project, where a novel *in vitro* model of prion infection and propagation will be created to test the impact of different ligands in the progression of PrP^{Sc} accumulation in neurons.

Chapter 4 Role of the M1 mAChR in a new prion infection model of *in vitro* primary neuronal cultures

4.1 Introduction

4.1.1 Prion disease mouse model

The prion disease mouse model our laboratory uses is based on the inoculation of RML into Tg37 hemizygous (3x Prion) mice, a transgenic MloxP mouse line that expresses approximately 3 times more levels of PrP^{C} than wild-type mice (Mallucci et al., 2002). The inoculum used for this prion disease mouse model consists of 20µl of 1% /w/v) brain homogenate from RML PrP^{Sc}-diseased mice (Bradley et al., 2017; Mallucci et al., 2003). These mice are manually intracerebrally inoculated with RML inoculum at the age of 3 to 6 weeks, flooding the animal's brain, to induce progressive prion disease. Around 12 weeks post-inoculation (w.p.i.) animals reach their terminally sick stage at which animals are humanly killed (Mallucci et al., 2003). As control, 3x Prion mice were inoculated with NBH, obtained from healthy animals. The lab has previously conducted time-course experiments with RML inoculated mice to understand the different biochemical and pathological characteristics of this specific strain prion disease. RML inoculated mice start to show PrP^{Sc} deposition in different brain regions, including the cortex, hippocampus and thalamus at 8 w.p.i., with levels increasing up to terminal stage (Scarpa, 2022). Markers of neurodegeneration and neuroinflammation such as APO-E and Clusterin are significantly increased over-time in the striatum, whilst SerpinA3N is also significantly increased in the cortex and hippocampus, showing disease progression (Scarpa, 2022). Spongiosis, astrogliosis and microgliosis are other phenotypic features of this prion disease model, with increased astrocyte and microglia reactivity correlation with disease progression. Finally, around 12 w.p.i., mice reach their terminal stage, presenting confirmatory indicators, and are therefore sacrificed. These indicators include ataxia, impairment of righting reflex, dragging of limbs, sustained hunched posture, and significant abnormal breathing.

Whilst this is the standard prion mouse model our lab uses, as well as being the model from which RML brain homogenates are used as future inoculum, other GEMMs are also inoculated with RML for different studies. These GEMMs all carry mutations, knock-ins or knock-outs of mAChRs, and therefore carry only one copy of the PRNP gene, subsequently leading to wild-type level expression of the

endogenous prion protein. Prion disease features, such as spongiosis, astrogliosis and microgliosis, are very similar to that of the tg37 hemizygous mouse model, however, the time-course of disease is longer due to the lower levels of endogenous PrP^C expression, with terminal disease stage being reached around 24 w.p.i. (Scarpa, 2022; Scarpa et al., 2021)

4.1.2 Cellular models of prion

Another strategy to study prion disease is the use of cellular models of prion infection and propagation, both in immortalised and non-immortalized cells. To create immortalized cell models supporting mouse prion propagation, scrapie prions had to firstly be "adapted" to the mouse PrP^C sequence (Chandler, 1961), in order to enable infection of mouse PrP^C due to the lack of naturally occurring prion disease in mice. This adaptation of scrapie prions to the mouse prion sequence led to the development of the Chandler/RML PrP^{Sc} strain, the most utilized PrP^{Sc} strain in the prion research field (Chandler, 1961). As mentioned above, other mouse prion strains were created, such as the ME7 and the 22L strains. A variety of immortalized cell lines have been used with these mouse scrapie strains to investigate prion infection, propagation and toxicity *in vitro*. Neuron-like cell lines include SMB-PS, N2a, GT1, CAD5, CBRL and 1C11 cells, all derived from different regions of the brain and all susceptible to prion infection by one or more mouse PrP^{Sc} strains (Berry et al., 2013; Birkett et al., 2001; Mahal et al., 2007; Mays et al., 2008; Mouillet-Richard et al., 2008; Nishida et al., 2005). More specifically, prion-infected mouse N2a neuroblastoma cells (ScN2a) have been the most widely used neuron-like immortalized cell lines to study prion propagation (Butler et al., 1988). However, CAD5 catecholaminergic cells have recently become more used due to their higher susceptibility to different mouse prion strains (Berry et al., 2013). These immortalized cell lines have also been genetically engineered over the years to improve the understanding of prion diseases. For example, the N2a #58 cells have been developed to over-express the PrP^C in N2a cells by six-fold (Nishida et al., 2000), allowing for more prolonged and higher levels of PrP^{Sc} infection, and therefore being more suitable models to assess anti-prion drugs. As well as neuron-like immortalized cell lines, non-neuronal cell lines expressing mouse PrP^C have also been shown to be susceptible

to mouse PrP^{Sc} infection, including fibroblast cell lines such as NIH-3T3 and L929 cells (Vorberg et al., 2004).

Mouse PrP^{Sc} infection, propagation and toxicity has also been studied in non-immortalized cells, including primary neuronal cells and organotypic slices.
Primary neuronal and astrocytic cultures are widely utilised due to their ability to conserve the phenotypic and biochemical identity from the region they are cultivated from and reproduce the effects of prion infection seen in mice. More specifically, neuronal and astrocytic cultures can be derived from wild-type as well as GEMMs, which can improve the understanding of prion infection, propagation and neurotoxicity. For example, different studies have shown that cortical, hippocampus and cerebellar granule neurons and astrocytes extracted from wild-type and over-expressing PrP^{C} mice, are susceptible to PrP^{Sc} infection (Cronier et al., 2004). These *in vitro* experiments have demonstrated the ability of brain homogenate originating from prion diseased mice, including the RML, ME7, 22L and 127S strains to infect and lead to the propagation of PrP^{Sc} over time in both primary neuronal and astrocytic cultures (Cronier et al., 2007; Philiastides et al., 2019; Soraya Victoria et al., 2016). In addition to primary cultures, organotypic slices have also been used in prion disease research, allowing the further investigation of prion disease. In contrast to primary cultures, organotypic slices maintain the distinct cell types and cell structure found in each specific brain region, which allows the precise study of prion infection, propagation and toxicity within particular brain areas (Falsig & Aguzzi, 2008). These slices show a more reliable and replicable prion pathology than primary cultures in comparison to *in vivo* studies, replicating specific pathologies such as neuronal death and vacuolar degeneration, both seen in mice prion disease (Campeau et al., 2013). However, for this study, neuronal cultures were more advantageous to use than the organotypic slices due to a higher experiment number that can be performed and number of ligands that can be tested using a lower number of animals. In addition, cellular cultures are preferential for signalling assays as well as the expression of M1 mAChR in the brain is mainly restricted to these cells.

To summarise, both immortalised and non-immortalised cellular models have been shown to be susceptible to different mouse prion strain infection, with many similarities and differences between and with-in them. This variety in cellular

models of prion has provided many options for prion disease studies, allowing to choose the best suited model depending on the research question.

4.1.3 Muscarinic receptors and prion

As mentioned in Chapter 1.1.5, many efforts have been put into the development or repurposing of drugs into anti-prion compounds to either target the prion protein or the effects of its accumulation in the brain. Recent studies have linked muscarinic receptors to the prion protein and prion disease. Muscarinic receptors are very widely expressed in the brain and are associated in the disease pathology of other NDs such as AD (Dwomoh, Tejeda, et al., 2022). More specifically, our group has shown through various *in vivo* studies in prion disease mice that the activation of the M1 mAChR can reduce disease pathology and slow down the progression of the disease (Dwomoh, Rossi, et al., 2022). Initial studies showed that prion disease is linked to the impairment of hippocampal cholinergic innervation, therefore causing learning deficits in prion infected mice (Bradley et al., 2017). This same study showed that treatment of prion diseased mice with xanomeline, a M1/M4-preferring mAChR orthosteric ligand, and BQCA, a highly selective M1 mAChR PAM, led complete restoration of memory deficits and the prolonged survival of prion diseased mice (Bradley et al., 2017). Another study looking at the effects of VU846, a next-generation M1 mAChR PAM, in prion-infected mice showed again restoration of learning and memory deficits and increased survival in prion diseased mice (Dwomoh, Rossi, et al., 2022). This research also included a proteomic study on hippocampi isolated tissue from control and prion-infected mice treated with vehicle and VU846. Analysis of control vs prion-infect mice showed a high upregulation of neurodegeneration, neuroinflammation and brain disorder-linked proteins, which were then showed to be down-regulated with chronic treatment of VU846 compared to vehicle treated prion diseased mice (Dwomoh, Rossi, et al., 2022).

In addition, a study conducted by Scarpa et al. (2021) showed that a genetically engineered M1 phospho-deficient mouse model was significantly more susceptible to prion disease after infection in comparison to wild-type mice, with higher levels of PrP^{Sc} accumulation at equal time-points and shorter survival times. The M1 mAChR was generated by mutating all the identified phosphorylation sites plus other potential ones located in the C-terminal and the third intracellular group.

These mutations did not change the strong $G_{q/11}$ coupling of the receptor, but in comparison to wild-type M1, the levels of arrestin recruitment and receptor internalisation were significantly decreased (Bradley et al., 2020). This study shows the importance of the M1 mAChR signalling pathway in prion disease, demonstrating a neuroprotective characteristic linked to the phosphorylation status of the receptor.

All the data collected by our group directly points at the M1 mAChR as a potential target to slow down prion disease, therefore requiring further investigation into other potential M1 mAChR compounds as well as to understand the molecular mechanisms by which activation of this muscarinic receptor is slowing down the accumulation of PrP^{Sc} and therefore prolonging the survival of prion-infected mice.

4.1.4 Aims

The main aim for this chapter was to create a novel *in vitro* prion infection and propagation model in primary neurons to reduce the usage of animals and to be able to test multiple compounds with potential to slow down misfolded prion-like propagation. Previously reported primary neuronal prion infection models use brain homogenates from diseased mice to directly infect the neurons, not showing robust prion infection until 14 or 21 d.p.i. (Cronier et al., 2004). Therefore, the aim was to accelerate the time-course of infection and propagation, by enriching PrP^{Sc} from prion diseased mouse brain homogenates used for infection. Once the model was created, different pharmacological tools were used to understand the impact of the M1 mAChR in this prion misfolding model using distinct primary neuronal strains with several mutations on the M1 mAChR, and a number of muscarinic ligands with different selectivity, efficacy and potency for the receptor, with the potential to slow or stop prion propagation.

4.2 Specific Methodology

4.2.1 Novel protocol of prion purification from prion diseased mice

The 3x Prion NBH (control) and RML (prion) inoculated mice, mentioned in Chapter 4.1.1) were sacrificed around 11 w.p.i. for PrP purification and enrichment. A novel method was used to enrich the misfolded PrP^{Sc} from the diseased brain homogenates (Figure 4-1). The protocol, as mentioned in Chapter 2.6, included low speed centrifugations , in order to lose a substantial amount of small soluble proteins. After a first high-speed ultracentrifugation to dispose of unwanted substrate, a 1% sodium lauroyl sarcosinate (sarcosyl) solution was used to solubilise the misfolded PrP^{Sc} present in the homogenates. Further ultracentrifugation steps were performed to further enrich the desired protein and to remove the sarcosyl solution. After each centrifugation step the pellet was resuspended in DPBS. At all stages of the enrichment protocol, small samples were collected for immunoblot analysis and observe the enrichment of the desired protein. Western blots of the control and prion brain tissue samples were performed, blotting with a prion protein antibody for the total prion (PrP^{Tot}), the same prion antibody after Proteinase K digestion for PrP^{Sc} and alpha tubulin antibody as a loading control, as mentioned in Chapter 2.7.

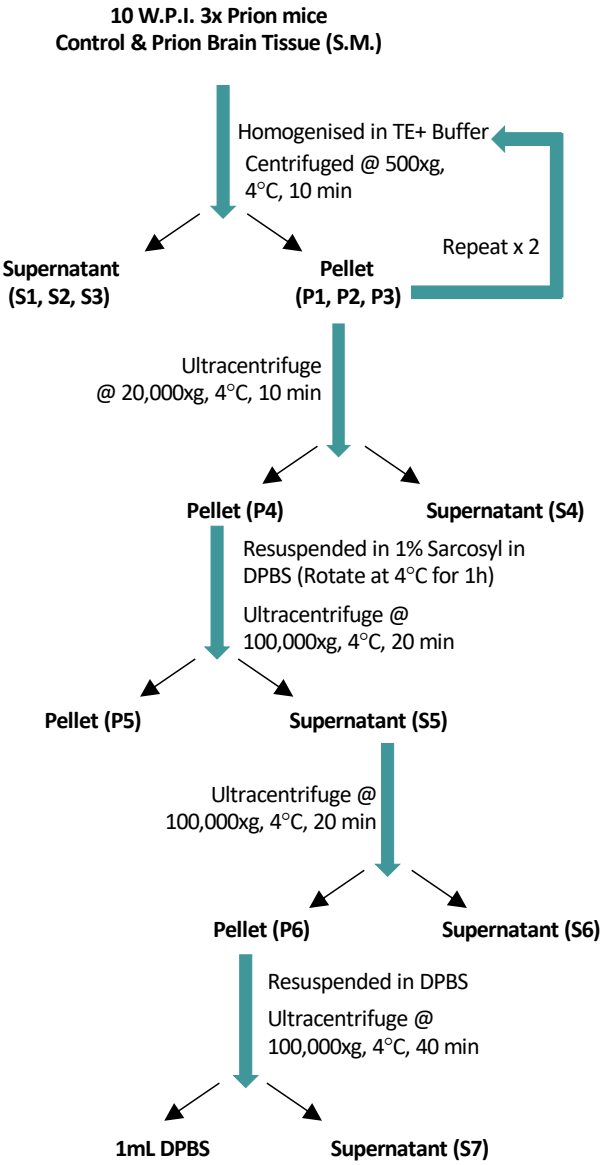

Figure 4-1 Novel protocol for prion protein enrichment from mouse brains. Schematic diagram summarizing the different steps of prion protein enrichment for both control and prion mouse brains.

4.3 Results

4.3.1 Characterisation of the novel prion purification protocol

Cellular endogenous prion was shown to be enriched from step to step in the normal brain tissue enriched samples, and no proteinase k-resistant PrP^{Sc} was observed in any of these samples as expected (Figure 4-2A). Total PrP^{C} was enriched in the prion brain tissue samples (Figure 4-2B) from step to step, and in addition, high enrichment in the proteinase k-resistant PrP^{Sc} in the final substrate (P7) was observed compared to the starting material (S.M.), which would then be used in infection experiments. Silver staining allowed for visualisation of total protein and demonstrated a large decrease in protein concentration between the S.M. and P7 prion samples (Figure 4-2C).

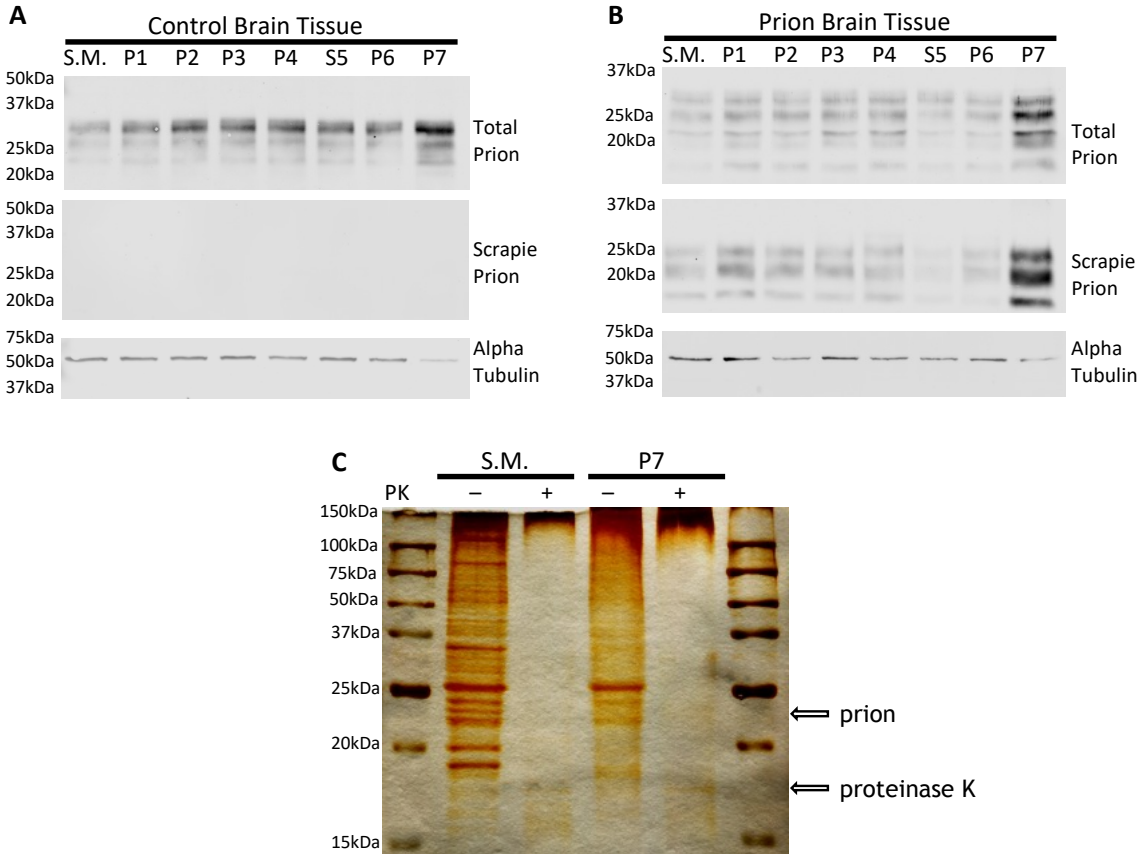

Figure 4-2 Prion protein enrichment from control and prion mouse brains. (A-B) Immunoblots of the different fractions from the prion enrichment of the **(A)** control (NBH) and **(B)** prion (RML) mouse brains using an anti-prion antibody for the PrP^{Tot}, anti-prion antibody after proteinase k digestion for PrP^{Sc} and anti-alpha tubulin antibody as a loading control. **(C)** Silver stain of the starting material and P7 (final material), with and without proteinase k digestion treatment, of the prion (RML) brain tissue.

4.3.2 Optimisation of novel *in vitro* model of PrP^{Sc} infection and propagation in primary neuronal cultures

Following the success of the prion enrichment protocol, P7 purified NBH (Figure 4-3A) and RML (Figure 4-3B) were used as control and prion infectious seed respectively in PrP^{Sc} infection experiments. A concentration-dependent pilot study, whereby DIV7 Prion-KO and 6x Prion neuronal cultures were incubated for 5 days with ascending concentrations of the misfolded-prion enriched fraction. Concentrations of the enriched fractions were calculated by performing a BCA quantification assay, which recorded the total amount of protein present in the enriched fractions. As expected, neurons which were not incubated or were treated with PBS showed no PrP^{Sc} deposition (Figure 4-3A). Neurons incubated with the different concentrations of misfolded-prion enriched fraction (prion seed) showed no cellular or PrP^{Sc} in the Prion-KO neurons (Figure 4-3A, B, C). In contrast, in the 6x Prion neurons, increasing deposition of PrP^{Sc} with increasing infection concentrations was observed. In Figure 4-3A, an incubation concentration of 1µg demonstrated no PrP^{Sc} deposition. The next three concentrations, 2µg, 3µg and 4µg, showed similar low levels of PrP^{Sc} in the blots (Figure 4-3B). Finally, the highest infection concentrations, 5 µg, 7.5 µg and 10 µg, showed an increasing trend of PrP^{Sc} deposition levels (Figure 4-3C), with 10µg leading to the largest amount of PrP^{Sc} present in the neurons (Figure 4-3D). Therefore, the 10 µg concentration was selected for future infection experiments.

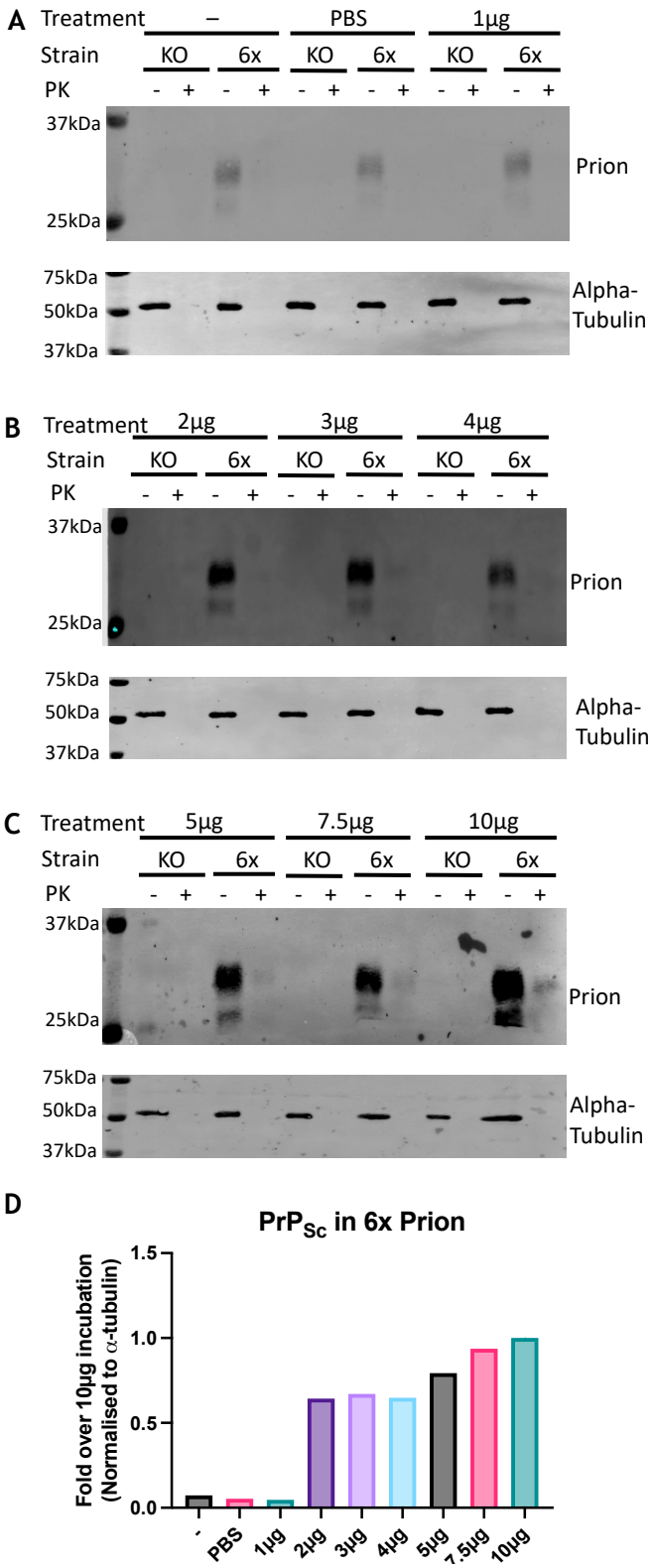

Figure 4-3 PrPSc deposition increases with higher concentrations of enriched substrate infections. Western blot analysis using an anti-prion antibody to observe total and PrP^{Sc} deposition with increasing concentrations of prion (purified RML) in Prion-KO and 6x Prion neuronal cultures. Samples were treated with vehicle or pK (1µg pk/1µg lysate protein) for 30min at 37°C to detect both PrP^{Tot} and pK-resistant PrP^{Sc}, respectively. **(A)** Membrane with no treatment, DPBS treatment and 1µg pRML infection. **(B)** Membrane with 2, 3 and 4µg pRML infections. **(C)** Membrane with 5, 7.5 and 10µg pRML infections. **(D)** 6x Prion neuronal culture band intensity analysis (EmpiriaStudio) for pK-resistant PrP^{Sc} deposition with different infection concentrations. (n=1).

Following the prion infection dose optimisation, further experiments were performed to assess the time course of the infection. Prion-KO and 6x Prion neuronal cultures infected with 10 µg of normally folded prion enriched fraction (control seed) and prion seed at DIV7 were collected at 7, 14 and 21 days post infection (d.p.i.) and assessed for PrP^{Sc} deposition.

Western blots of Prion-KO neurons showed no PrP^{C} or PrP^{Sc} deposition at either 7 or 14 d.p.i. with control infection (Figure 4-4A), however, prion infection did show both total and PrP^{Sc} deposition at both time-points. Importantly, the PrP^{Sc} levels are shown to be significantly reduced ($p<0.0001$, two-way ANOVA) from 7 to 14 d.p.i. (Figure 4-4C). In the 6x Prion neuronal cultures, incubation with control seed showed no PrP^{Sc} deposition at 7, 14 or 21 d.p.i. (Figure 4-4B), however, an increase in the levels of PrP^{Tot} was observed from one time-point to the next, as seen in Chapter 3, were neuronal maturation leads to increased PrP^{C} expression over time. The same increasing trend was visible for PrP^{Tot} of the prion seed incubated neurons, with no significant difference in PrP^{Tot} between control and prion infected neurons. However, in contrast to Prion-KO neurons, prion seed incubation did show a significant increase of PrP^{Sc} presence from 7 to 14 d.p.i, and from 14 to 21 d.p.i. ($p=0.047$ and $p=0.006$, respectively, two-way ANOVA) in 6x Prion neurons. The largest significant increase of prion scrapie levels was observed from 7 to 21 d.p.i. ($p=0.0001$, two-way ANOVA). These results demonstrate a successful neuronal *in vitro* model of PrP^{Sc} infection, were incubation with prion seed leads to infection and propagation of misfolded prion over time.

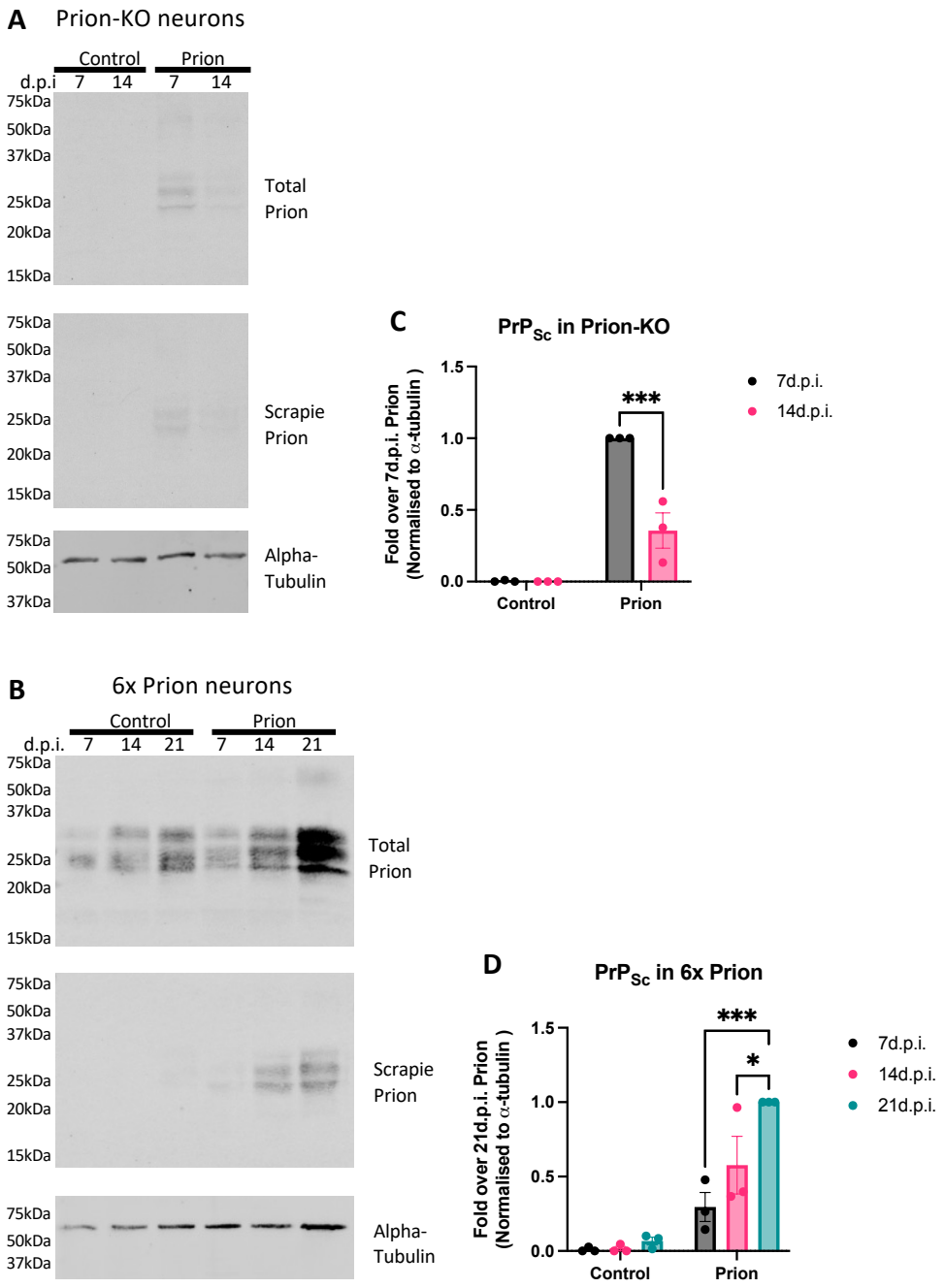

Figure 4-4 Enriched PrP^{Sc} can infect both in Prion-KO and 6x Prion neuronal cultures, however, propagation can only be observed in 6x Prion cultures. Western blot analysis using an anti-prion antibody to observe PrP^{Sc} deposition after 7-, 14- and 21- days post infection with control (NBH) and prion (RML) in **(A)** Prion-KO and **(B)** 6x Prion neuronal cultures samples (10µg). **(C)** Prion-KO and **(D)** 6x Prion band intensity analysis (EmpiriaStudio) for pK-resistant PrP^{Sc} deposition. Statistical analysis conducted was two-way ANOVA (Šídák's multiple comparisons). Data is expressed as mean ± SEM of three independent experiments. (n=3). *=P<0.05, ***=P<0.001.

4.3.3 Characterisation of the novel prion infection and propagation model

Daily light microscope images (1 to 7 d.p.i.) of the infected neuronal cultures, both control and prion infected, were taken to visualise morphological changes between them. No apparent visual changes in cell bodies, processes and number of cells were observed between control (Figure 4-5) and prion (Figure 4-6) infected neurons across the 7 day infection period, as well as no dead floating neurons present in the media. 10X images show similar increased number and density of neuronal processes between control and prion infected neurons, and 40X images show equal axonal growth originating from neuronal cell bodies between the two neuronal groups. In addition, no visual morphological differences could be observed between both control and prion infected neurons with non-infected neurons DIV7 and DIV14 (Figure 3-5).

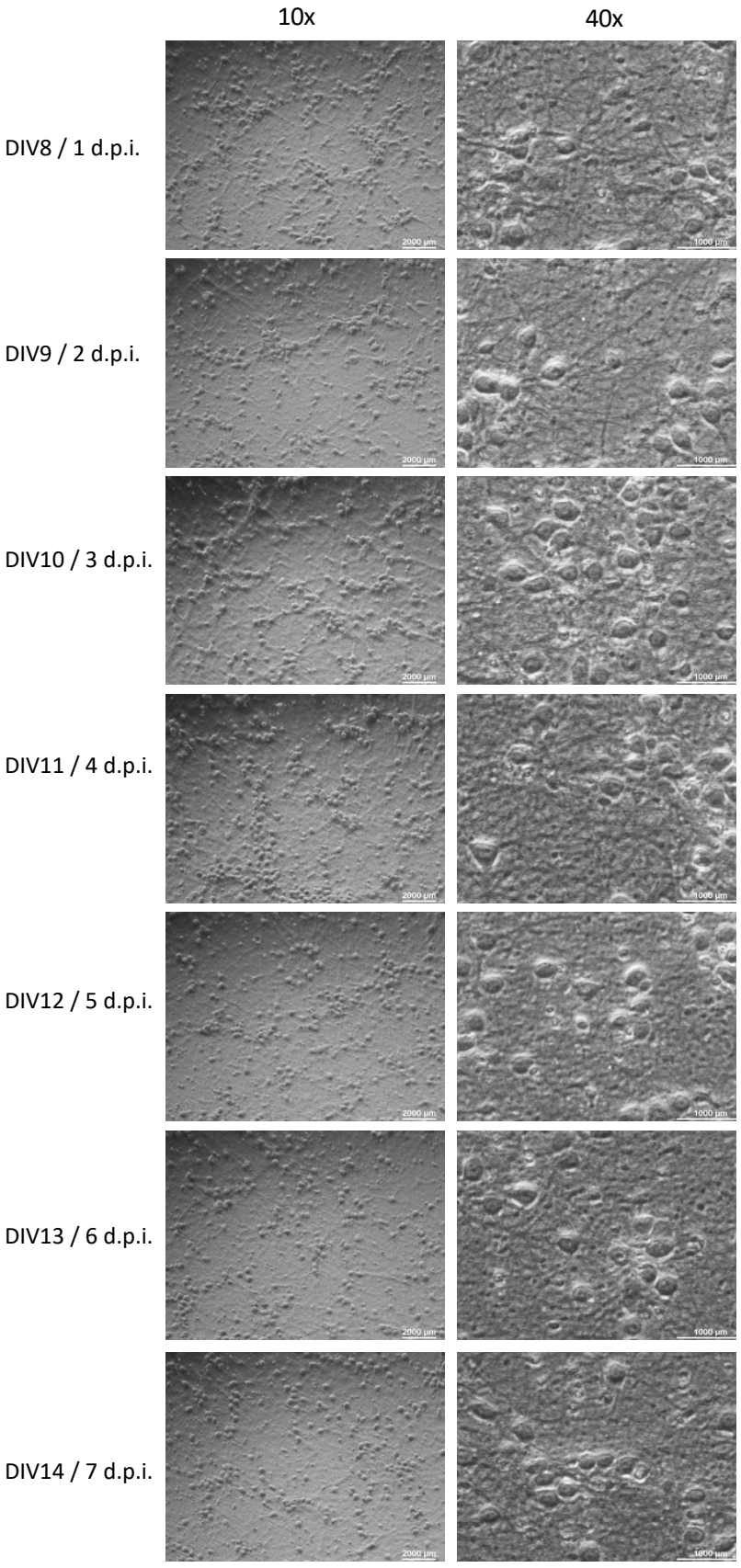

Figure 4-5 Infection with enriched prion from control mouse brains does not have any visible effect on 6x Prion neuronal cultures over a period of 7 days. Light microscope images at 10X and 40X magnification of pNBH infected 6x Prion neuronal cultures from 1d.p.i. (DIV8) to 7d.p.i. (DIV14). 10X Scale bar = 2000 µm and 40X Scale bar = 1000 µm.

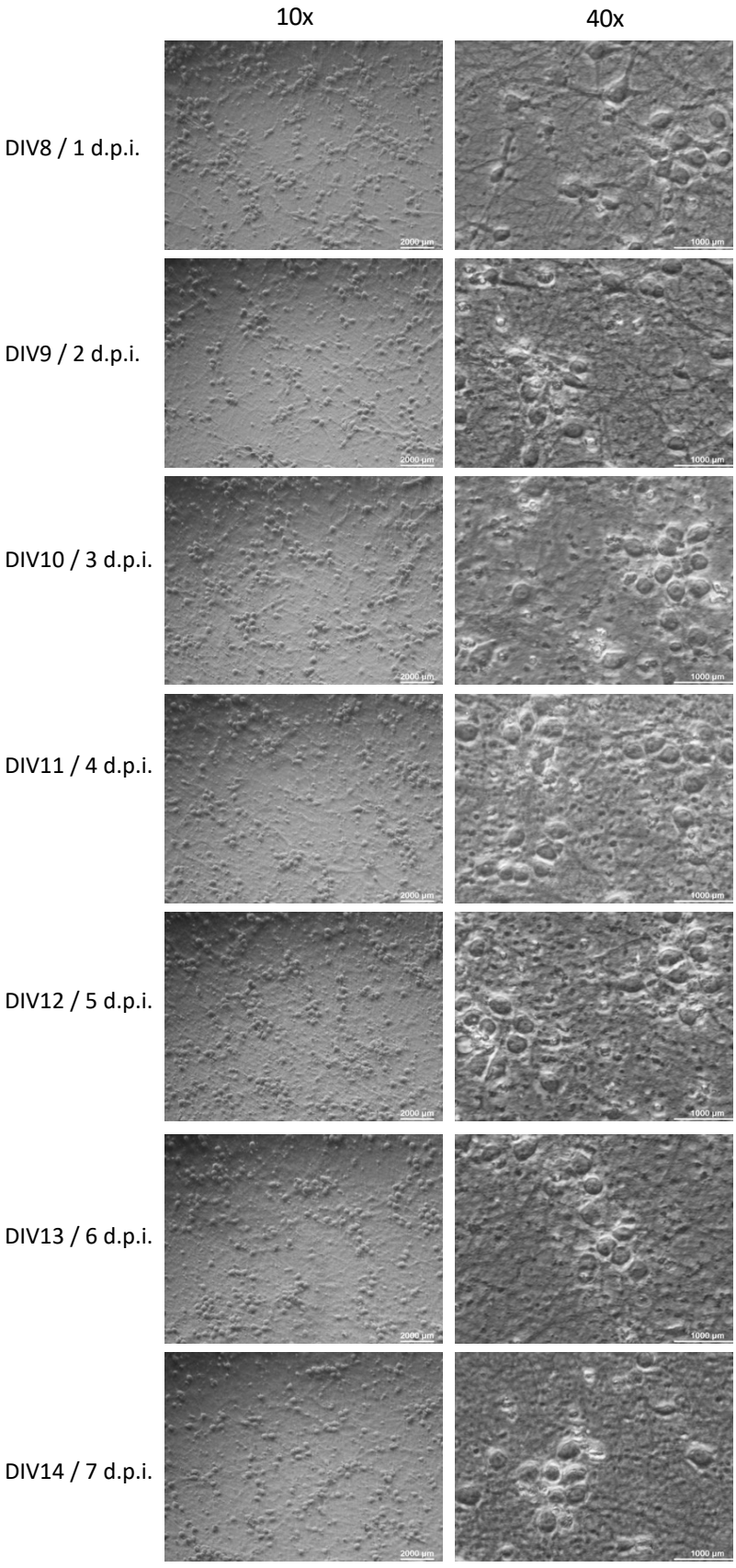

Figure 4-6 Infection with enriched prion from prion mouse brains does not have any visible effect on 6x Prion neuronal cultures over a period of 7 days. Light microscope images at 10X and 40X magnification of pRML infected 6x Prion neuronal cultures from 1d.p.i. (DIV8) to 7d.p.i. (DIV14). 10X Scale bar = 2000 µm and 40X Scale bar = 1000 µm.

Further analysis of 7 d.p.i. control seed versus prion seed infections in 6x Prion neuronal cultures was conducted. Western blots were performed to analyse the expression of distinct neuronal markers, including NeuN to quantify number of neurons, synapsin-1 for number synapses and choline acetyltransferase (ChAT) for number of cholinergic neurons (Figure 4-7A), showing no significant difference between control and prion seed infections (Figure 4-7B, C, D). Anti-M1 mAChR antibody showed that prion infection does not alter the expression of M1 mAChR in neurons compared to control infection (Figure 4-7A, E). Lastly, anti-LC3B and anti-caspase-3 antibodies were used to characterise autophagy and apoptosis (Figure 4-7A, F, G), respectively, showing identical band intensities and no significant difference for both control and prion infected 6x Prion neurons.

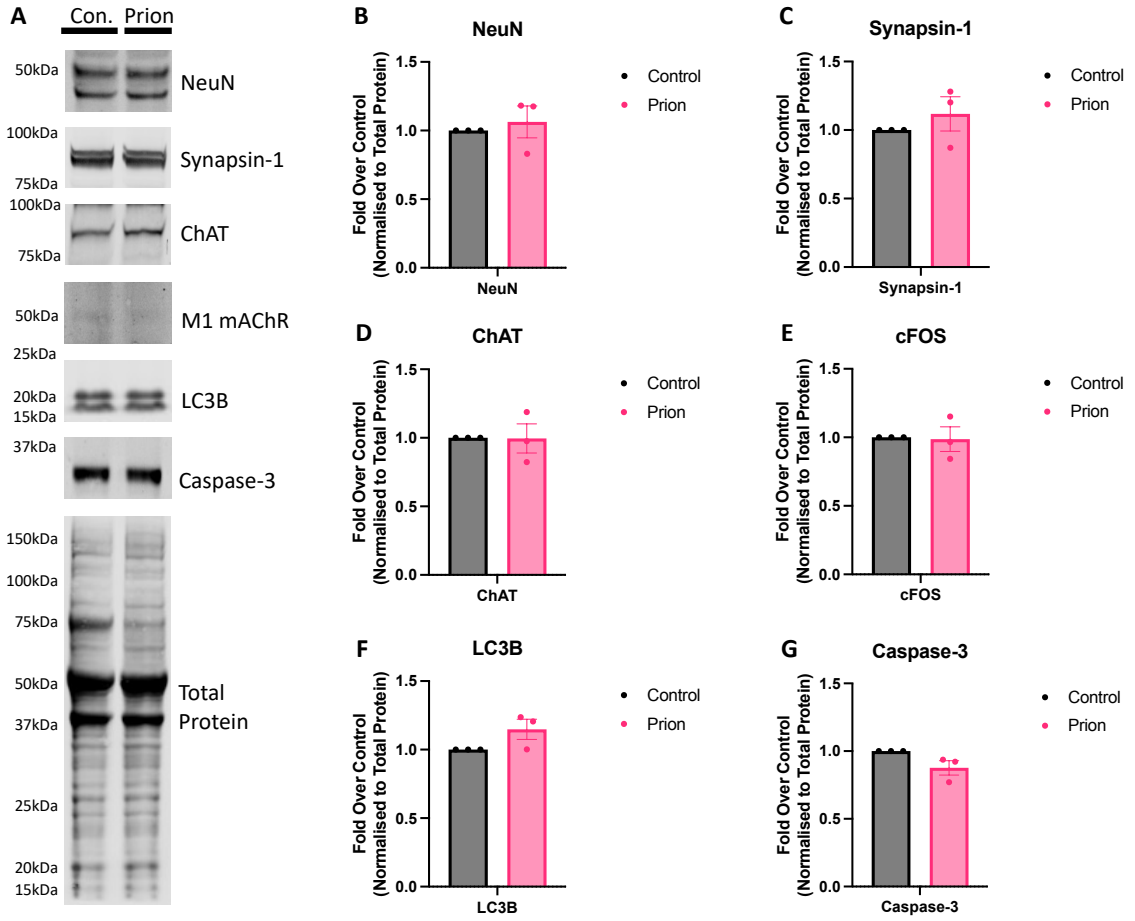

Figure 4-7 Neuron PrP^{Sc} infection does not have an adverse impact on neuronal health. (A) Western blot analysis of 6x Prion control (NBH) and prion (RML) 7d.p.i. neuron lysates (10µg) using different neuronal, muscarinic, autophagy and apoptosis markers. Western Blot band intensity analysis (EmpiriaStudio) of **(B)** anti-NeuN, **(C)** anti-Synapsin-1, **(D)** anti-ChAT, **(E)** anti-M1 mAChR, **(F)** anti-LC3B and **(G)** anti-caspase-3 antibodies. **(G)** Total protein stain was performed to normalise protein amounts. Bar graphs show normalised protein signal to control 6x Prion of each antibody. Statistical analysis conducted was unpaired T-test. Data is expressed as mean ± SEM of three independent experiments. (n=3).

4.3.4 Effect of M1 mAChR expression in PrP^{Sc} infection and propagation

The same infection protocol was performed on neuronal cultures from the three muscarinic GEMMs to understand how the expression and constitutive activation of the receptor would affect PrP^{Sc} deposition after infection.

Western blots were performed with M1-HA Wt, M1-KO and M1-DREADD neural lysates after control seed and prion seed 7 d.p.i. The M1-HA Wt cultures were used as controls. As expected, control infection showed similar levels of endogenous PrP^{Tot} across all three strains at the same time-point, as well as no PrP^{Sc} deposition (Figure 4-8A). Analysis of these bands (Figure 4-8C) showed a significant difference in prion expression between total and scrapie bands in all three strains (M1-HA p=0.0034, M1-DREADD p=0.0042, M1-KO p=0.0039, two-way ANOVA). Prion infection of the same neurons showed both the presence of PrP^{Tot} and PrP^{Sc} (Figure 4-8B). No differences were observed in PrP^{Sc} levels between the three neuronal strains; however, PrP^{Sc} levels were again significantly lower than PrP^{Tot} when comparing between the same strain (M1-HA p=0.0012, M1-DREADD p=0.0015, M1-KO p=0.0025, two-way ANOVA) (Figure 4-8D).

When comparing differences in PrP^{Tot} between control and prion infections (Figure 4-8E), analysis showed a significant statistical increase in PrP^{Tot} levels in prion infected neurons compared to control infected neurons of all three strains (M1-HA p=0.0009, M1-DREADD p=0.0011, M1-KO p=0.0036, two-way ANOVA). A significant difference was observed in PrP^{Sc} deposition levels when comparing prion seed infected cultures and control seed infected cultures in all neuronal strains (M1-HA p=0.01, M1-DREADD neurons p=0.009, and M1-KO p=0.031, two-way ANOVA) (Figure4-8F).

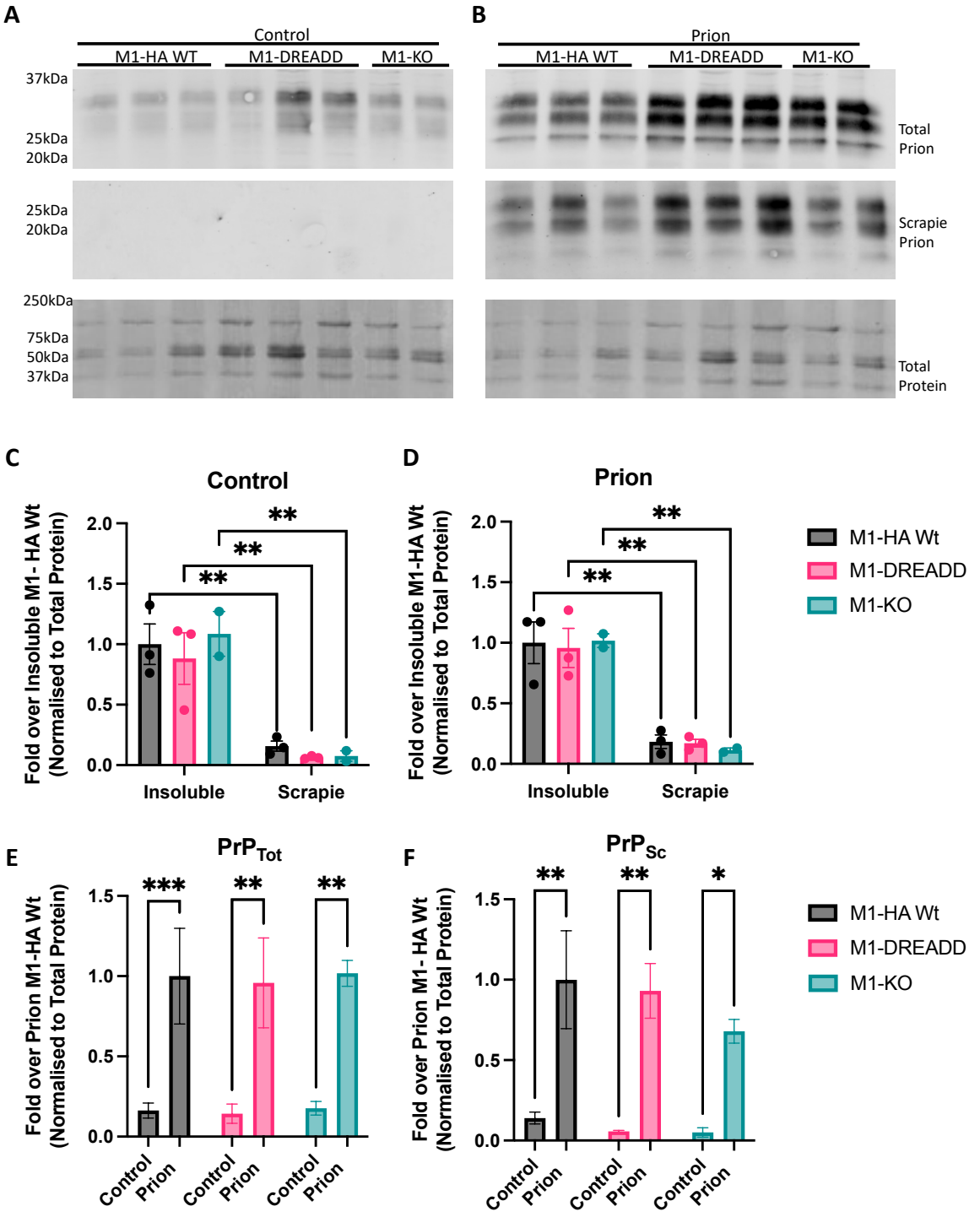

Figure 4-8 Equal levels of PrPSc deposition were observed across M1-WT, M1-DREADD and M1-KO neuronal cultures. Western blot analysis using an anti-prion antibody to observe PrP^{Sc} deposition in neuronal cultures after **(A)** control seed (NBH) and **(B)** prion seed (RML). Total protein stain was performed to normalise protein amounts. Band analysis (EmpiriaStudio) bar graphs of total and PrP^{Sc} from M1-HA Wt, M1-DREADD and M1-KO neurons after **(C)** control and **(D)** prion infections. Band analysis bar graphs comparing the amount of **(E)** total and **(F)** PrP^{Sc} present after control and prion infections of M1-HA Wt, M1-DREADD and M1-KO neurons. Statistical analysis conducted was two-way ANOVA (Šídák's multiple comparisons). Data is expressed as mean ± SEM of three independent experiments. (n=3). **=P<0.01, ***=P<0.001.

4.3.5 Muscarinic receptor activation effect on prion infection and propagation

Neurons from the 6x prion, M1-HA Wt, M1-KO and M1-DREADD mouse strains were infected at DIV7 with control seed or prion seed. From DIV6, prion infected neurons were chronically treated with a daily dose of 10 μM of vehicle, Oxo-M, CNO or HTL9936 until DIV14. Insoluble protein lysates of all strains were analysed using Western blot to observe the compound impact (muscarinic receptor activation) on PrP^{Sc} deposition. Control seed infections were included in all experiments as negative controls and were therefore not included in the statistical analysis of PrP^{Sc} bands.

Western blots from 6x Prion neurons showed no significant difference between PrP^{Sc} deposition in vehicle treated neurons and drug treated neurons after prion infection (Figure 4-9A, B). Although an increasing trend can be observed in with Oxo the graph (Figure 9-8B), statistical analysis revealed no significant difference in prion deposition compared to vehicle treatment. M1-HA Wt neurons showed no significant differences between vehicle and ligand treated neurons; however, analysis did reveal high variability in PrP^{Sc} depositions between experiments (Figure 4-9C, D). M1-KO neurons showed a nearly significant decrease in PrP^{Sc} deposition levels after CNO and HTL9936 treatments ($p=0.058$ and $p=0.068$, respectively) (Figure 4-9E,F). Finally, M1-DREADD neurons showed the closest similarity in PrP^{Sc} deposition between vehicle and drugs, with no significant difference between any of the treatments (Figure 4-9G,H). The results obtained from these experiments showed no significant changes in PrP^{Sc} accumulation across all neuronal strains using the different muscarinic ligands.

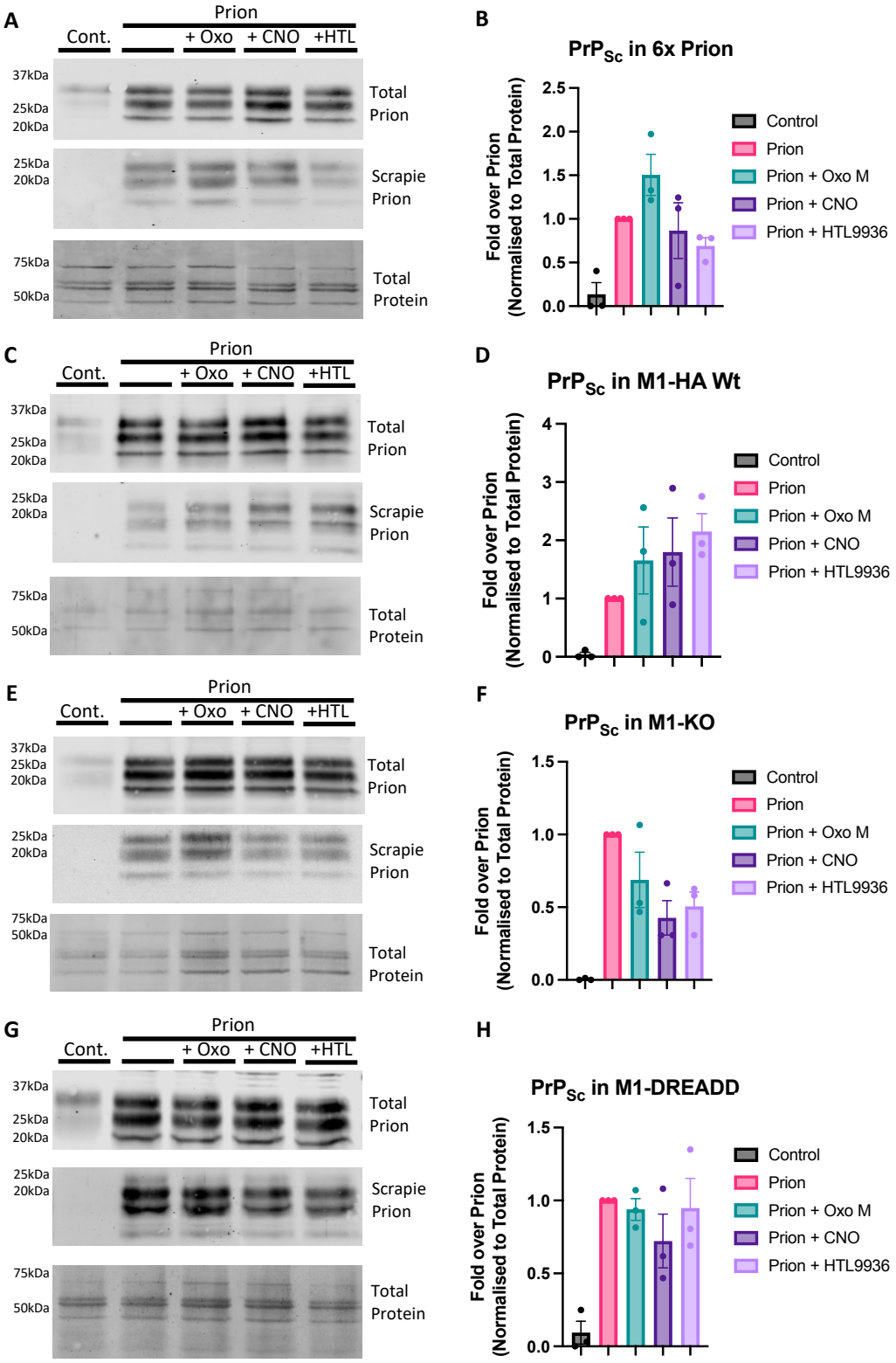

Figure 4-9 Activation of muscarinic receptors does not change the course of infection and propagation across different muscarinic GEMM neuronal culture strains. Western blot analysis using an anti-prion antibody to observe PrP^{Sc} deposition changes in neuronal cultures between control (pNBH), prion (pRML) and prion (pRML) infection with chronic dosages (10μM) of Oxotremorine-M, CNO and HTL9936 in **(A)** 6x Prion, **(C)** M1-HA Wt, **(E)** M1-KO and **(G)** M1-DREADD neuronal cultures. Neuronal culture lysates prepared as per previous experiments. pK-resistant PrP^{Sc} band intensity analysis (EmpiriaStudio) for protein expression in all four strains **(B, D, F and H respectively)** was performed. Statistical analysis conducted was ordinary one-way ANOVA (Tukey's multiple comparisons). Data is expressed as mean ± SEM of three independent experiments. (n=3).

4.3.6 M1 mAChR expression and signalling after chronic receptor activation

A non-permeable radioligand saturation binding assay, using tritiated [3H]-NMS, was performed to understand the effect of a chronic 7-day Oxo treatment to muscarinic receptor expression at the plasma membrane surface level in DIV14 neuronal cultures. 6x Prion neurons were used as they express wild-type levels of endogenous M1 mAChR. Cultures treated with Oxo for 7 days showed a significant increase in K_D ($p=0.33$, unpaired t-test) and the Bmax was significantly reduced ($p=0.022$, unpaired t-test) in comparison to vehicle treated neurons (Figure 4-9A, B and Table 4-1).

An IP1 accumulation assay was also performed on 6x Prion neurons after a chronic 7-day Oxo-M treatment to comprehend the impact of daily drug treatment on the activation and signalling of $G\alpha_{q/11}$ protein-dependent muscarinic receptors. Cultures treated with Oxo for 7 days showed a similar $LogEC_{50}$ compared to vehicle, however, the Emax was significantly reduced ($p=0.015$, unpaired t-test) (Figure 4-10C,D and Table 4-1).

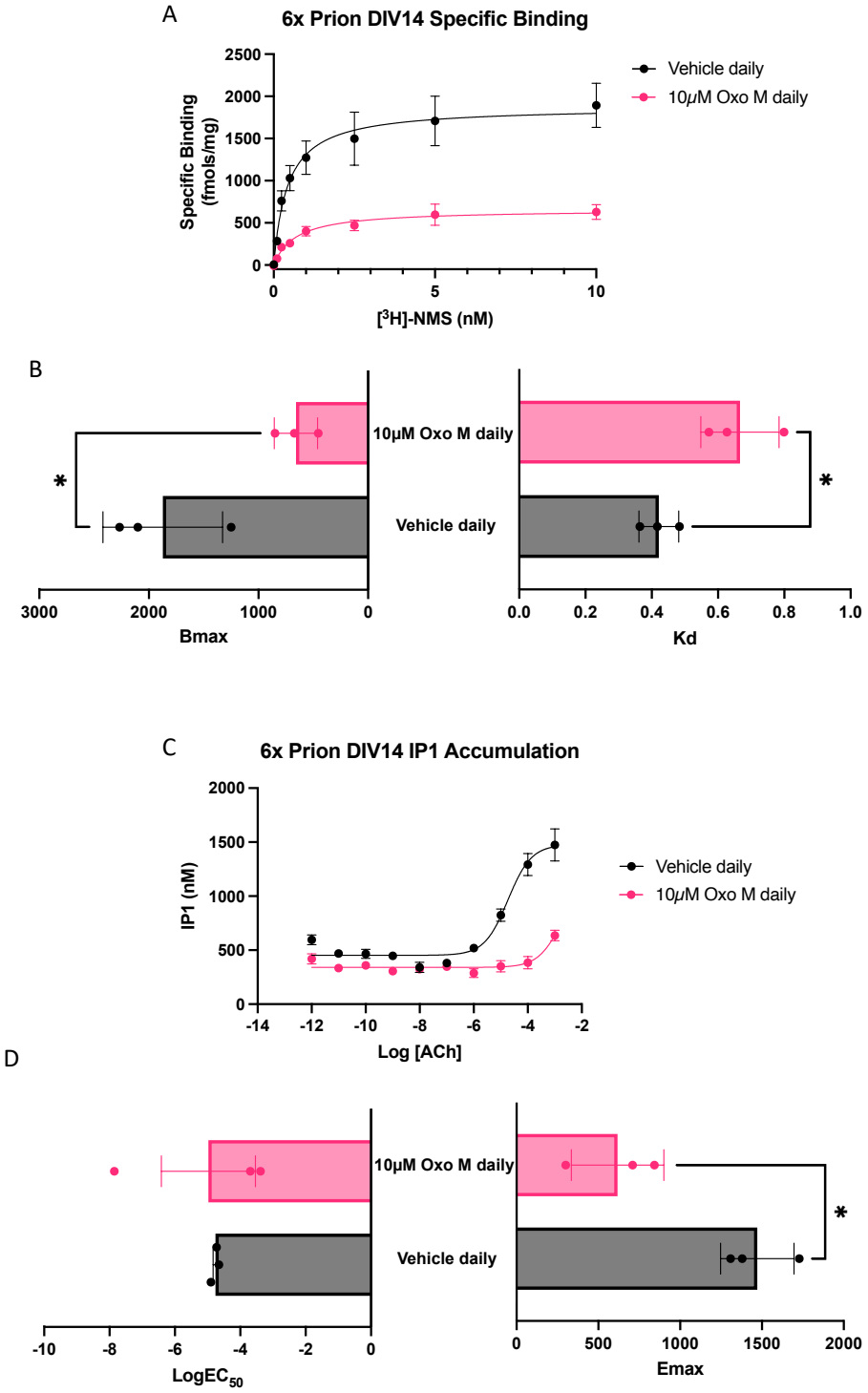

Figure 4-10 Expression and activation levels of muscarinic receptors on the plasma membrane of neuronal cultures decrease after daily treatment of Oxotremorine-M for 7 days. (A) Radioligand binding was measured on DIV14 6x Prion primary neuronal cultures after vehicle and Oxotremorine-M chronic treatments (10μM) from DIV6, following treatment with muscarinic receptor specific radioligand [^{3}H]-NMS. Neurons were stimulated for 2 hours with [^{3}H]-NMS concentrations ranging from 10nM to 0.1nM for a radioligand saturation concentration-response curve. **(B)** Maximum specific binding (Bmax) and affinity (Kd) values were compared between chronic treatments. Specific binding results were normalised to the protein concentration of three independent wells with the same number of plated neurons. Results were obtained from three independent experiments. (n=3). **(C)** Agonist-induced IP1 accumulation was measured with the same neuronal strain, at the same time-point and after the same Oxotremorine-M chronic treatment. Cells were stimulated with Acetylcholine for 1 hour ranging from 1mM down to 1pM to allow for an IP1 accumulation concentration-response curve. **(D)** Potency ($LogEC_{50}$) and efficacy (Emax) values were derived. Statistical analysis conducted was an unpaired T test. Results were obtained from three independent experiments. (n=3). *=P<0.05.

Ligand	[^{3}H]-NMS Saturation Binding					IP1 Accumulation				
	Bmax	*P*	Kd	*P*	*N*	$LogEC_{50}$	*P*	Emax	*P*	*N*
Vehicle	1873 ± 315.2	-	0.42 ± 0.03	-	3	-4.76 ± 0.07	-	1472 ± 130	-	3
10µM Oxo daily	658.0 ± 114.2	0.022 (*)	0.67 ± 0.07	0.033 (*)	3	-	0.59 n.s.	618 ± 163	0.015 (*)	3

Table 4-1 Muscarinic expression and efficacy on the outer membrane of 6x Prion neuronal cultures after daily treatment of Oxotremorine-M for 7 days. Maximum specific binding (Bmax) and affinity (Kd) values were compared between chronic treatments. Specific binding results were normalised to the protein concentration of three independent wells with the same number of plated neurons. Potency ($LogEC_{50}$) and efficacy (Emax) values were derived. Statistical analysis conducted was an unpaired T test. Results are mean ± SEM of three independent experiments. (n=3). *=P<0.05.

A permeable radioligand saturation binding assay, using tritiated [3H]-QNB, was performed to observe if muscarinic receptors had internalised after a chronic 7-day Oxo treatment in DIV14 neuronal cultures. Cultures treated with Oxo for 7 days showed a significant increase in K_D (p=0.011) and a significantly reduced Bmax (p=0.006) in comparison to vehicle treated neurons (Figure 4-11A, B and Table 4-2).

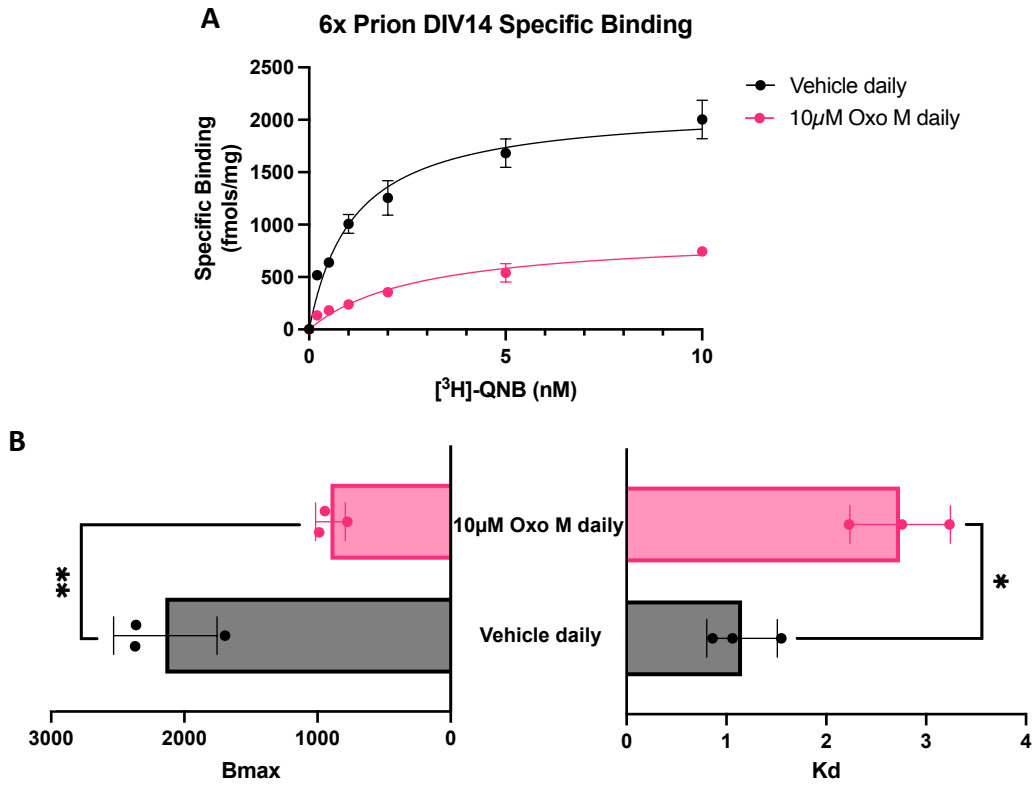

Figure 4-11 Daily treatment of Oxotremorine-M for 7 days leads to the reduced expression of muscarinic receptors both in the outer membrane and cytoplasm of 6x Prion neurons . (A) Radioligand binding was measured on DIV14 6x Prion primary neuronal cultures after vehicle and Oxotremorine-M chronic treatments (10μM) from DIV6, following treatment with permeable muscarinic receptor specific radioligand [^{3}H]-QNB. Neurons were stimulated for 2 hours with [^{3}H]-QNB concentrations ranging from 10nM to 0.1nM for a radioligand saturation concentration-response curve. **(B)** Maximum specific binding (Bmax) and affinity (Kd) values were compared between chronic treatments. Specific binding results were normalised to the protein concentration of three independent wells with the same number of plated neurons. Statistical analysis conducted was an unpaired T test. Results were obtained from three independent experiments. (n=3). *=P<0.05, **=P<0.01.

Ligand	[^{3}H]-QNB Saturation Binding				N
	Bmax	*P*	Kd	*P*	
Vehicle	2143 ± 223.8	-	1.16 ± 0.20	-	3
10μM Oxo daily	776.6 ± 64.34	0.006 (**)	2.74 ± 0.29	0.011 (*)	3

Table 4-2 Muscarinic expression and efficacy on the plasma membrane and inside the cytoplasm of 6x Prion neuronal cultures after daily treatment of Oxotremorine-M for 7 days. Maximum specific binding (Bmax) and affinity (Kd) values were compared between chronic treatments. Specific binding results were normalised to the protein concentration of three independent wells with the same number of plated neurons. Potency ($LogEC_{50}$) and efficacy (Emax) values were derived. Statistical analysis conducted was an unpaired T test. Results are mean ± SEM of three independent experiments. (n=3). *=P<0.05, **=P<0.01.

4.3.7 Muscarinic receptor activation effect on prion infection and propagation in a M1 mAChR phosphorylation-deficient mutant primary neuronal culture

Infection and drug treatment with Oxo was performed in M1-PD neuronal cultures, to test muscarinic activation in PrP^{Sc} propagation context in neurons where the M1 mAChR cannot be phosphorylated, and therefore internalised and degraded.

As expected, control infection showed no PrP^{Sc} deposition after pk digestion of the neuronal lysates (Figure 4-12A). Prion infection was shown to lead to PrP^{Sc} deposition in M1-PD neurons as seen by the bands in the immunoblots, however, neurons which were additionally treated daily with 10 µM of Oxo from DIV6 showed no significant difference compared to vehicle treated neurons (Figure 4-12A,B).

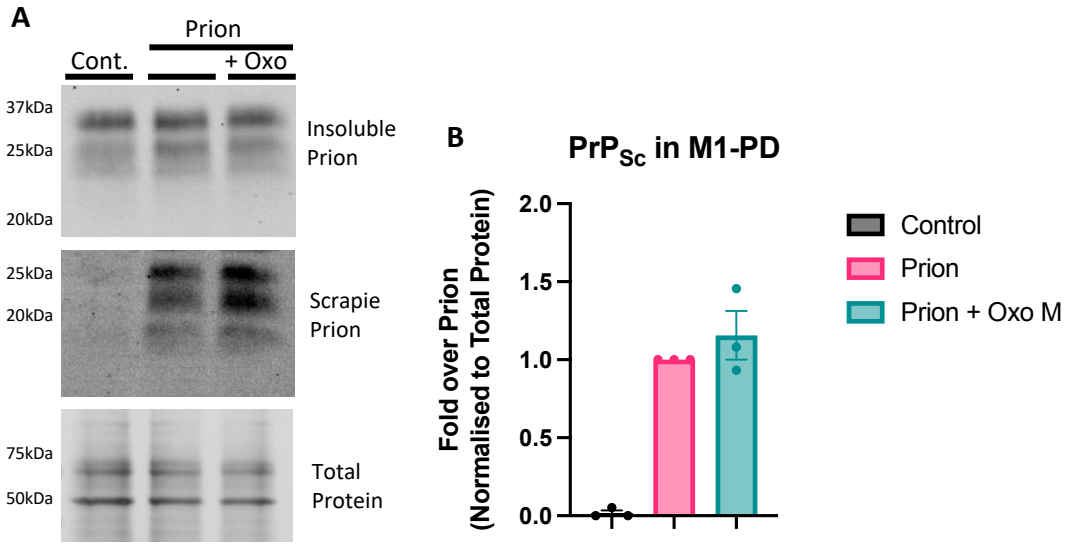

Figure 4-12 Activation of the phospho-deficient M1 muscarinic receptor does not change the course of infection and propagation neuronal cultures. (A) Western blot analysis using an anti-prion antibody to observe PrP^{Sc} deposition changes in neuronal cultures between control (pNBH), prion (pRML) and prion (pRML) infection with a chronic dosage (10µM) of Oxotremorine-M in M1-PD neuronal cultures. Neuronal culture lysates prepared as per previous experiments. **(B)** pK-resistant PrP^{Sc} band intensity analysis (EmpiriaStudio) for protein expression was performed. Total protein stain was performed to normalise the PrP^{Sc} amounts. Statistical analysis conducted was two-way ANOVA (Tukey's multiple comparisons). Data is expressed as mean ± SEM of three independent experiments. (n=3).

4.3.8 M1 mAChR expression and signalling after chronic receptor activation in a M1 mAChR phosphorylation-deficient mutant primary neuronal culture

A permeable radioligand saturation binding assay, using tritiated [3H]-QNB, was performed to observe what would occur to the M1 mAChR after a chronic 7-day Oxo-M treatment in DIV14 M1-PD neuronal cultures, when it cannot be internalised due to its lack of phosphorylation. Cultures treated with Oxo-M for 7 days showed no significant change in K_D, however they did show a significant reduction of the Bmax ($p=0.01$) in comparison to vehicle treated neurons (Figure 4-13A,B and Table 4-3).

An IP1 accumulation assay was also performed on the same neurons after a chronic 7-day Oxo-M treatment to analyse the impact of daily drug treatment on the activation and signalling of $G\alpha_{q/11}$ protein-dependent muscarinic receptors. Cultures treated with Oxo-M for 7 days showed a similar $LogEC_{50}$ compared to vehicle, however, the Emax was significantly reduced ($p=0.015$) (Figure 4-13C,D and Table 4-3).

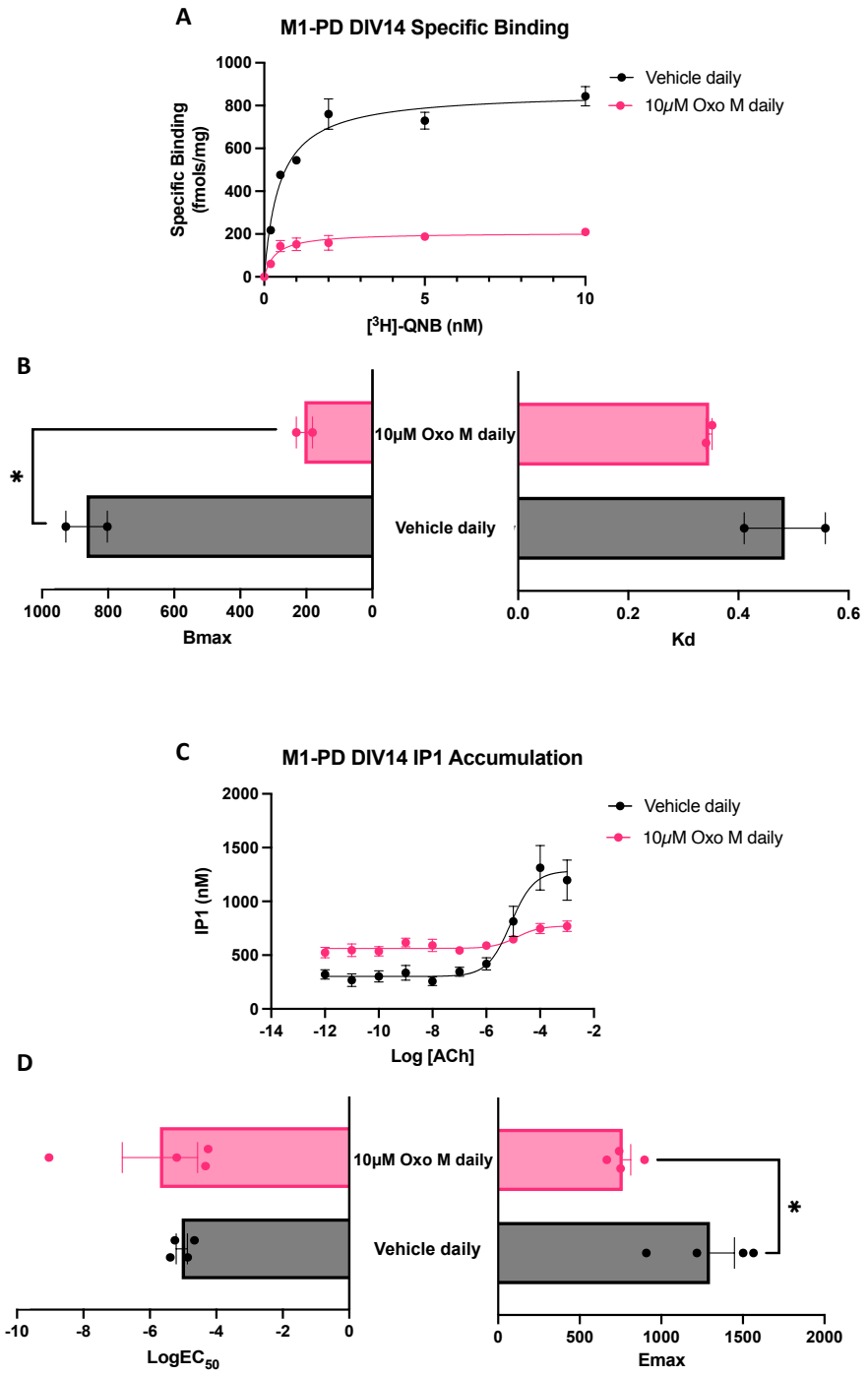

Figure 4-13 Expression and activation levels of muscarinic receptors on the plasma membrane and in the cytoplasm decrease in M1-PD neuronal cultures after daily treatment of Oxotremorine-M for 7 days. (A) Radioligand binding was measured on DIV14 M1-PD primary neuronal cultures after vehicle and Oxotremorine-M chronic treatments (10μM) from DIV6, following treatment with muscarinic receptor specific radioligand [^{3}H]-QNB. Neurons were stimulated for 2 hours with [^{3}H]-QNB concentrations ranging from 10nM to 0.1nM for a radioligand saturation concentration-response curve. **(B)** Maximum specific binding (Bmax) and affinity (Kd) values were compared between chronic treatments. Specific binding results were normalised to the protein concentration of three independent wells with the same number of plated neurons. Statistical analysis conducted was an unpaired T test. Results are mean ± SEM of three independent experiments. (n=2). **(C)** Agonist-induced IP1 accumulation was measured with the same neuronal strain, at the same time-point and after same Oxotremorine-M chronic treatment. Cells were stimulated with Acetylcholine for 1 hour ranging from 1mM down to 1pM to allow for an IP1 accumulation concentration-response curve. **(D)** Potency ($LogEC_{50}$) and efficacy (Emax) values were derived. Statistical analysis conducted was an unpaired T test. Results are mean ± SEM of three independent experiments. (n=4). *=P<0.05.

Ligand	[^{3}H]-QNB Saturation Binding				N	IP1 Accumulation				N
	Bmax	*P*	Kd	*P*		$LogEC_{50}$	*P*	Emax	$LogEC_{50}$	
Vehicle	865.2 ± 62.7	-	0.48 ± 0.07	-	2	-5.04 ± 0.17	-	1298 ± 150	-	4
10µM Oxo daily	205.7 ± 24.4	0.010 (*)	0.35 ± 0.01	0.020 n.s.	2	-5.70 ± 1.13	0.059 n.s.	764 ± 48.3	0.015 (*)	4

Table 4-3 Muscarinic expression and efficacy of M1-PD neuronal cultures after daily treatment of Oxotremorine-M for 7 days. Maximum specific binding (Bmax) and affinity (Kd) values were compared between chronic treatments. Specific binding results were normalised to the protein concentration of three independent wells with the same number of plated neurons. Potency ($LogEC_{50}$) and efficacy (Emax) values were derived. Statistical analysis conducted was an unpaired T test. Results are mean ± SEM of two/four independent experiments, respectively (n=2/4). *=P<0.05.

4.4 Discussion

This chapter's aim was to purify PrP^{Sc} from the brains of prion-diseased mice, in order to use this purified material as an infectious seed to create a novel *in vitro* model of prion infection and propagation in primary neuronal cultures. Several models of prion infected primary neuronal cultures have been reported before, with different mouse prion strains being used, leading to different biochemical and phenotypic outcomes, and different infection time-lines (Cronier et al., 2004; Tanaka et al., 2020). It is well known that PrP^{C}, with a predominantly α-helical fold conformation, sustains a sharp conversion into a more β-sheet structure, which characterises the disease-causing PrP^{Sc} (Wille et al., 2002). As the prion protein undergoes this major conformational change, its biochemical properties also change, becoming digestion-resistant to pK and insoluble in non-detergent solutions (Muramoto et al., 1996). This strong insolubility characteristic is what was relied on to obtain an enriched PrP^{Sc} from the diseased brain homogenates. As seen from the results (Figure 4-3), enrichment of PrP^{Sc} from the prion-infected brain homogenates, and reduction of the total protein levels in the last enriched fragments, in comparison to the starting material, was achieved. A purer PrP^{Sc} solution, to be used in *in vitro* infection experiments was attained. This protocol achieved high levels of misfolded prion enrichment comparable to other misfolded protein purification protocols, such as tau and α-synuclein, previously published

(J. L. Guo et al., 2016; McCormack et al., 2016) It is worth noting that enrichment of PrP^{C} in both control and prion-infected mice was also observed, demonstrating that although less insoluble than PrP^{Sc}, it can remain within the insoluble fraction demonstrating, previously reported by Yuan et al. (2006), as well as other proteins such as α-tubulin, which were used as a loading control.

Once the enriched PrP^{Sc} was obtained, optimising the PrP^{Sc} infection in primary neurons from 6x Prion mice was the next step. As previous studies have shown that the over-expression of endogenous PrP^{C} leads to faster infection and disease progression (Scarpa, 2022), 6x Prion mice were first used to demonstrate that infection and propagation could be attained. The initial concentration-dependent data demonstrated that infection of neurons with PrP^{Sc} can be achieved, observing PrP^{Sc} deposition at a much earlier time-point (5 d.p.i.) compared to results previously reported by other groups (Cronier et al., 2004; Tanaka et al., 2020). A concentration of 10µg/well was chosen for infections in 6-well plates, as this concentration resulted in the highest levels of PrP^{Sc} deposition.

A time-course study revealed opposing results after infection of Prion-KO and 6x Prion neurons. Levels of PrP^{Sc} in Prion-KO neurons significantly decreased from 7 to 14 d.p.i., suggesting the ability for PrP^{Sc} to infect neurons lacking the endogenous expression of prion. This result suggests an indirect mechanism by which PrP^{Sc} molecules can enter neuronal cells despite no endogenous PrP^{C} expression. This finding agrees with the effect of some anti-prion drugs, which do not target the prion protein directly, but reduce the levels of PrP^{Sc} accumulation (Mercer & Harris, 2019). However, the data also determines the inability of the same neuronal strain to propagate and accumulate PrP^{Sc}, due to the neurons not expressing endogenous PrP^{C}, therefore clearing out all PrP^{Sc} molecules from infection with time. Previous prion infection studies have shown the absence of PrP^{Sc} deposition in Prion-KO neuronal cultures at 28d.p.i. and beyond (Cronier et al., 2004), but never at earlier time-points, which might suggest why these results have not been seen before. This unknown mechanism by which inoculated PrP^{Sc} is cleared also occurs *in vivo* studies, were prion-infected Prn-$p^{0/0}$ mice are protected against PrP^{Sc} propagation and disease (Büeler et al., 1993), showing no PrP^{Sc} deposition in the mouse brains.

The presence of PrP^{Sc} within Prion-KO neurons at 7 d.p.i. was unexpected, as this was not observed in any of the previous concentration-dependent experiment. It was determined that the lysate preparation method was behind the difference between the results. The concentration-dependent experiment used complete sample lysates (supernatant and pellet) for Western blot analysis, whilst the time-course study used only the pellets of each sample for prion levels analysis. The sample preparation was changed in order to enrich PrP^{Sc} levels in the samples, as no PrP^{Sc} was present in supernatant fractions of prion infected neuronal samples, matching the high insolubility characteristic of PrP^{Sc} (Daude et al., 1997).

In contrast to Prion-KO neurons, PrP^{Sc} deposition increased with time in 6x Prion cultures. This data agrees with previously published studies (Cronier et al., 2004; Tanaka et al., 2020), were primary neurons expressing endogenous PrP^{C} can be infected with PrP^{Sc}, with deposition levels increasing with time. Infection of the neurons could be observed as soon as 7 d.p.i., demonstrating the ability of the enriched infectious prion material to infect neurons within 7 days. The attained results revealed significant increase in PrP^{Sc} levels between 7, 14 and 21 d.p.i., demonstrating that the infection leads to accumulation and propagation over time. From this data, it was determined 7 d.p.i. to be the best time-point for future experiments, due to robust levels of prion deposition after a short incubation period.

Characterisation of 7 d.p.i. 6x Prion neurons revealed no evident morphology difference between non-infected neurons, control-infected and prion-infected neurons. Images revealed the unaltered growth of the neuronal cells (Gordon et al., 2013). Western blot analysis of several neuronal markers showed no difference between control-infected and prion-infected neurons. This has been previously observed in *in vivo* studies, were no neuronal, presynaptic terminal and cholinergic neuron loss between control and prion infected mice in the hippocampal and cortical regions of the brain at 10 w.p.i. (Scarpa, 2022). M1 muscarinic expression was analysed using an M1 primary antibody, which revealed no change in the receptor expression levels as already demonstrated by previous prion infection *in vivo* studies carried out by our lab (Bradley et al., 2017). LC3B and Caspase-3 antibodies showed no significant difference between control and prion-infected neurons, suggesting the lack of increased cell death through

autophagy or apoptosis mechanisms respectively. These results show an absence of neurotoxicity and no change to neuron viability from the prion infection achieved in neuronal cultures at 7d.p.i., suggesting that misfolded prion does not directly cause neuronal death. This has previously been observed with other prion-like proteins such as Tau (Hallinan et al., 2019; Katsikoudi et al., 2020), were infection and propagation occur without a neurotoxic outcome for the neuronal cultures. In comparison to the *in vivo* studies carried out by our lab, neuroinflammatory markers were significantly elevated in the prion-diseased mice at 10 w.p.i., leading to neuronal loss in the later stages of the disease (Scarpa, 2022). The glial cells in charge of the neuroinflammatory responses are lacking in this *in vitro* model and are potentially the reason behind toxicity and cell death missing. Co-culture experiments with neurons and prion infected astrocytes, as well as primary neurons incubated in astrocyte-conditioned media from prion-infected astrocytes showed impairment in neuronal growth and maturation, as well as synapse integrity and spine density (Kushwaha et al., 2021). Other studies have also revealed glia-promoted neuronal death in other prion-infection models (Cronier et al., 2004), corroborating the hypothesis behind the lack of toxicity and neuronal death in these results. Although this model is not disease-causing, it can be utilized to investigate the mechanisms by which misfolded prions infects and propagate in neurons, and to discover the process to slow down or stop infection and propagation by testing ligands that directly or indirectly target PrP^{Sc}.

As the main goal for the whole project was to understand the role of the M1 mAChR in prion infection and propagation, the next step was to test the effects of M1 mAChR expression and endogenous activation using this prion model, by employing neuronal cultures from GEMMs with different mutations on the M1 mAChR (Chapter 1.3.5). The three mouse strains used were the M1-HA Wt, M1-KO and M1-DREADD, differing in the expression and activity of the receptor. Whilst M1-HA Wt express wild-type levels of the M1 mAChR, the M1-KO lack complete expression of it, and the M1-DREADD contains a two-point mutation in the receptor which inhibits the ability of the endogenous ligand ACh from activating the receptor. PrP^{Sc} levels after 7d.p.i. showed good accumulation across all strains, however no difference was observed, suggesting that the expression and endogenous activation of the receptor does not impact the speed at which infection occurs in neuronal cultures. As no further time-points were evaluated, whether the differences within the M1

mAChR would impact the propagation of PrP^{Sc} within neurons cannot be commented on. These results indicate that the M1 mAChR does not impact the uptake of PrP^{Sc} like other membrane proteins, such as dynamin-2 (Fehlinger et al., 2017). Whilst expression and endogenous activation of the receptor did not impact scrapie levels, it can be speculated that the additional activation of the M1 mAChR through muscarinic ligand treatments and as a consequence, the additional downstream signalling could potentially explain the decreased PrP^{Sc} levels seen from our labs *in vivo* experiments (Bradley et al., 2017; Dwomoh, Rossi, et al., 2022).

To examine this hypothesis, different selectivity, potency and efficacy ligands were used in the different neuronal cultures to interrogate how the induced activation of muscarinic receptors would alter infection and propagation of PrP^{Sc}. A 7 day chronic treatment of 10μM of each ligand was added to the neuronal cultures, from the day before prion infection up to the day before neuron collection, with no media changes involved. Other than some reduction trends of PrP^{Sc} in the M1-KO neurons with CNO and HTL9936 treatments, no significant changes were observed in PrP^{Sc} levels across the other strains and ligand treatments. The reduction trend in PrP^{Sc} levels after CNO in M1-KO neurons was an unexpected result, due to no DREADD receptor expression in these cells and therefore no direct target for CNO. Any off target hypothesis on why CNO would reduce PrP^{Sc} levels were discarded due to no reduction trends in the 6x Prion and M1-HA Wt neurons where, again, no DREADD receptor is expressed. The reduction trend in scrapie levels after HTL9936 treatment would suggest that the sole activation of the M4 receptor, as this ligand is selective for both the M1 and M4 mAChRs (Brown et al., 2021), is responsible behind the decreasing PrP^{Sc} levels. However, M1-DREADD neurons showed a different result to M1-KO neurons, were HTL9936 only activates the M4 receptor. From all these muscarinic ligand treatment results, it cannot be concluded that muscarinic activation leads to PrP^{Sc} deposition reduction. Instead, questions were posed on why this *in vitro* neuronal culture experiment does not correlate with previous *in vivo* experiments, were chronic muscarinic receptor treatment of prion mice lead to the slowing down of prion propagation compared to vehicle treated mice (Dwomoh, Rossi, et al., 2022). The lack of glial cells and the desensitization of muscarinic receptors were

the two hypotheses proposed for the differences between the *in vivo* and *in vitro* results.

To test the effects of chronic activation of muscarinic receptors in neuronal cultures, a radioligand binding assay and IP1 accumulation assay were carried out with 6x Prion neurons treated with Oxo for 7 days. Results demonstrated a significant decrease in muscarinic receptor expression at the plasma membrane and affinity for the radioligand, as well as a significant drop in the efficacy of ACh, the muscarinic endogenous ligand, to activate the $G_{q/11}$ signalling pathway, compared to vehicle treated neurons. A second binding assay was carried out with a membrane-permeable radioligand, in order to identify whether the muscarinic receptors had been internalised, however a significant decrease in receptor expression and affinity was also observed. These results suggest a possible desensitisation after internalisation or degradation of the muscarinic receptors due to the chronic ligand activation, in order to downregulate the receptor and inhibit further activation of the signalling pathway. Receptor desensitisation is a common feature of GPCRs when being over-activated to avoid excessive downstream signalling (Shankaran et al., 2007). Desensitisation most likely arises due to the lack of a glymphatic system, where excess products are eliminated or redistributed to prevent the over-activation of specific signalling pathway in the brain (Jessen et al., 2015). As no media changes were performed during the 7 day treatment to maintain the delicate environment neurons require to survive *in vitro*, Oxo would have excessively accumulated in the media, leading to the continuous activation of muscarinic receptors, and in consequence, lead to the desensitisation or degradation of the receptors. Although these two assays demonstrate a decrease in sensitised muscarinic receptor, no Western blot or qPCR was conducted to test for M1 mAChR protein expression and of M1 mRNA, respectively. From the PrP^{Sc} model characterisation, it is known that the M1 mAChR expression levels are unchanged between control-infected and prion-infected neurons (Figure 1-7), pointing at the chronic treatment with muscarinic ligands as the sole responsible for the muscarinic receptor desensitisation.

Neuronal cultures from M1-PD mice were prepared to test the prion infection model with chronic ligand treatments. This neuronal strain was chosen as the mice they are dissected from contain mutations in the 3rd intracellular loop and the C-

terminus preventing the phosphorylation, and therefore the internalisation of the M1 mAChR (Bradley et al., 2020). These neurons were used to observe the effect Oxo treatment would have on PrP^{Sc} infection, on an M1 mAChR which cannot be phosphorylated, internalised and desensitised. However, results showed no difference in prion deposition between vehicle and Oxo treated prion-infected cultures, and when testing muscarinic expression and activation in this strain of neurons, data again showed a significant decrease in muscarinic expression at both plasma membrane and cytosol levels, as well as a reduce efficacy of ACh to activate the $G_{q/11}$ signalling pathway. These results demonstrate that the desensitisation and/or degradation of the muscarinic receptors is not associated to the internalisation of the receptor after agonist binding as anticipated, and it is instead directly linked to the over-activation of the receptor, suggesting a distinct mechanism of desensitisation than through receptor phosphorylation.

Whilst previous studies carried in our lab have shown that *in vivo* chronic treatment of muscarinic receptors, specially the M1 mAChR, leads to therapeutic, disease-modifying outcomes by slowing down PrP^{Sc} progression (Bradley et al., 2017; Dwomoh et al., 2022; Scarpa et al., 2021), it was not possible to corroborate that data with the results obtained from this study. Instead, it can be concluded that an *in vitro* model of PrP^{Sc} infection and propagation, which will allow the study of these mechanisms, has been developed. This model has demonstrated that the accumulation of PrP^{Sc} in neurons is not the determining factor in this disease. The results have also demonstrated that the expression and endogenous activation of the M1 mAChR do not have a neuroprotective effect, as previously shown in *in vivo* studies (Scarpa, 2022; Scarpa et al., 2021), highlighting the possibility that the lack of astrocytes and microglia presence in these cultures and their role in neuroprotection, as a probable hypothesis for the differences between the *in vivo* and *in vitro* results. In addition, the presence of a neuronal mechanism to desensitise muscarinic receptors in response to chronic treatment with muscarinic agonists has been shown. All this data will allow to optimise *in vitro* experiments, using primary neuronal cultures, in which muscarinic compounds can be tested to further interrogate the question of the role of M1 mAChR in PrP^{Sc} infection, accumulation and propagation.

Chapter 5 Proteomic study of the new prion infection model of *in vitro* primary neuronal cultures

5.1 Introduction

5.1.1 Proteomic Studies of Protein Misfolding Diseases

Proteomics possesses the ability to thoroughly investigate protein expression alterations due to disease, informing us of potential new targets for drug discovery (Amiri-Dashatan et al., 2018). In addition to potential new targets, proteomics has also got the potential to discover early biomarkers of disease, allowing for the earlier treatment and possible prevention of such diseases before the onset of symptoms (Amiri-Dashatan et al., 2018). Proteomic studies have revealed that proteinopathies not only share the propagation of a misfolded protein but also many pathways activated during disease. Different mouse models for the same diseases showed similar proteome alterations, as well as some common altered pathways between disease.

Two examples of AD transgenic mouse models are the APP London transgenic mouse with a single mutation (V717I), and the Swedish transgenic mouse with a double mutation (K670M and N671L), which experiences amyloidosis around 2 years of age, accumulating amyloid-β in the neocortex and hippocampus (Richards et al., 2003). Proteomic studies of the APP Swedish model revealed alterations in the expression levels of proteins involved in neuroinflammation, metabolism, cellular transport and synaptic and axonal integrity, some of which are found to be differentially expressed in human AD brains (Butterfield et al., 2007), demonstrating the similarities between these mouse models and human AD. The Swedish/London (Swe/Lon) combination mutant mouse, combining the Swedish and London APP mice, has also revealed several upregulated proteins compared to healthy control animals (Sizova et al., 2007), that overlap with human AD patients (Schonberger et al., 2001; Tsuji et al., 2002). Again, these proteins demonstrate that this neurodegenerative disease alters inflammatory, metabolic markers, and synaptic and axonal integrity proteins compared to healthy control mice.

In addition to amyloid-β generating mouse models, tau mouse models have also been developed to study the effects of tau hyperphosphorylation and aggregation, in order to understand its role in AD and FTLD. One of these mouse models is a

mouse expressing the human P301S tau protein (Allen et al., 2002), which is a mutation that leads to an early-onset form of FTLD (Macdonald et al., 2019). This mouse model is characterised by the accumulation of hyperphosphorylated tau detected in the brain, one of the hallmarks of AD and FTLD. Proteomic studies using this mouse model revealed downregulation in mitochondrion-related proteins whilst upregulation in inflammatory-related and microtubule-related proteins (Tsumagari et al., 2022), demonstrating the proteome alteration caused due to accumulation of hyperphosphorylated tau. Although different mutations in different genes have been used to generate different mouse models of AD, similar proteome changes can be seen between the mouse models, such as metabolic and neuroinflammatory markers being altered in all mouse models investigated.

A commonly mouse model used to investigate PD is the 1-methyl-4-phenyl-1,2,3,6-tetrahydropyridine (MPTP)-treated mouse model. MPTP is a dopaminergic neurotoxin used to chemically induce parkinsonism (Schober, 2004). This toxin affects dopaminergic neurons, inducing human symptoms nearly identical to PD in mice (Przedborski & Vila, 2003). Chronic treatment of MPTP in mice leads to the progressive build-up of α-synuclein aggregates, neuroinflammation and neurodegeneration in the substantia nigra region of the brain (Zhang et al., 2017). Proteomic data obtained from MPTP-treated mice studies revealed alterations in mitochondrial-related protein expression (Jin et al., 2005), microglial-associated proteins linked to elevation of nitric oxide synthase observed in inflammation (Mclaughlin et al., 2006), as well as proteins involved in neurogenesis and cytoskeleton pathways (Diedrich et al., 2008). These proteome alterations seen in mouse models have also been reported in proteomic studies on PD human brains, were proteomic changes related to mitochondrial dysfunction, cytoskeleton impairment, and oxidative stress have also been identified (Kitsou et al., 2008).

5.1.2 Proteomic Studies in Prion Disease Models

The proteome of different prion disease models has been previously investigated, both in immortalised cell lines and animal models. A study using N2a neuroblastoma cells, an immortalised cell line which endogenously expresses PrP^{C}, revealed alteration in autophagy related proteins after scrapie prion infection (Hutti et al., 2020). The proteome-wide data in this study demonstrated an

upregulation in the cellular degradation machinery in comparison to uninfected cells (Hutti et al., 2020). In addition, animal models of prion disease have revealed proteome alterations as a consequence of the misfolding and propagation of PrP^{Sc}. One proteomic study looking at prion-infected mice with RML demonstrated protein expression alteration of neuroinflammatory, complement activation and cytoskeletal associated markers in both diseases (Moore et al., 2014). Molecular transport proteins were also found to be altered in disease, whilst differences in cell death and survival pathways were identified to be different between two different types of prion disease in mice (Moore et al., 2014).

Our lab (Dwomoh, Rossi, et al., 2022), performed a proteomic analysis to understand the changes occurring between NBH control-inoculated healthy mice and RML prion-inoculated diseased mice, as previously mentioned in Chapter 4.1.1. Proteins associated with neuronal dysfunction, inflammation, and AD were shown to be upregulated in this murine model of prion disease (Dwomoh, Rossi, et al., 2022). Additionally, this study also identified how targeting the M1 mAChR with the VU846 PAM in mouse prion disease modifies the hippocampal proteome. The data revealed a significant reduction of the majority of the proteins which had been significantly altered, bringing their expression closer to that of healthy mice. Specifically, VU846 reduced the expression levels of the neuroinflammation markers and increased levels of synaptic proteins previously altered by RML-inoculation (Dwomoh, Rossi, et al., 2022). This study reports the changes that occur at a protein level in prion diseased mice, but also that the activation of the M1 mAChR can revert these protein expression alterations. However, the data did not reveal any major changes occurring to neurons, with the majority of differently expressed proteins belonging to glial cells and inflammatory pathways. Such large glial changes could potentially be masking smaller significant alterations occurring within the neurons in prion disease. It is for this reason that further understanding on how PrP^{Sc} infection impacts neuronal cells directly by testing this new model, previously described in Chapter 4, is required.

5.1.3 Aims

The main aim for this chapter was to understand the alterations at the protein level that occur after PrP^{Sc} infection of primary neuronal cultures. Whilst previous studies have performed proteomics in immortalised cells lines (Hutti et al., 2020)

and animal models (Dwomoh, Rossi, et al., 2022; Moore et al., 2014) of prion disease to study prion protein degradation and disease impact at a protein level, respectively, no proteomic analysis has been performed in primary neuronal cultures infected with PrP^{Sc}. The majority of this proteomic studies have revealed major alterations in glial markers and neuroinflammatory pathways (Dwomoh, Rossi, et al., 2022; Moore et al., 2014), which could potentially be masking major changes happening within neuronal cells. Therefore, the aim was to perform a proteomic analysis of this novel prion infection model, previously described in Chapter 4, to investigate and characterise the protein changes which occur after prion infection. This data would permit us to understand what occurs to the neuronal cells in the presence of purified RML inoculum and identify altered proteins which could potentially be involved in the mechanism of infection and propagation of PrP^{Sc}.

5.2 Specific Methodology

5.2.1 Proteomic sample experimental outline

Primary neurons were prepared from 6x prion embryonic mice as explained in Chapter 2.4. Neurons were cultured for 7 days before either being left uninfected, NBH control-treated or RML prion-infected. At 7 d.p.i., the neuronal cultures were lysed, trypsin digested and labelled with TMT for mass spectrometry analysis as per Chapter 2.9. Figure 5-1 illustrates a diagrammatic representation of the protocol followed for the sample preparation for the proteomic study.

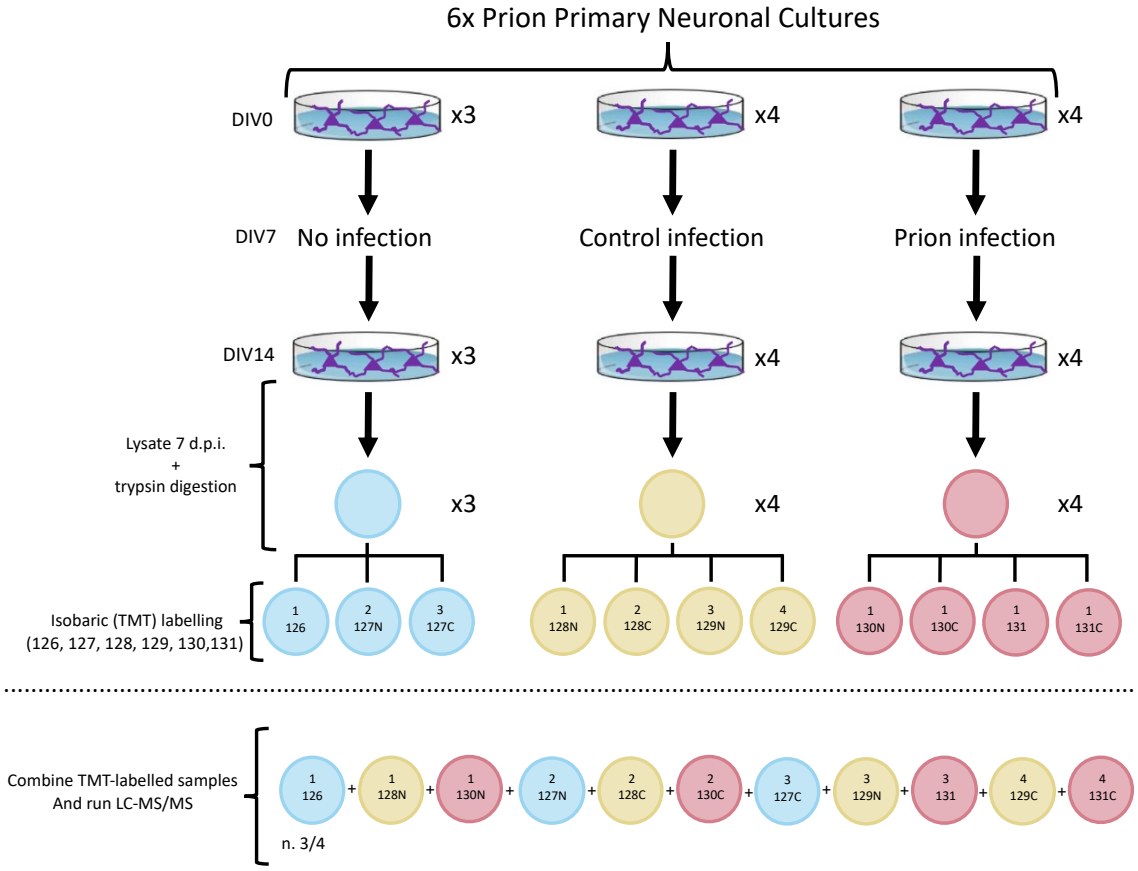

Figure 5-1 Flow diagram outlining the procedure carried out for the proteomic study between uninfected (blue), NBH control-treated (yellow) and RML prion-infected (red) 6x Prion primary neuronal cultures.

5.3 Results

5.3.1 Initial analysis of uninfected, NBH control-treated and RML prion-infected neuronal cultures' samples

Overall distribution density plots (Figure 5-2A) of the identified proteins demonstrate the high similarity within all samples from the three groups: uninfected, NBH control and RML prion. The high similarity across all samples indicates good experimental quality. The Principal Component Analysis (PCA) scatterplot (Figure 5-2B) between all three groups showed no clear separation between them. Sample replicates clustered together, showing high similarities in protein expression within the sample group, however, the different group samples showed no separation from each other, suggesting little differences between the protein expression of all samples.

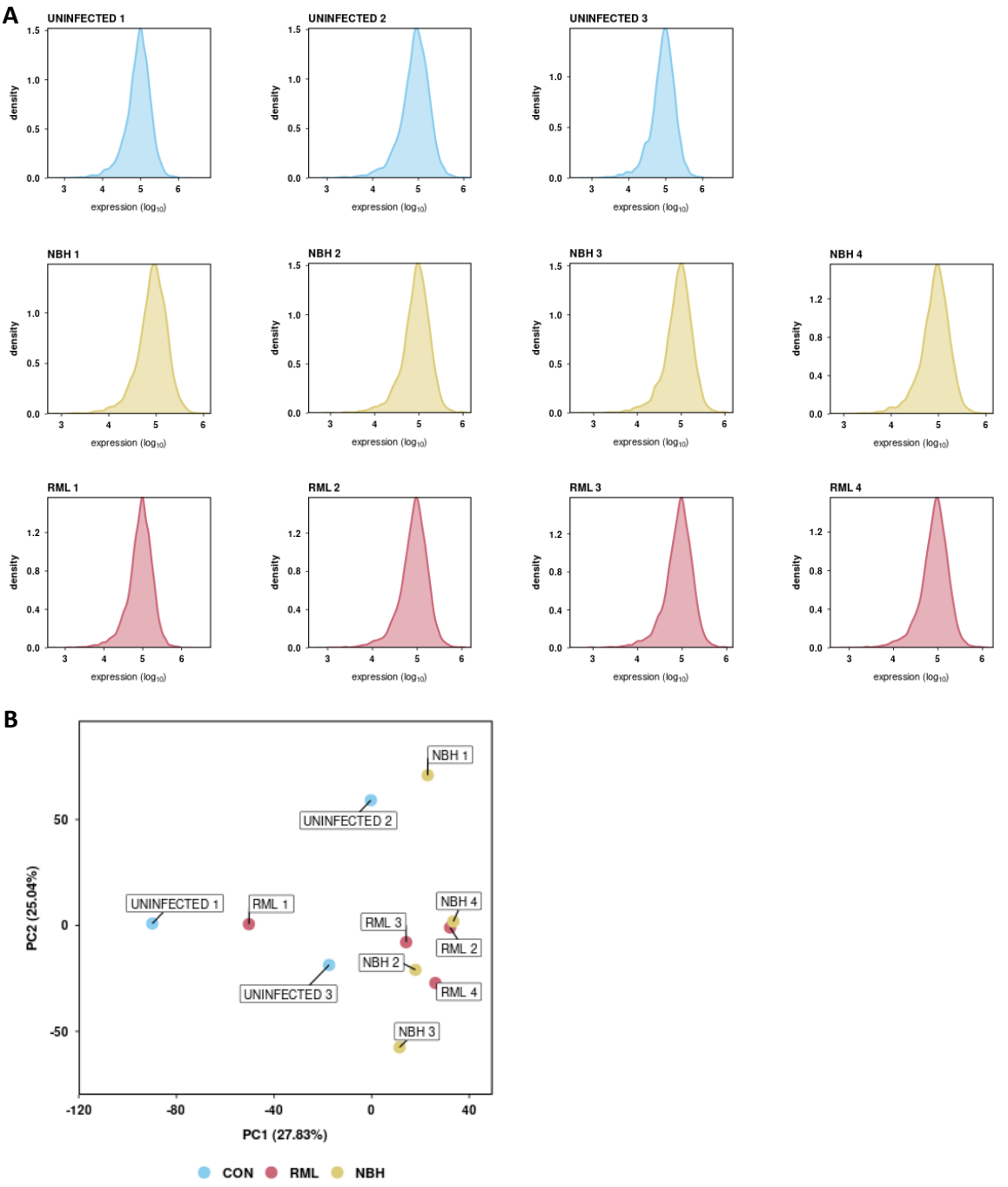

Figure 5-2 Density plots and PCA of all samples from the three groups. (A) Density plots revealing the overall distribution of all samples from the Uninfected (blue), NBH control (yellow) and RML prion (red) infection groups. X-axis shows the expression values on a log 10 scale. Y-axis shows the protein density. **(B)** PCA scatterplot, showing PC1 vs PC2. Each dot represents and individual sample (blue = uninfected, red= RML, yellow = NBH). Total variation percentage by each component is shown in the x- and y-axis. Z-core transformation was used to scale protein by protein basis all the protein expression values, prior to PCA, to control for high expressed proteins over representation.

5.3.2 General comparison between all 3 group samples

Spearman correlation analysis was performed out to observe the differences and similarities between all samples based on how weakly or strongly they correlate with each other across all protein expression results (Figure 5-3A). The total number of proteins identified, which met the robust criteria for analysis and quantification, was 5361. Protein expression statistical analysis revealed 69 proteins to be significantly differentially expressed in NBH control-treated compared to uninfected neurons, 77 proteins in RML prion-infected compared to uninfected neurons, and finally, 72 proteins in RML prion-infected compared to NBH control-treated neurons (Figure 5-3B). All these proteins were compared between all the sample groups in order to visualise any pattern within the data (Figure 5-3C).

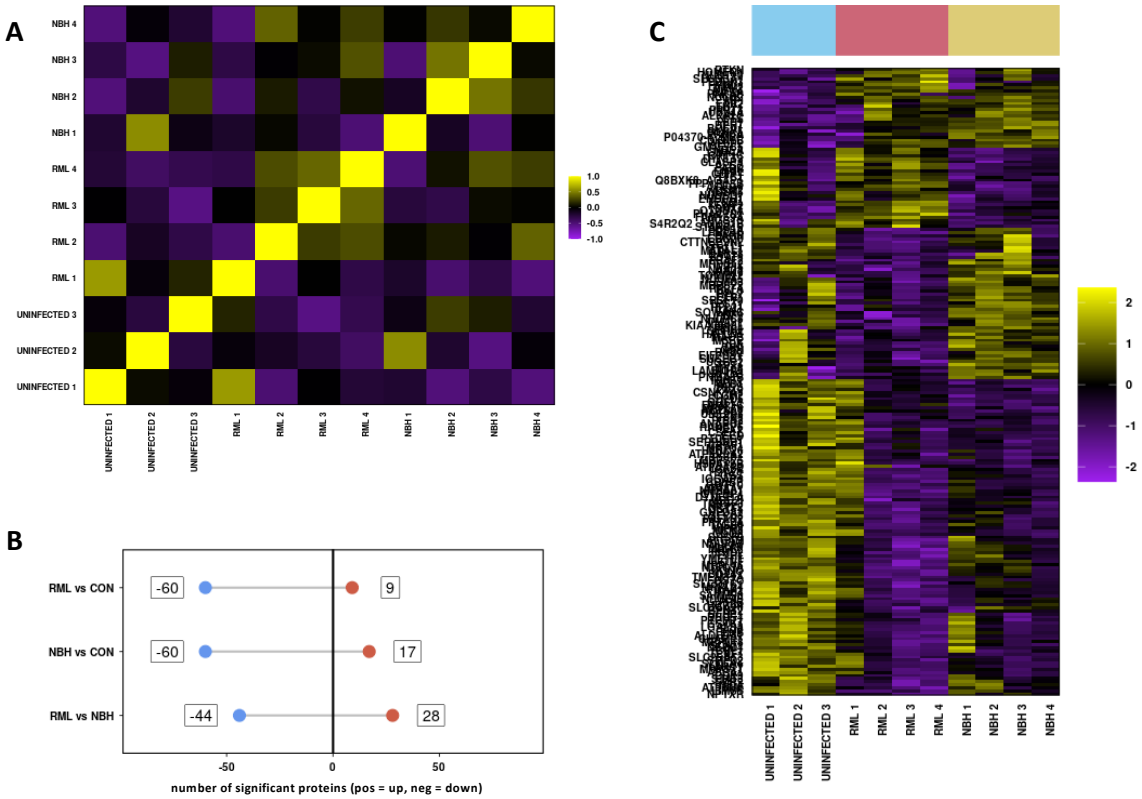

Figure 5-3 Heatmaps and significant protein changes between all three groups. (A) Heatmap of sample correlation between all samples from all three groups. Spearman Correlation was used to calculate the correlation between all protein expression values. The level of correlation is represented by colour intensity, with strong positive correlation in yellow, no correlation is black and strong anti-correlation in purple. **(B)** Bar chart revealing the number of significantly upregulated (red) and downregulated (blue) proteins between all three groups. **(C)** Hierarchically clustered heatmap of the significantly up- and downregulated proteins between uninfected (blue), NBH (yellow) and RML (red) groups. Samples are shown in the x-axis and proteins are shown on the y-axis. Colour intensity represents protein expression level, purple indicating low expression, and yellow indicating high expression. Expression levels have been row scaled into z−scores.

5.3.3 Impact of NBH control-treatment in primary neuronal cultures

In order to validate the NBH control-treated samples as a good control for this experiment, NBH control-treated neuronal cultures were first compared against uninfected neurons. Analysis between these two groups revealed a total of 77 proteins to be significantly different by p-value of less that 0.01, a total of 60 significantly downregulated proteins whilst only 17 were upregulated (Figure 5-4A). From the top 10 most differentially expressed proteins, ATP binding cassette subfamily A member 1 (ABCA1), TRPM8 channel associated factor 1 (TCAF1), coenzyme Q6, monooxygenase (COQ6) and CCM2 scaffold protein (CCM2) are all downregulated, whilst myelin basic protein (MBP) and glutaredoxin 5 (GLRX5) are examples of upregulated proteins (Figure 5-4B). The hierarchically clustered heatmap (Figure 5-4C) indicates all proteins which were either significantly up- or downregulated in NBH control-treated compared to uninfected neurons. All significantly upregulated and downregulated proteins in NBH control-treated neurons compared to uninfected neurons are listed in Supplementary Figure 5-1.

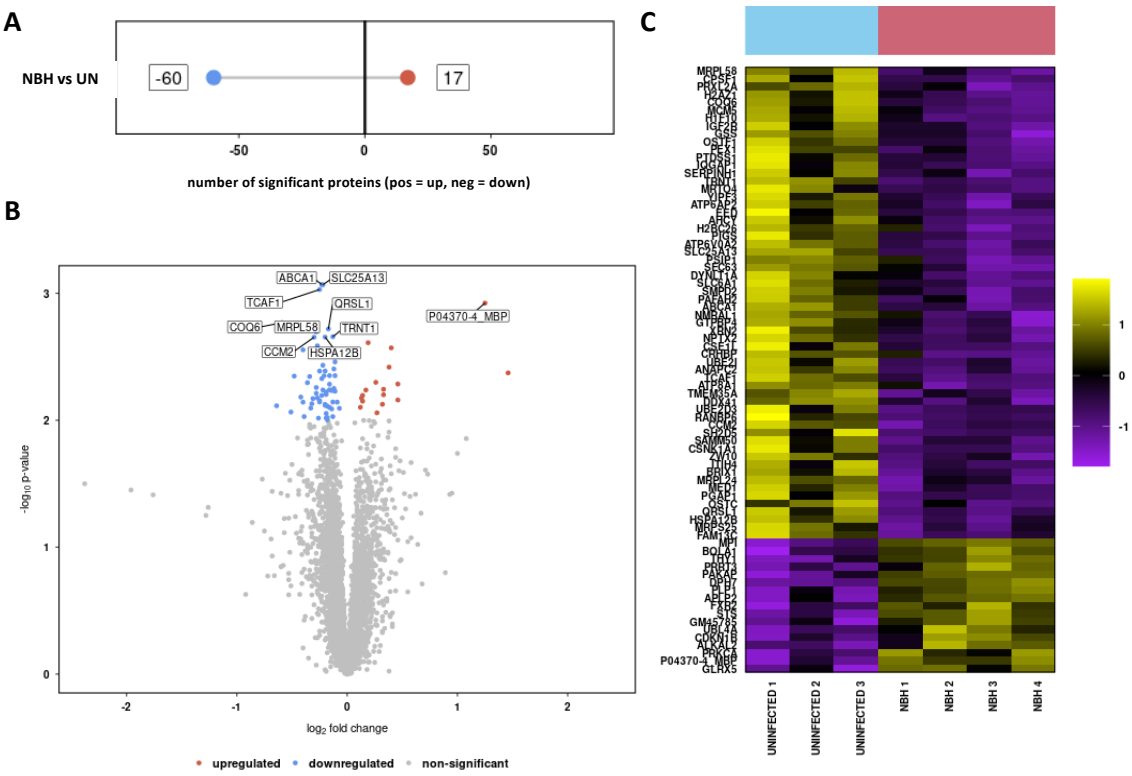

Figure 5-4 Upregulated and downregulated proteins by p-value in NBH control-treated vs uninfected neurons. (A) Bar chart revealing the number of significantly upregulated (red) and downregulated (blue) proteins comparing NBH control-treated to uninfected neurons. **(B)** Volcano plot comparing NBH control-treated to uninfected neuron proteins. Significantly differential proteins ($p < 0.01$, absolute log2 fold > 0.0) are shown in red (upregulated) and blue (downregulated), and non–significant proteins in grey. **(C)** Hierarchically clustered heatmap of the significantly up- and downregulated proteins comparing NBH control-treated to uninfected samples. Samples are shown in the x-axis and proteins are shown on the y-axis. Colour intensity represents protein expression level, purple indicating low expression, and yellow indicating high expression. Expression levels have been row scaled into z–scores.

5.3.4 Impact of RML prion-infection in primary neuronal cultures

The proteome expression of RML prion-infected neurons was compared to both uninfected neurons and NBH control-treated neurons to understand the impact of PrP^{Sc} infection compared to both vehicle and healthy brain purified material treated neurons.

Analysis between RML prion-infected neuron samples and uninfected neuron samples revealed a total of 60 significantly downregulated proteins whilst only 9 were upregulated by p-value of less that 0.01 (Figure 5-5A). From the top 10 most differentially expressed proteins, ergosterol biosynthesis 28 homolog (ERG28), KIAA0319-like protein (KIAA0319L), integrin subunit beta 6 (ITGB6) and LIM zinc finger domain containing 1 (LIMS1) are all downregulated, whilst TIAM Rac1

associated GEF 2 (TIAM2), formin like 1 (FMNL1) and PDZ domain containing ring finger 3 (PDZRN3) are examples of upregulated proteins (Figure 5-5B). The hierarchically clustered heatmap (Figure 5-5C) indicates all proteins which were either significantly up- or downregulated in RML prion-infected compared to uninfected neurons. All significantly upregulated and downregulated proteins in RML-prion infected neurons compared to uninfected neurons are listed in Supplementary Figure 5-2.

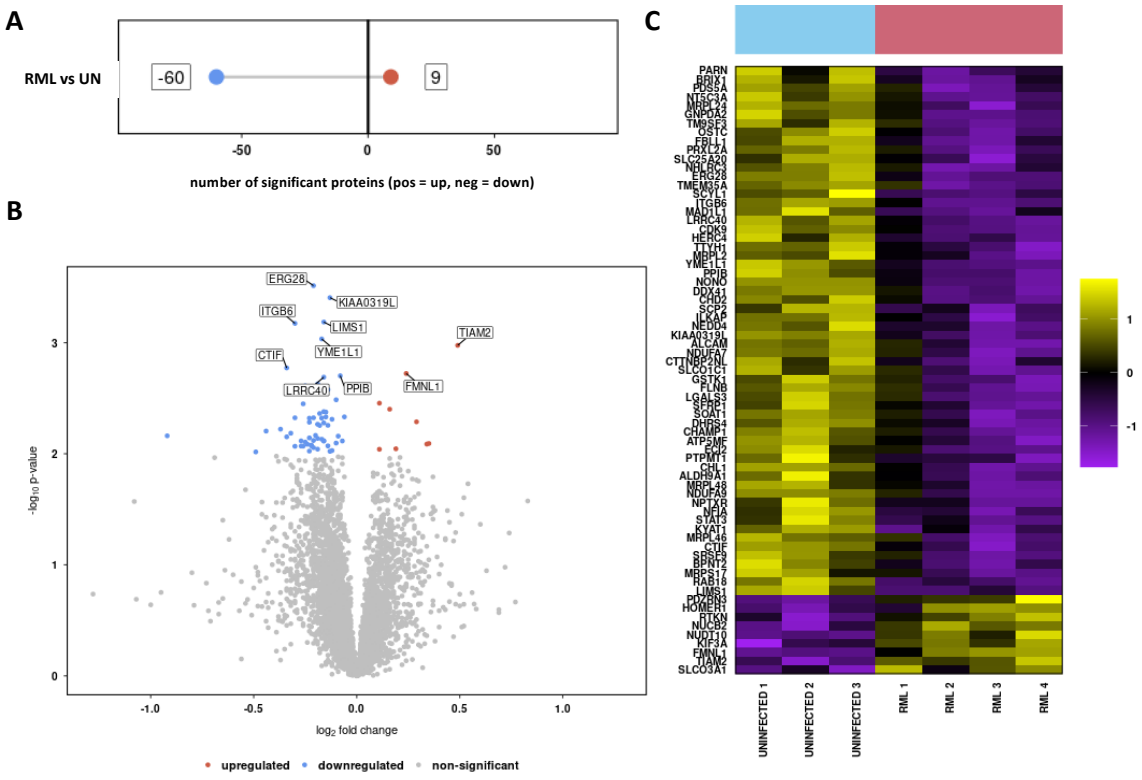

Figure 5-5 Upregulated and downregulated proteins by p-value in RML prion-infected vs uninfected neurons. (A) Bar chart revealing the number of significantly upregulated (red) and downregulated (blue) proteins comparing RML prion-infected to uninfected neurons. **(B)** Volcano plot comparing RML prion-infected to uninfected neuron proteins. Significantly differential proteins ($p < 0.01$, absolute log2 fold > 0.0) are shown in red (upregulated) and blue (downregulated), and non–significant proteins in grey. **(C)** Hierarchically clustered heatmap of the significantly up- and downregulated proteins comparing RML prion-infected to uninfected samples. Samples are shown in the x-axis and proteins are shown on the y-axis. Colour intensity represents protein expression level, purple indicating low expression, and yellow indicating high expression. Expression levels have been row scaled into z–scores.

Analysis between NBH control-treated and RML prion-infection groups revealed that out of the 5361 proteins identified, a total of 72 proteins were significantly different in RML samples compared to NBH. Specifically, 44 proteins were significantly downregulated and 28 were upregulated by an p-value of less that 0.01 in RML prion-infected neurons compared to NBH control-treated neurons

(Figure 5-6A). From the top 10 most differentially expressed proteins, translational controlled tumour protein 1 (TPT1), gelsolin (GSN), NHL repeat containing 3 (NHLRC3) and N-alpha-acetyltransferase 38 (NAA38) are all downregulated, whilst actin beta like 2 (ACTBL2), dynein light chain Tctex-type 3 (DYNLT3), potassium sodium-associated channel subfamily T member 2 (KCTN2) and regulator of G protein 13 (RGS13) are examples of upregulated proteins (Figure 5-6B). The hierarchically clustered heatmap (Figure 5-6C) indicates all proteins which were either significantly up- or downregulated in RML prion-infected compared to NBH control-treated neurons.

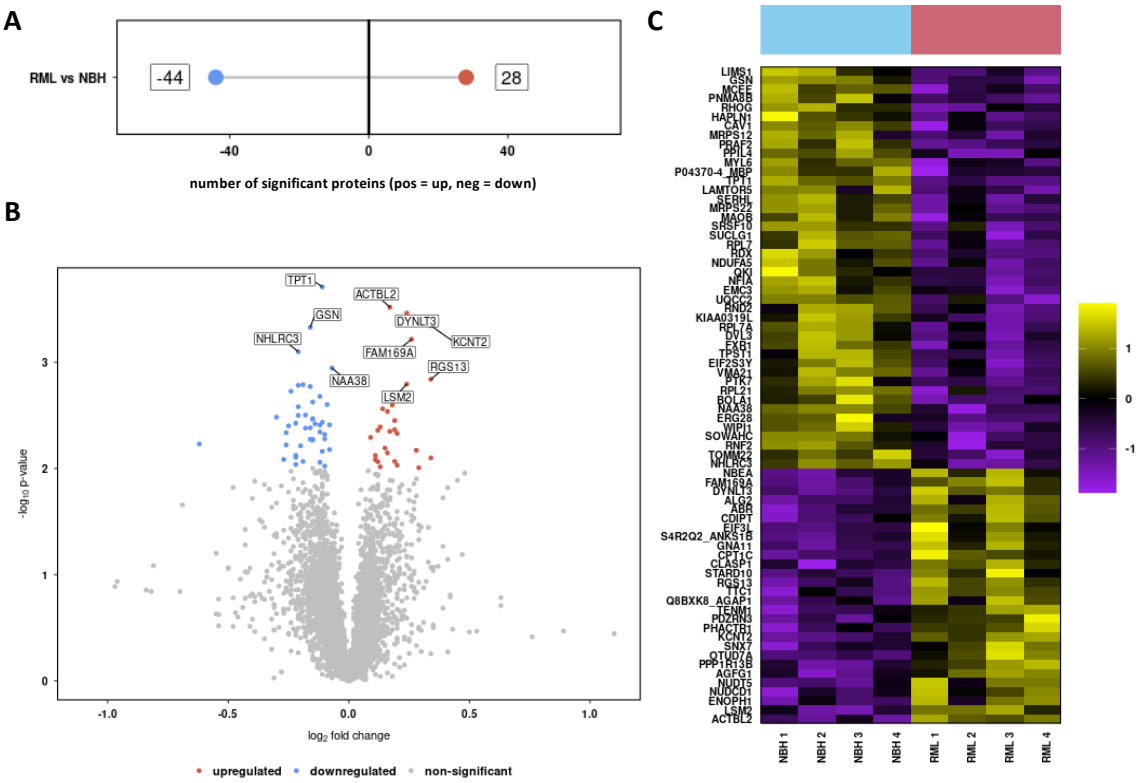

Figure 5-6 Upregulated and downregulated proteins by p-value in RML prion-infected vs NBH control-treated neurons. (A) Bar chart revealing the number of significantly upregulated (red) and downregulated (blue) proteins comparing RML prion-infected to NBH control-treated neurons. **(B)** Volcano plot comparing RML prion-infected to NBH control-treated neuron proteins. Significantly differential proteins ($p < 0.01$, absolute log2 fold > 0.0) are shown in red (upregulated) and blue (downregulated), and non−significant proteins in grey. **(C)** Hierarchically clustered heatmap of the significantly up- and downregulated proteins comparing RML prion-infected to NBH control-treated samples. Samples are shown in the x-axis and proteins are shown on the y-axis. Colour intensity represents protein expression level, purple indicating low expression, and yellow indicating high expression. Expression levels have been row scaled into z−scores.

5.3.5 RML prion-infection vs NBH control-treated primary neuronal cultures

As the aim of this proteomic study was to compare the differences between NBH control-treatment and RML prion-infection in neuronal cultures, further evaluation of the most differentially expressed proteins between both groups was performed. Statistical analysis revealed the top 10 most significantly upregulated proteins by p-value (Figure 5-7A) in RML-prion infection compared to NBH control-treated neurons. ACTBL2, a cytoskeletal associated protein, was found to be the most significantly upregulated protein (p=0.000303. A dynein regulatory protein, DYNLT3, was the second most upregulated protein (p=0.000344) after ACTBL2 (Figure 5-6B). Potassium sodium-activated channel subfamily T member 2 (KCNT2), family with sequence similarity 169 member A (FAM169A), RGS13, LSM2 homolog, U6 small nuclear RNA and mRNA degradation associated (LSM2), Gα protein subunit 11 (GNA11), OTU deubiquitinase 7A (OTUD7A), Tetratricopeptide repeat domain 1 (TTC1) and CDP-diacylglycerol-inositol 3-phosphatidyltransferase (CPT1C) are the other 8 most significantly up regulated proteins by p-value (Figure 5-7B). The protein names and functions of all significantly upregulated proteins are listed in Supplementary Figure 5-3.

A

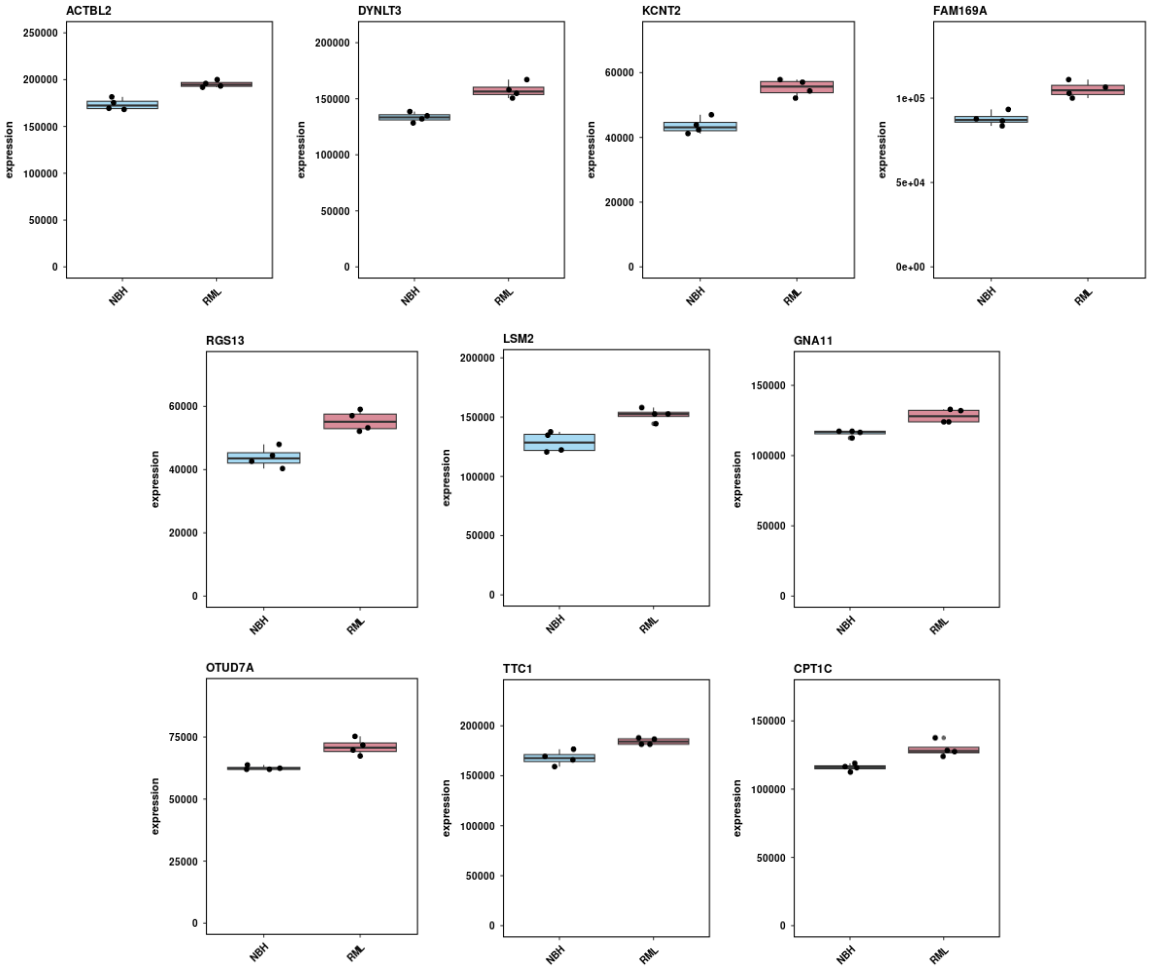

B

Gene	log2fold	p	p.adj
ACTBL2	0.17	0.0003027069	0.0003027069
DYNLT3	0.24	0.0003441933	0.0003441933
KCNT2	0.34	0.0004520204	0.0004520204
FAM169A	0.26	0.0006060627	0.0006060627
RGS13	0.34	0.0014464862	0.0014464862
LSM2	0.24	0.0016059822	0.0016059822
GNA11	0.15	0.0021443043	0.0021443043
OTUD7A	0.18	0.0025289020	0.0025289020
TTC1	0.14	0.0027383237	0.0027383237
CPT1C	0.16	0.0029095312	0.0029095312

Figure 5-7 Top 10 upregulated proteins. (A) Box plots of each of the 10 most upregulated proteins by p-value. Showing expression values for all samples in the sample groups: NBH control (blue) and RML prion (red). Each dot is one sample, with sample groups given on the x-axis and protein expression on the y-axis. The mean and standard error for each sample group is shown with lines. **(B)** Table showing the 10 most upregulated proteins by p-value. Upregulated proteins are higher in RML than in NBH.

The top 10 most significantly downregulated proteins by p-value (Figure 5-8A) were also shown. TPT1, a cellular growth and proliferation regulatory protein, was found to be the most significantly downregulated protein (p=0.000195) in RML prion-infected samples compared to NBH control-treated samples. GSN, another actin-associated protein, was found to be the second most upregulated protein (p=0.000468) (Figure 5-8B). NHLRC3, NAA38, methylmalonyl-CoA epimerase (MCEE), vacuolar ATPase assembly factor 21 (VMA21), mitochondrial ribosomal protein S22 (MRPS22), nuclear factor I A (NFIA), KIAA0319L and caveolin 1 (CAV1) are the other 8 most significantly up regulated proteins by p-value (Figure 5-8B). The protein names and functions of all significantly downregulated proteins are listed in Supplementary Figure 5-4.

A

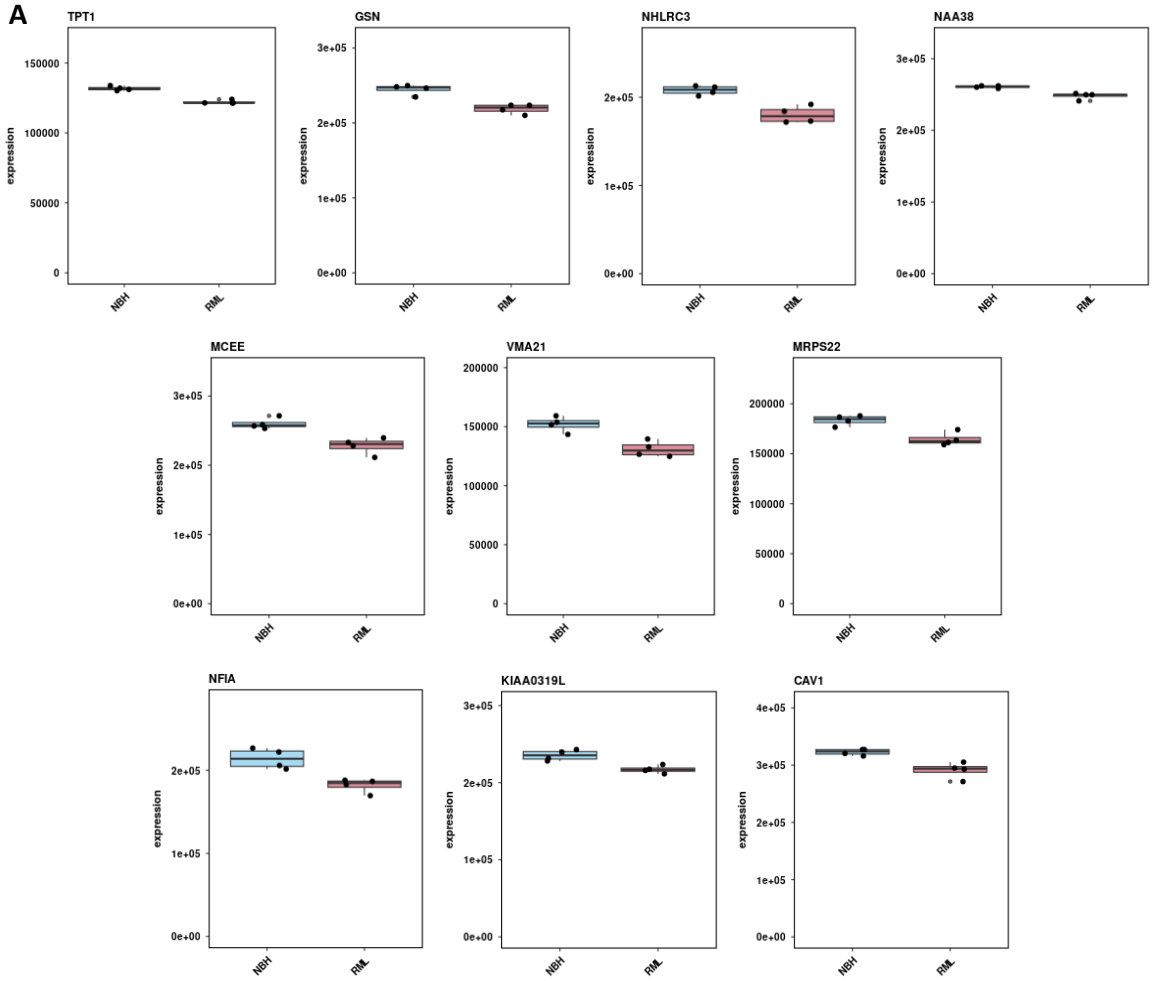

B

Gene	log2fold	p	p.adj
TPT1	-0.11	0.0001951400	0.0001951400
GSN	-0.16	0.0004683316	0.0004683316
NHLRC3	-0.21	0.0007951265	0.0007951265
NAA38	-0.07	0.0011329655	0.0011329655
MCEE	-0.19	0.0016234047	0.0016234047
VMA21	-0.21	0.0016469662	0.0016469662
MRPS22	-0.16	0.0016926530	0.0016926530
NFIA	-0.24	0.0018729972	0.0018729972
KIAA0319L	-0.12	0.0020924283	0.0020924283
CAV1	-0.15	0.0023672363	0.0023672363

Figure 5-8 Top 10 downregulated proteins. (A) Box plots showing for each of the 10 most downregulated proteins by p-value. Showing expression values for all samples in the sample groups: NBH control (blue) and RML prion (red). Each dot is one sample, with sample groups given on the x-axis and protein expression on the y-axis. The mean and standard error for each sample group is shown with lines. **(B)** Table showing the 10 most downregulated proteins in RML-infected samples compared to NBH neurons by p-value.

From the significantly upregulated and downregulated pool of proteins by log 2 fold change of more than 0.4, only two of them showed a nearly significant p value (Figure 5-9A). These two proteins were alpha-actinin 4 (ACTN4) (log2fold=0.45, p=0.012953) and actin filament-associated protein 1 (AFAP1) (log2fold=0.48,

p=0.011053) (Figure 5-9B). Western blot was performed to attempt to visualise the difference seen in alpha-actinin in the proteomic analysis, however, no significant difference in RML prion-infected neurons compared to NBH control-treated neurons was observed when probed using an anti-alpha-actinin antibody (Figure 5-9C,D).

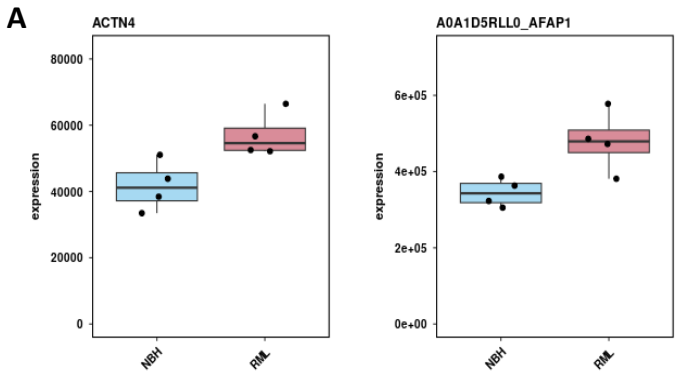

B

Gene	log2fold	p	p.adj
ACTN4	0.45	0.01295292	0.01295292
A0A1D5RLL0_AFAP1	0.48	0.01105273	0.01105273

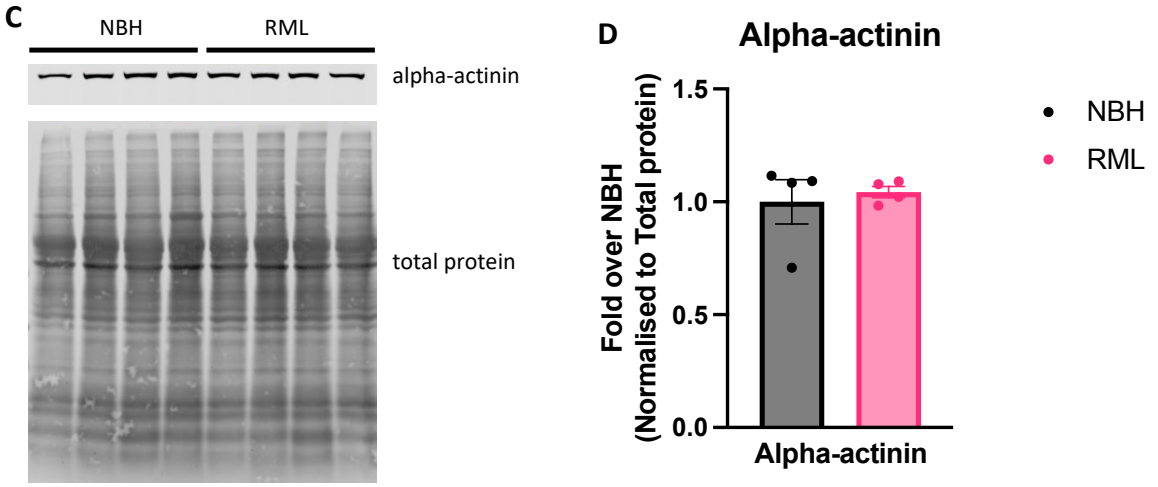

Figure 5-9 Upregulated proteins by p-value and log2fold. (A) Box plots showing upregulation of ACTN4 and AFAP1 proteins by log2fold change. Showing expression values for all samples in the sample groups: NBH control (blue) and RML prion (red). Each dot is one sample, with sample groups given on the x-axis and protein expression on the y-axis. The mean and standard error for each sample group is given as a red dot and line. **(B)** Table showing the ACTN4 and AFAP1 proteins upregulated by p-value and log2fold change. **(C)** Western Blot of NBH and RML sample probed with alpha-actinin antibody and total protein. **(D)** Band intensity analysis (EmpiriaStudio) for alpha-actinin. Statistical analysis conducted was unpaired T-test. Data is expressed as mean ± SEM of three independent experiments. (n=4).

5.4 Discussion

This chapter set out to characterise this *in vitro* infection and propagation model of PrP^{Sc} in primary neuronal cultures utilising a mass spectrometer proteomic analysis approach. Uninfected, NBH control-treated and RML prion-infected neurons were lysed at 7 d.p.i. and processed for mass spec. Analysis of both NBH control-treated and RML prion-infected neurons compared to uninfected neurons was performed to validate the effect of treating neuronal cultures with purified brain material and identify any protein expression changes due to treating the neurons with brain homogenate rather than infecting with PrP^{Sc}. Four proteins were found to be downregulated both in NBH and RML compared to uninfected neurons, three of which BRIX1, DDX41 and MRPL24, are associated to ribosomes and the production of proteins (Huang et al., 2020; Jiang et al., 2024; Tungalag et al., 2023), and OSTC, which contributes to dolichyl-diphosphooligosaccharide-protein glycotransferase activity (Chen et al., 2014). As these four proteins are being upregulated by both purified NBH and RML brain homogenates, it is suspected that this change is a result of the buffers and solutions used in the purification protocol, or any other protein present within the purified brain homogenate, such as growth factors. A potential chemical which could be behind these effects is sarcosyl, the detergent used in the purification protocol, which has been shown to impact RNA polymerases (Szentirmay & Sawadogo, 1994). A potential indirect effect from sarcosyl could be impacting the three ribosomal-associated proteins being downregulated. Although this is a possibility, it is unlikely due to the low concentration at which it would be present as well as the pellets being resuspended in PBS after solubilisation, as sarcosyl would have had other impacts on the neurons due to being a detergent. Another possibility could be the presence of other proteins, such as growth factors, within the purified brain materials used in these treatments, which could potentially be leading to the alteration of these proteins. Further analysis of the purified material being used to treat the neuronal samples to identify the remaining proteins after prion purification could reveal what possible protein/s could be behind these changes in protein expression.

This study revealed differentially expressed protein similarities between RML-infected and NBH-treated, and RML-infected and uninfected neurons,

demonstrating that the NBH control-treated neurons are a good control. An example of this is the BolA family member 1 (BOLA1) protein, which was found to be downregulated in RML prion-infected neurons compared to both NBH control-treated neurons and uninfected neurons. BOLA1 acts as a mitochondrial iron-sulfur (Fe-S) cluster assembly factor, facilitating the insertion of the (Fe-S) cluster into a subset of mitochondrial proteins (Willems et al., 2013). As mentioned in the introduction, proteomic studies in NDs have previously revealed the alteration and dysfunction of mitochondrial-related proteins (Jin et al., 2005; Kitsou et al., 2008), supporting the data that PrP^{Sc} infection is having an effect on some mitochondrial proteins in the neuronal cultures. Other mitochondrial-related proteins have also been found to be downregulated in the RML prion-infected neurons compared to the NBH control-treated neurons, specifically MRPL24, already mentioned above, and NDUFA5, TOMM22 and UQCC2, which are all localised in the mitochondria and mitochondrial outer membrane. NADH:ubiquinone oxidoreductase subunit A5 (NDUFA5), a protein localised in the inner mitochondrial membrane where it helps in the electron transfer from NADH to ubiquinol, has been found to be associated to both AD and PD (Ahmad et al., 2016; Talebi et al., 2016). Downregulation of this protein has been shown to have dysfunctional consequences on mitochondria in other NDs, specifically in diseased AD mouse models (George et al., 2010). Tsumagari et al. (2022) reported major downregulation in mitochondrial-associated proteins in their tau AD mouse model, with NDUFA10, from the same family as NDUFA 5, to be one of the most significantly downregulated proteins. They also saw downregulation in proteins associated with the tricarboxylic acid (TCA) cycle, demonstrating a functional dysregulation of this energy producing pathway. This data potentially suggests that this PrP^{Sc} infection model could be having a direct detrimental impact on mitochondrial energy production in neuronal cultures. These similarities in protein alteration between other NDs and the prion infection in neuronal cultures, allows us to understand that this prion infection model does have a detrimental impact upon the neuronal cultures. The changes observed might be subtle compared to neurodegeneration mouse models, where neuronal death, autophagy or apoptotic markers are being highly differentially expressed compared to control healthy mice, however, the short time-course of this experiment or the lack of glial cells are most likely preventing these markers from being differentially expressed in this *in vitro* model.

Unexpectedly, myelin basic protein (MBP) was found in the proteomic data analysis. MBP is major constituent of the myelin sheath of oligodendrocytes (Boggs, 2006), a cell type which should not be present in the cultures. Although myelin proteins are characteristic of oligodendrocytes, MBP has been reported to be expressed in differentiating neurons extracted from pre- and post-natal mice, with its expression levels decreasing dramatically once reached maturation (Landry et al., 1996; Miyazaki et al., 2024), explaining the expression of this protein in the neuronal cultures. This specific type of MBP was found in early neurodevelopmental neurons is referred to as golli-MBP contrary to the classic-MBP expressed in oligodendrocytes (Siu et al., 2015). Another potential explanation is the low presence of oligodendrocytes within the cultures. Although neurobasal complete media is a well-established neuronal media which prevents non-neuronal cells from growing (Brewer et al., 1993), it is possible for a low number of oligodendrocytes to be present within the cultures. MBP found to be downregulated in RML prion infected neurons compared to NBH control-treated, showing a downregulating impact of PrP^{Sc} on either golli-MBP present in the neurons or on any oligodendrocytes present.

Interestingly, the E3 ubiquitin ligase, DZ domain containing ring finger 3 (PDZRN3), was upregulated in RML prion-infected neurons compared to both uninfected and NBH control-treated neurons. E3 ubiquitin ligases are essential in mediating the degradation of proteins by the proteasome and play key roles in many essential biological pathways (Jeong et al., 2023). Upregulation of PDZRN3 could potentially be a result of PrP^{Sc} infection, propagation or toxicity, leading to the enhanced degradation of yet unidentified proteins in the neuronal cultures. Upregulation of PDZRN3 has been previously linked to dysfunction in synaptic growth and maturation in neuromuscular junction (Lu et al., 2007), as well as its expression linked to modulation of hippocampal synapse maturation (Kumari et al., 2017). Therefore, its upregulation after RML prion-infection, could potentially be having a negative dysfunction impact on the neuronal synapses of the neuronal cultures. The protein/s targeted by PDZRN3 in the neuronal cultures are unknown, however, PDZRN3 has been shown to be implicated in Wnt signalling, specifically Wnt5a-Ror signalling (Snavely et al., 2021). Wnt5a-Ror signalling is implicated in the regulation of morphogenic processes during vertebrate development, being a

crucial regulator of neurogenesis (Subashini et al., 2017). PDZRN3 has been shown to be degraded in the normal functioning of the Wnt5a-Ror pathway, however, in these results, an upregulation of PDZRN3 is observed (Snavely et al., 2021). This demonstrates dysregulation in PDZRN3 expression levels, which could possibly be having a detrimental effect on the Wnt pathways involved in the development and maturation of dendrites, synapses and spines of the neuronal cells. Contrary to PDZRN3, ring finger protein 2 (RNF2), another E3 ubiquitin ligase was found to be downregulated in RML prion-infected neurons compared to NBH control-treated neurons. RNF2 has been shown to regulate protein expression in neural tissues (Zaaroor-Regev et al., 2010), as well as regulating the neuronal differentiation of projection neurons in the development of the mouse neocortex (Morimoto-Suzki et al., 2014). RNF2 downregulation in RML prion-infected neurons could, again like PDZRN3, be having a potential detrimental effect on the development and maturation of dendrites, synapses and spines of the neurons, therefore exerting a neurotoxic effect by the infection with $PrP^{Sc.}$

Axon and synapse-associated proteins were also found to be altered by RML prion infection, one of which being the KIAA0319 like (KIAA0319L) protein. KIAA0319L is implicated in neuronal migration during neocortex development and have a role in axon guidance (Guidi et al., 2017). This protein is thought to confer susceptibility for dyslexia, as its disruption interferes in neuronal migration, a potential cause for this disease (Platt et al., 2013). Importantly, this protein is also known as adeno-associated virus (AAV) receptor, which is essential for the infection of AAVs. However, how PrP^{Sc} is impacting the KIAA0319L protein, and how its downregulation affects the neurons it is yet unknown, however, this information will allow us to further characterise and understand this protein in the context of prion disease. Another neuronal-associated protein, Hyaluronan and proteoglycan link protein 1 (HAPLN1), was also found to be downregulated in RML prion-infected neurons compared to NBH controls. HAPLN1 is both functionally and structurally important for the neuronal extracellular matrix (ECM), maintaining the integrity of the CNS and synaptic plasticity (Lemieux et al., 2023). HAPLN1 has also been shown to interact with PRNP in AD brains, showing a direct connection between HAPLN1 and prion and with NDs (Ulbrich et al., 2018). With such an important role, a reduction in the levels of this protein might have some detrimental impacts on the neuron's integrity as a result of PrP^{Sc}

infection. In addition, HAPLN2, a different protein from the same family, although not significantly altered in this model, has been directly linked to several NDs, specifically AD and PD, as well as schizophrenia (Wang et al., 2019). Interestingly, HAPLN2 has been found to colocalise with different E3 ubiquitin ligases (Wang et al., 2019), suggesting that PrP^{Sc} could have a detrimental effect on the same complex. HAPLN2 downregulation has also been demonstrated to lead to abnormal expression of ECM proteins and neuronal conductivity dysfunctionality (Wang et al., 2019). The direct family link between HAPLN2 and HAPLN1 suggests possible detrimental effects of the expression downregulation of HAPLN1 in this model. However, the specific mechanisms and detrimental effects the downregulation of HAPLN1 might be having on the neurons needs to be further investigated.

Several proteins associated to RHO GTPases were also found to be altered in RML prion-infected neurons compared to NBH control-treated ones. Tight regulation and cycling of RHO GTPases are essential for neurite outgrowth, playing an important role in neurite formation in primary neurons (Govek et al., 2005). Some RHO GTPase-associated protein examples to be downregulated after PrP^{Sc} infection are CAV1, Ras homolog family member G (RHOG) and RHO family GTPase 2 (RND2), whilst FAM169A was found to be upregulated. This dysfunction in protein expression of RHO GTPase-associated proteins suggests a possible detrimental effect on neurite development in the neuronal cultures, which could potentially lead to synaptic dysfunctions observed in several NDs (Senatore et al., 2013; Xiong et al., 2021).

Processes which rely on actin cytoskeleton, including endocytosis, have shown to play a very important role in prion formation and propagation in yeast cells (Ali et al., 2014; Ganusova et al., 2006). Several actin cytoskeletal proteins known to be involved in prion induction, propagation and elimination include SLAP2 (Baggett et al., 2003), a protein linking actin to clathrin; END3P (Zeng et al., 2001), implicated in actin cytoskeletal organisation and endocytosis, forming a complex with SLAP1, and ACT1P (Mishra et al., 2014), actin itself, which plays a role in cytoskeletal functions and endocytosis too. This direct relationship between actin cytoskeletal proteins and prion propagation matches the data attained in this study, with various actin-related cytoskeletal proteins altered in RML prion-infection samples compared to NBH control-infection samples. ACTBL2, or actin-

beta like 2 protein, was shown to be the most upregulated protein by p value between RML prion-infected neurons and NBH-control infected. This protein has previously been shown to have a major structural role in the postsynaptic actin cytoskeleton in different cells (Malek et al., 2021). ACTBL2 directly interacts with several proteins that have been showed to be altered in NDs such as dynactin subunit 3 (DCTN3) (Tsumagari et al., 2022) and MAPT, both of which are involved in AD. The data obtained in this study also showed a log2fold upregulation, and nearly significant p-value upregulation of ACTN4 and AFAP1 proteins. ACTN4, actinin alpha 4, is a protein that anchors actin to several intracellular structures. Actinin alpha 4 has been shown to be highly expressed in neuronal dendrites, specifically at excitatory synapses, where it interacts with several membrane receptors such as the metabotropic glutamate receptor 1 (mGluR1) (Kalinowska et al., 2015), as well as interacting with signalling and adhesion proteins (Hall et al., 2013). Most importantly, ACTN4 has previously been shown to have a direct interaction with PRNP (Ulbrich et al., 2018), which could potentially suggest a role of ACTN4 in prion infection and propagation due to its upregulation in this *in vitro* model. AFAP1, the actin filament-associated protein 1, is a motor-fibre associated protein involved in organising a network which links other proteins to the actin cytoskeleton, including protein kinase C (Baisden et al., 2001). These two actin-linking and -binding proteins could potentially be playing a role interacting with PrP^{Sc} before being endocytosed, by other actin-associated proteins, into neurons. Their contribution to the propagation of PrP^{Sc} would potentially explain their upregulation in RML prion-infected neurons compared to NBH control-treated neurons. Phosphatase and actin regulator 1 (PHACTR1) was also found to be significantly upregulated after PrP^{Sc} infection. PHACTR1 is expressed in cortical neurons throughout the development of the brain (Hamada et al., 2018), and has been linked to neurodevelopmental disorders, as well as NDs like early-onset parkinsonism in children (Previtali et al., 2023). Another protein associated to actin and the cytoskeleton which was altered in RML prion-infected neurons was LIM zinc finger containing domain 1 (LIMS1). LIMS1 is an adaptor protein involved in integrin-mediated cell adhesion, which supports cell movement through indirect linkages to the actin cytoskeleton (Parsons et al., 2010). LIMS1 has been reported as essential for the maintenance of communication between synapses and neuronal polarity during neuronal development (Muñoz et al., 2021). As mentioned in this chapter's introduction, not only do cytoskeletal protein,

specifically actin-related proteins, have a role in prion diseases, but they are also seen to be upregulated in AD , ALS and PD neurodegeneration (Diedrich et al., 2008; Kitsou et al., 2008; Tsumagari et al., 2022). The impact of the dysregulation of these cytoskeleton proteins in this neuronal model could be similar to the one observed in NDs, making this prion neuronal model relevant for the study of this disease.

In conclusion, this proteomic study revealed several groups of proteins to be altered in the RML prion-infection compared to out NBH control-treated neurons. Despite the fact these changes did not cause neuronal death in this *in vitro* system, it does not mean that these alterations are not key in the health and survival of neurons within the brain. In comparison to *in vivo* proteomic studies (Dwomoh, Rossi, et al., 2022), this study did not reveal as many proteins altered after PrP^{Sc} infection. However, it did highlight several potential proteins which could be directly and/or indirectly participating in the mechanism by which PrP^{Sc} enters, infects and propagates in neurons, and certain aspects of toxicity and dysfunction as a consequence of prion infection. Neuronal-, mitochondrial-, ribosomal-, and actin-related proteins were found to be altered by PrP^{Sc} infection, as well as E3 ubiquitin ligases and RHO GTPase-associated proteins (Figure 5-10). The protein expression changes indicate the impact this novel infection model has upon neurons, and more importantly, highlights proteins possibly involved in the mechanisms of prion infection, propagation and/or toxicity in neurons. As mentioned in Chapter 4, the absence of astrocytes in this cultures is the main reason behind the lack of neuroinflammatory markers being expressed and upregulated, and therefore no neuroinflammation-mediated degeneration occurring to the neurons. Other studies have shown glia-promoted neuronal death in prion-infection models (Cronier et al., 2004), which corroborates the lack of degeneration hypothesis. Due to the lack of all glial cells in the cultures, it can be speculated that the effect of PrP^{Sc} might be different compared to its effect on a dual culture with glia or a brain, leading to distinct differentially expressed proteins and alterations that could not be seeing in the other infection models. Instead, a model that can infect and propagate neurons with PrP^{Sc}, allowing to investigate the pathways and mechanisms involved in infection and propagation, to research potential targets and drugs which can slow down or inhibit this process, has been created. The lack of astrocytes, in this scenario, would

facilitate this research when specifically targeting neurons, and further proteomic analysis using neuronal cultures from GEMMs or specific drugs will allow for better understanding behind the intricate mechanisms of prion infection and propagation.

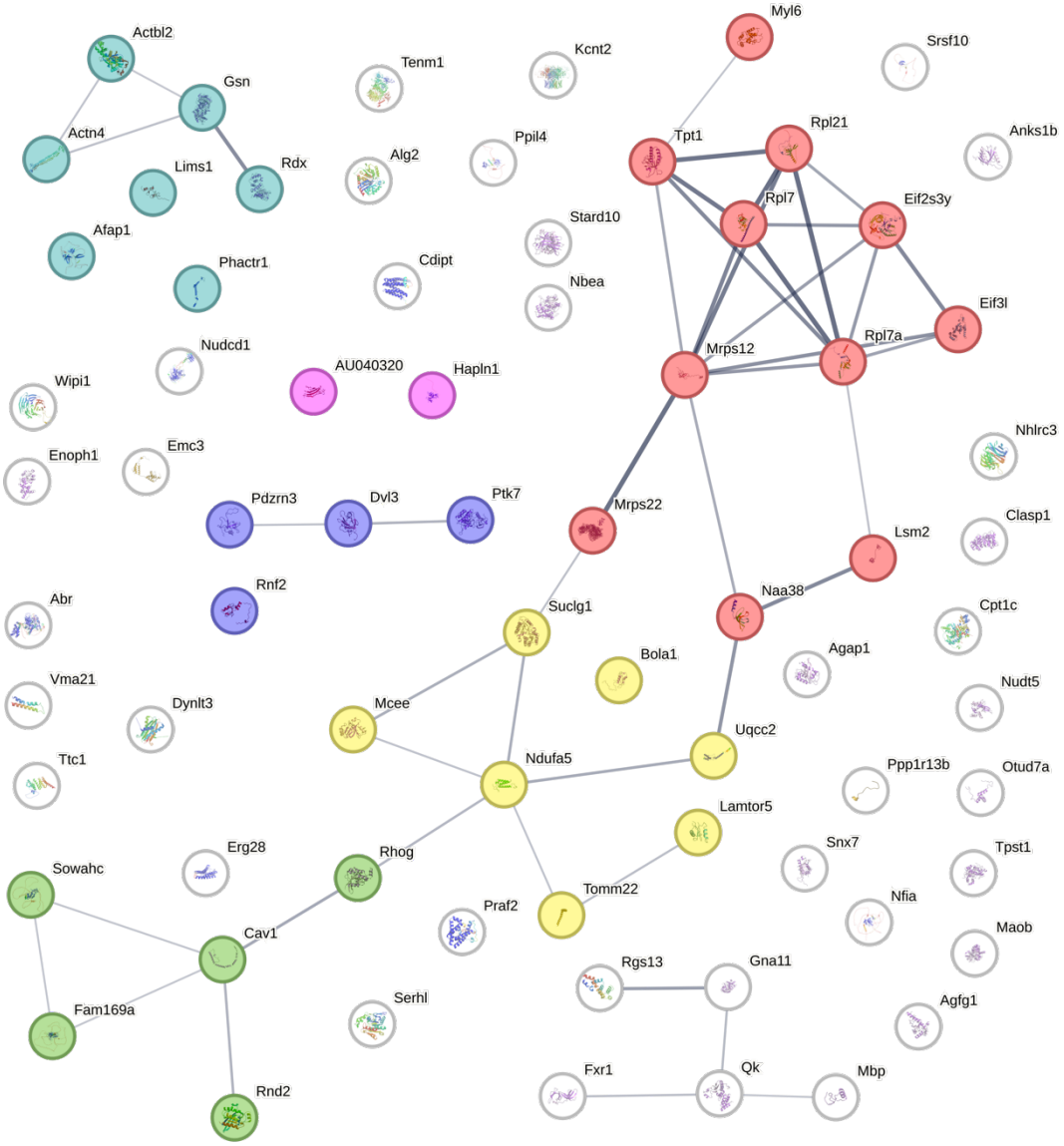

Figure 5-10 STRING map of all differentially expressed proteins between RML prion-infected and NBH control-treated neurons. Summary map showing all significantly up- and downregulated proteins between the RML infected and NBH treated sample groups. Lines joining the different proteins represent protein-to-protein interactions. Line thickness represents the strength of the data supporting the interaction. Different coloured proteins belong to different protein cluster groups (turquoise = actin/cytoskeleton-associated, blue = E3 ubiquitin ligase and Wnt pathway-associated, purple = axon/synapse -associated, green = RHO GTPase-associated, yellow = mitochondrion-associated and red = ribosomal-associated proteins) (Figure created using https://string-db.org/)

Chapter 6 Final Discussion

The understanding by which misfolded prion aggregates has considerably expanded in recent years (Scheckel & Aguzzi, 2018), however, the way in which these aggregates propagate throughout the brain is still unclear. It is thought that the mechanism of prion misfolding and propagation is replicated by other misfolding proteins in other NDs (Duyckaerts et al., 2019). These misfolding proteins include amyloid-ß, tau, α-synuclein and TDP-43, and their respective neurodegenerative diseases AD, PD, ALS and FTLD. Whilst extensive research to generate drugs that counteract the symptoms generated by these diseases has been performed (Mathur et al., 2023), targeting these misfolded proteins directly has not been able to alter or slow down the disease in humans.

In order to investigate the role of the M1 mAChR in altering prion infection, the study presented here formed a new model of *in vitro* infection and propagation of PrP^{Sc} in several strains of primary neuronal cultures. The infectious material used for the PrP^{Sc} infections was obtained from the purification and enrichment of misfolded prions from prion diseased mouse brains. The enrichment protocol used was adapted from a hyperphosphorylated tau purification protocol. Clear enrichment of PrP^{Sc} was achieved whilst purifying the brain homogenates. Other prion purification protocols previously published (Wenborn et al., 2015), in which they utilise pK throughout the process, removing all other proteins except for the insoluble PrP^{Sc}. However, this protocol leaves the purified homogenate containing protein products which could result harmful when being used neuronal cultures. Treatment with the purified homogenates from the novel enrichment protocol clearly demonstrate a robust infection of the neuronal cultures, with PrP^{Sc} being propagated within these cultures over time when these express endogenous PrP^{C}. Contrary to PrP^{C} expressing neurons, neurons without the *PRNP* gene were able to uptake PrP^{Sc}, however, these misfolded prions were degraded over time due to the lack of PrP^{C} to misfold. These results allow to validate and separate the mechanisms of infection and propagation from each other, demonstrating the need of PrP^{C} expression for propagation as seen in 6x Prion neurons, but not for infection, as seen in Prion-KO neuronal cultures. This data demonstrates an indirect mechanism by which PrP^{Sc} is able to be up taken by neurons without the endogenous expression of PrP^{C}, possibly involving HSPGs (Horonchik et al., 2005).

As discussed in Chapter 4, past studies have reported no PrP^{Sc} presence in Prion-KO neuronal cultures at 28 d.p.i. and beyond (Cronier et al., 2004), but never at earlier time-points like shown in the data presented in this study. *In vivo* studies have demonstrated prion-infected $Prnp^{0/0}$ mice are protected against PrP^{Sc} propagation and disease (Büeler et al., 1993), showing no PrP^{Sc} deposition in the mouse brains. It has been widely demonstrated that PrP^{Sc} requires the expression of PrP^{C} in order to initiate further prion misfolding, aggregation and propagation throughout the brain (Brandner et al., 1996; Büeler et al., 1993; Sailer et al., 1994). The lack of PrP^{Sc} deposition in prion knockout mice after inoculation, indicates the presence of a clearing mechanism by which PrP^{Sc} is degraded from the brain when PrP^{C} is not expressed. This model of PrP^{Sc} infection in Prion-KO neurons will allow to investigate the mechanism of infection independently of propagation, permitting to test different ligands and genetic mutations to see their effect on the uptake of PrP^{Sc} into neurons. In addition, known endocytosis pathways for proteins into cells such as HSPGs and receptor-mediated endocytosis could be tested in this model, understanding their role in prion infection.

Opposite to Prion-KO neurons, 6x Prion neurons demonstrated a clear increase in PrP^{Sc} deposition on a time-course experiment, validating that using the novel PrP^{Sc} infection model with PrP^{C} endogenously expressing neurons, you can achieve further misfolding and propagation of PrP^{Sc}. In contrast to using prion knockout neurons to study infection, PrP^{C} endogenously expressing neurons will permit to investigate the mechanisms of PrP^{Sc} propagation and test ligands that could potentially interrupt PrP^{Sc} propagation once infection is established. The ability to use the same purified material in different neuronal strains to study distinct aspects of prion disease will permit to understand both distinct mechanisms, as well as to target them separately, allowing for the generation of drugs which can be used at different stages of the disease. Investigating the mechanisms by which misfolded proteins propagate from cell-to-cell has previously been investigated by several groups with different misfolded protein such as Tau (Frost et al., 2009; Wu et al., 2013). Limitations such as antibody specificity between PrP^{Sc} and PrP^{C} prevent us from further characterising the propagation mechanism through immunocytochemistry as done in the above studies, however, the use of microfluidic chambers could allow to further characterise the mechanism of

propagation between neurons utilising different strains of neuronal cultures and strains of PrP^{Sc}.

As continuously referred to, this is a model of PrP^{Sc} infection and propagation, not a model of disease. This limitation was observed due to the lack of neuronal degeneration and death markers, making this model not ideal for investigating prion disease and its effects, such as toxicity and cell death. The lack of degeneration and neuronal death is possibly due to the absence of glial cells within culture (Li et al., 2019). Glial cells are directly involved in the neuroinflammatory responses to disease and are involved in the processes of neurodegeneration and cell death, shown by previous prion studies (Cronier et al., 2004). However, the consistency and robustness in neuronal culture infection demonstrates the ability of this model to be used in infection and propagation studies, to further characterise these two mechanisms and testing ligands which could slow down or stop either of them.

Further characterisation of the infection and propagation model was assessed through a proteomic study, to discover the alterations PrP^{Sc} infection was having on neuronal cells at a protein level. This study aimed to unravel proteins which could potentially be directly involved in the infection and propagation of PrP^{Sc}, and to assess whether any kind of dysregulation to neuronal health systems was happening. Proteins involved in autophagy, apoptosis and cell death were not found to be altered between control treatment and prion infection, demonstrating again that this model is ideal to study both infection and propagation of PrP^{Sc} due to the lack of neuronal compromise and death. However, this asks the question of what causes neuronal death in prion disease. This question brings back the hypothesis in which the lack of glial cells within the neuronal cultures is preventing this model from showing any neurodegeneration of the neurons. Due to the lack of astrocytes, the data showed no expression changes in classical neuroinflammatory proteins (GFAP, Vimentin) seen in *in vivo* studies (Dwomoh, Rossi, et al., 2022), demonstrating the need of glial cells in order to achieve a disease model. In contrast, the proteomic study did reveal a range of mitochondrial-, ribosomal- and actin-related proteins altered in the PrP^{Sc} infected neurons compared to the uninfected and control treated ones. Dysregulation of mitochondrial, ribosomal and cytoskeletal systems has previously been

demonstrated by proteomic studies in different NDs, such as AD and PD (Ahmad et al., 2016; Diedrich et al., 2008; Kitsou et al., 2008; Previtali et al., 2023; Talebi et al., 2016; Tsumagari et al., 2022; Ulbrich et al., 2018). E3 ubiquitin ligases were also found to be altered, both increasing and decreasing the degradation of proteins in the neurons, potentially having a detrimental impact after PrP^{Sc} infection (Morimoto-Suzki et al., 2014; Zaaroor-Regev et al., 2010). The disruption of these systems within the neurons provides proof of the detrimental impact that the PrP^{Sc} infection is having, however, these changes are not enough to drive neuronal death. It can be speculated these changes in mitochondrial, ribosomal and cytoskeletal proteins in the brain in an *in vivo* study or *in vitro* with the presence of glial cells could potentially have a more detrimental effect on the neurons or other cells in the brain, possibly driving their deaths in those models. In addition to all these findings, a limitation has to be noted from this experiment. Whilst total proteomic analyses of neuronal cultures allows to quantify the differences in protein expression between different sample conditions, they do not show alterations in protein localisation, a very important factor which alters protein function. Studies have demonstrated the effect of PrP^{Sc} infections on spine retractions, with actin localisation changing but not altered in expression (Fang et al., 2016). Dissection of particular regions within neuronal cells, for example the soma from the dendrites, followed by proteomic analysis of the specific regions would provide a better understanding of the specific changes occurring within each region, and allow to dissect the effects of PrP^{Sc} infection in neuronal cells.

Out of all the existing drugs, 30% of them all target the same family of receptor protein, the GPCRs (Zhang & Xie, 2012). GPCRs and their pathways have previously been targeted in neurodegenerative diseases, especially for AD. In AD, cholinergic hypofunction is one of the main hallmarks, where levels of ACh released into the synaptic cleft to activate the M1 mAChR, a class of GPCR, are significantly reduced (Mufson et al., 2008). Drugs such as donepezil, rivastigmine and galantamine, all acetylcholinesterase inhibitors drugs, have been extensively used on AD patients, inhibiting the breakdown of ACh and allowing for the activation and downstream signalling of the M1 mAChR (Colovic et al., 2013). Although these drugs counteract symptoms at the early stages of AD, they stop having the same positive effects at later stages as well as producing a number of side effects (Bodick et al., 1997).

Several M1 mAChR PAMs have been tested in prion mouse models (Bradley et al., 2017; Dwomoh, Rossi, et al., 2022), showing great potential in reversing learning and memory deficits as well as slowing down the disease course, increasing mouse survival. Other studies inhibiting the phosphorylation of the M1 mAChR have also demonstrated to aggravate prion disease in mice (Scarpa et al., 2021). These studies continue to directly point to muscarinic receptors, specifically at the M1 mAChR, as a potential candidate for the next generation of AD and prion disease modifying drugs, with the ability to slow down and alter disease progression.

Investigating the impact of M1 mAChR expression and mutations on prion infection in this neuronal model did not show similar results to what seen *in vivo* (Bradley et al., 2017; Dwomoh, Rossi, et al., 2022; Scarpa et al., 2021). Expression of the M1 DREADD receptor and the knock-out of the CHRM1 gene showed no difference in infection compared to the control. Increased PrP^{Sc} levels at the same time-points in infection were expected in both genetically engineered strains due to the lack of endogenous M1 mAChR expression and activation, however, results showed no significant difference. This hypothesis was developed following the research by Scarpa et al. (2021), were the inhibition of M1 mAChR phosphorylation in mice lead to the acceleration of PrP^{Sc} accumulation and a lower survival period. The deactivation of the M1 mAChR with a DREADD mutation or knocking the gene out completely, was hypothesised to have a more severe effect due to the loss of all downstream signalling of the M1 mAChR, losing the neuroprotective effects of the M1 mAChR. In addition, activation of the different M1 mAChR variants in all neuronal strains resulted in no significant difference in the infection and propagation rate. This did not support previous data published by our lab (Bradley et al., 2017; Dwomoh, Rossi, et al., 2022), where the treatment with M1 mAChR ligands on prion infected mice lead to lower PrP^{Sc} accumulation and longer survival periods. However, the results from the separate studies point at an indirect mechanism, by which activation of the M1 mAChR in mouse brain, slows down PrP^{Sc} accumulation. This is possibly through the reduction of inflammation as seen in the *in vivo* proteomic data, or that the overall brain system, such as specific neuron types, is required to observe the neuroprotective effects of M1 MAChR activation. In parallel to this experiment, we tested muscarinic expression and downstream signalling after chronic ligand treatment, to observe any changes in the biochemistry and pharmacology of the receptors. Results showed a 50%

desensitisation of muscarinic receptors in the cultures, suggesting the absence of a clearing mechanisms within the cultures which could clear excess ligand, and therefore causing a cholinergic crisis. This downregulation of the muscarinic receptors has previously been observed in other GPCRs, specifically the β-adrenergic receptor, by the chronic exposure of β-adrenergic ligands (Strader et al., 1984). The lack of astrocyte expression could potentially be the reason behind these results, as astrocytes are in charge of clearing waste and excess neurotransmitters within the brain (Weber & Barros, 2015). Astrocytes have also been shown to drive the neuroinflammatory responses in neurodegenerative diseases leading to neuronal death (Acosta et al., 2017; Brandebura et al., 2022; Hirsch & Hunot, 2009; Li et al., 2019; Szutowicz et al., 2014), as well as shown to being essential in *in vitro* models for neuronal degeneration to occur when misfolded protein infections are performed (Kushwaha et al., 2021). Not only would glia presence lead to degeneration in this model, but they would also clear up unused muscarinic ligand, possibly avoiding the desensitisation of the M1 mAChR after the chronic treatments performed.

In conclusion, it can be stated that a novel, quicker way to purify and enrich PrP^{Sc} from prion diseased mice was developed, and that it can be used to infect and propagate PrP^{Sc} in neuronal cultures over time. The lack of degeneration is an advantage in the case of this study, as it allows to investigate the mechanisms involved in the infection and propagation of PrP^{Sc} in healthy neuronal cells. Continuation of this research would involve the incorporation of an acute treatment with muscarinic ligands side-by-side to the chronic ones already employed, would permit to see the distinct effects both treatment plans have on prion disease and levels of PrP^{Sc} in the cultures. This would allow us to observe the impact of muscarinic ligands without desensitising the receptor. Another way to test the concentrations of PrP^{Sc} accumulation in the neurons with a better quantitative approach, in comparison to Western blotting, is real-time quaking-induced conversion (RT-QuIC) (Green, 2019; Wilham et al., 2010). This high throughput assay uses purified recombinant PrP^{C} as a substrate for any PrP^{Sc} present in the neuronal lysates to convert and aggregate. Thioflavin S, a fluorescent dye, binds to protein aggregates, allowing to quantify the levels of PrP^{Sc} present in the lysates (Shin et al., 2021). In addition, testing our infection model on dual cultures of primary neurons and astrocytes (Ioannou et al., 2019),

as well as primary neuronal cultures grown in astrocyte-conditioned media would be a possibility. Studies by Kushwaha et al. (2021), demonstrated that the presence of astrocytes in culture or culturing neurons in astrocyte-conditioned media, lead to the degeneration of neuronal cells when infected with PrP^{Sc}. The absence of astrocyte or astrocyte-conditioned media in the cultures is most likely the reason behind the lack of degeneration and neuronal death markers observed in this prion infection model (Brandebura et al., 2022). The addition of glia into this system would potentially allow us to use this model not just as an infection and propagation *in vitro* model of PrP^{Sc}, but also as a disease model (Kushwaha et al., 2021). Although this could also bring a new layer of complexity to the model, it would provide further understanding on the role of glia in prion disease. A new proteomic study could be conducted at this point to identify the main differences caused by PrP^{Sc} infection in single primary neuronal cultures or dual-neuron glia cultures. Dissection of the cell types and/or regions within the cells for more localised proteomic analysis would also allow to obtain deeper understanding on the effects of PrP^{Sc}. Potentially, not only would astrocytes presence lead to neurodegeneration, but it could also impact the effect of muscarinic ligand treatment, helping with the recycling of unused ligand as well as any indirect effect the ligands might be having on astrocytes and prion disease which is observed in animal models.

Appendices

Upregulated Proteins	Protein Names	Downregulated Proteins	Protein Names
ALKAL2	ALK and LTK ligand 2	ABCA1	ATP binding cassette subfamily A member 1
APLP2	Amyloid beta precursor like protein 2	AHCY	Adenosylhomocysteinase
BOLA1	BolA family member 1	ANAPC2	Anaphase promoting complex subunit 2
CDKN1B	Cyclin dependent kinase inhibitor 1B	ATP6AP2	ATPase H+ transporting accessory protein 2
DPH7	Diphthamide biosynthesis 7	ATP6V0A2	ATPase H+ transporting V0 subunit a2
FXR2	FMR1 autosomal homolog 2	ATP8A1	ATPase phospholipid transporting 8A1
GLRX5	Glutaredoxin 5	BRIX1	Biogenesis of ribosomes BRX1
GM45785	GM45785 (mouse protein)	CCM2	CCM2 scaffold protein
MBP	Myelin basic protein	COQ6	Coenzyme Q6, monooxygenase
MPI	Mannose phosphate isomerase	CPSF1	Cleavage and polyadenylation specific factor 1
PAKAP	Paralemmin A kinase anchor protein (mouse protein)	CRHBP	Corticotropin releasing hormone binding protein
PLP1	Proteolipid protein 1	CSE1L	Chromosome segregation 1 like
PRKCA	Protein kinase C alpha	CSNK1A1	Casein kinase 1 alpha 1
PRRT3	Proline rich transmembrane protein 3	DDX41	DEAD-box helicase 41
STS	Steroid sulfatase	DYNLT1A	Dynein light chain Tctex-type 1A (mouse gene)
THY1	Thy-1 cell surface antigen	EED	Embryonic extoderm development
UBL4A	Ubiquitin like 4A	FAM13C	Family with sequence similarity 13 member C
		GSS	Glutathione synthetase
		GTPBP4	GTP binding protein 4
		H1F10	H1.10 linker histone (mouse gene)
		H2AZ1	H2A.Z variant histone 1
		H2BC26	H2B clustered histone 26
		HSPA12B	Heat shock protein family A member 12B
		IGF2R	Insulin like growth factor 2 receptor
		IQGAP1	IQ motif containing GTPases activating protein 1
		ITIH4	Inter-alpha-trypsin inhibitor heavy chain 4
		MCM5	Minichromosome maintenance complex component 5
		MED1	Mediator complex subunit 1
		MRPL24	Mitochondrial ribosomal protein L24
		MRPL58	Mitochondrial ribosomal protein L58
		MRPS25	Mitochondrial ribosomal protein S25
		MRTO4	MRT4 homolog, ribosome maturation factor
		NMRAL1	NmrA like redox sensor 1
		NPTX2	Neuronal pentraxin 2
		OSTC	Oligosaccharyltransferase complex non-catalytic subunit
		OSTF1	Osteoclast stimulating factor 1
		PAFAH2	Platelet activating factor acetylhydrolase 2
		PEX1	Peroxisomal biogenesis factor 1
		PGAP1	Post-GPI attachment to proteins inositol deacylase 1
		PIGS	Phosphatidylinositol glycan anchor biosynthesis class S
		PRXL2A	Peroxiredoxin like 2A
		PSIP1	PC4 and SFRS1 interacting protein 1
		PTDSS1	Phosphatidylserine synthase 1
		QRSL1	Glutaminyl-tRNA amidotransferase subunit QRSL1
		RANBP6	Ran binding protein 6
		SAMM50	SAMM50 sorting and assembly machinery component
		SEC63	SEC63 homolog, protein translocation regulator
		SERPINH1	Serpin family H member 1
		SH2D5	SH2 domain containing 5
		SLC25A13	Solute carrier family 25 member 13
		SLC6A1	Solute carrier family 6 member 1
		SMPD2	Sphingomyelin phosphodiesterase 2
		TCAF1	TRPM8 channel associated factor 1
		TMEM35A	Transmembrane protein 35A
		TRNT1	TRNA nucleotidyl transferase 1
		UBE2D3	Ubiquitin conjugating enzyme E2 D3
		UBE2I	Ubiquitin conjugating enzyme E2 I
		XRN2	5'-3' exoribonuclease 2
		YIPF3	Yip1 domain family member 3
		ZW10	Zw10 kinetochore protein

Table S-1 Protein names of the significantly different proteins in NBH control-treated neurons compared to uninfected neurons. (All protein names obtained from proteinatlas.org and ncbi.nlm.nih.gov)

Upregulated Protein	Protein Names	Downregulated Proteins	Protein Names
FMNL1	Formin like 1	ALCAM	Activated leukocyte cell adhesion molecule
HOMER1	Homer scaffold protein 1	ALDH9A1	Aldehyde dehydrogenesae 9 family member A1
KIF3A	Kinesin family member 3A	ATP5MF	ATP synthase membrane subunit f
NUCB2	Nucleobindin 2	BPNT2	3'(2'), 5'-bisphosphate nucleotidase 2
NUDT10	Nudix hydrolase 10	BRIX1	Biogenesis of ribosomes BRX1
PDZRN3	PDZ domain containing ring finger 3	CDK9	Cyclin dependent kinase 9
RTKN	Rhotekin	CHAMP1	Chromosome alignment maintaining phosphoprotein 1
SLC03A1	Solute carrier organic anion transporter family member 3A1	CDH2	Cadherin 2
TIAM2	TIAM Rac1 associated GEF 2	CHL1	Cell adhesion molecule L1 like
		CTIF	Cap binding complex dependent translation initiation factor
		CTTNBP2NL	CTTNBP2 N-terminal like
		DDX41	DEAD-box helicase 41
		DHRS4	Dehydrogenase/reductase 4
		ECI2	Enoyl-CoA delta isomerase 2
		ERG28	Ergosterol biosynthesis 28 homolog
		FBLL1	Fibrillarin like 1
		FLNB	Filamin B
		GNPDA2	Glucosamine-6-phosphate deaminase 2
		GSTK1	Glutathione S-transferase kappa 1
		HERC4	HECT and RLD domain containing E3 ubiquitin protein ligase 4
		ILKAP	ILK associated serine/threonine phosphatase
		ITGB6	Integrin subunit beta 6
		KIAA0319L	KIAA0319 like
		KYAT1	Kynurenine aminotransferase 1
		LGALS3	Galectin 3
		LIMS1	LIM zinc finger domain containing 1
		LRRC40	Leucine rich repeat containing 40
		MAD1L1	Mitotic arrest deficient 1 like 1
		MRPL2	Mitochondrial ribosomal protein L2
		MRPL24	Mitochondrial ribosomal protein L24
		MRPL46	Mitochondrial ribosomal protein L46
		MRPL48	Mitochondrial ribosomal protein L48
		MRPS17	Mitochondrial ribosomal protein S17
		NDUFA7	NADH:ubiquinone oxidoreductase subunit A7
		NDUFA9	NADH:ubiquinone oxidoreductase subunit A9
		NEDD4	NEDD4 E3 ubiquitin protein ligase
		NFIA	Nuclear factor I A
		NHLRC3	NHL repeat containing 3
		NONO	Non-POU domain containing octamer binding
		NPTXR	Neuronal pentraxin receptor
		NT5C3A	5'-nucleotidase, cytosolic IIIA
		OSTC	Oligosaccharyltransferase complex non-catalytic subunit
		PARN	Poly(A)-specific ribonuclease
		PDS5A	PDS5 cohesin associated factor A
		PPIB	Peptidylprolyl isomerase B
		PRXL2A	Peroxiredoxin like 2A
		PTPMT1	Protein tyrosine phosphatase mitochondrial 1
		RAB18	RAB18, member RAS oncogene family
		SCP2	Sterol carrier protein 2
		SCYL1	SCY1 like pseudokinase 1
		SFRP1	Secreted frizzled related protein 1
		SLC25A20	Solute carrier family 25 member 20
		SLCO1C1	Solute carrier organic anion transporter family member 1C1
		SOAT1	Sterol O-acyltransferase 1
		SRSF9	Serine and arginine rich splicing factor 9
		STAT3	Signal transducer and activator of transcription 3
		TM9SF3	Transmembrane 9 superfamily member 3
		TMEM25A	Transmembrane protein 25A
		TTYH1	Tweety family member 1
		YME1L1	YME1 like 1 ATPase

Table S-2 Protein names of the significantly different proteins in RML prion-infected neurons compared to uninfected neurons. (All protein names obtained from proteinatlas.org and ncbi.nlm.nih.gov)

Upregulated Proteins	Protein Names	Function
NBEA	Neurobeachin	Binds to protein kinase A type II regulatory subunits and anchors/targets them to the membrane. May also anchor the kinase to cytoskeletal and/or organelle-associated proteins
FAM169A	Family with sequence similarity 169 member A	Neuropeptide signalling.
DYNLT3	Dynein light chain Tctex-type 3	One of several non-catalytic accessory components of the cytoplasmic dynein 1 complex. Involved in linking dynein to cargos and to adapter proteins regulating dynein function.
ALG2	alpha 1,3 mannosyltransferase,	Member of the glycosyltransferase 1 family.
ABR	ABR activator of RhoGEF and GTPase	Protein with a unique structure having two opposing regulatory activities toward small GTP-binding proteins. Protein contains a GTPase-activating protein domain, a domain found in members of the Rho family of GTP-binding proteins.
CDIPT	CDP-diacylglycerol--inositol 3-phosphatidyltransferase	Catalyses the biosynthesis of phosphatidylinositol and the phosphatidylinositol:inositol exchange reaction.
EIF3L	Eukaryotic translation initiation factor 3 subunit L	Enables RNA binding activity. Contributes to translation initiation factor activity. Involved in translational initiation and viral translational termination-reinitiation. Located in membrane. Part of eukaryotic translation initiation factor 3 complex
ANKS1B	Ankyrin repeat and sterile alpha motif domain containing 1B	Regulation of nucleoplasmic coilin protein interactions in neuronal and transformed cells.
GNA11	Gα protein subunit 11	Involved as modulators or transducers in transmembrane signalling systems, acting as an activator of phospholipase C
CPT1C	Carnitine palmitoyltransferase 1C	Plays a role in lipid metabolic process.
CLASP1	Cytoplasmic linker associated protein 1	Nonmotor microtubule-associated proteins that interact with cytoplasmic linker proteins (CLIPs). Involved in the regulation of microtubule dynamics at the kinetochore and throughout the spindle.
STARD10	StAR related lipid transfer domain containing 10	Predicted to enable lipid binding activity. Predicted to be involved in lipid transport.
RGS13	Regulator of G protein signaling 13	Protein inhibits signal transduction, it increases the GTPase activity of G protein α-subunits, driving them into their inactive GDP-bound form. Binds to both G(q)-α and G(i)-α.
TTC1	Tetratricopeptide repeat domain 1	Plays role in protein-protein interactions, and binds to the Gα subunit of G protein-coupled receptors, activating the Ras signalling pathway.
AGAP1	ArfGAP with GTPase domain, ankyrin repeat and PH domain 1	Member of an ADP-ribosylation factor GTPase-activating protein family. Involved in membrane trafficking and cytoskeleton dynamics. Direct regulator of the adaptor-related protein complex 3 on endosomes.
TENM1	Teneurin transmembrane protein 1	Involved in neural development, regulating the establishment of proper connectivity within the nervous system.
PDZRN3	PDZ domain containing ring finger 3	E3 ubiquitin-protein ligase
PHACTR1	Phosphatase and actin regulator 1	Binds actin monomers. Role in multiple processes: regulation of actin cytoskeleton dynamics, actin stress fibers formation, cell motility and survival, and formation of tubules by endothelial cells. Involved in the regulation of cortical neuron migration and dendrite arborization.
KCNT2	Potassium Sodium-Activated Channel Subfamily T Member 2	Enables chloride-activated potassium channel activity.
SNX7	Sorting nexin 7	Involved in the regulation of endocytosis and in several stages of intracellular trafficking
OTUD7A	OTU deubiquitinase 7A	Acts as a deubiquitinating enzyme and possible tumour suppressor. Acts on TNF receptor associated factor 6 (TRAF6), controlling nuclear factor kappa B expression.
PPP1R13B	Protein phosphatase 1 regulatory subunit 13B	Regulator that plays a central role in regulation of apoptosis via its interaction with p53/TP53
AGFG1	ArfGAP with FG repeats 1	Related to nucleoporins, a protein class mediating nucleocytoplasmic transport. Plays role in RNA trafficking or localisation.
NUDT5	Nudix hydrolase 5	Catalyses the hydrolysis of modified nucleoside diphosphates, including ADP-ribose (ADPR) and 8-oxoGua-containing 8-oxo-dADP and 8-oxo-dGDP.
NUDCD1	NudC domain containing 1	Involved in synaptic function of neurons
ENOPH1	Enolase-phosphatase 1	Enables acireductone synthase activity. Involved in L-methionine salvage from methylthioadenosine.
LSM2	LSM2 homolog, U6 small nuclear RNA and mRNA degradation associated	Role in pre-mRNA splicing as component of the U4/U6-U5 tri-snRNP complex. Involved in spliceosome assembly and as component of the precatalytic spliceosome complex.
ACTBL2	Actin beta-like 2	Enables protein kinase binding activity. Structural protein of the postsynaptic actin cytoskeleton.

Table S-3 Protein names and functions of the 28 significantly upregulated proteins. (Protein names and functions obtained from proteinatlas.org and ncbi.nlm.nih.gov)

Downregulated Proteins	Protein Names	Function
LIMS1	LIM zinc finger domain containing 1	Adaptor protein. Likely involved in integrin signalling. Protein may play role in integrin-mediated cell adhesion or spreading.
GSN	Gelsolin	Binds to the "plus" ends of actin monomers and filaments to prevent monomer exchange
MCEE	Methylmalonyl-CoA epimerase	Catalyses the interconversion of D- and L-methylmalonyl-CoA during the degradation of branched chain amino acids
PNMA8B	PNMA family member 8B	Involved in neuronal signalling
RHOG	Ras homolog family member G	Promote reorganization of the actin cytoskeleton and regulate cell shape, attachment, and motility. Facilitates translocation of a functional guanine nucleotide exchange factor (GEF) complex from the cytoplasm to the plasma membrane where ras-related C3 botulinum toxin substrate 1 is activated to promote lamellipodium formation and cell migration.
HAPLN1	Hyaluronan and proteoglycan link protein 1	Predicted to be involved in central nervous system development and skeletal system development
CAV1	Caveolin 1	Scaffolding protein of the caveolae plasma membranes found in most cell types. Links integrin subunits to the tyrosine kinase FYN, an initiating step in coupling integrins to the Ras-ERK pathway and promoting cell cycle progression
MRPS12	Mitochondrial ribosomal protein S2	Key component of the ribosomal small subunit and controls the decoding fidelity and susceptibility to aminoglycoside antibiotics
PRAF2	PRA1 domain family member 2	Predicted to be involved in L-glutamate transmembrane transport
PPIL4	Peptidylprolyl isomerase like 4	Member of the cyclophilin family of peptidylprolyl isomerases. The cyclophilins are a highly conserved family, members of which play an important role in protein folding, immunosuppression by cyclosporin A, and infection of HIV-1 virions
MYL6	Myosin light chain 6	Encodes a myosin alkali light chain.
MBP	Myelin basic protein	Major constituent of the myelin sheath of oligodendrocytes and Schwann cells in the nervous system. However, MBP-related transcripts are also present in the bone marrow and the immune system
TPT1	Translational controlled tumour protein 1	Regulator of cellular growth and proliferation
LAMTOR5	Late endosomal/lysosomal adaptor, MAPK and MTOR activator 5	Involved in amino acid sensing and activation of mTORC1, a signaling complex promoting cell growth in response to growth factors, energy levels, and amino acids. Activated by amino acids through a mechanism involving the lysosomal V-ATPase, the Ragulator functions as a guanine nucleotide exchange factor activating the small GTPases Rag. Activated Ragulator and Rag GTPases function as a scaffold recruiting mTORC1 to lysosomes where it is in turn activated. When complexed to BIRC5, interferes with apoptosome assembly, preventing recruitment of pro-caspase-9 to oligomerized APAF1, thereby selectively suppressing apoptosis initiated via the mitochondrial/cytochrome c pathway.
SERHL	Serine hydrolase like 2	Predicted to enable hydrolase activity
MRPS22	Mitochondrial ribosomal protein S22	Enables hydrolase activity
MAOB	Monoamine oxidase B	Catalyses the oxidative deamination of biogenic and xenobiotic amines and plays an important role in the metabolism of neuroactive and vasoactive amines in the central nervous sytem and peripheral tissues
SRSF10	Serine and arginine rich splicing factor 10	Member of the serine-arginine (SR) family of proteins, which are involved in constitutive and regulated RNA splicing
SUCLG1	Succinate-CoA ligase GDP/ADP-forming subunit alpha	This enzyme is targeted to the mitochondria and catalyzes the conversion of succinyl CoA and ADP or GDP to succinate and ATP or GTP
RPL7	Ribosomal protein L7	The protein can inhibit cell-free translation of mRNAs, suggesting that it plays a regulatory role in the translation apparatus
RDX	Radixin	Cytoskeletal protein that may be important in linking actin to the plasma membrane
NDUFA5	NADH:ubiquinone oxidoreductase subunit A5	Localized to the inner mitochondrial membrane, where it is thought to aid in the transfer of electrons from NADH to ubiquinone
QKI	QKI, KH domain containing RNA binding	RNA-binding protein that regulates pre-mRNA splicing, export of mRNAs from the nucleus, protein translation, and mRNA stability. The encoded protein is involved in myelinization and oligodendrocyte differentiation and may play a role in schizophrenia
NFIA	Nuclear factor I A	Member of the NF1 (nuclear factor 1) family of transcription factors
EMC3	ER membrane protein complex subunit 3	Contributes to membrane insertase activity. Involved in protein insertion into ER membrane by stop-transfer membrane-anchor sequence and tail-anchored membrane protein insertion into ER membrane. Is integral component of endoplasmic reticulum membrane
UQCC2	Ubiquinol-cytochrome c reductase complex assembly factor 2	Nucleoid protein localized to the mitochondria inner membrane. The encoded protein affects regulation of insulin secretion, mitochondrial ATP production, and myogenesis through modulation of mitochondrial respiratory chain activity
RND2	Rho family GTPase 2	Member of the Rho GTPase family, whose members play a key role in the regulation of actin cytoskeleton organization in response to extracellular growth factors. This particular family member has been implicated in the regulation of neuronal morphology and endosomal trafficking
KIAA0319L	KIAA0319 like	Implicated in neuronal migration during neocortex development
RPL7A	Ribosomal protein L7a	Interacts with a subclass of nuclear hormone receptors, including thyroid

		hormone receptor, and inhibit their ability to transactivate by preventing their binding to their DNA response elements
DVL3	Dishevelled segment polarity protein 3	Involved in the signal transduction pathway mediated by multiple Wnt genes.
FXR1	FMR1 autosomal homolog 1	RNA binding protein that interacts with the functionally-similar proteins FMR1 and FXR2. These proteins shuttle between the nucleus and cytoplasm and associate with polyribosomes, predominantly with the 60S ribosomal subunit
TPST1	Tyrosylprotein sulfotransferase 1	Enables protein homodimerization activity and protein-tyrosine sulfotransferase activity
EIF2S3Y	eukaryotic translation initiation factor 2, subunit 3, structural gene Y-linked (mouse gene)	Predicted to enable translation initiation factor activity. Predicted to contribute to tRNA binding activity. Predicted to be involved in formation of translation preinitiation complex and positive regulation of translational fidelity.
PTK7	Protein tyrosine kinase 7 (inactive)	Inactive tyrosine kinase involved in Wnt signaling pathway. Component of both the non-canonical (also known as the Wnt/planar cell polarity signaling) and the canonical Wnt signaling pathway. Functions in cell adhesion, cell migration, cell polarity, proliferation, actin cytoskeleton reorganization and apoptosis
RPL21	Ribosomal protein L21	The protein belongs to the L21E family of ribosomal proteins. It is located in the cytoplasm
BOLA1	BolA family member 1	Acts as a mitochondrial iron-sulfur (Fe-S) cluster assembly factor that facilitates (Fe-S) cluster insertion into a subset of mitochondrial proteins
NAA38	N-alpha-acetyltransferase 38	Involved in negative regulation of apoptotic process
ERG28	Ergosterol biosynthesis 28 homolog	Enables identical protein binding activity
WIPI1	WD repeat domain, phosphoinositide interacting 1	Regulates the assembly of multiprotein complexes by presenting a beta-propeller platform for simultaneous and reversible protein-protein interactions
SOWAHC	Sosondowah ankyrin repeat domain family member C	
RNF2	Ring finger protein 2	E3 ubiquitin-protein ligase that mediates monoubiquitination of 'Lys-119' of histone H2A (H2AK119Ub), thereby playing a central role in histone code and gene regulation
TOMM22	Translocase of outer mitochondrial membrane 22	Integral membrane protein of the mitochondrial outer membrane
NHLRC3	NHL repeat containing 3	May be involved in various enzymatic processes, including protein modification by ubiquitination
VMA21	Vacuolar ATPase assembly factor 21	This gene encodes a chaperone for assembly of lysosomal vacuolar ATPase

Table S-4 Protein names and functions of the 44 significantly downregulated proteins. (All protein names and functions obtained from proteinatlas.org and ncbi.nlm.nih.gov)

List of References

Abeliovich, A., Schmitz, Y., Fariñas, I., Choi-Lundberg, D., Ho, W. H., Castillo, P. E., Shinsky, N., Garcia Verdugo, J. M., Armanini, M., Ryan, A., Hynes, M., Phillips, H., Sulzer, D., & Rosenthal, A. (2000). Mice lacking alpha-synuclein display functional deficits in the nigrostriatal dopamine system. *Neuron*, *25*(1), 239–252. https://doi.org/10.1016/S0896-6273(00)80886-7

Abrams, J. Y., Schonberger, L. B., Belay, E. D., Maddox, R. A., Leschek, E. W., Mills, J. L., Wysowski, D. K., & Fradkin, J. E. (2011). Lower risk of Creutzfeldt-Jakob disease in pituitary growth hormone recipients initiating treatment after 1977. *The Journal of Clinical Endocrinology and Metabolism*, *96*(10). https://doi.org/10.1210/JC.2011-1357

Acosta, C., Anderson, H. D., & Anderson, C. M. (2017). Astrocyte dysfunction in Alzheimer disease. *Journal of Neuroscience Research*, *95*(12), 2430–2447. https://doi.org/10.1002/JNR.24075

Aguzzi, A., Heikenwalder, M., & Polymenidou, M. (2007). Insights into prion strains and neurotoxicity. *Nature Reviews Molecular Cell Biology 2007 8:7*, *8*(7), 552–561. https://doi.org/10.1038/nrm2204

Ahmad, K., Baig, M. H., Gupta, G. K., Kamal, M. A., Pathak, N., & Choi, I. (2016). Identification of common therapeutic targets for selected neurodegenerative disorders: An in silico approach. *Journal of Computational Science*, *17*, 292–306. https://doi.org/10.1016/J.JOCS.2016.03.007

Ahn, M., Ghaemmaghami, S., Huang, Y., Phuan, P. W., May, B. C. H., Giles, K., DeArmond, S. J., & Prusiner, S. B. (2012). Pharmacokinetics of quinacrine efflux from mouse brain via the P-glycoprotein efflux transporter. *PloS One*, *7*(7). https://doi.org/10.1371/JOURNAL.PONE.0039112

Ali, M., Chernova, T. A., Newnam, G. P., Yin, L., Shanks, J., Karpova, T. S., Lee, A., Laur, O., Subramanian, S., Kim, D., McNally, J. G., Seyfried, N. T.,

Chernoff, Y. O., & Wilkinson, K. D. (2014). Stress-dependent proteolytic processing of the actin assembly protein Lsb1 modulates a yeast prion. *The Journal of Biological Chemistry*, *289*(40), 27625–27639. https://doi.org/10.1074/JBC.M114.582429

Allen, B., Ingram, E., Takao, M., Smith, M. J., Jakes, R., Virdee, K., Yoshida, H., Holzer, M., Craxton, M., Emson, P. C., Atzori, C., Migheli, A., Anthony Crowther, R., Ghetti, B., Spillantini, M. G., & Goedert, M. (2002). Abundant Tau Filaments and Nonapoptotic Neurodegeneration in Transgenic Mice Expressing Human P301S Tau Protein. *The Journal of Neuroscience*, *22*(21), 9340. https://doi.org/10.1523/JNEUROSCI.22-21-09340.2002

Alonso, A. D. C., Mederlyova, A., Novak, M., Grundke-Iqbal, I., & Iqbal, K. (2004). Promotion of hyperphosphorylation by frontotemporal dementia tau mutations. *The Journal of Biological Chemistry*, *279*(33), 34873–34881. https://doi.org/10.1074/JBC.M405131200

Alonso, A. D. C., Zaidi, T., Novak, M., Grundke-Iqbal, I., & Iqbal, K. (2001). Hyperphosphorylation induces self-assembly of tau into tangles of paired helical filaments/straight filaments. *Proceedings of the National Academy of Sciences of the United States of America*, *98*(12), 6923–6928. https://doi.org/10.1073/PNAS.121119298

Alpers, M., & Rail, L. (1971). Kuru and Creutzfeldt-Jakob disease: clinical and aetiological aspects. *Proceedings of the Australian Association of Neurologists*, *8*, 7–15.

Amiri-Dashatan, N., Koushki, M., Abbaszadeh, H. A., Rostami-Nejad, M., & Rezaei-Tavirani, M. (2018). Proteomics Applications in Health: Biomarker and Drug Discovery and Food Industry. *Iranian Journal of Pharmaceutical Research : IJPR*, *17*(4), 1523. /pmc/articles/PMC6269565/

Anisuzzaman, A. S. M., Uwada, J., Masuoka, T., Yoshiki, H., Nishio, M., Ikegaya, Y., Takahashi, N., Matsuki, N., Fujibayashi, Y., Yonekura, Y., Momiyama, T., & Muramatsu, I. (2013). Novel contribution of cell surface and intracellular

M1-muscarinic acetylcholine receptors to synaptic plasticity in hippocampus. *Journal of Neurochemistry*, *126*(3), 360–371. https://doi.org/10.1111/JNC.12306

Armbruster, B. N., Li, X., Pausch, M. H., Herlitze, S., & Roth, B. L. (2007). Evolving the lock to fit the key to create a family of G protein-coupled receptors potently activated by an inert ligand. *Proceedings of the National Academy of Sciences of the United States of America*, *104*(12), 5163–5168. https://doi.org/10.1073/PNAS.0700293104/SUPPL_FILE/00293FIG8.PDF

Artikis, E., Kraus, A., & Caughey, B. (2022). Structural biology of ex vivo mammalian prions. *The Journal of Biological Chemistry*, *298*(8). https://doi.org/10.1016/J.JBC.2022.102181

Astolfi, A., Spagnolli, G., Biasini, E., & Barreca, M. L. (2020). The Compelling Demand for an Effective PrPC-Directed Therapy against Prion Diseases. *ACS Medicinal Chemistry Letters*, *11*(11), 2063–2067. https://doi.org/10.1021/ACSMEDCHEMLETT.0C00528

Baggett, J. J., D'Aquino, K. E., & Wendland, B. (2003). The Sla2p talin domain plays a role in endocytosis in Saccharomyces cerevisiae. *Genetics*, *165*(4), 1661–1674. https://doi.org/10.1093/GENETICS/165.4.1661

Baisden, J. M., Qian, Y., Zot, H. M., & Flynn, D. C. (2001). The actin filament-associated protein AFAP-110 is an adaptor protein that modulates changes in actin filament integrity. *Oncogene 2001 20:44*, *20*(44), 6435–6447. https://doi.org/10.1038/sj.onc.1204784

Ballatore, C., Lee, V. M. Y., & Trojanowski, J. Q. (2007). Tau-mediated neurodegeneration in Alzheimer's disease and related disorders. In *Nature Reviews Neuroscience* (Vol. 8, Issue 9, pp. 663–672). https://doi.org/10.1038/nrn2194

Barret, A., Tagliavini, F., Forloni, G., Bate, C., Salmona, M., Colombo, L., De Luigi, A., Limido, L., Suardi, S., Rossi, G., Auvré, F., Adjou, K. T., Salès, N.,

Williams, A., Lasmézas, C., & Deslys, J. P. (2003). Evaluation of quinacrine treatment for prion diseases. *Journal of Virology*, *77*(15), 8462–8469. https://doi.org/10.1128/JVI.77.15.8462-8469.2003

Bayer, T. A. (2015). Proteinopathies, a core concept for understanding and ultimately treating degenerative disorders? In *European Neuropsychopharmacology* (Vol. 25, Issue 5, pp. 713–724). Elsevier. https://doi.org/10.1016/j.euroneuro.2013.03.007

Beach, T. G., Adler, C. H., Lue, L. F., Sue, L. I., Bachalakuri, J., Henry-Watson, J., Sasse, J., Boyer, S., Shirohi, S., Brooks, R., Eschbacher, J., White, C. L., Akiyama, H., Caviness, J., Shill, H. A., Connor, D. J., Sabbagh, M. N., & Walker, D. G. (2009). Unified Staging System for Lewy Body Disorders: Correlation with Nigrostriatal Degeneration, Cognitive Impairment and Motor Dysfunction. *Acta Neuropathologica*, *117*(6), 613. https://doi.org/10.1007/S00401-009-0538-8

Berg, K. A., & Clarke, W. P. (2018). Making Sense of Pharmacology: Inverse Agonism and Functional Selectivity. *International Journal of Neuropsychopharmacology*, *21*(10), 962. https://doi.org/10.1093/IJNP/PYY071

Berry, D. B., Lu, D., Geva, M., Watts, J. C., Bhardwaj, S., Oehler, A., Renslo, A. R., DeArmond, S. J., Prusiner, S. B., & Giles, K. (2013). Drug resistance confounding prion therapeutics. *Proceedings of the National Academy of Sciences of the United States of America*, *110*(44). https://doi.org/10.1073/PNAS.1317164110/-/DCSUPPLEMENTAL

Bessen, R. A., Kocisko, D. A., Raymond, G. J., Nandan, S., Lansbury, P. T., & Caughey, B. (1995). Non-genetic propagation of strain-specific properties of scrapie prion protein. *Nature*, *375*(6533), 698–700. https://doi.org/10.1038/375698A0

Bett, C., Joshi-Barr, S., Lucero, M., Trejo, M., & Liberski, P. (2012). Biochemical Properties of Highly Neuroinvasive Prion Strains. *PLoS Pathog*, *8*(2), 1002522. https://doi.org/10.1371/journal.ppat.1002522

Biffi, E., Regalia, G., Menegon, A., Ferrigno, G., & Pedrocchi, A. (2013). The Influence of Neuronal Density and Maturation on Network Activity of Hippocampal Cell Cultures: A Methodological Study. *PLoS ONE*, *8*(12). https://doi.org/10.1371/JOURNAL.PONE.0083899

Birkett, C. R., Hennion, R. M., Bembridge, D. A., Clarke, M. C., Chree, A., Bruce, M. E., & Bostock, C. J. (2001). Scrapie strains maintain biological phenotypes on propagation in a cell line in culture. *EMBO Journal*, *20*(13), 3351–3358. https://doi.org/10.1093/EMBOJ/20.13.3351

Bodick, N. C., Offen, W. W., Levey, A. I., Cutler, N. R., Gauthier, S. G., Satlin, A., Shannon, H. E., Tollefson, G. D., Rasmussen, K., Bymaster, F. P., Hurley, D. J., Potter, W. Z., & Paul, S. M. (1997). Effects of Xanomeline, a Selective Muscarinic Receptor Agonist, on Cognitive Function and Behavioral Symptoms in Alzheimer Disease. *Archives of Neurology*, *54*(4), 465–473. https://doi.org/10.1001/ARCHNEUR.1997.00550160091022

Boggs, J. M. (2006). Myelin basic protein: a multifunctional protein. *Cellular and Molecular Life Sciences : CMLS*, *63*(17), 1945–1961. https://doi.org/10.1007/S00018-006-6094-7

Bolognini, D., Barki, N., Butcher, A. J., Hudson, B. D., Sergeev, E., Molloy, C., Moss, C. E., Bradley, S. J., Le Gouill, C., Bouvier, M., Tobin, A. B., & Milligan, G. (2019). Chemogenetics defines receptor-mediated functions of short chain free fatty acids. *Nature Chemical Biology 2019 15:5*, *15*(5), 489–498. https://doi.org/10.1038/s41589-019-0270-1

Braak, H., & Braak, E. (1991). Neuropathological stageing of Alzheimer-related changes. *Acta Neuropathologica*, *82*(4), 239–259. https://doi.org/10.1007/BF00308809

Braak, H., Brettschneider, J., Ludolph, A. C., Lee, V. M., Trojanowski, J. Q., & Tredici, K. Del. (2013). Amyotrophic lateral sclerosis--a model of corticofugal axonal spread. *Nature Reviews. Neurology*, *9*(12), 708–714. https://doi.org/10.1038/NRNEUROL.2013.221

Bradley, S. J., Bourgognon, J. M., Sanger, H. E., Verity, N., Mogg, A. J., White, D. J., Butcher, A. J., Moreno, J. A., Molloy, C., Macedo-Hatch, T., Edwards, J. M., Wess, J., Pawlak, R., Read, D. J., Sexton, P. M., Broad, L. M., Steinert, J. R., Mallucci, G. R., Christopoulos, A., … Tobin, A. B. (2017). M1 muscarinic allosteric modulators slow prion neurodegeneration and restore memory loss. *The Journal of Clinical Investigation*, *127*(2), 487. https://doi.org/10.1172/JCI87526

Bradley, S. J., Molloy, C., Valuskova, P., Dwomoh, L., Scarpa, M., Rossi, M., Finlayson, L., Svensson, K. A., Chernet, E., Barth, V. N., Gherbi, K., Sykes, D. A., Wilson, C. A., Mistry, R., Sexton, P. M., Christopoulos, A., Mogg, A. J., Rosethorne, E. M., Sakata, S., … Tobin, A. B. (2020). Biased M1-muscarinic-receptor-mutant mice inform the design of next-generation drugs. *Nature Chemical Biology*. https://doi.org/10.1038/s41589-019-0453-9

Brandebura, A. N., Paumier, A., Onur, T. S., & Allen, N. J. (2022). Astrocyte contribution to dysfunction, risk and progression in neurodegenerative disorders. *Nature Reviews Neuroscience 2022 24:1*, *24*(1), 23–39. https://doi.org/10.1038/s41583-022-00641-1

Brandner, S., Isenmann, S., Raeber, A., Fischer, M., Sailer, A., Kobayashi, Y., Marino, S., Weissmann, C., & Aguzzi, A. (1996). Normal host prion protein necessary for scrapie-induced neurotoxicity. *Nature*, *379*(6563), 339–343. https://doi.org/10.1038/379339A0

Brandner, S., & Jaunmuktane, Z. (2017). Prion disease: experimental models and reality. *Acta Neuropathologica*, *133*, 197–222. https://doi.org/10.1007/s00401-017-1670-5

Brewer, G. J., Torricelli, J. R., Evege, E. K., & Price, P. J. (1993). Optimized survival of hippocampal neurons in B27-supplemented Neurobasal, a new serum-free medium combination. *Journal of Neuroscience Research*, *35*(5), 567–576. https://doi.org/10.1002/JNR.490350513

Brooke, S. M. (2018). *Evaluation of a Chemical Genetic Approach to be used in vivo to Investigate the Role of the M1 Muscarinic Acetylcholine Receptor in Learning, Memory, and Neurodegenerative Disease*.

Brooks, D. J. (2000). Dopamine agonists: their role in the treatment of Parkinson's disease. *Journal of Neurology, Neurosurgery & Psychiatry*, *68*(6), 685–689. https://doi.org/10.1136/JNNP.68.6.685

Brown, A. J. H., Bradley, S. J., Marshall, F. H., Brown, G. A., Bennett, K. A., Brown, J., Cansfield, J. E., Cross, D. M., de Graaf, C., Hudson, B. D., Dwomoh, L., Dias, J. M., Errey, J. C., Hurrell, E., Liptrot, J., Mattedi, G., Molloy, C., Nathan, P. J., Okrasa, K., … Tobin, A. B. (2021). From structure to clinic: Design of a muscarinic M1 receptor agonist with potential to treatment of Alzheimer's disease. *Cell*, *184*(24), 5886-5901.e22. https://doi.org/10.1016/J.CELL.2021.11.001

Brown, K., & Mastrianni, J. A. (2010). The prion diseases. *Journal of Geriatric Psychiatry and Neurology*, *23*(4), 277–298. https://doi.org/10.1177/0891988710383576

Brown, P., Brandel, J. P., Preese, M., & Sato, T. (2006). Iatrogenic Creutzfeldt-Jakob disease: the waning of an era. *Neurology*, *67*(3), 389–393. https://doi.org/10.1212/01.WNL.0000231528.65069.3F

Bruce, M. E., & Dickinson, A. G. (1987). Biological evidence that scrapie agent has an independent genome. *The Journal of General Virology*, *68 (Pt 1)*(1), 79–89. https://doi.org/10.1099/0022-1317-68-1-79

Buckley, N. J., Bonner, T. I., & Brann, M. R. (1988). Localization of a family of muscarinic receptor mRNAs in rat brain. *The Journal of Neuroscience*, *8*(12), 4646. https://doi.org/10.1523/JNEUROSCI.08-12-04646.1988

Büeler, H., Aguzzi, A., Sailer, A., Greiner, R. A., Autenried, P., Aguet, M., & Weissmann, C. (1993). Mice devoid of PrP are resistant to scrapie. *Cell*, *73*(7), 1339–1347. https://doi.org/10.1016/0092-8674(93)90360-3

Büeler, H., Fischer, M., Lang, Y., Bluethmann, H., Lipp, H. P., Dearmond, S. J., Prusiner, S. B., Aguet, M., & Weissmann, C. (1992). Normal development and behaviour of mice lacking the neuronal cell-surface PrP protein. *Nature 1992 356:6370*, *356*(6370), 577–582. https://doi.org/10.1038/356577a0

Burton, M. D., & Johnson, R. W. (2012). Interleukin-6 trans-signaling in the senescent mouse brain is involved in infection-related deficits in contextual fear conditioning. *Brain, Behavior, and Immunity*, *26*(5), 732–738. https://doi.org/10.1016/J.BBI.2011.10.008

Butler, D. A., Scott, M. R. D., Bockman, J. M., Borchelt,', D. R., Taraboulos, A., Hsiao, K. K., Kingsbury, D. T., & Prusiner13, S. B. (1988). Scrapie-infected murine neuroblastoma cells produce protease-resistant prion proteins. *Journal of Virology*, *62*(5), 1558–1564. https://doi.org/10.1128/JVI.62.5.1558-1564.1988

Butler, Y. R., Liu, Y., Kumbhar, R., Zhao, P., Gadhave, K., Wang, N., Li, Y., Mao, X., & Wang, W. (2022). α-Synuclein fibril-specific nanobody reduces prion-like α-synuclein spreading in mice. *Nature Communications 2022 13:1*, *13*(1), 1–13. https://doi.org/10.1038/s41467-022-31787-2

Butterfield, D. A., Reed, T., Newman, S. F., & Sultana, R. (2007). Roles of Amyloid ß-Peptide-Associated Oxidative Stress and Brain Protein Modifications in the Pathogenesis of Alzheimer's Disease and Mild Cognitive Impairment. *Free Radical Biology & Medicine*, *43*(5), 658. https://doi.org/10.1016/J.FREERADBIOMED.2007.05.037

Cairns, N. J., Neumann, M., Bigio, E. H., Holm, I. E., Troost, D., Hatanpaa, K. J., Foong, C., White, C. L., Schneider, J. A., Kretzschmar, H. A., Carter, D., Taylor-Reinwald, L., Paulsmeyer, K., Strider, J., Gitcho, M., Goate, A. M., Morris, J. C., Mishra, M., Kwong, L. K., … Mackenzie, I. R. A. (2007). TDP-43 in familial and sporadic frontotemporal lobar degeneration with ubiquitin inclusions. *The American Journal of Pathology*, *171*(1), 227–240. https://doi.org/10.2353/AJPATH.2007.070182

Campeau, J. L., Wu, G., Bell, J. R., Rasmussen, J., & Sim, V. L. (2013). Early Increase and Late Decrease of Purkinje Cell Dendritic Spine Density in Prion-Infected Organotypic Mouse Cerebellar Cultures. *PLOS ONE*, *8*(12), e81776. https://doi.org/10.1371/JOURNAL.PONE.0081776

Carman, C. V., & Benovic, J. L. (1998). G-protein-coupled receptors: turn-ons and turn-offs. *Current Opinion in Neurobiology*, *8*(3), 335–344. https://doi.org/10.1016/S0959-4388(98)80058-5

Carroll, J. A., Striebel, J. F., Race, B., Phillips, K., & Chesebro, B. (2015). Prion Infection of Mouse Brain Reveals Multiple New Upregulated Genes Involved in Neuroinflammation or Signal Transduction. *Journal of Virology*, *89*(4), 2388–2404. https://doi.org/10.1128/JVI.02952-14/SUPPL_FILE/ZJV999090076SO1.PDF

Carroll, J. A., Striebel, J. F., Rangel, A., Woods, T., Phillips, K., Peterson, K. E., Race, B., & Chesebro, B. (2016). Prion Strain Differences in Accumulation of PrPSc on Neurons and Glia Are Associated with Similar Expression Profiles of Neuroinflammatory Genes: Comparison of Three Prion Strains. *PLoS Pathogens*, *12*(4). https://doi.org/10.1371/JOURNAL.PPAT.1005551

Caughey, B., & Race, R. E. (1992). Potent inhibition of scrapie-associated PrP accumulation by congo red. *Journal of Neurochemistry*, *59*(2), 768–771. https://doi.org/10.1111/J.1471-4159.1992.TB09437.X

Chai, X., Dage, J. L., & Citron, M. (2012). Constitutive secretion of tau protein by an unconventional mechanism. *Neurobiology of Disease*, *48*(3), 356–366. https://doi.org/10.1016/J.NBD.2012.05.021

Chandler, R. L. (1961). ENCEPHALOPATHY IN MICE PRODUCED BY INOCULATION WITH SCRAPIE BRAIN MATERIAL. *The Lancet*, *277*(7191), 1378–1379. https://doi.org/10.1016/S0140-6736(61)92008-6

Chaudhuri, T. K., & Paul, S. (2006). Protein-misfolding diseases and chaperone-based therapeutic approaches. *The FEBS Journal*, *273*(7), 1331–1349. https://doi.org/10.1111/J.1742-4658.2006.05181.X

Chen, C. M., Tseng, C. N., Cho, J. J., Lee, Y. Z., Kao, C. L., Cheng, Y. Bin, Hong, Y. R., & Cho, C. L. (2014). Heat shock induces expression of OSTC/DC2, a novel subunit of oligosaccharyltransferase, in vitro and in vivo. *The Kaohsiung Journal of Medical Sciences*, *30*(5), 219–223. https://doi.org/10.1016/J.KJMS.2014.01.003

Chen, G. F., Xu, T. H., Yan, Y., Zhou, Y. R., Jiang, Y., Melcher, K., & Xu, H. E. (2017). Amyloid beta: structure, biology and structure-based therapeutic development. *Acta Pharmacologica Sinica 2017 38:9*, *38*(9), 1205–1235. https://doi.org/10.1038/aps.2017.28

Chesebro, B. (1998). BSE and prions: uncertainties about the agent. *Science (New York, N.Y.)*, *279*(5347), 42–43. https://doi.org/10.1126/SCIENCE.279.5347.42

Christopoulos, A. (2014). Advances in G protein-coupled receptor allostery: from function to structure. *Molecular Pharmacology*, *86*(5), 463–478. https://doi.org/10.1124/MOL.114.094342

Christopoulos, A., Changeux, J.-P., Catterall, W. A., Fabbro, D., Burris, T. P., Cidlowski, J. A., Olsen, R. W., Peters, J. A., Neubig, R. R., Pin, J.-P., Sexton, P. M., Kenakin, T. P., Ehlert, F. J., Spedding, M., & Langmead, C. J. (2014). International Union of Basic and Clinical Pharmacology. XC. Multisite

Pharmacology: Recommendations for the Nomenclature of Receptor Allosterism and Allosteric Ligands. *Pharmacological Reviews*, *66*(4), 918–947. https://doi.org/10.1124/PR.114.008862

Collinge, J. (2005). Molecular neurology of prion disease. *Journal of Neurology, Neurosurgery, and Psychiatry*, *76*(7), 906–919. https://doi.org/10.1136/JNNP.2004.048660

Collinge, J., Whitfield, J., McKintosh, E., Beck, J., Mead, S., Thomas, D. J., & Alpers, M. P. (2006). Kuru in the 21st century--an acquired human prion disease with very long incubation periods. *Lancet (London, England)*, *367*(9528), 2068–2074. https://doi.org/10.1016/S0140-6736(06)68930-7

Colovic, M. B., Krstic, D. Z., Lazarevic-Pasti, T. D., Bondzic, A. M., & Vasic, V. M. (2013). Acetylcholinesterase Inhibitors: Pharmacology and Toxicology. *Current Neuropharmacology*, *11*(3), 315–335. https://doi.org/10.2174/1570159x11311030006

Conway, K. A., Lee, S. J., Rochet, J. C., Ding, T. T., Williamson, R. E., & Lansbury, P. T. (2000). Acceleration of oligomerization, not fibrillization, is a shared property of both α-synuclein mutations linked to early-onset Parkinson's disease: Implications for pathogenesis and therapy. *Proceedings of the National Academy of Sciences of the United States of America*, *97*(2), 571. https://doi.org/10.1073/PNAS.97.2.571

Costanzo, M., Abounit, S., Marzo, L., Danckaert, A., Chamoun, Z., Roux, P., & Zurzolo, C. (2013). Transfer of polyglutamine aggregates in neuronal cells occurs in tunneling nanotubes. *Journal of Cell Science*, *126*(16), 3678–3685. https://doi.org/10.1242/JCS.126086/263594/AM/TRANSFER-OF-POLYGLUTAMINE-AGGREGATES-IN-NEURONAL

Creutzfeldt, H. G. (1989). On a particular focal disease of the central nervous system (preliminary communication), 1920. *Alzheimer Disease and Associated Disorders*, *3*(1–2), 3–25.

Cronier, S., Beringue, V., Bellon, A., Peyrin, J.-M., & Laude, H. (2007). Prion Strain- and Species-Dependent Effects of Antiprion Molecules in Primary Neuronal Cultures. *Journal of Virology*, *81*(24), 13794–13800. https://doi.org/10.1128/JVI.01502-07/ASSET/DA1C56F2-66B9-4F6B-A7C7-DE64D74AD827/ASSETS/GRAPHIC/ZJV0240700010005.JPEG

Cronier, S., Laude, H., & Peyrin, J. M. (2004). Prions can infect primary cultured neurons and astrocytes and promote neuronal cell death. *Proceedings of the National Academy of Sciences of the United States of America*, *101*(33), 12271–12276. https://www.pnas.org/doi/abs/10.1073/pnas.0402725101

Dale, N. C., Johnstone, E. K. M., & Pfleger, K. D. G. (2022). GPCR heteromers: An overview of their classification, function and physiological relevance. *Frontiers in Endocrinology*, *13*, 931573. https://doi.org/10.3389/FENDO.2022.931573/BIBTEX

Daude, N., Lehmann, S., & Harris, D. A. (1997). Identification of intermediate steps in the conversion of a mutant prion protein to a Scrapie-like form in cultured cells. *Journal of Biological Chemistry*, *272*(17), 11604–11612. https://doi.org/10.1074/jbc.272.17.11604

Dauer, W., & Przedborski, S. (2003). Parkinson's Disease: Mechanisms and Models. *Neuron*, *39*(6), 889–909. https://doi.org/10.1016/S0896-6273(03)00568-3

Dawson, V. L., & Dawson, T. M. (1996). Function of Nitric Oxide in Neuronal Cell Death. *Comprehensive Biotechnology, Second Edition*.

Depta, L., Whitmarsh-Everiss, T., & Laraia, L. (2022). Structure, function and small molecule modulation of intracellular sterol transport proteins. *Bioorganic & Medicinal Chemistry*, *68*. https://doi.org/10.1016/J.BMC.2022.116856

Dhapola, R., Hota, S. S., Sarma, P., Bhattacharyya, A., Medhi, B., & Reddy, D. H. K. (2021). Recent advances in molecular pathways and therapeutic

implications targeting neuroinflammation for Alzheimer's disease. *Inflammopharmacology*, *29*(6), 1669. https://doi.org/10.1007/S10787-021-00889-6

Dhuri, K., Bechtold, C., Quijano, E., Pham, H., Gupta, A., Vikram, A., & Bahal, R. (2020). Antisense Oligonucleotides: An Emerging Area in Drug Discovery and Development. *Journal of Clinical Medicine*. https://doi.org/10.3390/jcm9062004

Diaz-Espinoza, R., & Soto, C. (2012). High-resolution structure of infectious prion protein: the final frontier. *Nature Structural & Molecular Biology*, *19*(4), 370–377. https://doi.org/10.1038/NSMB.2266

Dickinson, A. G., Meikle, V. M. H., & Fraser, H. (1968). *Identification of a gene which controls the incubation period of some strains of scrapie agent in mice*.

Diedrich, M., Mao, L., Bernreuther, C., Zabel, C., Nebrich, G., Kleene, R., & Klose, J. (2008). Proteome analysis of ventral midbrain in MPTP-treated normal and L1cam transgenic mice. *Proteomics*, *8*(6), 1266–1275. https://doi.org/10.1002/PMIC.200700754

Doh-ura, K., Iwaki, T., & Caughey, B. (2000). Lysosomotropic agents and cysteine protease inhibitors inhibit scrapie-associated prion protein accumulation. *Journal of Virology*, *74*(10), 4894–4897. https://doi.org/10.1128/JVI.74.10.4894-4897.2000

Duce, J. A., Tsatsanis, A., Cater, M. A., James, S. A., Robb, E., Wikhe, K., Leong, S. L., Perez, K., Johanssen, T., Greenough, M. A., Cho, H. H., Galatis, D., Moir, R. D., Masters, C. L., McLean, C., Tanzi, R. E., Cappai, R., Barnham, K. J., Ciccotosto, G. D., … Bush, A. I. (2010). Iron-export ferroxidase activity of β-amyloid precursor protein is inhibited by zinc in Alzheimer's disease. *Cell*, *142*(6), 857–867. https://doi.org/10.1016/J.CELL.2010.08.014

Dujardin, S., Bégard, S., Caillierez, R., Lachaud, C., Delattre, L., Carrier, S., Loyens, A., Galas, M. C., Bousset, L., Melki, R., Aurégan, G., Hantraye, P., Brouillet, E., Buée, L., & Colin, M. (2014). Ectosomes: A New Mechanism for Non-Exosomal Secretion of Tau Protein. *PLOS ONE*, *9*(6), e100760. https://doi.org/10.1371/JOURNAL.PONE.0100760

Duyckaerts, C., Clavaguera, F., & Potier, M. C. (2019). The prion-like propagation hypothesis in Alzheimer's and Parkinson's disease. *Current Opinion in Neurology*, *32*(2), 266–271. https://doi.org/10.1097/WCO.0000000000000672

Dwomoh, L., Rossi, M., Scarpa, M., Khajehali, E., Molloy, C., Herzyk, P., Mistry, S. N., Bottrill, A. R., Sexton, P. M., Christopoulos, A., Conn, P. J., Lindsley, C. W., Bradley, S. J., & Tobin, A. B. (2022). M1 muscarinic receptor activation reduces the molecular pathology and slows the progression of prion-mediated neurodegenerative disease. *Science Signaling*, *15*(760). https://doi.org/10.1126/SCISIGNAL.ABM3720

Dwomoh, L., Tejeda, G. S., & Tobin, A. B. (2022). Targeting the M1 muscarinic acetylcholine receptor in Alzheimer's disease. *Neuronal Signaling*, *6*(1), 20210004. https://doi.org/10.1042/NS20210004

Falsig, J., & Aguzzi, A. (2008). The prion organotypic slice culture assay—POSCA. *Nature Protocols 2008 3:4*, *3*(4), 555–562. https://doi.org/10.1038/nprot.2008.13

Fang, C., Imberdis, T., Garza, M. C., Wille, H., & Harris, D. A. (2016). A Neuronal Culture System to Detect Prion Synaptotoxicity. *PLoS Pathogens*, *12*(5). https://doi.org/10.1371/JOURNAL.PPAT.1005623

Fehlinger, A., Wolf, H., Hossinger, A., Duernberger, Y., Pleschka, C., Riemschoss, K., Liu, S., Bester, R., Paulsen, L., Priola, S. A., Groschup, M. H., Schätzl, H. M., & Vorberg, I. M. (2017). Prion strains depend on different endocytic routes for productive infection. *Scientific Reports*, *7*(1). https://doi.org/10.1038/S41598-017-07260-2

Ferrada, C., Moreno, E., Casadó, V., Bongers, G., Cortés, A., Mallol, J., Canela, E. I., Leurs, R., Ferré, S., Lluís, C., & Franco, R. (2009). Marked changes in signal transduction upon heteromerization of dopamine D1 and histamine H3 receptors. *British Journal of Pharmacology*, *157*(1), 64–75. https://doi.org/10.1111/J.1476-5381.2009.00152.X

Ferreira, S. T., Clarke, J. R., Bomfim, T. R., & De Felice, F. G. (2014). Inflammation, defective insulin signaling, and neuronal dysfunction in Alzheimer's disease. *Alzheimer's and Dementia*, *10*(1 SUPPL.). https://doi.org/10.1016/J.JALZ.2013.12.010

Fisher, A. (2012). Cholinergic modulation of amyloid precursor protein processing with emphasis on M1 muscarinic receptor: perspectives and challenges in treatment of Alzheimer's disease. *Journal of Neurochemistry*, *120*, 22–33. https://doi.org/10.1111/j.1471-4159.2011.07507.x

Fisher, A., Pittel, Z., Haring, R., Bar-Ner, N., Kliger-Spatz, M., Natan, N., Egozi, I., Sonego, H., Marcovitch, I., & Brandeis, R. (2003). M1 Muscarinic Agonists Can Modulate Some of the Hallmarks in Alzheimer's Disease: Implications in Future Therapy. *Journal of Molecular Neuroscience*, *20*(3), 349–356. https://doi.org/10.1385/JMN:20:3:349

Forlenza, O. V., Spink, J. M., Dayanandan, R., Anderton, B. H., Olesen, O. F., & Lovestone, S. (2000). Muscarinic agonists reduce tau phosphorylation in non-neuronal cells via GSK-3β inhibition and in neurons. *Journal of Neural Transmission*, *107*(10), 1201–1212. https://doi.org/10.1007/s007020070034

Foster, J. D., & Dickinson, A. G. (1988). The unusual properties of CH1641, a sheep-passaged isolate of scrapie. *The Veterinary Record*.

Franco, A., Velasco-Carneros, L., Alvarez, N., Orozco, N., Moro, F., Prado, A., & Muga, A. (2021). Unzipping the Secrets of Amyloid Disassembly by the Human Disaggregase. *Cells 2021, Vol. 10, Page 2745*, *10*(10), 2745. https://doi.org/10.3390/CELLS10102745

Frost, B., Jacks, R. L., & Diamond, M. I. (2009). Propagation of tau misfolding from the outside to the inside of a cell. *The Journal of Biological Chemistry*, *284*(19), 12845–12852. https://doi.org/10.1074/JBC.M808759200

Gambetti, P., Kong, Q., Zou, W., Parchi, P., & Chen, S. G. (2003). Sporadic and familial CJD: classification and characterisation. *British Medical Bulletin*, *66*(1), 213–239. https://doi.org/10.1093/BMB/66.1.213

Ganusova, E. E., Ozolins, L. N., Bhagat, S., Newnam, G. P., Wegrzyn, R. D., Sherman, M. Y., & Chernoff, Y. O. (2006). Modulation of prion formation, aggregation, and toxicity by the actin cytoskeleton in yeast. *Molecular and Cellular Biology*, *26*(2), 617–629. https://doi.org/10.1128/MCB.26.2.617-629.2006

George, A. J., Gordon, L., Beissbarth, T., Koukoulas, I., Holsinger, R. M. D., Perreau, V., Cappai, R., Tan, S. S., Masters, C. L., Scott, H. S., & Li, Q. X. (2010). A serial analysis of gene expression profile of the Alzheimer's disease Tg2576 mouse model. *Neurotoxicity Research*, *17*(4), 360–379. https://doi.org/10.1007/S12640-009-9112-3/TABLES/6

George, J. M. (2002). The synucleins. *Genome Biology*, *3*(1), reviews3002.1. https://doi.org/10.1186/GB-2001-3-1-REVIEWS3002

Gericke, A., Sniatecki, J. J., Mayer, V. G. A., Goloborodko, E., Patzak, A., Wess, J., & Pfeiffer, N. (2011). Role of M1, M3, and M5 muscarinic acetylcholine receptors in cholinergic dilation of small arteries studied with gene-targeted mice. *American Journal of Physiology - Heart and Circulatory Physiology*, *300*(5), H1602. https://doi.org/10.1152/AJPHEART.00982.2010

Geschwind, M. D. (2015). Prion Diseases. *Continuum (Minneapolis, Minn.)*, *21*(6 NEUROINFECTIOUS DISEASE), 1612. https://doi.org/10.1212/CON.0000000000000251

Geschwind, M. D., Kuo, A. L., Wong, K. S., Haman, A., Devereux, G., Raudabaugh, B. J., Johnson, D. Y., Torres-Chae, C. C., Finley, R., Garcia,

P., Thai, J. N., Cheng, H. Q., Neuhaus, J. M., Forner, S. A., Duncan, J. L., Possin, K. L., Dearmond, S. J., Prusiner, S. B., & Miller, B. L. (2013). Quinacrine treatment trial for sporadic Creutzfeldt-Jakob disease. *Neurology*, *81*(23), 2015. https://doi.org/10.1212/WNL.0B013E3182A9F3B4

Geser, F., Martinez-Lage, M., Robinson, J., Uryu, K., Neumann, M., Brandmeir, N. J., Xie, S. X., Kwong, L. K., Elman, L., McCluskey, L., Clark, C. M., Malunda, J., Miller, B. L., Zimmerman, E. A., Qian, J., Van Deerlin, V., Grossman, M., Lee, V. M. Y., & Trojanowski, J. Q. (2009). Clinical and pathological continuum of multisystem TDP-43 proteinopathies. *Archives of Neurology*, *66*(2), 180–189. https://doi.org/10.1001/ARCHNEUROL.2008.558

Geuens, T., Bouhy, D., & Timmerman, V. (2016). The hnRNP family: insights into their role in health and disease. *Human Genetics*, *135*(8), 851–867. https://doi.org/10.1007/S00439-016-1683-5

Giacobini, E., & Becker, R. E. (2007). One hundred years after the discovery of Alzheimer's disease. A turning point for therapy? *Journal of Alzheimer's Disease*, *12*(1), 37–52. https://doi.org/10.3233/JAD-2007-12105

Giles, K., Berry, D. B., Condello, C., Hawley, R. C., Gallardo-Godoy, A., Bryant, C., Oehler, A., Elepano, M., Bhardwaj, S., Patel, S., Silber, B. M., Guan, S., Dearmond, S. J., Renslo, A. R., & Prusiner, S. B. (2015). Different 2-Aminothiazole Therapeutics Produce Distinct Patterns of Scrapie Prion Neuropathology in Mouse Brains. *The Journal of Pharmacology and Experimental Therapeutics*, *355*(1), 2–12. https://doi.org/10.1124/JPET.115.224659

Giles, K., Olson, S. H., & Prusiner, S. B. (2017). Developing Therapeutics for PrP Prion Diseases. *Cold Spring Harbor Perspectives in Medicine*. https://doi.org/10.1101/cshperspect.a023747

Glass, C. K., Saijo, K., Winner, B., Marchetto, M. C., & Gage, F. H. (2010). Mechanisms underlying inflammation in neurodegeneration. *Cell*, *140*(6), 918–934. https://doi.org/10.1016/J.CELL.2010.02.016

Goedert, M., Spillantini, M. G., Jakes, R., Rutherford, D., & Crowther, R. A. (1989). Multiple isoforms of human microtubule-associated protein tau: sequences and localization in neurofibrillary tangles of Alzheimer's disease. *Neuron*, *3*(4), 519–526. https://doi.org/10.1016/0896-6273(89)90210-9

Goin, J. C., & Nathanson, N. M. (2006). Quantitative Analysis of Muscarinic Acetylcholine Receptor Homo- and Heterodimerization in Live Cells: REGULATION OF RECEPTOR DOWN-REGULATION BY HETERODIMERIZATION. *Journal of Biological Chemistry*, *281*(9), 5416–5425. https://doi.org/10.1074/JBC.M507476200

Goodman, J., Krupnick, J. G., Santini, F., Gurevich, V. V., Penn, R. B., Gagnon, A. W., Keen, J. H., & Benovic, J. L. (1996). Beta-arrestin acts as a clathrin adaptor in endocytosis of the beta2-adrenergic receptor. *Nature*, *383*(6599), 447–450. https://doi.org/10.1038/383447A0

Gordon, J., Amini, S., & White, M. K. (2013). General overview of neuronal cell culture. *Methods in Molecular Biology (Clifton, N.J.)*, *1078*, 1. https://doi.org/10.1007/978-1-62703-640-5_1

Gousset, K., Schiff, E., Langevin, C., Marijanovic, Z., Caputo, A., Browman, D. T., Chenouard, N., de Chaumont, F., Martino, A., Enninga, J., Olivo-Marin, J. C., Männel, D., & Zurzolo, C. (2009). Prions hijack tunnelling nanotubes for intercellular spread. *Nature Cell Biology 2009 11:3*, *11*(3), 328–336. https://doi.org/10.1038/ncb1841

Govek, E. E., Newey, S. E., & Van Aelst, L. (2005). The role of the Rho GTPases in neuronal development. *Genes & Development*, *19*(1), 1–49. https://doi.org/10.1101/GAD.1256405

Green, A. J. E. (2019). RT-QuIC: a new test for sporadic CJD. *Practical Neurology*, *19*(1), 49–55. https://doi.org/10.1136/PRACTNEUROL-2018-001935

Guidi, L. G., Mattley, J., Martinez-Garay, I., Monaco, A. P., Linden, J. F., Velayos-Baeza, A., & Molnr, Z. (2017). Knockout Mice for Dyslexia Susceptibility Gene Homologs KIAA0319 and KIAA0319L have Unaffected Neuronal Migration but Display Abnormal Auditory Processing. *Cerebral Cortex*, *27*(12), 5831–5845. https://doi.org/10.1093/CERCOR/BHX269

Guo, J. L., Narasimhan, S., Changolkar, L., He, Z., Stieber, A., Zhang, B., Gathagan, R. J., Iba, M., McBride, J. D., Trojanowski, J. Q., & Lee, V. M. Y. (2016). Unique pathological tau conformers from alzheimer's brains transmit tau pathology in nontransgenic mice. *Journal of Experimental Medicine*, *213*(12), 2635–2654. https://doi.org/10.1084/jem.20160833

Guo, W., Chen, Y., Zhou, X., Kar, A., Ray, P., Chen, X., Rao, E. J., Yang, M., Ye, H., Zhu, L., Liu, J., Xu, M., Yang, Y., Wang, C., Zhang, D., Bigio, E. H., Mesulam, M., Shen, Y., Xu, Q., … Wu, J. Y. (2011). An ALS-associated mutation affecting TDP-43 enhances protein aggregation, fibril formation and neurotoxicity. *Nature Structural & Molecular Biology*, *18*(7), 822–831. https://doi.org/10.1038/NSMB.2053

Haass, C., Koo, E. H., Mellon, A., Hung, A. Y., & Selkoe, D. J. (1992). Targeting of cell-surface beta-amyloid precursor protein to lysosomes: alternative processing into amyloid-bearing fragments. *Nature*, *357*(6378), 500–503. https://doi.org/10.1038/357500A0

Haga, T. (2013). Molecular properties of muscarinic acetylcholine receptors. *Proceedings of the Japan Academy. Series B, Physical and Biological Sciences*, *89*(6), 226. https://doi.org/10.2183/PJAB.89.226

Haïk, S., Brandel, J. P., Salomon, D., Sazdovitch, V., Delasnerie-Laupêtre, N., Laplanche, J. L., Faucheux, B. A., Soubrié, C., Boher, E., Belorgey, C., Hauw, J. J., & Alpérovitch. (2004). Compassionate use of quinacrine in Creutzfeldt-Jakob disease fails to show significant effects. *Neurology*, *63*(12), 2413–2415. https://doi.org/10.1212/01.WNL.0000148596.15681.4D

Hall, D. D., Dai, S., Tseng, P. Y., Malik, Z., Nguyen, M., Matt, L., Schnizler, K., Shephard, A., Mohapatra, D. P., Tsuruta, F., Dolmetsch, R. E., Christel, C. J., Lee, A., Burette, A., Weinberg, R. J., & Hell, J. W. (2013). Competition between α-actinin and Ca^{2+}-calmodulin controls surface retention of the L-type Ca^{2+} channel Ca(V)1.2. *Neuron*, *78*(3), 483–497. https://doi.org/10.1016/J.NEURON.2013.02.032

Halliday, M., & Mallucci, G. R. (2015). Review: Modulating the unfolded protein response to prevent neurodegeneration and enhance memory Modulating the unfolded protein response to prevent neurodegeneration and enhance memory. *Neuropathology and Applied Neurobiology*, *41*, 414–427. https://doi.org/10.1111/nan.12211

Hallinan, G. I., Vargas-Caballero, M., West, J., & Deinhardt, K. (2019). Tau Misfolding Efficiently Propagates between Individual Intact Hippocampal Neurons. *Journal of Neuroscience*, *39*(48), 9623–9632. https://doi.org/10.1523/JNEUROSCI.1590-19.2019

Hamada, N., Ogaya, S., Nakashima, M., Nishijo, T., Sugawara, Y., Iwamoto, I., Ito, H., Maki, Y., Shirai, K., Baba, S., Maruyama, K., Saitsu, H., Kato, M., Matsumoto, N., Momiyama, T., & Nagata, K. I. (2018). De novo PHACTR1 mutations in West syndrome and their pathophysiological effects. *Brain*, *141*(11), 3098–3114. https://doi.org/10.1093/BRAIN/AWY246

Hamaguchi, T., Sakai, K., Noguchi-Shinohara, M., Nozaki, I., Takumi, I., Sanjo, N., Sadakane, A., Nakamura, Y., Kitamoto, T., Saito, N., Mizusawa, H., & Yamada, M. (2013). Insight into the frequent occurrence of dura mater graft-associated Creutzfeldt-Jakob disease in Japan. *Journal of Neurology, Neurosurgery, and Psychiatry*, *84*(10), 1171–1175. https://doi.org/10.1136/JNNP-2012-304850

Hamilton, S. E., Loose, M. D., Qi, M., Levey, A. I., Hille, B., Mcknight, G. S., Idzerda, R. L., & Nathanson, N. M. (1997). Disruption of the m1 receptor gene ablates muscarinic receptor-dependent M current regulation and seizure activity in mice. *Proceedings of the National Academy of Sciences of*

the United States of America, *94*(24), 13311–13316. https://doi.org/10.1073/PNAS.94.24.13311/ASSET/643DF80C-B63F-4937-A8A1-B27352A81601/ASSETS/GRAPHIC/PQ2473204006.JPEG

Hampel, H., Hardy, J., Blennow, K., Chen, C., Perry, G., Kim, S. H., Villemagne, V. L., Aisen, P., Vendruscolo, M., Iwatsubo, T., Masters, C. L., Cho, M., Lannfelt, L., Cummings, J. L., & Vergallo, A. (2021). The Amyloid-β Pathway in Alzheimer's Disease. *Molecular Psychiatry 2021 26:10*, *26*(10), 5481–5503. https://doi.org/10.1038/s41380-021-01249-0

Han, J., Wu, J., & Silke, J. (2020). An overview of mammalian p38 mitogen-activated protein kinases, central regulators of cell stress and receptor signaling . *F1000 Research*. https://doi.org/10.12688/f1000research.22092.1

Hasegawa, M., Arai, T., Nonaka, T., Kametani, F., Yoshida, M., Hashizume, Y., Beach, T. G., Buratti, E., Baralle, F., Morita, M., Nakano, I., Oda, T., Tsuchiya, K., & Akiyama, H. (2008). Phosphorylated TDP-43 in frontotemporal lobar degeneration and amyotrophic lateral sclerosis. *Annals of Neurology*, *64*(1), 60–70. https://doi.org/10.1002/ANA.21425

Hasselmo, M., & Sarter, M. (2011). Modes and models of forebrain cholinergic neuromodulation of cognition. *Neuropsychopharmacology : Official Publication of the American College of Neuropsychopharmacology*, *36*(1), 52–73. https://doi.org/10.1038/NPP.2010.104

Hauser, A. S., Attwood, M. M., Rask-Andersen, M., Schiöth, H. B., & Gloriam, D. E. (2017). Trends in GPCR drug discovery: new agents, targets and indications. *Nature Reviews. Drug Discovery*, *16*(12), 829–842. https://doi.org/10.1038/NRD.2017.178

Hauser, R. A. (2009). Levodopa: Past, Present, and Future. *European Neurology*, *62*(1), 1–8. https://doi.org/10.1159/000215875

Hebert, D. N., & Molinari, M. (2007). In and out of the ER: protein folding, quality control, degradation, and related human diseases. *Physiological Reviews*, *87*(4), 1377–1408. https://doi.org/10.1152/PHYSREV.00050.2006

Hensley, K., Carney, J. M., Mattson, M. P., Aksenova, M., Harris, M., Wu, J. F., Floyd, R. A., & Butterfield, D. A. (1994). A model for beta-amyloid aggregation and neurotoxicity based on free radical generation by the peptide: relevance to Alzheimer disease. *Proceedings of the National Academy of Sciences of the United States of America*, *91*(8), 3270–3274. https://doi.org/10.1073/PNAS.91.8.3270

Heyser, C. J., Masliah, E., Samimi, A., Campbell, I. L., & Gold, L. H. (1997). Progressive decline in avoidance learning paralleled by inflammatory neurodegeneration in transgenic mice expressing interleukin 6 in the brain. *Proceedings of the National Academy of Sciences of the United States of America*, *94*(4), 1500–1505. https://doi.org/10.1073/PNAS.94.4.1500

Hirsch, E. C., & Hunot, S. (2009). Neuroinflammation in Parkinson's disease: a target for neuroprotection? *The Lancet. Neurology*, *8*(4), 382–397. https://doi.org/10.1016/S1474-4422(09)70062-6

Hollingsworth, S. A., Kelly, B., Valant, C., Michaelis, J. A., Mastromihalis, O., Thompson, G., Venkatakrishnan, A. J., Hertig, S., Scammells, P. J., Sexton, P. M., Felder, C. C., Christopoulos, A., & Dror, R. O. (2019). Cryptic pocket formation underlies allosteric modulator selectivity at muscarinic GPCRs. *Nature Communications*, *10*(1). https://doi.org/10.1038/S41467-019-11062-7

Holmes, B. B., DeVos, S. L., Kfoury, N., Li, M., Jacks, R., Yanamandra, K., Ouidja, M. O., Brodsky, F. M., Marasa, J., Bagchi, D. P., Kotzbauer, P. T., Miller, T. M., Papy-Garcia, D., & Diamond, M. I. (2013). Heparan sulfate proteoglycans mediate internalization and propagation of specific proteopathic seeds. *Proceedings of the National Academy of Sciences of the United States of America*, *110*(33), E3138–E3147. https://doi.org/10.1073/PNAS.1301440110/SUPPL_FILE/SM01.MOV

Holper, S., Watson, R., & Yassi, N. (2022). Tau as a Biomarker of Neurodegeneration. *International Journal of Molecular Sciences 2022, Vol. 23, Page 7307*, *23*(13), 7307. https://doi.org/10.3390/IJMS23137307

Horonchik, L., Tzaban, S., Ben-Zaken, O., Yedidia, Y., Rouvinski, A., Papy-Garcia, D., Barritault, D., Vlodavsky, I., & Taraboulos, A. (2005). Heparan Sulfate Is a Cellular Receptor for Purified Infectious Prions. *Journal of Biological Chemistry*, *280*(17), 17062–17067. https://doi.org/10.1074/JBC.M500122200

Hoyt, F., Alam, P., Artikis, E., Schwartz, C. L., Hughson, A. G., Race, B., Baune, C., Raymond, G. J., Baron, G. S., Kraus, A., & Caughey, B. (2022). Cryo-EM of prion strains from the same genotype of host identifies conformational determinants. *PLOS Pathogens*, 2022.09.19.508587. https://doi.org/10.1101/2022.09.19.508587

Huang, G., Li, H., & Zhang, H. (2020). Abnormal Expression of Mitochondrial Ribosomal Proteins and Their Encoding Genes with Cell Apoptosis and Diseases. *International Journal of Molecular Sciences 2020, Vol. 21, Page 8879*, *21*(22), 8879. https://doi.org/10.3390/IJMS21228879

Huang, W., Zhou, Y., Tu, L., Ba, Z., Huang, J., Huang, N., & Luo, Y. (2020). TDP-43: From Alzheimer's Disease to Limbic-Predominant Age-Related TDP-43 Encephalopathy. *Frontiers in Molecular Neuroscience*, *13*. https://doi.org/10.3389/FNMOL.2020.00026

Hulme, E. C., Birdsall, N. J. M., & Buckley, N. J. (1990). Muscarinic receptor subtypes. *Annual Review of Pharmacology and Toxicology*, *30*, 633–673. https://doi.org/10.1146/ANNUREV.PA.30.040190.003221

Hulme, E. C., Lu, Z. L., Saldanha, J. W., & Bee, M. S. (2003). Structure and activation of muscarinic acetylcholine receptors. *Biochemical Society Transactions*, *31*(Pt 1), 29–34. https://doi.org/10.1042/BST0310029

Hutti, C. R., Welle, K. A., Hryhorenko, J. R., & Ghaemmaghami, S. (2020). Global analysis of protein degradation in prion infected cells. *Scientific Reports 2020 10:1*, *10*(1), 1–13. https://doi.org/10.1038/s41598-020-67505-5

Ilyaskina, O. S., Lemoine, H., & Bünemann, M. (2018). Lifetime of muscarinic receptor–G-protein complexes determines coupling efficiency and G-protein subtype selectivity. *Proceedings of the National Academy of Sciences*, *115*(19), 5016–5021. https://doi.org/10.1073/PNAS.1715751115

Insel, P. S., Mormino, E. C., Aisen, P. S., Thompson, W. K., & Donohue, M. C. (2020). Neuroanatomical spread of amyloid ß and tau in Alzheimer's disease: implications for primary prevention. *Brain Communications*, *2*(1). https://doi.org/10.1093/BRAINCOMMS/FCAA007

Ioannou, M. S., Liu, Z., & Lippincott-Schwartz, J. (2019). A Neuron-Glia Co-culture System for Studying Intercellular Lipid Transport. *Current Protocols in Cell Biology*, *84*(1), e95. https://doi.org/10.1002/CPCB.95

Iqbal, K., Liu, F., & Gong, C. X. (2016). Tau and neurodegenerative disease: The story so far. In *Nature Reviews Neurology* (Vol. 12, Issue 1, pp. 15–27). Nature Publishing Group. https://doi.org/10.1038/nrneurol.2015.225

Iqbal, K., Liu, F., Gong, C. X., del Alonso, A. C., & Grundke-Iqbal, I. (2009). Mechanisms of tau-induced neurodegeneration. *Acta Neuropathologica*, *118*(1), 53. https://doi.org/10.1007/S00401-009-0486-3

Iqbal, K., Liu, F., & Gong, C.-X. (2018). Recent developments with tau-based drug discovery. *Expert Opinion on Drug Discovery*, *13*(5), 399–410. https://doi.org/10.1080/17460441.2018.1445084

Iqbal, K., Zaidi, T., Wen, G. Y., Grundke-Iqbal, I., Merz, P. A., Shaikh, S. S., Wisniewski, H. M., Alafuzoff, I., & Winblad, B. (1986). Defective brain microtubule assembly in Alzheimer's disease. *Lancet (London, England)*, *2*(8504), 421–426. https://doi.org/10.1016/S0140-6736(86)92134-3

Jakob, A. (1989). Concerning a disorder of the central nervous system clinically resembling multiple sclerosis with remarkable anatomic findings (spastic pseudosclerosis). Report of a fourth case. *Alzheimer Disease and Associated Disorders*, *3*(1–2), 26–45.

Janetopoulos, C., Jin, T., & Devreotes, P. (2001). Receptor-mediated activation of heterotrimeric G-proteins in living cells. *Science (New York, N.Y.)*, *291*(5512), 2408–2411. https://doi.org/10.1126/SCIENCE.1055835

Jarpe, M. B., Knall, C., Mitchell, F. M., Buhl, A. M., Duzic, E., & Johnson, G. L. (1998). [d-Arg1,d-Phe5,d-Trp7,9,Leu11]Substance P Acts as a Biased Agonist toward Neuropeptide and Chemokine Receptors. *Journal of Biological Chemistry*, *273*(5), 3097–3104. https://doi.org/10.1074/JBC.273.5.3097

Jarrahian, A., Watts, V. J., & Barker, E. L. (2004). D2 Dopamine Receptors Modulate Gα-Subunit Coupling of the CB1 Cannabinoid Receptor. *Journal of Pharmacology and Experimental Therapeutics*, *308*(3), 880–886. https://doi.org/10.1124/JPET.103.057620

Jeong, Y., Oh, A. R., Jung, Y. H., Gi, H. J., Kim, Y. U., & Kim, K. J. (2023). Targeting E3 ubiquitin ligases and their adaptors as a therapeutic strategy for metabolic diseases. *Experimental & Molecular Medicine 2023 55:10*, *55*(10), 2097–2104. https://doi.org/10.1038/s12276-023-01087-w

Jessen, N. A., Munk, A. S. F., Lundgaard, I., & Nedergaard, M. (2015). The Glymphatic System – A Beginner's Guide. *Neurochemical Research*, *40*(12), 2583. https://doi.org/10.1007/S11064-015-1581-6

Jiang, C., Sun, L., Wen, S., Tian, Y., Xu, C., Xu, Q., & Xue, H. (2024). BRIX1 promotes ribosome synthesis and enhances glycolysis by selected translation of GLUT1 in colorectal cancer. *The Journal of Gene Medicine*, *26*(1), e3632. https://doi.org/10.1002/JGM.3632

Jiménez, E., & Montiel, M. (2005). Activation of MAP kinase by muscarinic cholinergic receptors induces cell proliferation and protein synthesis in

human breast cancer cells. *Journal of Cellular Physiology*, *204*(2), 678–686. https://doi.org/10.1002/JCP.20326

Jin, J., Meredith, G. E., Chen, L., Zhou, Y., Xu, J., Shie, F. S., Lockhart, P., & Zhang, J. (2005). Quantitative proteomic analysis of mitochondrial proteins: relevance to Lewy body formation and Parkinson's disease. *Brain Research. Molecular Brain Research*, *134*(1), 119–138. https://doi.org/10.1016/J.MOLBRAINRES.2004.10.003

Jin, S., Kedia, N., Illes-Toth, E., Haralampiev, I., Prisner, S., Herrmann, A., Wanker, E. E., & Bieschke, J. (2016). Amyloid-β(1–42) Aggregation Initiates Its Cellular Uptake and Cytotoxicity. *Journal of Biological Chemistry*, *291*(37), 19590–19606. https://doi.org/10.1074/JBC.M115.691840

Jo, M., Lee, S., Jeon, Y. M., Kim, S., Kwon, Y., & Kim, H. J. (2020). The role of TDP-43 propagation in neurodegenerative diseases: integrating insights from clinical and experimental studies. *Experimental & Molecular Medicine 2020 52:10*, *52*(10), 1652–1662. https://doi.org/10.1038/s12276-020-00513-7

Johnson, B. S., Snead, D., Lee, J. J., McCaffery, J. M., Shorter, J., & Gitler, A. D. (2009). TDP-43 is intrinsically aggregation-prone, and amyotrophic lateral sclerosis-linked mutations accelerate aggregation and increase toxicity. *The Journal of Biological Chemistry*, *284*(30), 20329–20339. https://doi.org/10.1074/JBC.M109.010264

Jung, S.-R., Kushmerick, C., Seo, J. B., Koh, D.-S., & Hille, B. (2017). Muscarinic receptor regulates extracellular signal regulated kinase by two modes of arrestin binding. *Proceedings of the National Academy of Sciences*, *114*(28), E5579–E5588. https://doi.org/10.1073/PNAS.1700331114

Kaakkola, S. (2000). Clinical pharmacology, therapeutic use and potential of COMT inhibitors in Parkinson's disease. *Drugs*, *59*(6), 1233–1250. https://doi.org/10.2165/00003495-200059060-00004/FIGURES/TAB6

Kalia, L. V., & Lang, A. E. (2015). Parkinson's disease. *Lancet (London, England)*, *386*(9996), 896–912. https://doi.org/10.1016/S0140-6736(14)61393-3

Kalinowska, M., Chávez, A. E., Lutzu, S., Castillo, P. E., Bukauskas, F. F., & Francesconi, A. (2015). Actinin-4 Governs Dendritic Spine Dynamics and Promotes Their Remodeling by Metabotropic Glutamate Receptors. *The Journal of Biological Chemistry*, *290*(26), 15909. https://doi.org/10.1074/JBC.M115.640136

Kamal, M., Gbahou, F., Guillaume, J. L., Daulat, A. M., Benleulmi-Chaachoua, A., Luka, M., Chen, P., Anaraki, D. K., Baroncini, M., La Cour, C. M., Millan, M. J., Prevot, V., Delagrange, P., & Jockers, R. (2015). Convergence of melatonin and serotonin (5-HT) signaling at MT2/5-HT2C receptor heteromers. *Journal of Biological Chemistry*, *290*(18), 11537–11546. https://doi.org/10.1074/jbc.M114.559542

Kametani, F., & Hasegawa, M. (2018). Reconsideration of amyloid hypothesis and tau hypothesis in Alzheimer's disease. In *Frontiers in Neuroscience* (Vol. 12, Issue JAN). Frontiers Media S.A. https://doi.org/10.3389/fnins.2018.00025

Kanekiyo, T., Zhang, J., Liu, Q., Liu, C. C., Zhang, L., & Bu, G. (2011). Heparan Sulphate Proteoglycan and the Low-Density Lipoprotein Receptor-Related Protein 1 Constitute Major Pathways for Neuronal Amyloid-β Uptake. *Journal of Neuroscience*, *31*(5), 1644–1651. https://doi.org/10.1523/JNEUROSCI.5491-10.2011

Karch, C. M., Jeng, A. T., & Goate, A. M. (2012). Extracellular Tau Levels Are Influenced by Variability in Tau That Is Associated with Tauopathies. *Journal of Biological Chemistry*, *287*(51), 42751–42762. https://doi.org/10.1074/JBC.M112.380642

Karran, E., Mercken, M., & Strooper, B. De. (2011). The amyloid cascade hypothesis for Alzheimer's disease: an appraisal for the development of therapeutics. *Nature Reviews Drug Discovery 2011 10:9*, *10*(9), 698–712. https://doi.org/10.1038/nrd3505

Katsikoudi, A., Ficulle, E., Cavallini, A., Sharman, G., Guyot, A., Zagnoni, M., Eastwood, B. J., Hutton, M., & Bose, S. (2020). Quantitative propagation of assembled human Tau from Alzheimer's disease brain in microfluidic neuronal cultures. *The Journal of Biological Chemistry*, *295*(37), 13079. https://doi.org/10.1074/JBC.RA120.013325

Kertesz, A., & Munoz, D. (2004). Relationship between Frontotemporal Dementia and Corticobasal Degeneration/ Progressive Supranuclear Palsy. *Dement Geriatr Cogn Disord*, *17*, 282–286. https://doi.org/10.1159/000077155

Khajehali, E., Bradley, S., Van Der Westhuizen, E. T., Molloy, C., Valant, C., Finlayson, L., Lindsley, C. W., Sexton, P. M., Tobin, A. B., & Christopoulos, A. (2020). Restoring Agonist Function at a Chemogenetically Modified M1 Muscarinic Acetylcholine Receptor. *ACS Chemical Neuroscience*, *11*(24), 4270–4279. https://doi.org/10.1021/ACSCHEMNEURO.0C00540/SUPPL_FILE/CN0C00540_SI_001.PDF

Kimberlin, R. H., & Walker, C. A. (1978). Evidence that the transmission of one source of scrapie agent to hamsters involves separation of agent strains from a mixture. *Journal of General Virology*, *39*(3), 487–496. https://doi.org/10.1099/0022-1317-39-3-487/CITE/REFWORKS

Kitsou, E., Pan, S., Zhang, J. P., Shi, M., Zabeti, A., Dickson, D. W., Albin, R., Gearing, M., Kashima, D. T., Wang, Y., Beyer, R. P., Zhou, Y., Pan, C., Caudle, W. M., & Zhang, J. (2008). Identification of proteins in human substantia nigra. *PROTEOMICS – Clinical Applications*, *2*(5), 776–782. https://doi.org/10.1002/PRCA.200800028

Klawonn, A. M., Wilhelms, D. B., Lindström, S. H., Singh, A. K., Jaarola, M., Wess, J., Fritz, M., & Engblom, D. (2018). Muscarinic M4 receptors on cholinergic and dopamine D1 receptor-expressing neurons have opposing functionality for positive reinforcement and influence impulsivity. *Frontiers in Molecular Neuroscience*, *11*, 139. https://doi.org/10.3389/FNMOL.2018.00139/BIBTEX

Knaus, K. J., Morillas, M., Swietnicki, W., Malone, M., Surewicz, W. K., & Yee, V. C. (2001). Crystal structure of the human prion protein reveals a mechanism for oligomerization. *Nature Structural Biology*, *8*(9), 770–774. https://doi.org/10.1038/NSB0901-770

Kovacs, G. G., & Budka, H. (2008). Prion diseases: From protein to cell pathology. *American Journal of Pathology*, *172*(3), 555–565. https://doi.org/10.2353/ajpath.2008.070442

Koyama, S., Noguchi, H., Yagita, K., Hamasaki, H., Shijo, M., Yoshimura, M., Inoshita, K., Sasagasako, N., & Honda, H. (2022). Characteristic distribution and molecular properties of normal cellular prion protein in human endocrine and exocrine tissues. *Scientific Reports*. https://doi.org/10.1038/s41598-022-19632-4

Krance, S. H., Luke, R., Shenouda, M., Israwi, A. R., Colpitts, S. J., Darwish, L., Strauss, M., & Watts, J. C. (2020). Cellular models for discovering prion disease therapeutics: Progress and challenges. *Journal of Neurochemistry*, *153*(2), 150–172. https://doi.org/10.1111/JNC.14956

Kraus, A., Hoyt, F., Schwartz, C. L., Hansen, B., Artikis, E., Hughson, A. G., Raymond, G. J., Race, B., Baron, G. S., & Caughey, B. (2021). High-resolution structure and strain comparison of infectious mammalian prions. *Molecular Cell*, *81*(21), 4540-4551.e6. https://doi.org/10.1016/J.MOLCEL.2021.08.011/ATTACHMENT/641C7AF4-9AE0-4813-A590-CF38E76ACB44/MMC1.PDF

Krejčí, A., & Tuček, S. (2002). Quantitation of mRNAs for M(1) to M(5) subtypes of muscarinic receptors in rat heart and brain cortex. *Molecular Pharmacology*, *61*(6), 1267–1272. https://doi.org/10.1124/MOL.61.6.1267

Kumari, P., Srinivasan, B., & Banerjee, S. (2017). Modulation of hippocampal synapse maturation by activity-regulated E3 ligase via non-canonical pathway. *Neuroscience*, *364*, 226–241. https://doi.org/10.1016/J.NEUROSCIENCE.2017.08.057

Kurt, T. D., & Sigurdson, C. J. (2016). Cross-species transmission of CWD prions. *Prion*, *10*(1), 83. https://doi.org/10.1080/19336896.2015.1118603

Kushwaha, R., Sinha, A., Makarava, N., Molesworth, K., & Baskakov, I. V. (2021). Non-cell autonomous astrocyte-mediated neuronal toxicity in prion diseases. *Acta Neuropathologica Communications*, *9*(1). https://doi.org/10.1186/S40478-021-01123-8

L, I., A, L., & M, P. (1995). Congo red prolongs the incubation period in scrapie-infected hamsters. *Journal of Virology*, *69*(1), 506–508. https://doi.org/10.1128/JVI.69.1.506-508.1995

L. Sim, V. (2012). Prion disease: chemotherapeutic strategies. *Infectious Disorders Drug Targets*, *12*(2), 144–160. https://doi.org/10.2174/187152612800100161

Landry, C. F., Ellison, J. A., Pribyl, T. M., Campagnoni, C., Kampf, K., & Campagnoni, A. T. (1996). Myelin basic protein gene expression in neurons: developmental and regional changes in protein targeting within neuronal nuclei, cell bodies, and processes. *The Journal of Neuroscience : The Official Journal of the Society for Neuroscience*, *16*(8), 2452–2462. https://doi.org/10.1523/JNEUROSCI.16-08-02452.1996

Le Dur, A., Laï, T. L., Stinnakre, M. G., Laisné, A., Chenais, N., Rakotobe, S., Passet, B., Reine, F., Soulier, S., Herzog, L., Tilly, G., Rézaei, H., Béringue, V., Vilotte, J. L., & Laude, H. (2017). Divergent prion strain evolution driven by PrPC expression level in transgenic mice. *Nature Communications 2017 8:1*, *8*(1), 1–11. https://doi.org/10.1038/ncomms14170

Lebois, E., Thorn, C., Edgerton, J., Popiolek, M., & Xi, S. (2018). Muscarinic receptor subtype distribution in the central nervous system and relevance to aging and Alzheimer's disease. *Neuropharmacology*, *136*(Pt C), 362–373. https://doi.org/10.1016/J.NEUROPHARM.2017.11.018

Lebon, G., Langmead, C. J., Tehan, B. G., & Hulme, E. C. (2009). Mutagenic mapping suggests a novel binding mode for selective agonists of M1 muscarinic acetylcholine receptors. *Molecular Pharmacology*, *75*(2), 331–341. https://doi.org/10.1124/MOL.108.050963

Lee, C. S., Sauer, H., & Björklund, A. (1996). Dopaminergic neuronal degeneration and motor impairments following axon terminal lesion by intrastriatal 6-hydroxydopamine in the rat. *Neuroscience*, *72*(3), 641–653. https://doi.org/10.1016/0306-4522(95)00571-4

Lemieux, S. P., Lev-Ram, V., Tsien, R. Y., & Ellisman, M. H. (2023). Perineuronal nets and the neuronal extracellular matrix can be imaged by genetically encoded labeling of HAPLN1 in vitro and in vivo. *BioRxiv*. https://doi.org/10.1101/2023.11.29.569151

Levey, A. I. (1993). Immunological localization of m1-m5 muscarinic acetylcholine receptors in peripheral tissues and brain. *Life Sciences*, *52*(5–6), 441–448. https://doi.org/10.1016/0024-3205(93)90300-R

Levey, A. I. (1996). Muscarinic acetylcholine receptor expression in memory circuits: Implications for treatment of Alzheimer disease. *Proceedings of the National Academy of Sciences of the United States of America*, *93*(24), 13541. https://doi.org/10.1073/PNAS.93.24.13541

Levey, A. I., Edmunds, S. M., Koliatsos, V., Wiley, R. G., & Heilman', C. J. (1995). Expression of ml-m4 Muscarinic Acetylcholine Receptor Proteins in Rat Hippocampus and Regulation by Cholinergic Innervation. *The Journal of Neuroscience*, *15*(5), 4077–4092.

Li, H. L., Wang, H. H., Liu, S. J., Deng, Y. Q., Zhang, Y. J., Tian, Q., Wang, X. C., Chen, X. Q., Yang, Y., Zhang, J. Y., Wang, Q., Xu, H., Liao, F. F., & Wang, J. Z. (2007). Phosphorylation of tau antagonizes apoptosis by stabilizing beta-catenin, a mechanism involved in Alzheimer's neurodegeneration. *Proceedings of the National Academy of Sciences of the*

United States of America, *104*(9), 3591–3596. https://doi.org/10.1073/PNAS.0609303104

Li, K., Li, J., Zheng, J., & Qin, S. (2019). Reactive Astrocytes in Neurodegenerative Diseases. *Aging and Disease*, *10*(3), 664. https://doi.org/10.14336/AD.2018.0720

Liang, M., Martin, M. W., & Harden, T. K. (1987). [3H]propylbenzilylcholine mustard-labeling of muscarinic cholinergic receptors that selectively couple to phospholipase C or adenylate cyclase in two cultured cell lines. *Molecular Pharmacology*, *32*(4).

Lloyd, S. E., Mead, S., & Collinge, J. (2013). Genetics of prion diseases. *Current Opinion in Genetics & Development*, *23*(3), 345–351. https://doi.org/10.1016/J.GDE.2013.02.012

Lourenco, M. V., Clarke, J. R., Frozza, R. L., Bomfim, T. R., Forny-Germano, L., Batista, A. F., Sathler, L. B., Brito-Moreira, J., Amaral, O. B., Silva, C. A., Freitas-Correa, L., Espírito-Santo, S., Campello-Costa, P., Houzel, J. C., Klein, W. L., Holscher, C., Carvalheira, J. B., Silva, A. M., Velloso, L. A., … De Felice, F. G. (2013). TNF-α mediates PKR-dependent memory impairment and brain IRS-1 inhibition induced by Alzheimer's β-amyloid oligomers in mice and monkeys. *Cell Metabolism*, *18*(6), 831–843. https://doi.org/10.1016/J.CMET.2013.11.002

Lu, Z., Je, H. S., Young, P., Gross, J., Lu, B., & Feng, G. (2007). Regulation of synaptic growth and maturation by a synapse-associated E3 ubiquitin ligase at the neuromuscular junction. *The Journal of Cell Biology*, *177*(6), 1077. https://doi.org/10.1083/JCB.200610060

Luttrell, L. M., & Kenakin, T. P. (2011). Refining efficacy: allosterism and bias in G protein-coupled receptor signaling. *Methods in Molecular Biology (Clifton, N.J.)*, *756*, 3–35. https://doi.org/10.1007/978-1-61779-160-4_1

Lysek, D. A., Schorn, C., Nivon, L. G., Esteve-Moya, V., Christen, B., Calzolai, L., Von Schroetter, C., Fiorito, F., Hermann, T., Günter, P., & Wüthrich, K. (2005). Prion protein NMR structures of cats, dogs, pigs, and sheep. *Proceedings of the National Academy of Sciences of the United States of America*, *102*(3), 640. https://doi.org/10.1073/PNAS.0408937102

Macdonald, J. A., Bronner, I. F., Drynan, L., Fan, J., Curry, A., Fraser, G., Lavenir, I., & Goedert, M. (2019). Assembly of transgenic human P301S Tau is necessary for neurodegeneration in murine spinal cord. *Acta Neuropathologica Communications*, *7*(1), 44. https://doi.org/10.1186/S40478-019-0695-5/FIGURES/8

Mackenzie, I. R. A., Neumann, M., Baborie, A., Sampathu, D. M., Du Plessis, D., Jaros, E., Perry, R. H., Trojanowski, J. Q., Mann, D. M. A., & Lee, V. M. Y. (2011). A harmonized classification system for FTLD-TDP pathology. *Acta Neuropathologica*, *122*(1), 111–113. https://doi.org/10.1007/S00401-011-0845-8

Maeda, S., Qu, Q., Robertson, M. J., Skiniotis, G., & Kobilka, B. K. (2019). Structures of the M1 and M2 muscarinic acetylcholine receptor/G-protein complexes. *Science*, *364*(6440), 552–557. https://doi.org/10.1126/science.aaw5188

Mahal, S. P., Baker, C. A., Demczyk, C. A., Smith, E. W., Julius, C., & Weissmann, C. (2007). Prion strain discrimination in cell culture: The cell panel assay. *Proceedings of the National Academy of Sciences of the United States of America*, *104*(52), 20908–20913. https://doi.org/10.1073/PNAS.0710054104/SUPPL_FILE/10054FIG5.JPG

Makarava, N., Mychko, O., Chang, J. C. Y., Molesworth, K., & Baskakov, I. V. (2021). The degree of astrocyte activation is predictive of the incubation time to prion disease. *Acta Neuropathologica Communications*, *9*(1). https://doi.org/10.1186/S40478-021-01192-9

Malek, N., Michrowska, A., Mazurkiewicz, E., Mrówczyńska, E., Mackiewicz, P., & Mazur, A. J. (2021). The origin of the expressed retrotransposed gene ACTBL2 and its influence on human melanoma cells' motility and focal adhesion formation. *Scientific Reports 2021 11:1*, *11*(1), 1–26. https://doi.org/10.1038/s41598-021-82074-x

Mallucci, G., Dickinson, A., Linehan, J., Klöhn, P. C., Brandner, S., & Collinge, J. (2003). Depleting Neuronal PrP in Prion Infection Prevents Disease and Reverses Spongiosis. *Science*, *302*(5646), 871–874. https://doi.org/10.1126/science.1090187

Mallucci, G. R., Ratté, S., Asante, E. A., Linehan, J., Gowland, I., Jefferys, J. G. R., & Collinge, J. (2002). Post-natal knockout of prion protein alters hippocampal CA1 properties, but does not result in neurodegeneration. *The EMBO Journal*, *21*(3), 202. https://doi.org/10.1093/EMBOJ/21.3.202

Mandelkow, E. M., Biernat, J., Drewes, G., Gustke, N., Trinczek, B., & Mandelkow, E. (1995). Tau domains, phosphorylation, and interactions with microtubules. *Neurobiology of Aging*, *16*(3), 355–362. https://doi.org/10.1016/0197-4580(95)00025-A

Manka, S. W., Wenborn, A., Betts, J., Joiner, S., Saibil, H. R., Collinge, J., & Wadsworth, J. D. F. (2023). A structural basis for prion strain diversity. *Nature Chemical Biology |*, *19*, 607–613. https://doi.org/10.1038/s41589-022-01229-7

Mann, D., Teuber, C., Tennigkeit, S. A., Schröter, G., Gerwert, K., Kötting, C., & Pai, E. F. (2016). Mechanism of the intrinsic arginine finger in heterotrimeric G proteins. *Proceedings of the National Academy of Sciences of the United States of America*, *113*(50), E8041–E8050. https://doi.org/10.1073/PNAS.1612394113/SUPPL_FILE/PNAS.1612394113.SAPP.PDF

Manson, J. C., Clarke, A. R., Hooper, M. L., Aitchison, L., McConnell, I., & Hope, J. (1994). 129/Ola mice carrying a null mutation in PrP that abolishes mRNA

production are developmentally normal. *Molecular Neurobiology*, *8*(2–3), 121–127. https://doi.org/10.1007/BF02780662

Marsango, S., Jenkins, L., Pediani, J. D., Bradley, S. J., Ward, R. J., Hesse, S., Biener, G., Stoneman, M. R., Tobin, A. B., Raicu, V., & Milligan, G. (2022). The M1 muscarinic receptor is present in situ as a ligand-regulated mixture of monomers and oligomeric complexes. *Proceedings of the National Academy of Sciences of the United States of America*, *119*(24), e2201103119. https://doi.org/10.1073/PNAS.2201103119/SUPPL_FILE/PNAS.2201103119.SAPP.PDF

Marsh, A. P. (2019). Molecular mechanisms of proteinopathies across neurodegenerative disease: a review. *Neurological Research and Practice*, *1*(1), 1–7. https://doi.org/10.1186/S42466-019-0039-8/FIGURES/1

Matamoros-Angles, A., Hervera, A., Soriano, J., Martí, E., Carulla, P., Llorens, F., Nuvolone, M., Aguzzi, A., Ferrer, I., Gruart, A., Delgado-García, J. M., & Del Río, J. A. (2022). Analysis of co-isogenic prion protein deficient mice reveals behavioral deficits, learning impairment, and enhanced hippocampal excitability. *BMC Biology 2021 20:1*, *20*(1), 1–25. https://doi.org/10.1186/S12915-021-01203-0

Mathur, S., Gawas, C., Ahmad, I. Z., Wani, M., & Tabassum, H. (2023). Neurodegenerative disorders: Assessing the impact of natural vs drug-induced treatment options. *Aging Medicine*, *6*(1), 82. https://doi.org/10.1002/AGM2.12243

Mays, C. E., Kang, H. E., Kim, Y., Shim, S. H., Bang, J. E., Woo, H. J., Cho, Y. H., Kim, J. B., & Ryou, C. (2008). CRBL cells: Establishment, characterization and susceptibility to prion infection. *Brain Research*, *1208*, 170–180. https://doi.org/10.1016/J.BRAINRES.2008.02.103

McAlary, L., Chew, Y. L., Lum, J. S., Geraghty, N. J., Yerbury, J. J., & Cashman, N. R. (2020). Amyotrophic Lateral Sclerosis: Proteins, Proteostasis, Prions,

and Promises. *Frontiers in Cellular Neuroscience*, *14*. https://doi.org/10.3389/FNCEL.2020.581907

McAlary, L., Plotkin, S. S., Yerbury, J. J., & Cashman, N. R. (2019). Prion-Like Propagation of Protein Misfolding and Aggregation in Amyotrophic Lateral Sclerosis. *Frontiers in Molecular Neuroscience*, *12*. https://doi.org/10.3389/FNMOL.2019.00262

McCormack, A., Chegeni, N., Chegini, F., Colella, A., Power, J., Keating, D., & Chataway, T. (2016). Purification of α-synuclein containing inclusions from human post mortem brain tissue. *Journal of Neuroscience Methods*, *266*, 141–150. https://doi.org/10.1016/J.JNEUMETH.2016.03.016

McKhann, G. M., Albert, M. S., Grossman, M., Miller, B., Dickson, D., & Trojanowski, J. Q. (2001). Clinical and pathological diagnosis of frontotemporal dementia: report of the Work Group on Frontotemporal Dementia and Pick's Disease. *Archives of Neurology*, *58*(11), 1803–1809. https://doi.org/10.1001/ARCHNEUR.58.11.1803

Mclaughlin, P., Zhou, Y., Ma, T., Liu, J., Zhang, W., Hong, J. S., Kovacs, M., & Zhang, J. (2006). Proteomic analysis of microglial contribution to mouse strain-dependent dopaminergic neurotoxicity. *Glia*, *53*(6), 567–582. https://doi.org/10.1002/GLIA.20294

McLean, C. A., Storey, E., Gardner, R. J. M., Tannenberg, A. E. G., Cervenáková, L., & Brown, P. (1997). The D178N (cis-129M) 'fatal familial insomnia' mutation associated with diverse clinicopathologic phenotypes in an Australian kindred. *Neurology*, *49*(2), 552–558. https://doi.org/10.1212/WNL.49.2.552

Meade-White, K. D., Barbian, K. D., Race, B., Favara, C., Gardner, D., Taubner, L., Porcella, S., & Race, R. (2009). Characteristics of 263K Scrapie Agent in Multiple Hamster Species. *Emerging Infectious Diseases*, *15*(2), 207. https://doi.org/10.3201/EID1502.081173

Mercer, R. C., & Harris, D. A. (2019). Identification of anti-prion drugs and targets using toxicity-based assays. *Current Opinion in Pharmacology*, *44*, 20–27. https://doi.org/10.1016/J.COPH.2018.12.005

Michel, M. C., & Charlton, S. J. (2018). Biased Agonism in Drug Discovery—Is It Too Soon to Choose a Path? *Molecular Pharmacology*, *93*(4), 259–265. https://doi.org/10.1124/MOL.117.110890

Mioshi, E., Hsieh, S., Savage, S., Hornberger, M., & Hodges, J. R. (2010). Clinical staging and disease progression in frontotemporal dementia. *Neurology*, *74*(20), 1591–1597. https://doi.org/10.1212/WNL.0B013E3181E04070

Mironov, A., Latawiec, D., Wille, H., Bouzamondo-Bernstein, E., Legname, G., Williamson, R. A., Burton, D., DeArmond, S. J., Prusiner, S. B., & Peters, P. J. (2003). Cytosolic Prion Protein in Neurons. *Journal of Neuroscience*, *23*(18), 7183–7193. https://doi.org/10.1523/JNEUROSCI.23-18-07183.2003

Mishra, M., Huang, J., & Balasubramanian, M. K. (2014). The yeast actin cytoskeleton. *FEMS Microbiology Reviews*, *38*(2), 213–227. https://doi.org/10.1111/1574-6976.12064

Miyazaki, H., Nishioka, S., Yamanaka, T., Abe, M., Imamura, Y., Miyasaka, T., Kakuda, N., Oohashi, T., Shimogori, T., Yamakawa, K., Ikawa, M., & Nukina, N. (2024). Generation and characterization of cerebellar granule neurons specific knockout mice of Golli-MBP. *Transgenic Research*, 1–19. https://doi.org/10.1007/S11248-024-00382-0/FIGURES/5

Mondal, R., Sandhu, Y. K., Kamalia, V. M., Delaney, B. A., Syed, A. U., Nguyen, G. A. H., Moran, T. R., Limpengco, R. R., Liang, C., & Mukherjee, J. (2023). Measurement of Aß Amyloid Plaques and Tau Protein in Postmortem Human Alzheimer's Disease Brain by Autoradiography Using [18F]Flotaza, [125I]IBETA, [124/125I]IPPI and Immunohistochemistry Analysis Using QuPath. *Biomedicines*, *11*(4). https://doi.org/10.3390/BIOMEDICINES11041033

Moore, R. A., Sturdevant, D. E., Chesebro, B., & Priola, S. A. (2014). Proteomics Analysis of Amyloid and Nonamyloid Prion Disease Phenotypes Reveals Both Common and Divergent Mechanisms of Neuropathogenesis. *Journal of Proteome Research*, *13*(11), 4620. https://doi.org/10.1021/PR500329W

Morales, R., Abid, K., & Soto, C. (2007). The prion strain phenomenon: Molecular basis and unprecedented features. *Biochimica et Biophysica Acta*, *1772*(6), 681. https://doi.org/10.1016/J.BBADIS.2006.12.006

Moran, S. P., Dickerson, J. W., Cho, H. P., Xiang, Z., Maksymetz, J., Remke, D. H., Lv, X., Doyle, C. A., Rajan, D. H., Niswender, C. M., Engers, D. W., Lindsley, C. W., Rook, J. M., & Conn, P. J. (2018). M1-positive allosteric modulators lacking agonist activity provide the optimal profile for enhancing cognition. *Neuropsychopharmacology*, *43*(8), 1763. https://doi.org/10.1038/S41386-018-0033-9

Morimoto-Suzki, N., Hirabayashi, Y., Tyssowski, K., Shinga, J., Vidal, M., Koseki, H., & Gotoh, Y. (2014). The polycomb component Ring1B regulates the timed termination of subcerebral projection neuron production during mouse neocortical development. *Development*, *141*(22), 4343–4353. https://doi.org/10.1242/DEV.112276

Morris, J. (2015). Amyotrophic Lateral Sclerosis (ALS) and Related Motor Neuron Diseases: An Overview. *The Neurodiagnostic Journal*, *55*(3), 180–194. https://doi.org/10.1080/21646821.2015.1075181

Mothe, B., & Brander, C. (2020). Small steps forward for HIV vaccine development. *Nature Medicine*. https://doi.org/10.1038/s41591-020-0835-2

Mouillet-Richard, S., Nishida, N., Pradines, E., Laude, H., Schneider, B., Féraudet, C. C., Grassi, J., Launay, J. M., Lehmann, S., & Kellermann, O. (2008). Prions impair bioaminergic functions through serotonin- or catecholamine-derived neurotoxins in neuronal cells. *Journal of Biological Chemistry*, *283*(35), 23782–23790. https://doi.org/10.1074/jbc.M802433200

Mufson, E. J., Counts, S. E., Perez, S. E., & Ginsberg, S. D. (2008). Cholinergic system during the progression of Alzheimer's disease: therapeutic implications. *Expert Review of Neurotherapeutics*, *8*(11), 1703. https://doi.org/10.1586/14737175.8.11.1703

Muñoz, E. R., Caccese, J. B., Wilson, B. E., Shuler, K. T., Santos, F. V., Cabán, C. T., Jeka, J. J., Langford, D., & Hudson, M. B. (2021). Effects of purposeful soccer heading on circulating small extracellular vesicle concentration and cargo. *Journal of Sport and Health Science*, *10*(2), 122–130. https://doi.org/10.1016/J.JSHS.2020.11.006

Muramoto, T., Scott, M., Cohen, F. E., & Prusiner, S. B. (1996). Recombinant scrapie-like prion protein of 106 amino acids is soluble. *Proceedings of the National Academy of Sciences of the United States of America*, *93*(26), 15457. https://doi.org/10.1073/PNAS.93.26.15457

Nakić, N., Tran, T. H., Novokmet, M., Andreoletti, O., Lauc, G., & Legname, G. (2021). Site-specific analysis of N-glycans from different sheep prion strains. *PLOS Pathogens*, *17*(2), e1009232. https://doi.org/10.1371/JOURNAL.PPAT.1009232

Nakielny, S., & Dreyfuss, G. (1997). Nuclear export of proteins and RNAs. *Current Opinion in Cell Biology*, *9*(3), 420–429. https://doi.org/10.1016/S0955-0674(97)80016-6

Nathan, P. J., Watson, J., Lund, J., Davies, C. H., Peters, G., Dodds, C. M., Swirski, B., Lawrence, P., Bentley, G. D., O'Neill, B. V., Robertson, J., Watson, S., Jones, G. A., Maruff, P., Croft, R. J., Laruelle, M., & Bullmore, E. T. (2013). The potent M1 receptor allosteric agonist GSK1034702 improves episodic memory in humans in the nicotine abstinence model of cognitive dysfunction. *International Journal of Neuropsychopharmacology*, *16*(4), 721–731. https://doi.org/10.1017/S1461145712000752

Nelson, P. T., Alafuzoff, I., Bigio, E. H., Bouras, C., Braak, H., Cairns, N. J., Castellani, R. J., Crain, B. J., Davies, P., Tredici, K. Del, Duyckaerts, C.,

Frosch, M. P., Haroutunian, V., Hof, P. R., Hulette, C. M., Hyman, B. T., Iwatsubo, T., Jellinger, K. A., Jicha, G. A., … Beach, T. G. (2012). Correlation of alzheimer disease neuropathologic changes with cognitive status: A review of the literature. In *Journal of Neuropathology and Experimental Neurology* (Vol. 71, Issue 5, pp. 362–381). https://doi.org/10.1097/NEN.0b013e31825018f7

Nenasheva, T. A., Neary, M., Mashanov, G. I., Birdsall, N. J. M., Breckenridge, R. A., & Molloy, J. E. (2013). Abundance, distribution, mobility and oligomeric state of M2 muscarinic acetylcholine receptors in live cardiac muscle. *Journal of Molecular and Cellular Cardiology*, *57*(1), 129. https://doi.org/10.1016/J.YJMCC.2013.01.009

Neumann, M., Sampathu, D. M., Kwong, L. K., Truax, A. C., Micsenyi, M. C., Chou, T. T., Bruce, J., Schuck, T., Grossman, M., Clark, C. M., McCluskey, L. F., Miller, B. L., Masliah, E., Mackenzie, I. R., Feldman, H., Feiden, W., Kretzschmar, H. A., Trojanowski, J. Q., & Lee, V. M. Y. (2006). Ubiquitinated TDP-43 in frontotemporal lobar degeneration and amyotrophic lateral sclerosis. *Science (New York, N.Y.)*, *314*(5796), 130–133. https://doi.org/10.1126/SCIENCE.1134108

Neves, S. R., Ram, P. T., & Iyengar, R. (2002). G protein pathways. *Science (New York, N.Y.)*, *296*(5573), 1636–1639. https://doi.org/10.1126/SCIENCE.1071550

Nishida, N., Harris, D. A., Vilette, D., Laude, H., Frobert, Y., Grassi, J., Casanova, D., Milhavet, O., & Lehmann, S. (2000). Successful Transmission of Three Mouse-Adapted Scrapie Strains to Murine Neuroblastoma Cell Lines Overexpressing Wild-Type Mouse Prion Protein. *Journal of Virology*, *74*(1), 320–325. https://doi.org/10.1128/JVI.74.1.320-325.2000/ASSET/894832DC-01A7-40F1-82C0-DCC40EF9D837/ASSETS/GRAPHIC/JV0101043005.JPEG

Nishida, N., Katamine, S., & Manuelidis, L. (2005). Reciprocal interference between specific CJD and scrapie agents in neural cell cultures. *Science*,

310(5747), 493–496. https://doi.org/10.1126/SCIENCE.1118155/SUPPL_FILE/NISHIDA.SOM.PDF

Nussinov, R., & Tsai, C.-J. (2012). The Different Ways through Which Specificity Works in Orthosteric and Allosteric Drugs. *Current Pharmaceutical Design*, *18*(9), 1311. https://doi.org/10.2174/138161212799436377

O'Brien, R. J., & Wong, P. C. (2011). Amyloid Precursor Protein Processing and Alzheimer's Disease. *Annual Review of Neuroscience*, *34*, 185. https://doi.org/10.1146/ANNUREV-NEURO-061010-113613

Ohara, K., Uchiyama, H., Ohara, K., Haga, T., & Ichiyama, A. (1990). Interaction of deglycosylated muscarinic receptors with ligands and G proteins. *European Journal of Pharmacology*, *189*(6), 341–346. https://doi.org/10.1016/0922-4106(90)90030-2

Oikawa, T., Nonaka, T., Terada, M., Tamaoka, A., Hisanaga, S. I., & Hasegawa, M. (2016). α-Synuclein Fibrils Exhibit Gain of Toxic Function, Promoting Tau Aggregation and Inhibiting Microtubule Assembly. *Journal of Biological Chemistry*, *291*(29), 15046–15056. https://doi.org/10.1074/JBC.M116.736355

Okamura, N., & Yanai, K. (2017). Brain imaging: Applications of tau PET imaging. In *Nature reviews. Neurology* (Vol. 13, Issue 4, pp. 197–198). NLM (Medline). https://doi.org/10.1038/nrneurol.2017.38

Oldham, W. M., & Hamm, H. E. (2008). Heterotrimeric G protein activation by G-protein-coupled receptors. *Nature Reviews. Molecular Cell Biology*, *9*(1), 60–71. https://doi.org/10.1038/NRM2299

Olsson, F., Schmidt, S., Althoff, V., Munter, L. M., Jin, S., Rosqvist, S., Lendahl, U., Multhaup, G., & Lundkvist, J. (2014). Characterization of intermediate steps in amyloid beta (Aß) production under near-native conditions. *The Journal of Biological Chemistry*, *289*(3), 1540–1550. https://doi.org/10.1074/JBC.M113.498246

Orr, C. F., Rowe, D. B., Mizuno, Y., Mori, H., & Halliday, G. M. (2005). A possible role for humoral immunity in the pathogenesis of Parkinson's disease. *Brain : A Journal of Neurology*, *128*(Pt 11), 2665–2674. https://doi.org/10.1093/BRAIN/AWH625

Pagel, O., Loroch, S., Sickmann, A., & Zahedi, R. P. (2015). Current strategies and findings in clinically relevant post-translational modification-specific proteomics. *Expert Review of Proteomics*, *12*(3), 235–253. https://doi.org/10.1586/14789450.2015.1042867

Palmio, J., Suhonen, J., Keränen, T., Hulkkonen, J., Peltola, J., & Pirttilä, T. (2009). Cerebrospinal fluid tau as a marker of neuronal damage after epileptic seizure. *Seizure*, *18*(7), 474–477. https://doi.org/10.1016/J.SEIZURE.2009.04.006

Pan, K. M., Baldwin, M., Nguyen, J., Gasset, M., Serban, A., Groth, D., Mehlhorn, I., Huang, Z., Fletterick, R. J., Cohen, F. E., & Prusiner, S. B. (1993). Conversion of alpha-helices into beta-sheets features in the formation of the scrapie prion proteins. *Proceedings of the National Academy of Sciences of the United States of America*, *90*(23), 10962–10966. https://doi.org/10.1073/PNAS.90.23.10962

Panda, D., Samuel, J. C., Massie, M., Feinstein, S. C., & Wilson, L. (2003). Differential regulation of microtubule dynamics by three- and four-repeat tau: implications for the onset of neurodegenerative disease. *Proceedings of the National Academy of Sciences of the United States of America*, *100*(16), 9548–9553. https://doi.org/10.1073/PNAS.1633508100

Parsons, J. T., Horwitz, A. R., & Schwartz, M. A. (2010). Cell adhesion: integrating cytoskeletal dynamics and cellular tension. *Nature Reviews. Molecular Cell Biology*, *11*(9), 633. https://doi.org/10.1038/NRM2957

Patel, C. B., Noor, N., & Rockman, H. A. (2010). Functional Selectivity in Adrenergic and Angiotensin Signaling Systems. *Molecular Pharmacology*, *78*(6), 983–992. https://doi.org/10.1124/MOL.110.067066

Pattison, I. H., & Millson, G. C. (1961). Scrapie Produced Experimentally in Goats With Special Reference To the Clinical Syndrome. *Journal of Comparative Pathology and Therapeutics*, *71*, 101-IN10. https://doi.org/10.1016/S0368-1742(61)80013-1

Philiastides, A., Manuel Ribes, J., Chun-Mun Yip, D., Schmidt, C., Benilova, I., & Klöhn, P.-C. (2019). A New Cell Model for Investigating Prion Strain Selection and Adaptation. *Viruses*. https://doi.org/10.3390/v11100888

Platt, M. P., Adler, W. T., Mehlhorn, A. J., Johnson, G. C., Wright, K. A., Choi, R. T., Tsang, W. H., Poon, M. W., Yeung, S. Y., Waye, M. M. Y., Galaburda, A. M., & Rosen, G. D. (2013). Embryonic disruption of the candidate dyslexia susceptibility gene homolog Kiaa0319-like results in neuronal migration disorders. *Neuroscience*, *248*, 585–593. https://doi.org/10.1016/J.NEUROSCIENCE.2013.06.056

Politis, M., Wu, K., Molloy, S., Bain, P. G., Chaudhuri, K. R., & Piccini, P. (2010). Parkinson's disease symptoms: The patient's perspective. *Movement Disorders*, *25*(11), 1646–1651. https://doi.org/10.1002/MDS.23135

Polymeropoulos, M. H., Lavedan, C., Leroy, E., Ide, S. E., Dehejia, A., Dutra, A., Pike, B., Root, H., Rubenstein, J., Boyer, R., Stenroos, E. S., Chandrasekharappa, S., Athanassiadou, A., Papapetropoulos, T., Johnson, W. G., Lazzarini, A. M., Duvoisin, R. C., Di Iorio, G., Golbe, L. I., & Nussbaum, R. L. (1997). Mutation in the alpha-synuclein gene identified in families with Parkinson's disease. *Science (New York, N.Y.)*, *276*(5321), 2045–2047. https://doi.org/10.1126/SCIENCE.276.5321.2045

Poorkaj, P., Bird, T. D., Wijsman, E., Nemens, E., Garruto, R. M., Anderson, L., Andreadis, A., Wiederholt, W. C., Raskind, M., & Schellenberg, G. D. (1998). Tau is a candidate gene for chromosome 17 frontotemporal dementia. *Annals of Neurology*, *43*(6), 815–825. https://doi.org/10.1002/ANA.410430617

Powell, A., Matar, E., & Lewis, S. J. G. (2022). Treating hallucinations in Parkinson's disease. *Expert Review of Neurotherapeutics*, *22*(6), 455–468. https://doi.org/10.1080/14737175.2021.1851198

Previtali, R., Leidi, A., Basso, M., Izzo, G., Stignani, C., Spaccini, L., Iascone, M., Veggiotti, P., & Bova, S. M. (2023). Case report: Early-onset parkinsonism among the neurological features in children with PHACTR1 variants. *Frontiers in Neurology*, *14*, 1181015. https://doi.org/10.3389/FNEUR.2023.1181015/BIBTEX

Priemer, G., Balkema-Buschmann, A., Hills, B., Groschup, M. H., & Johnson, C. J. (2013). *Biochemical Characteristics and PrP Sc Distribution Pattern in the Brains of Cattle Experimentally Challenged with H-type and L-type Atypical BSE*. https://doi.org/10.1371/journal.pone.0067599

Priller, C., Bauer, T., Mitteregger, G., Krebs, B., Kretzschmar, H. A., & Herms, J. (2006). Synapse formation and function is modulated by the amyloid precursor protein. *The Journal of Neuroscience : The Official Journal of the Society for Neuroscience*, *26*(27), 7212–7221. https://doi.org/10.1523/JNEUROSCI.1450-06.2006

Prions, 95 Proceedings of the National Academy of Sciences of the United States of America 13363 (1998). https://www.pnas.org/doi/abs/10.1073/pnas.95.23.13363

Prusiner, S. B. (1998a). Prions. *Proceedings of the National Academy of Sciences of the United States of America*, *95*(23), 13363–13383. https://doi.org/10.1073/pnas.95.23.13363

Prusiner, S. B., McKinley, M. P., Bowman, K. A., Bolton, D. C., Bendheim, P. E., Groth, D. F., & Glenner, G. G. (1983). Scrapie prions aggregate to form amyloid-like birefringent rods. *Cell*, *35*(2 Pt 1), 349–358. https://doi.org/10.1016/0092-8674(83)90168-X

Przedborski, S., & Vila, M. (2003). The 1-methyl-4-phenyl-1,2,3,6-tetrahydropyridine mouse model: a tool to explore the pathogenesis of Parkinson's disease. *Annals of the New York Academy of Sciences*, *991*, 189–198.

Puoti, G., Bizzi, A., Forloni, G., Safar, J. G., Tagliavini, F., & Gambetti, P. (2012). Sporadic human prion diseases: molecular insights and diagnosis. *The Lancet Neurology*, *11*(7), 618–628. https://doi.org/10.1016/S1474-4422(12)70063-7

Qiu, C., Kivipelto, M., & Von Strauss, E. (2009). Epidemiology of Alzheimer's disease: Occurrence, determinants, and strategies toward intervention. In *Dialogues in Clinical Neuroscience* (Vol. 11, Issue 2, pp. 111–128).

Quintanilla, R. A., Orellana, D. I., González-Billault, C., & Maccioni, R. B. (2004). Interleukin-6 induces Alzheimer-type phosphorylation of tau protein by deregulating the cdk5/p35 pathway. *Experimental Cell Research*, *295*(1), 245–257. https://doi.org/10.1016/j.yexcr.2004.01.002

Rabinovici, G. D., & Miller, B. L. (2010). Frontotemporal Lobar Degeneration: Epidemiology, Pathophysiology, Diagnosis and Management. *CNS Drugs*, *24*(5), 375. https://doi.org/10.2165/11533100-000000000-00000

Rabinovici, G. D., Wang, P. N., Levin, J., Cook, L., Pravdin, M., Davis, J., DeArmond, S. J., Barbaro, N. M., Martindale, J., Miller, B. L., & Geschwind, M. D. (2006). First symptom in sporadic Creutzfeldt-Jakob disease. *Neurology*, *66*(2), 286–287. https://doi.org/10.1212/01.WNL.0000196440.00297.67

Ravits, J., Laurie, P., Fan, Y., & Moore, D. H. (2007). Implications of ALS focality: rostral-caudal distribution of lower motor neuron loss postmortem. *Neurology*, *68*(19), 1576–1582. https://doi.org/10.1212/01.WNL.0000261045.57095.56

Ravits, J. M., & La Spada, A. R. (2009). ALS motor phenotype heterogeneity, focality, and spread: deconstructing motor neuron degeneration. *Neurology*, *73*(10), 805. https://doi.org/10.1212/WNL.0B013E3181B6BBBD

Raymond, G. J., Zhao, H. T., Race, B., Raymond, L. D., Williams, K., Swayze, E. E., Graffam, S., Le, J., Caron, T., Stathopoulos, J., O'Keefe, R., Lubke, L. L., Reidenbach, A. G., Kraus, A., Schreiber, S. L., Mazur, C., Cabin, D. E., Carroll, J. B., Minikel, E. V., … Vallabh, S. M. (2019). Antisense oligonucleotides extend survival of prion-infected mice. *JCI Insight*, *4*(16). https://doi.org/10.1172/JCI.INSIGHT.131175

Richards, J. G., Higgins, G. A., Ouagazzal, A. M., Ozmen, L., Kew, J. N. C., Bohrmann, B., Malherbe, P., Brockhaus, M., Loetscher, H., Czech, C., Huber, G., Bluethmann, H., Jacobsen, H., & Kemp, J. A. (2003). PS2APP Transgenic Mice, Coexpressing hPS2mut and hAPPswe, Show Age-Related Cognitive Deficits Associated with Discrete Brain Amyloid Deposition and Inflammation. *The Journal of Neuroscience*, *23*(26), 8989. https://doi.org/10.1523/JNEUROSCI.23-26-08989.2003

Riederer, P., & Laux, G. (2011). MAO-inhibitors in Parkinson's Disease. *Experimental Neurobiology*, *20*(1), 1. https://doi.org/10.5607/EN.2011.20.1.1

Riek, R., Hornemann, S., Wider, G., Billeter, M., Glockshuber, R., & Wuthrich, K. (1996). NMR structure of the mouse prion protein domain PrP(121–231). *Nature*, *382*(6587), 180–182. https://doi.org/10.1038/382180A0

Riesner, D. (2003). Biochemistry and structure of PrPC and PrPSc. *British Medical Bulletin*, *66*(1), 21–33. https://doi.org/10.1093/BMB/66.1.21

Rivera-Milla, E., Stuermer, C. A. O., & Málaga-Trillo, E. (2003). An evolutionary basis for scrapie disease: identification of a fish prion mRNA. *Trends in Genetics*, *19*(2), 72–75. https://doi.org/10.1016/S0168-9525(02)00032-X

Rizek, P., Kumar, N., & Jog, M. S. (2016). An update on the diagnosis and treatment of Parkinson disease. *CMAJ*, *188*(16), 1157–1165. https://doi.org/10.1503/CMAJ.151179/-/DC1

Rosenbaum, D. M., Rasmussen, S. G. F., & Kobilka, B. K. (2009). The structure and function of G-protein-coupled receptors. *Nature*, *459*(7245), 356. https://doi.org/10.1038/NATURE08144

Saborio, G. P., Permanne, B., & Soto, C. (2001). Sensitive detection of pathological prion protein by cyclic amplification of protein misfolding. *Nature*, *411*(6839), 810–813. https://doi.org/10.1038/35081095

Safar, J., Gajdusek, D. C., Gibbs, C. J., & Roller, P. P. (1994). Scrapie amyloid (prion) protein has the conformational characteristics of an aggregated molten globule folding intermediate. *Biochemistry*, *33*(27), 8375–8383. https://doi.org/10.1021/BI00193A027

Sailer, A., Büeler, H., Fischer, M., Aguzzi, A., & Weissmann, C. (1994). No propagation of prions in mice devoid of PrP. *Cell*, *77*(7), 967–968. https://doi.org/10.1016/0092-8674(94)90436-7

Saman, S., Kim, W. H., Raya, M., Visnick, Y., Miro, S., Saman, S., Jackson, B., McKee, A. C., Alvarez, V. E., Lee, N. C. Y., & Hall, G. F. (2012). Exosome-associated Tau Is Secreted in Tauopathy Models and Is Selectively Phosphorylated in Cerebrospinal Fluid in Early Alzheimer Disease. *Journal of Biological Chemistry*, *287*(6), 3842–3849. https://doi.org/10.1074/JBC.M111.277061

Sanders, D. W., Kaufman, S. K., Holmes, B. B., & Diamond, M. I. (2016). Prions and Protein Assemblies that Convey Biological Information in Health and Disease. *Neuron*, *89*(3), 433–448. https://doi.org/10.1016/J.NEURON.2016.01.026

Santa-Maria, I., Varghese, M., Księzak-Reding, H., Dzhun, A., Wang, J., & Pasinetti, G. M. (2012). Paired Helical Filaments from Alzheimer Disease

Brain Induce Intracellular Accumulation of Tau Protein in Aggresomes. *Journal of Biological Chemistry*, *287*(24), 20522–20533. https://doi.org/10.1074/JBC.M111.323279

Scarpa, M. (2022). *Phosphorylation of the M1 muscarinic acetylcholine receptor provides neuroprotection in mouse prion disease*.

Scarpa, M., Hesse, S., & Bradley, S. J. (2020). M1 muscarinic acetylcholine receptors: A therapeutic strategy for symptomatic and disease-modifying effects in Alzheimer's disease? *Advances in Pharmacology (San Diego, Calif.)*, *88*, 277–310. https://doi.org/10.1016/BS.APHA.2019.12.003

Scarpa, M., Molloy, C., Jenkins, L., Strellis, B., Budgett, R. F., Hesse, S., Dwomoh, L., Marsango, S., Tejeda, G. S., Rossi, M., Ahmed, Z., Milligan, G., Hudson, B. D., Tobin, A. B., & Bradley, S. J. (2021). Biased M1 muscarinic receptor mutant mice show accelerated progression of prion neurodegenerative disease. *Proceedings of the National Academy of Sciences of the United States of America*, *118*(50), e2107389118. https://doi.org/10.1073/PNAS.2107389118/SUPPL_FILE/PNAS.2107389118.SAPP.PDF

Scarr, E. (2012). Muscarinic Receptors: Their Roles in Disorders of the Central Nervous System and Potential as Therapeutic Targets. *CNS Neuroscience & Therapeutics*, *18*(5), 369–379. https://doi.org/10.1111/J.1755-5949.2011.00249.X

Schapira, A. H. V., Chaudhuri, K. R., & Jenner, P. (2017). Non-motor features of Parkinson disease. *Nature Reviews. Neuroscience*, *18*(7), 435–450. https://doi.org/10.1038/NRN.2017.62

Scheckel, C., & Aguzzi, A. (2018). Prions, prionoids and protein misfolding disorders. *Nature Reviews Genetics*, *19*(7), 405–418. https://doi.org/10.1038/s41576-018-0011-4

Schliebs, R., & Arendt, T. (2006). The significance of the cholinergic system in the brain during aging and in Alzheimer's disease. *J Neural Transm*, *113*, 1625–1644. https://doi.org/10.1007/s00702-006-0579-2

Schober, A. (2004). Classic toxin-induced animal models of Parkinson's disease: 6-OHDA and MPTP. *Cell and Tissue Research*, *318*(1), 215–224. https://doi.org/10.1007/S00441-004-0938-Y

Schonberger, S. J., Edgar, P. F., Kydd, R., Faull, R. L. M., & Cooper, G. J. S. (2001). Proteomic analysis of the brain in Alzheimer's disease: Molecular phenotype of a complex disease process. *PROTEOMICS*, *1*(12), 1519. https://doi.org/10.1002/1615-9861(200111)1:12<1519::AID-PROT1519>3.0.CO;2-L

Scotter, E. L., Chen, H. J., & Shaw, C. E. (2015). Erratum to: TDP-43 Proteinopathy and ALS: Insights into Disease Mechanisms and Therapeutic Targets. *Neurotherapeutics : The Journal of the American Society for Experimental NeuroTherapeutics*, *12*(2), 515–518. https://doi.org/10.1007/S13311-015-0351-0

Selkoe, D. J., & Hardy, J. (2016). The amyloid hypothesis of Alzheimer's disease at 25 years. *EMBO Molecular Medicine*, *8*(6), 595–608. https://doi.org/10.15252/emmm.201606210

Senatore, A., Restelli, E., & Chiesa, R. (2013). Synaptic Dysfunction in Prion Diseases: A Trafficking Problem? *International Journal of Cell Biology*, *2013*, 15. https://doi.org/10.1155/2013/543803

Shankaran, H., Steven, H. S., & Resat, H. (2007). Receptor downregulation and desensitization enhance the information processing ability of signalling receptors. *BMC Systems Biology*, *1*, 48. https://doi.org/10.1186/1752-0509-1-48

Shi, J., Shaw, C. L., Du Plessis, D., Richardson, A. M. T., Bailey, K. L., Julien, C., Stopford, C., Thompson, J., Varma, A., Craufurd, D., Tian, J., Pickering-

Brown, S., Neary, D., Snowden, J. S., & Mann, D. M. A. (2005). Histopathological changes underlying frontotemporal lobar degeneration with clinicopathological correlation. *Acta Neuropathologica*, *110*(5), 501–512. https://doi.org/10.1007/S00401-005-1079-4/TABLES/4

Shin, J., Park, S., Lee, H. Y., & Kim, Y. S. (2021). Thioflavin-positive tau aggregates complicating quantification of amyloid plaques in the brain of 5XFAD transgenic mouse model. *Scientific Reports 2021 11:1*, *11*(1), 1–9. https://doi.org/10.1038/s41598-021-81304-6

Shmerling, D., Hegyi, I., Fischer, M., Blättler, T., Brandner, S., Götz, J., Rülicke, T., Flechsig, E., Cozzio, A., Von Mering, C., Hangartner, C., Aguzzi, A., & Weissmann, C. (1998). Expression of amino-terminally truncated PrP in the mouse leading to ataxia and specific cerebellar lesions. *Cell*, *93*(2), 203–214. https://doi.org/10.1016/S0092-8674(00)81572-X

Shukla, A. K., Manglik, A., Kruse, A. C., Xiao, K., Reis, R. I., Tseng, W. C., Staus, D. P., Hilger, D., Uysal, S., Huang, L. Y., Paduch, M., Tripathi-Shukla, P., Koide, A., Koide, S., Weis, W. I., Kossiakoff, A. A., Kobilka, B. K., & Lefkowitz, R. J. (2013). Structure of active β-arrestin-1 bound to a G-protein-coupled receptor phosphopeptide. *Nature*, *497*(7447), 137–141. https://doi.org/10.1038/NATURE12120

Siu, C. R., Balsor, J. L., Jones, D. G., & Murphy, K. M. (2015). Classic and Golli Myelin Basic Protein have distinct developmental trajectories in human visual cortex. *Frontiers in Neuroscience*, *9*(APR), 138. https://doi.org/10.3389/FNINS.2015.00138

Sizova, D., Charbaut, E., Delalande, F., Poirier, F., High, A. A., Parker, F., Van Dorsselaer, A., Duchesne, M., & Diu-Hercend, A. (2007). Proteomic analysis of brain tissue from an Alzheimer's disease mouse model by two-dimensional difference gel electrophoresis. *Neurobiology of Aging*, *28*(3), 357–370. https://doi.org/10.1016/J.NEUROBIOLAGING.2006.01.011

Snavely, S. E. K., Susman, M. W., Kunz, R. C., Tan, J., Srinivasan, S., Cohen, M. D., Okada, K., Lamb, H., Choi, S. S., Karuna, E. P., Scales, M. K., Gygi, S. P., Greenberg, M. E., & Ho, H. Y. H. (2021). Proteomic analysis identifies the E3 ubiquitin ligase Pdzrn3 as a regulatory target of Wnt5a-Ror signaling. *Proceedings of the National Academy of Sciences of the United States of America*, *118*(25), e2104944118. https://doi.org/10.1073/PNAS.2104944118/SUPPL_FILE/PNAS.2104944118.SD01.XLSX

Solforosi, L., Milani, M., Mancini, N., Clementi, M., & Burioni, R. (2013). A closer look at prion strains: Characterization and important implications. *Prion*, *7*(2), 99. https://doi.org/10.4161/PRI.23490

Soraya Victoria, G., Arkhipenko, A., Zhu, S., Syan, S., & Zurzolo, C. (2016). Astrocyte-to-neuron intercellular prion transfer is mediated by cell-cell contact. *Scientific Reports*. https://doi.org/10.1038/srep20762

Soto, C., & Satani, N. (2011). The intricate mechanisms of neurodegeneration in prion diseases. *Trends Mol Med*. https://doi.org/10.1016/j.molmed.2010.09.001

Sparkes, R. S., Simon, M., Cohn, V. H., Fournier, R. E., Lem, J., Klisak, I., Heinzmann, C., Blatt, C., Lucero, M., & Mohandas, T. (1986). Assignment of the human and mouse prion protein genes to homologous chromosomes. *Proceedings of the National Academy of Sciences of the United States of America*, *83*(19), 7358. https://doi.org/10.1073/PNAS.83.19.7358

Spillantini, M. G., Bird, T. D., & Ghetti, B. (1998). Frontotemporal dementia and Parkinsonism linked to chromosome 17: a new group of tauopathies. *Brain Pathology (Zurich, Switzerland)*, *8*(2), 387–402. https://doi.org/10.1111/J.1750-3639.1998.TB00162.X

Stallaert, W., Christopoulos, A., & Bouvier, M. (2011). Ligand functional selectivity and quantitative pharmacology at G protein-coupled receptors.

Expert Opinion on Drug Discovery, *6*(8), 811–825. https://doi.org/10.1517/17460441.2011.586691

Staus, D. P., Hu, H., Robertson, M. J., Kleinhenz, A. L. W., Wingler, L. M., Capel, W. D., Latorraca, N. R., Lefkowitz, R. J., & Skiniotis, G. (2020). Structure of the M2 muscarinic receptor-ß-arrestin complex in a lipid nanodisc. *Nature*, *579*(7798), 297–302. https://doi.org/10.1038/S41586-020-1954-0

Stefani, M. (2010). Biochemical and biophysical features of both oligomer/fibril and cell membrane in amyloid cytotoxicity. *The FEBS Journal*, *277*(22), 4602–4613. https://doi.org/10.1111/J.1742-4658.2010.07889.X

Stefanis, L. (2012). α-Synuclein in Parkinson's Disease. *Cold Spring Harbor Perspectives in Medicine*, *2*(2). https://doi.org/10.1101/CSHPERSPECT.A009399

Strader, C. D., Sibley, D. R., & Lefkowitz, R. J. (1984). Association of sequestered beta-adrenergic receptors with the plasma membrane: a novel mechanism for receptor down regulation. *Life Sciences*, *35*(15), 1601–1610. https://doi.org/10.1016/0024-3205(84)90359-X

Strumbo, B., Ronchi, S., Bolis, L. C., & Simonic, T. (2001). Molecular cloning of the cDNA coding for Xenopus laevis prion protein. *FEBS Letters*, *508*(2), 170–174. https://doi.org/10.1016/S0014-5793(01)03027-7

Subashini, C., Dhanesh, S. B., Chen, C. M., Riya, P. A., Meera, V., Divya, T. S., Kuruvilla, R., Buttler, K., & James, J. (2017). Wnt5a is a crucial regulator of neurogenesis during cerebellum development. *Scientific Reports*, *7*. https://doi.org/10.1038/SREP42523

Sun, C. S., Wang, C. Y. H., Chen, B. P. W., He, R. Y., Liu, G. C. H., Wang, C. H., Chen, W., Chern, Y., & Huang, J. J. T. (2014). The influence of pathological mutations and proline substitutions in TDP-43 glycine-rich peptides on its

amyloid properties and cellular toxicity. *PloS One*, *9*(8). https://doi.org/10.1371/JOURNAL.PONE.0103644

Swinnen, B., & Robberecht, W. (2014). The phenotypic variability of amyotrophic lateral sclerosis. *Nature Reviews. Neurology*, *10*(11), 661–670. https://doi.org/10.1038/NRNEUROL.2014.184

Szentirmay, M. N., & Sawadogo, M. (1994). Sarkosyl block of transcription reinitiation by RNA polymerase II as visualized by the colliding polymerases reinitiation assay. *Nucleic Acids Research*, *22*(24), 5341. https://doi.org/10.1093/NAR/22.24.5341

Szutowicz, A., Bielarczyk, H., Ronowska, A., Gul-Hinc, S., Klimaszewska-ŁAta, J., Dýs, A., Zýsk, M., & Pawełczyk, T. (2014). Intracellular redistribution of acetyl-CoA, the pivotal point in differential susceptibility of cholinergic neurons and glial cells to neurodegenerative signals. *Biochemical Society Transactions*, *42*(4), 1101–1106. https://doi.org/10.1042/BST20140078

Takács, V. T., Cserép, C., Schlingloff, D., Pósfai, B., Szőnyi, A., Sos, K. E., Környei, Z., Dénes, Á., Gulyás, A. I., Freund, T. F., & Nyiri, G. (2018). Co-transmission of acetylcholine and GABA regulates hippocampal states. *Nature Communications 2018 9:1*, *9*(1), 1–15. https://doi.org/10.1038/s41467-018-05136-1

Takami, M., Nagashima, Y., Sano, Y., Ishihara, S., Morishima-Kawashima, M., Funamoto, S., & Ihara, Y. (2009). γ-Secretase: Successive Tripeptide and Tetrapeptide Release from the Transmembrane Domain of β-Carboxyl Terminal Fragment. *The Journal of Neuroscience*, *29*(41), 13042. https://doi.org/10.1523/JNEUROSCI.2362-09.2009

Talebi, R., Ahmadi, A., Afraz, F., & Abdoli, R. (2016). Parkinson's disease and lactoferrin: Analysis of dependent protein networks. *Gene Reports*, *4*, 177–183. https://doi.org/10.1016/J.GENREP.2016.05.006

Tanaka, M., Chien, P., Naber, N., Cooke, R., & Weissman, J. S. (2004). Conformational variations in an infectious protein determine prion strain differences. *Nature*, *428*(6980), 323–328. https://doi.org/10.1038/NATURE02392

Tanaka, M., Takeshi Yamasaki, Hasebe, R., Suzuki, A., & Motohiro Horiuchi. (2020). Enhanced phosphorylation of PERK in primary cultured neurons as an autonomous neuronal response to prion infection. *PLOS ONE*. https://doi.org/10.1371/journal.pone.0234147

Thal, D. M., Sun, B., Feng, D., Nawaratne, V., Leach, K., Felder, C. C., Bures, M. G., Evans, D. A., Weis, W. I., Bachhawat, P., Kobilka, T. S., Sexton, P. M., Kobilka, B. K., & Christopoulos, A. (2016). Crystal structures of the M1 and M4 muscarinic acetylcholine receptors. *Nature*, *531*(7594), 335–340. https://doi.org/10.1038/NATURE17188

Thomas, R. L., Mistry, R., Langmead, C. J., Wood, M. D., & Challiss, R. A. J. (2008). G Protein Coupling and Signaling Pathway Activation by M 1 Muscarinic Acetylcholine Receptor Orthosteric and Allosteric Agonists. *THE JOURNAL OF PHARMACOLOGY AND EXPERIMENTAL THERAPEUTICS*, *327*(2), 2021. https://doi.org/10.1124/jpet.108.141788

Thompson, K. J., Khajehali, E., Bradley, S. J., Navarrete, J. S., Huang, X. P., Slocum, S., Jin, J., Liu, J., Xiong, Y., Olsen, R. H. J., Diberto, J. F., Boyt, K. M., Pina, M. M., Pati, D., Molloy, C., Bundgaard, C., Sexton, P. M., Kash, T. L., Krashes, M. J., … Tobin, A. B. (2018). DREADD Agonist 21 Is an Effective Agonist for Muscarinic-Based DREADDs in Vitro and in Vivo. *ACS Pharmacol Transl Sci*, *1*(1), 61–72. https://doi.org/10.1021/acsptsci.8b00012

Tobin, A. B. (2008). G-protein-coupled receptor phosphorylation: where, when and by whom. *British Journal of Pharmacology*, *153*(S1), S167–S176. https://doi.org/10.1038/SJ.BJP.0707662

Tsuji, T., Shiozaki, A., Kohno, R., Yoshizato, K., & Shimohama, S. (2002). Proteomic profiling and neurodegeneration in Alzheimer's disease.

Neurochemical Research, *27*(10), 1245–1253. https://doi.org/10.1023/A:1020941929414

Tsumagari, K., Sato, Y., Shimozawa, A., Aoyagi, H., Okano, H., & Kuromitsu, J. (2022). Co-expression network analysis of human tau-transgenic mice reveals protein modules associated with tau-induced pathologies. *IScience*, *25*(8). https://doi.org/10.1016/J.ISCI.2022.104832

Tungalag, S., Shinriki, S., Hirayama, M., Nagamachi, A., Kanai, A., Inaba, T., & Matsui, H. (2023). Ribosome profiling analysis reveals the roles of DDX41 in translational regulation. *International Journal of Hematology*, *117*(6), 876–888. https://doi.org/10.1007/S12185-023-03558-2/FIGURES/4

Turner, P. R., O'Connor, K., Tate, W. P., & Abraham, W. C. (2003). Roles of amyloid precursor protein and its fragments in regulating neural activity, plasticity and memory. *Progress in Neurobiology*, *70*(1), 1–32. https://doi.org/10.1016/S0301-0082(03)00089-3

Ulbrich, S., Janning, P., Seidel, R., Matschke, J., Gonsberg, A., Jung, S., Glatzel, M., Engelhard, M., Winklhofer, K. F., & Tatzelt, J. (2018). Alterations in the brain interactome of the intrinsically disordered N-terminal domain of the cellular prion protein (PrPC) in Alzheimer's disease. *Plos One*, *13*(5), e0197659–e0197659. https://doi.org/10.1371/JOURNAL.PONE.0197659

Valant, C., Robert Lane, J., Sexton, P. M., & Christopoulos, A. (2012). The best of both worlds? Bitopic orthosteric/allosteric ligands of g protein-coupled receptors. *Annual Review of Pharmacology and Toxicology*, *52*, 153–178. https://doi.org/10.1146/ANNUREV-PHARMTOX-010611-134514

Vallabh, S. M., Minikel, E. V., Schreiber, S. L., & Lander, E. S. (2020). Towards a treatment for genetic prion disease: trials and biomarkers. *The Lancet Neurology*, *19*(4), 361–368. https://doi.org/10.1016/S1474-4422(19)30403-X

van Keulen, L. J. M., Langeveld, J. P. M., Dolstra, C. H., Jacobs, J., Bossers, A., & van Zijderveld, F. G. (2015). TSE strain differentiation in mice by immunohistochemical PrPSc profiles and triplex Western blot. *Neuropathology and Applied Neurobiology*, *41*(6), 756–779. https://doi.org/10.1111/NAN.12181/SUPPINFO

Veazey, C., Aki, S. O. E., Cook, K. F., Lai, E. C., & Kunik, M. E. (2005). Prevalence and treatment of depression in Parkinson's disease. *Journal of Neuropsychiatry and Clinical Neurosciences*, *17*(3), 310–323. https://doi.org/10.1176/JNP.17.3.310/ASSET/IMAGES/LARGE/RK0028T2.JPEG

Volpicelli, L. A., & Levey, A. I. (2004). Muscarinic acetylcholine receptor subtypes in cerebral cortex and hippocampus. *Progress in Brain Research*, *145*, 59–66. https://doi.org/10.1016/S0079-6123(03)45003-6

Vorberg, I., Raines, A., Story, B., & Priola, S. A. (2004). Susceptibility of Common Fibroblast Cell Lines to Transmissible Spongiform Encephalopathy Agents. *Journal of Infectious Diseases*, *189*(3), 431–439. https://doi.org/10.1086/381166/2/189-3-431-FIG005.GIF

Wadsworth, J. D. F., Joiner, S., Linehan, J. M., Asante, E. A., Brandner, S., & Collinge, J. (2008). The origin of the prion agent of kuru: molecular and biological strain typing. *Philosophical Transactions of the Royal Society B: Biological Sciences*, *363*(1510), 3747. https://doi.org/10.1098/RSTB.2008.0069

Wadsworth, J. D. F., Joiner, S., Linehan, J. M., Desbruslais, M., Fox, K., Cooper, S., Cronier, S., Asante, E. A., Mead, S., Brandner, S., Hill, A. F., & Collinge, J. (2008). Kuru prions and sporadic Creutzfeldt-Jakob disease prions have equivalent transmission properties in transgenic and wild-type mice. *Proceedings of the National Academy of Sciences of the United States of America*, *105*(10), 3885–3890. https://doi.org/10.1073/PNAS.0800190105

Wakabayashi, K., Tanji, K., Mori, F., & Takahashi, H. (2007). The Lewy body in Parkinson's disease: molecules implicated in the formation and degradation of alpha-synuclein aggregates. *Neuropathology : Official Journal of the Japanese Society of Neuropathology*, *27*(5), 494–506. https://doi.org/10.1111/J.1440-1789.2007.00803.X

Wang, Q., Wang, C., Ji, B., Zhou, J., Yang, C., & Chen, J. (2019). Hapln2 in Neurological Diseases and Its Potential as Therapeutic Target. *Frontiers in Aging Neuroscience*, *11*, 422782. https://doi.org/10.3389/FNAGI.2019.00060/BIBTEX

Wang, W. Y., Tan, M. S., Yu, J. T., & Tan, L. (2015). Role of pro-inflammatory cytokines released from microglia in Alzheimer's disease. *Annals of Translational Medicine*, *3*(10). https://doi.org/10.3978/J.ISSN.2305-5839.2015.03.49

Weber, B., & Barros, L. F. (2015). The Astrocyte: Powerhouse and Recycling Center. *Cold Spring Harbor Perspectives in Biology*, *7*(12), 20396–20397. https://doi.org/10.1101/CSHPERSPECT.A020396

Weihl, C. C., Temiz, P., Miller, S. E., Watts, G., Smith, C., Forman, M., Hanson, P. I., Kimonis, V., & Pestronk, A. (2008). TDP-43 accumulation in inclusion body myopathy muscle suggests a common pathogenic mechanism with frontotemporal dementia. *Journal of Neurology, Neurosurgery, and Psychiatry*, *79*(10), 1186–1189. https://doi.org/10.1136/JNNP.2007.131334

Wenborn, A., Terry, C., Gros, N., Joiner, S., D'Castro, L., Panico, S., Sells, J., Cronier, S., Linehan, J. M., Brandner, S., Saibil, H. R., Collinge, J., & Wadsworth, J. D. F. (2015). A novel and rapid method for obtaining high titre intact prion strains from mammalian brain. *Scientific Reports 2015 5:1*, *5*(1), 1–13. https://doi.org/10.1038/srep10062

Wess, J. (1993). Molecular basis of muscarinic receptor function. *Trends in Pharmacological Sciences*, *14*(8), 308–313. https://doi.org/10.1016/0165-6147(93)90049-P

Wess, J., Eglen, R. M., & Gautam, D. (2007). Muscarinic acetylcholine receptors: Mutant mice provide new insights for drug development. In *Nature Reviews Drug Discovery* (Vol. 6, Issue 9, pp. 721–733). https://doi.org/10.1038/nrd2379

Wijesekera, L. C., & Leigh, P. N. (2009). Amyotrophic lateral sclerosis. *Orphanet Journal of Rare Diseases*, *4*(1), 1–22. https://doi.org/10.1186/1750-1172-4-3/TABLES/5

Wilham, J. M., Orrú, C. D., Bessen, R. A., Atarashi, R., Sano, K., Race, B., Meade-White, K. D., Taubner, L. M., Timmes, A., & Caughey, B. (2010). Rapid End-Point Quantitation of Prion Seeding Activity with Sensitivity Comparable to Bioassays. *PLOS Pathogens*, *6*(12), e1001217. https://doi.org/10.1371/JOURNAL.PPAT.1001217

Will, R. G. (2003). Acquired prion disease: iatrogenic CJD, variant CJD, kuru. *British Medical Bulletin*, *66*, 255–265. https://doi.org/10.1093/BMB/66.1.255

Will, R. G. (2008). Bovine Spongiform Encephalopathy ☆. *Academic Press*. https://doi.org/10.1016/B978-0-12-801238-3.02540-X

Wille, H., Michelitsch, M. D., Guénebaut, V., Supattapone, S., Serban, A., Cohen, F. E., Agard, D. A., & Prusiner, S. B. (2002). Structural studies of the scrapie prion protein by electron crystallography. *Proceedings of the National Academy of Sciences of the United States of America*, *99*(6), 3563–3568. https://doi.org/10.1073/PNAS.052703499/ASSET/AC84A7FD-8A28-4EDD-8831-375E6CD0075A/ASSETS/GRAPHIC/PQ0527034004.JPEG

Willems, P., Wanschers, B. F. J., Esseling, J., Szklarczyk, R., Kudla, U., Duarte, I., Forkink, M., Nooteboom, M., Swarts, H., Gloerich, J., Nijtmans, L., Koopman, W., & Huynen, M. A. (2013). BOLA1 Is an Aerobic Protein That Prevents Mitochondrial Morphology Changes Induced by Glutathione Depletion. *Antioxidants & Redox Signaling*, *18*(2), 129. https://doi.org/10.1089/ARS.2011.4253

Winklhofer, K. F., Tatzelt, J., & Haass, C. (2008). The two faces of protein misfolding: Gain- and loss-of-function in neurodegenerative diseases. In *EMBO Journal* (Vol. 27, Issue 2, pp. 336–349). https://doi.org/10.1038/sj.emboj.7601930

Wootten, D., Christopoulos, A., Marti-Solano, M., Babu, M. M., & Sexton, P. M. (2018). Mechanisms of signalling and biased agonism in G protein-coupled receptors. *Nature Reviews Molecular Cell Biology 2018 19:10*, *19*(10), 638–653. https://doi.org/10.1038/s41580-018-0049-3

Wu, J. W., Herman, M., Liu, L., Simoes, S., Acker, C. M., Figueroa, H., Steinberg, J. I., Margittai, M., Kayed, R., Zurzolo, C., Di Paolo, G., & Duff, K. E. (2013). Small misfolded Tau species are internalized via bulk endocytosis and anterogradely and retrogradely transported in neurons. *The Journal of Biological Chemistry*, *288*(3), 1856–1870. https://doi.org/10.1074/JBC.M112.394528

Wulf, M. A., Senatore, A., & Aguzzi, A. (2017). The biological function of the cellular prion protein: an update. *BMC Biology 2017 15:1*, *15*(1), 1–13. https://doi.org/10.1186/S12915-017-0375-5

Xilouri, M., Emmanouilidou, E., Polissidis, A., Chavarría, C., Ivagnes, R., & Souza, J. M. (2022). Extracellular Alpha-Synuclein: Mechanisms for Glial Cell Internalization and Activation. *Biomolecules 2022, Vol. 12, Page 655*, *12*(5), 655. https://doi.org/10.3390/BIOM12050655

Xiong, M., Zou, L., Meng, L., Zhang, X., Tian, Y., Zhang, G., Yang, J., Chen, G., Xiong, J., Ye, K., & Zhang, Z. (2021). A γ-adducin cleavage fragment induces neurite deficits and synaptic dysfunction in Alzheimer's disease. *Progress in Neurobiology*, *203*, 102074. https://doi.org/10.1016/J.PNEUROBIO.2021.102074

Xu, L., & Pu, J. (2016). Alpha-Synuclein in Parkinson's Disease: From Pathogenetic Dysfunction to Potential Clinical Application. *Parkinson's Disease*, *2016*. https://doi.org/10.1155/2016/1720621

Yuan, J., Xiao, X., McGeehan, J., Dong, Z., Cali, I., Fujioka, H., Kong, Q., Kneale, G., Gambetti, P., & Zou, W. Q. (2006). Insoluble aggregates and protease-resistant conformers of prion protein in uninfected human brains. *The Journal of Biological Chemistry*, *281*(46),34848–34858. https://doi.org/10.1074/JBC.M602238200

Zaaroor-Regev, D., De Bie, P., Scheffner, M., Noy, T., Shemer, R., Heled, M., Stein, I., Pikarsky, E., & Ciechanover, A. (2010). Regulation of the polycomb protein Ring1B by self-ubiquitination or by E6-AP may have implications to the pathogenesis of Angelman syndrome. *Proceedings of the National Academy of Sciences of the United States of America*, *107*(15), 6788–6793. https://doi.org/10.1073/PNAS.1003108107/SUPPL_FILE/PNAS.1003108107_SI.PDF

Zeng, G., Yu, X., & Cai, M. (2001). Regulation of yeast actin cytoskeleton-regulatory complex Pan1p/Sla1p/End3p by serine/threonine kinase Prk1p. *Molecular Biology of the Cell*, *12*(12), 3759–3772. https://doi.org/10.1091/MBC.12.12.3759

Zhang, Q.-S., Heng, Y., Mou, Z., Huang, J.-Y., Yuan, Y.-H., & Chen, N.-H. (2017). Reassessment of subacute MPTP-treated mice as animal model of Parkinson's disease. *Acta Pharmacologica Sinica*, *38*(10), 1317–1328. https://doi.org/10.1038/aps.2017.49

Zhang, R., & Xie, X. (2012). Tools for GPCR drug discovery. *Acta Pharmacologica Sinica*, *33*(3), 372–384. https://doi.org/10.1038/APS.2011.173

Zhang, Y. J., Xu, Y. F., Cook, C., Gendron, T. F., Roettges, P., Link, C. D., Lin, W. L., Tong, J., Castanedes-Casey, M., Ash, P., Gass, J., Rangachari, V., Buratti, E., Baralle, F., Golde, T. E., Dickson, D. W., & Petrucelli, L. (2009). Aberrant cleavage of TDP-43 enhances aggregation and cellular toxicity. *Proceedings of the National Academy of Sciences of the United States of America*, *106*(18), 7607–7612. https://doi.org/10.1073/PNAS.0900688106

Zhang, Z., Nie, S., & Chen, L. (2018). Targeting prion-like protein spreading in neurodegenerative diseases. In *Neural Regeneration Research* (Vol. 13, Issue 11, pp. 1875–1878). Wolters Kluwer Medknow Publications. https://doi.org/10.4103/1673-5374.239433